Engineering Highly-functional, Self-regenerative Skeletal Muscle Tissues with Enhanced Vascularization and Survival *In Vivo*

by

Mark Edward Juhas

Department of Biomedical Engineering
Duke University

Date:_____

Approved:

_____
Nenad Bursac, Supervisor

_____
Charles Gersbach

_____
Christopher Kontos

_____
George Truskey

_____
Jennifer West

Dissertation submitted in partial fulfillment of the
requirements for the degree of Doctor of Philosophy in the
Department of Biomedical Engineering in the
Graduate School of Duke University

2016

ABSTRACT

Engineering Highly-functional, Self-regenerative Skeletal Muscle Tissues with Enhanced Vascularization and Survival *In Vivo*

by

Mark Edward Juhas

Department of Biomedical Engineering
Duke University

Date:_____

Approved:

_____
Nenad Bursac, Supervisor

_____
Charles Gersbach

_____
Christopher Kontos

_____
George Truskey

_____
Jennifer West

An abstract of a dissertation submitted in partial fulfillment of the requirements for the degree of Doctor of Philosophy in the Department of Biomedical Engineering in the Graduate School of Duke University

2016

Abstract

Tissue engineering of biomimetic skeletal muscle may lead to development of new therapies for myogenic repair and generation of improved *in vitro* models for studies of muscle function, regeneration, and disease. For the optimal therapeutic and *in vitro* results, engineered muscle should recreate the force-generating and regenerative capacities of native muscle, enabled respectively by its two main cellular constituents, the mature myofibers and satellite cells (SCs). Still, after 20 years of research, engineered muscle tissues fall short of mimicking contractile function and self-repair capacity of native skeletal muscle. To overcome this limitation, we set the thesis goals to: 1) generate a highly functional, self-regenerative engineered skeletal muscle and 2) explore mechanisms governing its formation and regeneration *in vitro* and survival and vascularization *in vivo*.

By studying myogenic progenitors isolated from neonatal rats, we first discovered advantages of using an adherent cell fraction for engineering of skeletal muscles with robust structure and function and the formation of a SC pool. Specifically, when synergized with dynamic culture conditions, the use of adherent cells yielded muscle constructs capable of replicating the contractile output of native neonatal muscle, generating >40 mN/mm^2 of specific force. Moreover, tissue structure and cellular heterogeneity of engineered muscle constructs closely resembled those of native muscle, consisting of aligned, striated myofibers embedded in a matrix of basal lamina proteins and SCs that resided in native-like niches. Importantly, we identified rapid formation of myofibers early during engineered muscle culture as a critical condition leading to SC homing and conversion to a quiescent, non-proliferative state. The SCs

retained natural regenerative capacity and activated, proliferated, and differentiated to rebuild damaged myofibers and recover contractile function within 10 days after the muscle was injured by cardiotoxin (CTX). The resulting regenerative response was directly dependent on the abundance of SCs in the engineered muscle that we varied by expanding starting cell population under different levels of basic fibroblast growth factor (bFGF), an inhibitor of myogenic differentiation. Using a dorsal skinfold window chamber model in nude mice, we further demonstrated that within 2 weeks after implantation, initially avascular engineered muscle underwent robust vascularization and perfusion and exhibited improved structure and contractile function beyond what was achievable *in vitro*.

To enhance translational value of our approach, we transitioned to use of adult rat myogenic cells, but found that despite similar function to that of neonatal constructs, adult-derived muscle lacked regenerative capacity. Using a novel platform for live monitoring of calcium transients during construct culture, we rapidly screened for potential enhancers of regeneration to establish that many known pro-regenerative soluble factors were ineffective in stimulating *in vitro* engineered muscle recovery from CTX injury. This led us to introduce bone marrow-derived macrophages (BMDMs), an established non-myogenic contributor to muscle repair, to the adult-derived constructs and to demonstrate remarkable recovery of force generation (>80%) and muscle mass (>70%) following CTX injury. Mechanistically, while similar patterns of early SC activation and proliferation upon injury were observed in engineered muscles with and without BMDMs, a significant decrease in injury-induced apoptosis occurred only in the presence of BMDMs. The importance of preventing apoptosis was further demonstrated

by showing that application of caspase inhibitor (Q-VD-OPh) yielded myofiber regrowth and functional recovery post-injury. Gene expression analysis suggested muscle-secreted tumor necrosis factor-α (TNFα) as a potential inducer of apoptosis as common for muscle degeneration in diseases and aging *in vivo*. Finally, we showed that BMDM incorporation in engineered muscle enhanced its growth, angiogenesis, and function following implantation in the dorsal window chambers in nude mice.

In summary, this thesis describes novel strategies to engineer highly contractile and regenerative skeletal muscle tissues starting from neonatal or adult rat myogenic cells. We find that age-dependent differences of myogenic cells distinctly affect the self-repair capacity but not contractile function of engineered muscle. Adult, but not neonatal, myogenic progenitors appear to require co-culture with other cells, such as bone marrow-derived macrophages, to allow robust muscle regeneration *in vitro* and rapid vascularization *in vivo*. Regarding the established roles of immune system cells in the repair of various muscle and non-muscle tissues, we expect that our work will stimulate the future applications of immune cells as pro-regenerative or anti-inflammatory constituents of engineered tissue grafts. Furthermore, we expect that rodent studies in this thesis will inspire successful engineering of biomimetic human muscle tissues for use in regenerative therapy and drug discovery applications.

Contents

Abstract iv

List of Tables xiii

List of Figures xiv

Acknowledgements xviii

1. Introduction 1

2. Background 6

2.1 Skeletal muscle regeneration and myogenesis 6

2.1.1 The satellite cell and its niche 8

2.1.2. Macrophages and skeletal muscle regeneration 9

2.2 Defective regeneration and disease 11

2.3 Muscle repair strategies 13

2.3.1. Candidates for cellular therapy 14

2.3.2. Engineering environments for therapeutic use 16

2.3.2.1. Engineering SC niche 17

2.3.2.2. In situ regeneration using engineered scaffolds 18

2.3.3. Tissue-engineered muscle 20

2.4 Engineering skeletal muscle 21

2.4.1 Preparation of myogenic cell source 21

2.4.1.1 Satellite cell isolation 22

2.4.1.2 Myoblast cell culture 23

2.4.1.3 Maintaining regenerative capacity in vitro 25

2.4.2 Engineering functional muscle constructs 26

2.4.2.1 Generating 3D muscle....27
2.4.2.2 Maturation of engineered muscle in vitro....30
2.4.3 In vitro assessment of engineered muscle....30
2.4.3.1 Muscle structure and morphology....31
2.4.3.2 Contractile function....32
2.4.3.3 Calcium handling....33
2.4.4 Implantation of engineered muscle in vivo....33
3. Identification of the roles of cellular source and culture condition in muscle myogenesis and function....36
3.1 Rationale and experimental plan....36
3.2 Methods....37
3.2.1 Myogenic cell preparation....37
3.2.2 Fabrication of engineered muscle....37
3.2.3 Immunostaining analysis....38
3.2.4 Assessment of contractile function....40
3.2.5 Statistics....41
3.3 Results....42
3.3.1 Effects of culture and cell source on muscle area....42
3.3.2 Effects of culture and cell source on contractility....43
3.3.3 Effects of culture and cell source on hypertrophy and fusion....44
3.3.5 Retention of satellite cells....46
3.3.6 Cellular dynamics during fusion events....47
3.3.7 Structural characteristics of engineered muscle....53
3.3.8 Maturation of engineered muscle....54

3.4 Discussion 57
3.4.1 Optimizing cell source and culture conditions 57
3.4.1.1 Effects on engineered muscle compaction 58
3.4.1.2 Effects on myofiber maturity 61
3.4.1.3 Maintaining a satellite cell population and tracking early fusion events 62
3.4.1.4 Formation of the satellite cell niche 63
3.4.2 Comparing optimized constructs to native muscle 64
3.5 Summary and Implications 65
4. Assessing the ability of neonatal-derived engineer muscle to respond to injury in vitro and survive following in vivo implantation 67
4.1 Rationale and experimental plan 67
4.2 Methods 68
4.2.1 Cell isolation and culture 68
4.2.2 Engineered muscle formation 69
4.2.3 In vitro regeneration assay 69
4.2.4 Implantation of engineered muscle bundles 70
4.2.5 Intravital imaging of blood vessels 71
4.2.6 Intravital imaging of intracellular Ca^{2+} transients 72
4.2.7 In vitro and ex vivo measurements of Ca^{2+} transients 74
4.2.8 In vitro and ex vivo force measurements 74
4.2.9 Immunostaining 74
4.2.10 Nucleus counting image analysis 75
4.2.11 Analysis of myofiber and blood vessel alignment 75
4.2.12 Statistics 75

4.3 Results 76
4.3.1 Evaluation of homeostatic state of engineered muscle 76
4.3.2 Response of engineered muscle to in vitro injury 77
4.3.3 Expansion of neonatal cells to maintain SC pool and enhance function 80
4.3.4 Effect of $Pax7^+$ SCs on in vitro regeneration 82
4.3.5. Vascularization of implanted engineered muscle 83
4.3.6 Myogenesis in implanted engineered muscle 86
4.3.7 Function of implanted engineered muscle 88
4.4 Discussion 91
4.4.1 Characterization of satellite cell pool 91
4.4.2 In vitro regeneration of engineered bundles in response to CTX injury 93
4.4.3 Importance of satellite pool for in vitro regeneration 95
4.4.4 Implantation of engineered muscle 97
4.4.4.1 Vascularization of implanted tissue 97
4.4.4.2 Benefit of pre-differentiated muscle implant 98
4.4.4.3 Continued functional and structural maturation of implanted muscle 99
4.5 Summary and Implications 99
5. Engineering highly functional muscle tissues derived from adult cell isolates capable of self-repair and survival in vivo 101
5.1. Rationale and experimental plan 101
5.2 Methods 102
5.2.1 Myogenic cell preparation 102
5.2.2 Bone marrow-derived macrophage isolation and differentiation 103
5.2.3 BMDM polarization 104

5.2.4 Engineered muscle formation and culture 105

5.2.3 Real-time in vitro regeneration assay 105

5.2.4 Cellular proliferation assay 106

5.2.4 Supplementation of pro-regenerative and anti-apoptotic factors 106

5.2.5 Quantitative RT-PCR 106

5.2.6 Immunostaining 107

5.2.7 Implantation of adult-derived engineered muscle bundles 107

5.2.8 Intravital imaging of blood vessels and intracellular Ca^{2+} transients 108

5.2.9 In vitro and ex vivo functional testing 108

5.3 Results 108

5.3.1 Formation of adult-derived engineered muscle 108

5.3.2 Regenerative ability of adult-derived constructs following CTX injury 109

5.3.3 Attempt to enhance SC maintenance within engineered muscle bundles 111

5.3.4 Supplementation of pro-regenerative factors following CTX injury 113

5.3.5 Incorporation of bone marrow-derived macrophages into engineered muscle 116

5.3.6 Regenerative capacity of muscle-BMDM constructs following CTX injury 118

5.3.7. Mechanisms of BMDM-induced in vitro regeneration 121

5.3.8. Assessing paracrine effects of BMDMs within engineered muscle following injury 128

5.3.9 Effect of macrophage phenotype for regeneration following CTX injury 132

5.3.10. Roles of BMDMs in implanted muscle survival, vascularization, and function 136

5.3.10.1 Effect of M0 BMDMs on engineered muscle vascularization following implantation 137

5.3.10.2 Effect of M0 BMDMs on engineered muscle function and survival following implantation....138

5.3.10.4 Effect of BMDM polarization on survival, vascularization, and function of engineered muscle implants....141

5.4 Discussion....142

5.4.1 Generation of adult-derived engineered muscle....143

5.4.2 Enhancing the regeneration of adult-derived muscle....144

5.4.3 Effect of bone marrow-derived macrophages on regeneration....145

5.4.4 Understanding the mechanisms behind BMDM-induced regeneration....146

5.4.5 Effect of BMDMs polarization on regeneration following CTX injury....149

5.4.6 Effect of BMDMs on in vivo vascularization, function, and survival of engineered muscle....150

5.5 Summary and Implications....153

6. Summary....155

7. Future Applications....158

Lastly, our *in vivo* work provides a foundation for many future implantation studies. The ability of engineered muscle tissues to serve for volumetric muscle loss therapy....161

References....163

Biography....187

List of Tables

Table 2.1 Cellular candidates for myogenic repair 16

Table 3.1 Primary antibody list for chapter 3.....39

Table 3.2 Secondary antibody list for chapter 3 40

Table 4.1 Additional primary antibodies used in chapter 4 75

Table 5.1 QT-PCR primer list 107

Table 5.2 Additional primary antibodies used in Section 5 107

List of Figures

Figure 2.1: Regenerative response of injured skeletal muscle. 6

Figure 2.2 Myogenesis during regeneration. 8

Figure 2.3 Current cellular-based therapies for muscle repair. 14

Figure 2.3 Methods to isolate and expand myogenic cells. 26

Figure 2.4 Methods for implantation of engineered muscle. 35

Figure 3.1 Cross-sectional analysis on engineered muscle. 43

Figure 3.2 Contractile force generation of engineered muscle. 44

Figure 3.3 Quantification of myofiber hypertrophy. 45

Figure 3.4 Fusion efficiency in engineered muscle. 46

Figure 3.5 Maintenance of satellite cell pool. 47

Figure 3.6 Cellular dynamics within engineered muscle during fusion. 48

Figure 3.7 Co-expression of myogenic markers within engineered muscle during fusion. 49

Figure 3.8 Early formation of sarcomeres within engineered muscle. 51

Figure 3.9 Early compaction of dynamically cultured bundles. 52

Figure 3.10 Exterior layer of fibroblasts in engineered muscle during fusion. 52

Figure 3.11 Input cell population for engineering of skeletal muscle bundles. 53

Figure 3.12 Structural characterization of engineered muscle. 54

Figure 3.13 Maturation of engineered muscle. 55

Figure 3.14 Functional characterization of engineered muscle bundles. 56

Figure 3.15 Characterization of engineered muscle from non-adherent cell fraction cultured dynamically. 58

Figure 3.16 Peripheral fibroblast layer in engineered muscle. 60

Figure 3.17 Pax7^{+} cells homed to myofibers at day 4. 64

Figure 4.1 In vitro assessment of engineered muscle regeneration. 70

Figure 4.2 Method for calculating blood vessel density in implanted engineered muscle bundles.....72

Figure 4.3 Measurements of intracellular calcium transient and contractile force generation in implanted engineered muscle bundles. 73

Figure 4.4 Acquisition of homeostatic cell composition within engineered muscle bundles.....77

Figure 4.5 Regenerative response of engineered muscle to in vitro cardiotoxin (CTX) injury. 79

Figure 4.6 Expansion of neonatal myogenic cells in bFGF supplemented media.....80

Figure 4.7 Engineered muscle from myogenic cells expanded in bFGF.....81

Figure 4.9 SCs and regeneration.....82

Figure 4.10 Vascular integration of implanted engineered muscle. 84

Figure 4.11 Structural characterization of 2-day old undifferentiated engineered (UnD) muscle bundles. 85

Figure 4.12 Vascular organization in implanted engineered muscle bundles. 85

Figure 4.13 Capillary lumen diameters in implanted engineered muscle bundles. 86

Figure 4.14 Myogenesis and structural differentiation of implanted engineered muscle bundles.....87

Figure 4.15 Myofiber alignment in pre-differentiated and undifferentiated implanted engineered muscle bundles.....87

Figure 4.16 Calcium transients and force generation of implanted engineered muscle..89

Figure 4.17 Kinetics of electrically-induced calcium transient and twitch force responses in engineered muscle bundles. 90

Figure 4.18 The formation of SC niche within engineered muscle tissue. 93

Figure 5.1 Adult-derived engineered muscle.....109

Figure 5.2 Adult-derived engineered muscle regenerative response. 110

Figure 5.3 SC pool and regenerative ability in adult-derived muscle. 111

Figure 5.4 Enhanced retention of myogenic cells with regenerative potential using specific growth factors. 112

Figure 5.5 Engineered muscle from growth factor expanded cells. 113

Figure 5.6 MHCK7 promoter in engineered muscle. 115

Figure 5.7 Effect of pro-regenerative factors on engineered muscle following injury. ... 116

Figure 5.8 Structure and function of bone marrow-derived macrophage (BMDM)-muscle co-cultured engineered bundles. 117

Figure 5.9 Functional recovery of muscle-BMDM constructs following CTX injury. 119

Figure 5.10 Structural recovery of muscle-BMDM constructs following CTX injury. 120

Figure 5.11 The regrowth of myofibers in muscle-BMDM constructs after CTX injury. . 121

Figure 5.12 Early myogenic responses in adult-derived engineered muscle after CTX injury. 122

Figure 5.13 Cell proliferation during *in vitro* muscle bundle regeneration in response to CTX injury. 123

Figure 5.14 Caspase activity in engineered muscle bundles following CTX injury. 125

Figure 5.15. Effects of Q-VD-OPh on regeneration following CTX injury. 127

Figure 5.16 In vitro regeneration of engineered muscle bundles in paracrine system following severe CTX injury. 129

Figure 5.17 In vitro regeneration of engineered muscle bundles in paracrine system following mild CTX injury. 131

Figure 5.18 Cleaved-caspase-3 activity following mild CTX injury in paracrine muscle bundles. 132

Figure 5.19 Bone marrow-derived macrophage polarization. 133

Figure 5.20 Expression of polarization markers within engineered muscle. 134

Figure 5.21 Effect of BMDM polarization on functional recovery following CTX injury. . 135

Figure 5.22 The effect of BMDM polarization on structural recovery following CTX injury. 136

Figure 5.23 Vascularization of implanted adult-derived engineered muscle bundles....138

Figure 5.24 Function of adult-derived engineered muscle implants. 140

Figure 5.25 Survival of adult-derived engineered muscle following implantation. 141

Figure 5.26. Effect of BMDM polarization on vascularization, function, and survival of engineered muscle implants. 142

Figure 5.27. TNFα gene expression following injury. 148

Figure 5.28. BMDMs contribution during regeneration. 149

Figure 5.29. Invasion of macrophages following implantation. 153

Acknowledgements

The work presented in this thesis would not have been possible without the constant support I've received throughout my time at Duke University. I would first like to thank my family for their encouragement and unwavering confidence in me: my parents, David and Judith, my sister, Elizabeth, my brother, Brett, my brother-in-law, Doug, and my new nephew, Landon. I'm also grateful for the friends I have made in Durham, those who were always available for a late night at The Federal, especially Gordon, Nikolas, Matt, Caslin, Katy, Frank, and Sean. A very special thanks goes to Robin for unconditional support and being a constant source of joy and excitement.

I would also like to express my gratitude to all members of the Bursac lab for their assistance over the years. In particular, I would like to thank Christopher Jackman for immeasurable technical support, Liqing Li and Hung Nguyen for lentiviral development, Jason Wang for assistance running experiments, Jasmine Li for molecular biology advice, Ilya Shadrin, Ying Qian, Asvin Ganapathi, and George Engelmayr for surgical procedures, and Jean Ye for her exceptional cell culture talents. I would further like to acknowledge senior lab members for their guidance and training, including Sara Hinds, Weining Bian, Luke McSpadden, Ava Krol, Nima Badie, Alastair Khodabudkus, Aaron Carlson, Lauran Madden, Huda Asfour, and, most importantly, Robert Kirkton. Within the Duke community, I would like to thank our collaborators, Gregory Palmer and Andrew Fontanella, and members of the Light Microscopy and Optical Molecular Imaging and Analysis core facilities. Additionally, the Biomedical Engineering department and its staff have provided an excellent environment to grow as an academic

and infinite support during my tenure. I would also like to acknowledge consultation from members at other universities including Benedicte Chazaud and Thomas Rando.

Finally, I would also like to thank the members of my thesis committee and especially, my advisor, Nenad Bursac. His passion for science and drive for excellence created an inspiring work environment. With his guidance and patience, I have been able to develop as a scientist and a professional.

1. Introduction

Over the last several decades intensive efforts of biologists, physicians, and bioengineers have unraveled the important contributions of molecular signaling, systemic and cellular factors, cell-matrix interactions, and stem cell niches to skeletal muscle function, regeneration and disease [1-3]. While these studies have led to the discovery of various therapeutic targets and improved clinical outcomes, muscle-related diseases still impose significant health and economic burdens on society. For continued advances towards efficient clinical therapies it will be essential to develop methods for better control of *in vitro* and *in vivo* environments to enable accurate studies of cellular functions and interactions, recreate stem cell niches both *in vitro* and *in vivo*, and encourage survival and integration of implanted cells [4-6]. One strategy utilized by many researchers has been the engineering of three-dimensional (3D) muscle tissues to recreate the structural complexity and functionality of the native organ for use in both regenerative therapies and as a bridge between traditional studies of muscle biology in individual cells or groups of cells and physiological tests at the organ or whole body level [5, 6]. Although quite promising for the field of muscle repair, tissue-engineered skeletal muscle has been previously inadequate in recreating native muscle's contractile and regenerative functions [7-22].

The work described in this thesis is motivated by the need for 1) highly functional engineered skeletal muscle tissues capable of physiological function with the potential for on-site replacement and 2) *in vitro* platforms to efficiently model muscle contractility, development, regeneration, and disease to support therapeutic development and screening. We established novel methodology to generate muscle constructs with biomimetic structure and cellular heterogeneity, comprised of functional SCs and

aligned, striated myofibers, which generate forces comparable to aged-matched native tissue. Following rigorous assessment, we demonstrate the ability of the maintained SC population within the engineered tissue to respond in a natural manner to injury *in vitro* and regenerate muscle mass and recover force production. Further, upon *in vivo* implantation, using a unique imaging platform in live mice, we monitored engineered tissues in real-time as they became vascularized and matured over the course of two weeks. Finally, we transitioned from neonatal to adult cell types and, through the use of a real-time *in vitro* regeneration assay, discovered the beneficial effect of incorporating immune cells in the engineered muscle to enhance both regeneration *in vitro* and survival *in vivo*. These studies represent a significant step towards developing human-based muscle replacement therapeutics and physiologically accurate, *in vitro* models of skeletal muscle.

Chapter 2 of this thesis provides background information on the natural processes governing skeletal muscle regeneration and describes conditions and pathologies in which, this otherwise robust process, is impeded or exhausted. The SC, the cellular keystone for new muscle formation, and its niche, a complex orchestra of local and systemic signals, will be discussed in detail. The chapter will present current cellular and genetic therapies for a diverse set of muscular diseases. Importantly, the paradigm of engineering 3D skeletal muscle for use in regenerative therapies or as a model system will be discussed. Specifically, the methods used to form engineered tissues and optimize their performance both *in vitro* and *in vivo* as well as current applications will be addressed.

In Chapter 3, we identified optimal culturing conditions and cell preparation using primary, neonatal rat cells to engineer muscle tissues with superior force generation and

cellular maturity compared to previously reported attempts. We revealed the benefit of using an adherent fraction of cells with maintained regenerative and proliferative properties combined with dynamic culture to yield constructs capable of replicating the function and architecture of natural muscle. Importantly, we identified critical conditions for the maintenance of SCs in engineered muscle *in vitro*, namely the differentiated myofibers, which played a critical role in regaining SC quiescence at early time points in culture.

In Chapter 4, we focused our studies on assessing the ability of neonatal-derived engineered muscle tissues to regenerate *in vitro* and survive and vascularize *in vivo*. Specifically, the functionality of the SC population in engineered muscle was tested using an *in vitro* regeneration assay in which the muscle was injured with the application of cardiotoxin (CTX) to induce myofiber damage. Upon muscle injury, the initially quiescent SCs demonstrated the ability to activate, proliferate, and differentiate, yielding the recovery of muscle mass and contractile function. Next, the ability of engineered muscle to survive, vascularize, and experience sustained growth and maturation *in vivo* was assessed. To continuously monitor engineered tissue after implantation, we transduced the myogenic cells with a genetically-encoded calcium (Ca^{2+}) indicator, GCaMP3, and implanted the muscle constructs in a dorsal skinfold chamber in nude mice. While initially avascular, these engineered neonatal-derived muscle tissues underwent robust vascularization and perfusion, and exhibited continued myogenesis and improved contractile function *in vivo*, all of which were significantly enhanced by myogenic pre-differentiation of tissue constructs before implantation.

In Chapter 5, we transitioned from using neonatal to using adult myogenic cells in attempt to enhance the clinical relevance of the work and assess the ability of adult-

derived engineered muscle to regenerate *in vitro* and survive *in vivo*. Using cell expansion and culture methods optimized for neonatal cells, we showed the ability to engineer adult-derived muscle with architecture and force generating capacity comparable to those of neonatal-derived muscle. However, in contrast to their neonatal counterparts, adult-derived tissues did not undergo regeneration upon CTX injury, leading us to further investigate methods to enhance their regenerative potential. We developed a "regeneration assay" whereby GCaMP-reported calcium transients in engineered muscle were recorded live with a fast fluorescent camera at different times after CTX injury. Based on this assay, we found that various pro-regenerative growth factors did not support *in vitro* muscle recovery from CTX damage. We next introduced bone marrow-derived macrophages (BMDMs) in engineered muscle, as a non-myogenic cell type known to associate with natural muscle regeneration. The BMDMs proved vital in preventing apoptotic loss of myofibers that typically provide a scaffold for subsequent SC-induced muscle repair and thus rescued the ability of adult-derived muscles to regenerate. Finally, with the use of the *in vivo* platform developed in Chapter 4, we showed the benefits of added BMDMs for vascularization, continued muscle growth, and increased force generating capacity of implanted adult-derived engineered muscles.

In Chapter 6, we provided a summary of all the work described in this thesis and in Chapter 7 we discussed future applications of these findings, specifically towards the development of muscle regenerative therapies and *in vitro* platforms for therapeutic discovery.

Overall, this thesis demonstrates methods to engineer biomimetic skeletal muscle tissues capable of recapitulating the contractile and regenerative potential of natural muscle. The hereto developed methodologies and mechanistic findings are

expected to: 1) accelerate the implementation of three-dimensional, tissue-engineered skeletal muscle models for *in vitro* and *in vivo* studies of muscle growth, regeneration, and disease; 2) bolster the consideration of incorporating immune cells within engineered tissues to support their regeneration, vascularization, and survival *in vivo*; and 3) stimulate the development of *in vitro* human microphysiological platforms with real-time monitoring capabilities for the accelerated discovery or new drug, cell, and gene therapies for skeletal muscle dysfunction.

2. Background

2.1 Skeletal muscle regeneration and myogenesis

Skeletal muscle has a remarkable capacity for regeneration which allows the tissue to undergo daily renewal and fully recover following small, everyday injuries or acute damage even in a matured state [2], a phenomenon absent in most other tissues. The regenerative process involves the synchronized action of resident and circulating myogenic cells, local non-muscle cells, and inflammatory cells, at cellular and molecular levels, that rapidly yield the production of new muscle[2, 23], provisional ECM, and supporting vascular networks (Figure 2.1) [24].

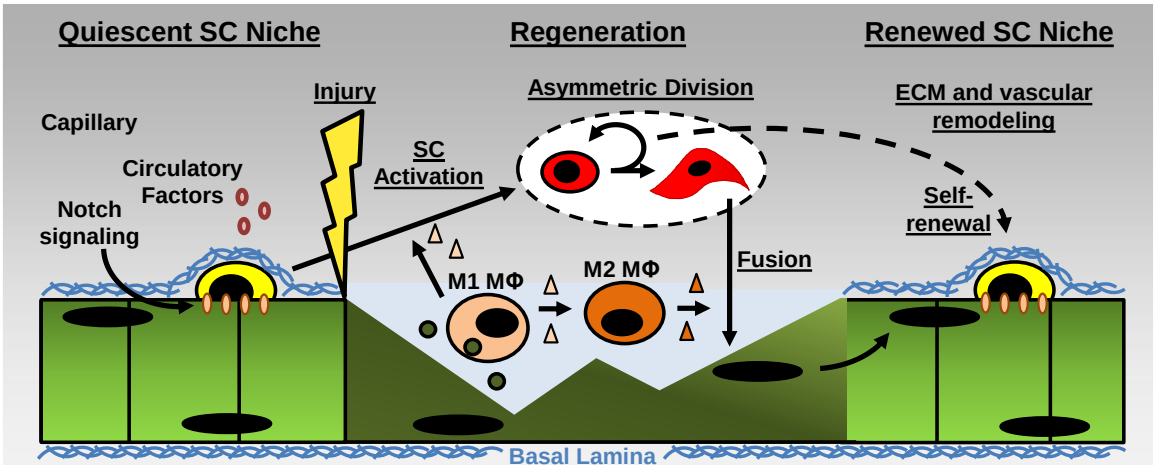

Figure 2.1: Regenerative response of injured skeletal muscle. A simplified schematic of the satellite cell (SC) niche at homeostasis and following an acute injury. Niche quiescence maintained via local juxtacrine and paracrine signaling is disturbed following injury. In response to injury-induced myofiber debris, M1 and M2 macrophages (MΦ) secrete factors that lead to SC activation, asymmetric division, and formation of myogenic precursors primed for fusion that participate in repair of damaged and creation of new myofibers. After regeneration, the SC niche is reestablished along with its extracellular matrix (ECM) and vascular components.

In general, the formation of new muscle following injury can be separated into a *degenerative* and a *regenerative* phase. The degenerative phase is responsible for clearing necrotic myofibers, as well as activating the subsequent regenerative phase. Following injury, the myofiber sarcolemma is disrupted and intracellular components,

such as creatine kinase, leak into the extracellular space [25]. Inflammatory cells, the majority being neutrophils, begin to infiltrate within 1-6 hours [26]. By 48 hours, pro-inflammatory M1 phenotype macrophages are the predominant inflammatory cell at the site of injury. The cells work to clear necrotic debris through phagocytosis, further amplify the inflammatory response, and activate SCs for regeneration through the release of soluble cues [26, 27], including tumor necrosis factor-α (TNFα) [28] and interleukin 6 (IL-6) [29]. The regenerative phase is activated by cellular responses occurring in the degenerative phase, and involves skeletal myogenesis occurring concurrently with ECM production and angiogenesis at the injured site. Myogenesis is initiated by the local activation of SCs by cytokines excreted in the degenerative phase. SCs, normally quiescent in adult muscle, reside beneath the basal lamina surrounding myofibers and are marked by expression of the paired-box transcription factor, Pax7 [2]. Once activated, $Pax7^+$ SCs gain expression of the myogenic regulatory factor, MyoD, and begin to proliferate (Figure 2.2A). The new pool of cells will either commit to a myogenic lineage and undergo differentiation or lose MyoD expression and return to quiescence, refilling the SC pool for future regenerative events [1, 2]. The commitment to a myogenic fate is marked by a loss of Pax7 expression and expression of the mature muscle marker, myogenin; these cells are termed myoblasts (Figure 2.2B) [1, 2]. This process, known as differentiation, is activated by release of cytokines, such as insulin-like growth factor-1 (IGF-1) and IL-10, from M2 phenotype macrophages [27]. The expansion and differentiation of the myogenic cell population is essential, as it will act as the source of new myonuclei at the injury site [30, 31]. At this point, mature myoblasts will either undergo primary fusion, in which they will fuse to one another to form new multinucleated myotubes which will later mature into myofibers, or secondary fusion, in

which they will fuse to pre-existing, damaged myofibers to restore or even augment their function (Figure 2.2C) [2]. Concurrent with myogenesis, residing fibroblasts proliferate and migrate to the injury site to transiently form a supportive ECM in response to the release of the pro-fibrotic transforming growth factor-β (TGF-β) [32]. Simultaneously, increased expression of angiogenic factors, including vascular endothelial growth factor (VEGF) and angiopoeitin-1/2, yields the formation of new capillaries along with the formation of new myofibers ensuring the maintenance of blood supply (Figure 2.1) [33, 34]. These three components of regenerative process, myogenesis, fibrosis, and angiogenesis, act to provide a proper environment for the muscle regrowth and maturation and restore compromised contractile function.

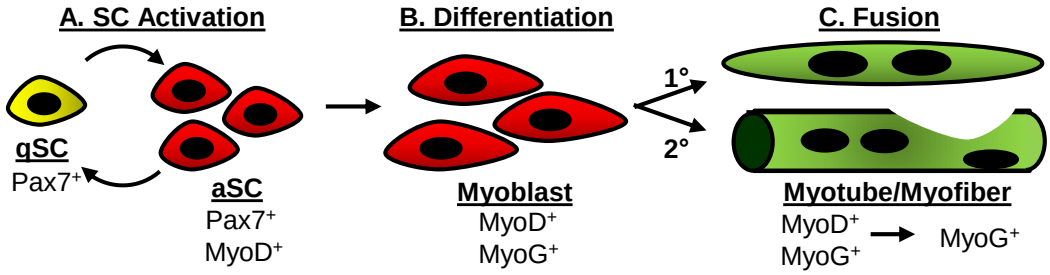

Figure 2.2 Myogenesis during regeneration. (A-B) A schematic of myogenesis describing (A) satellite cell (SC) activation, (B) differentiation, and (C) fusion, including the cells involved in the processes and their transcription factor expression. qSC: quiescent SC, aSC: activated SC.

2.1.1 The satellite cell and its niche

The notion that stem cells exist in specialized compartments, or “niches”, dates back more than forty years ago when it was proposed that stem cells maintain their potential by existing in specialized tissue compartments [35]. These niches are composed of local cellular and extracellular support systems that are essential for the stem cells that reside there to be held in reserve to support tissue homeostasis and repair over a lifetime. For SCs, the niche is only beginning to be understood. The muscle fiber is a major cellular component as each SC resides closely apposed to the

sarcolemma of its parent myofiber [36] via the cell-cell adhesion molecule, M-cadherin [1]. Moreover, SCs lay beneath a basal lamina matrix that consists of laminin and collagen IV, among other ECM proteins, and exist in a relatively soft micro-environment (~12 kPa) [37]. More recently, the concept of the stem cell niche has been broadened to include the systemic milieu. As exemplified by studies of stem cell aging and the decline in tissue regenerative potential with age, it became clear, first from the use of heterochronic parabiosis and, more recently, by heterochronic plasma transfer, that stem cell function can be markedly affected by circulatory factors [38, 39]. Importantly, disruption of the SC niche, noticed in aging [40], genetic defects [41], and matrix remodeling during fibrosis [42], has significantly detrimental impacts on the regenerative capacity of SCs.

2.1.2. Macrophages and skeletal muscle regeneration

As mentioned above, myogenesis during the regeneration process is highly regulated by events of the inflammatory response, most predominantly by pro- (M1) and anti-inflammatory (M2) macrophages. The commonly accepted paradigm is: first, the infiltration of M1 macrophages and the subsequent activation of SCs, followed by the transition from M1 to M2 macrophages and the induction of myoblast differentiation [27] (Figure 2.1). More specifically, upon the induction of injury, circulating monocytes, attracted by specific chemokines such as monocyte chemoattractant protein-1 (MCP1/CCL2), arrive at the damaged site [43]. The MCP1/CCL2 receptor, CCR2, is expressed in a Ly-C6^{high} monocyte population, making these cells the first to arrive at the scene. Ly-C6^{high} monocytes are a pro-inflammatory population capable of phagocytosis and, importantly, of M1 macrophage polarization [43]. Soluble factors, including TNFα, IL-1β, IL-13, interferon-γ (IFNγ), and nitric oxide, are secreted by the M1 population

stimulating both SC activation and the recruitment of more M1 cells [27, 44]. Within about 48 hours, Ly-6C^{high} cells are progressively replaced with Ly-6C^{low} cells, a population which will source anti-inflammatory M2 macrophages [27, 44, 45]. Similar to the autocrine actions of M1 cells, M2 macrophages secrete factors to inhibit M1 polarization, IL-10 and TGFβ, as well as recruit more M2 cells, IGF-1 and IL4 [44]. M2-secreted factors are linked to myoblast mobilization [46], cellular growth, and fusion [44] during muscle regeneration.

Another point of interest is the role of skeletal muscle-resident macrophages within the tissue. Tissue-resident macrophages are normally associated with homeostatic maintenance of an organ. The presence and contribution of such macrophages vary from tissue to tissue [47]. Resident macrophages are active as the first line in defense to activate the inflammatory response. As mentioned prior, skeletal muscle-resident macrophages, preferentially located in the connective tissue regions of the epimysium and perimysium, are secretors of monocyte-attracting chemokines [48]. Although active in initial recruitment, tissue-resident macrophages are commonly classified as “M2-like” and serve greater roles in the resolution of inflammation [49]. Included in this part, is the regulation of apoptotic cell clearance [50]. The specific roles and significance of skeletal muscle-resident macrophages are still in question. The population, which represents only a miniscule fraction of cellular content in the tissue [51], exists as an interesting target to ensure or restore proper regeneration *in vivo*.

The effect of macrophages on myogenic cells has been explored *in vitro* and researchers have utilized the pro-regenerative cell type as a method to aid in transplantation studies. Macrophages can be derived through either isolation of blood monocytes or, for a more efficient yield, through isolation of bone marrow monocytes

[52]. In *in vitro* culture, macrophage-colony stimulating factor (M-CSF) is commonly used to drive the differentiation of monocytes to a macrophage phenotype [53]. M-CSF is a factor found *in vivo* that regulates tissue-resident macrophage numbers [54] and is critical for macrophage differentiation, proliferation, and survival [55]. Notable work using *in vitro*-derived macrophages include the identification of their tendency to migrate towards SCs upon induced injury and their support of SCs to escape apoptotic events and enhance muscle formation [56]. Further, researchers have identified contact-mediated mechanisms through adhesion proteins which prevent apoptosis in proliferating myoblasts [57]. Finally, in co-transplantation studies, macrophages significantly enhance myoblast survival, expansion, and migration *in vivo* [52].

2.2 Defective regeneration and disease

Muscular disorders are commonly a result of chronic degenerative diseases due to genetic defects in muscle cells or neurological maladies, volumetric muscle loss following severe trauma, or muscle wasting stemmed from systemic disease. Chronic degenerative disease, such as muscular dystrophy, expose muscle to constant injury, eliciting continuous cycles of degeneration and regeneration, and can eventually lead to devastating fibrosis and exhaustion of the myogenic capacity conferred by SCs [58]. In Duchenne muscular dystrophy (DMD), the most severe form of muscular dystrophy, muscle lacks the membrane bound protein dystrophin as a result of a genetic mutation [59]. In the absence of dystrophin, the cellular membrane becomes vulnerable and the sarcolemma undergoes repeated tearing [60]. As a result, myofibers are susceptible to degeneration due to elevated intracellular calcium levels [61], oxidative damage [62], and focal damage to the myofiber. Regenerating myofibers, also containing the dystrophin mutation, retain the defect and are prone to further degeneration. The

persistent cycles of degeneration result in sustained activation of the wound healing response and chronic inflammation [63]. As previously mentioned, inflammatory cells recruit and activate ECM-producing cell types and, eventually, functional muscle is replaced with fibrotic and adipose tissue. Impaired regeneration in cases of chronic degeneration can be a result of various mechanisms including the reduced myogenic potential [64, 65] and proliferative capacity [66], marked by decreased telomere length [58], of SCs. Additionally, the fibrotic environment and disarrayed ECM may further hinder the capability of myogenesis to fully restore muscle function. There are no current cures for any of the dystrophies, although there is a burgeoning field of experimental therapeutics moving into clinical trials, with approaches ranging from pharmacological to viral gene therapies [67, 68]. Stem cell therapies have been long envisioned, but are only in their infancy [69]. Recent success of CRISPR-Cas9 *in vivo* genome editing technology to restore expression of a modified dystrophin protein in mice, gives significant hope for a genetic-based remedy [70-72].

Instances in which a significant amount of muscle is lost, i.e., greater than 20% of total muscle, are referred to as volumetric muscle loss (VML). As reviewed elsewhere [24], in these severe injuries the fibrotic response to stabilize the tissue proceeds more rapidly than myogenesis. Accelerated ECM deposition creates an environment that hinders the formation of new muscle and angiogenesis. In some cases, a dense cap of scar tissue may form resulting in denervation of the distal tissue as it lacks neuronal input. Overall, there is a general agreement that successful treatment of VML will likely involve timely surgical delivery of a large volume implant to rapidly add or recruit new muscle before the chronic scar is formed [5].

A separate category of muscle disorders involves conditions that result in muscle atrophy and wasting. Examples include cachexia associated with chronic diseases, especially cancer, chronic obstructive pulmonary disease (COPD), chronic renal disease, and chronic infections such as AIDS [73]. Muscle atrophy also occurs in the setting of injury or disease of peripheral nerves and motor neurons, such as amyotrophic lateral sclerosis (ALS), and there is prominent muscle wasting in paralyzed limbs of patients with spinal cord injuries [74]. Further, age-related muscle loss, or sarcopenia, is a major source of disability in the elderly [74]. In such cases, muscle atrophy is commonly attributed to either the disruption of SC activity, whether it's through chronic over-activation of the pool [75] or destruction of the healthy niche [40], or an increased propensity of myofiber apoptosis through caspase-3-dependent pathways [76]. In addition to the loss of strength and mobility, there are also systemic effects of muscle loss related to the role of muscle as an endocrine tissue, a feature that is increasingly being recognized and studied [77].

2.3 Muscle repair strategies

Various cell- and material-based approaches have been explored in animal and clinical studies to aid in the replacement of injured or diseased skeletal muscle or restoration of its regenerative capacity (Figure 2.3). Researchers have identified various cellular candidates capable of myogenic differentiation and the formation of new muscle following transplantation. Further, engineers have developed cellular niches for optimal cellular conditioning *in vitro* and co-delivery systems capable of introducing a combination of growth factors, bio-absorbable scaffolds, and stem or progenitor cells to augment cell viability, vascularization, and myogenesis *in vivo*. Further, the generation of three-dimensional, tissue-engineered muscle constructs has been explored to recreate

the structural, mechanical, and functional properties of natural muscle in attempt to promote rapid muscle repair *in vivo*.

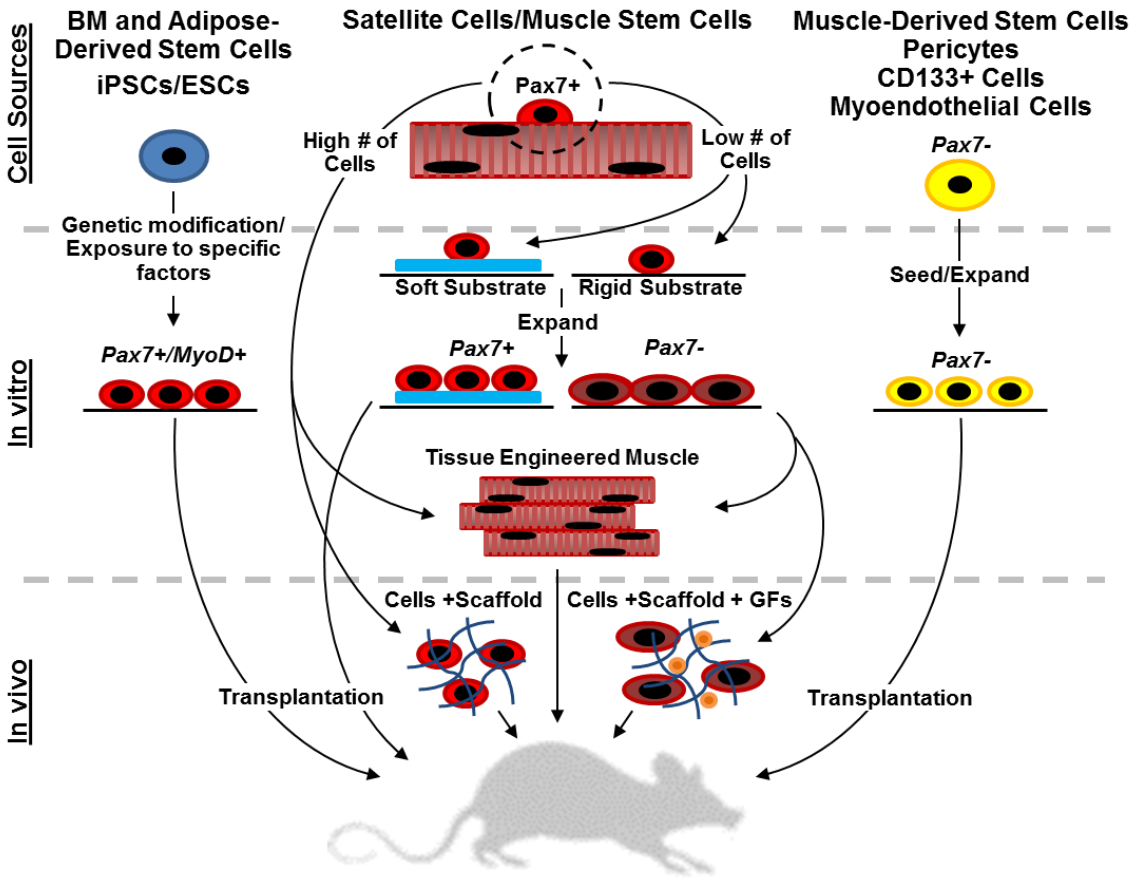

Figure 2.3 Current cellular-based therapies for muscle repair. Diagram displaying various cell-based therapies for skeletal muscle disease and repair.

2.3.1. Candidates for cellular therapy

Skeletal muscle presents a variety of possible cell source candidates for use in cellular therapies, as listed in Table 2.1. An optimal cell source for muscle repair would need to be accessible, proliferative *in vitro*, self-renewing, capable of efficient engraftment and regeneration of muscle *in vivo*, and able to add to the local muscle stem cell pool to allow for continued regeneration. As expected, SCs have been a highly investigated cell source for transplantation studies due to their requisite roles in the

regenerative process. SCs can be isolated from single muscle fibers and expanded *in vitro*; however, expansion causes them to commit to a myoblast ($Pax7^-$) fate. Early studies which attempted the implantation of expanded myoblast populations to damaged muscle observed high cell mortality followed by loss of regenerative capacity [78, 79]. In contrast, implanted freshly isolated ($Pax7^+$) SCs were able to fuse to existing muscle, home to the SC niche [78, 80, 81], rescue muscle function, and provide continued capacity for repair, emphasizing the importance of maintained “stemness” for the process of muscle repair and regeneration. In the case of larger muscle ablation, SC transplantation will need to be able to fully recover muscle mass, suggesting the need for an engineered scaffold to provide structural support for volumetric tissue reconstruction.

Besides the SC, other cell types have been identified for potential use in muscle repair. Ideally, these cells should be: 1) easy to isolate, 2) readily expandable *in vitro*, 3) engraft and improve muscle function in vivo, and 4) able to integrate within the local muscle stem cell pool. Human myoendothelial cells (co-expressing myogenic and endothelial cell markers) [82] and vessel-associated pericytes [83] are two expandable cell types able to regenerate muscle and fill the SC compartment upon transplantation into mice, but are still hard to isolate, similar to SC. Blood-derived $CD133^+$ cells are easily accessible and upon systemic delivery can contribute to muscle regeneration and fill stem cell niche [84], yet, may be difficult to expand *in vitro* [85] and harder to engraft than their muscle-derived counterparts [84]. Human $Pax7^+$ myogenic cells derived from adult bone marrow stromal cells through Notch1 intracellular domain gene transfer [86] and, more recently, from induced pluripotent stem cells (iPSCs) by conditional lentiviral expression of Pax7 [87], have been shown to engraft, fill the SC niche upon

implantation, and aid in subsequent rounds of regeneration in diseased mice. However, these results are achieved only by viral methods and in immunocompromised setting, and derived myogenic cells are not yet tested for their ability to rebuild large volumes of muscle tissue or recapitulate human muscle function *in vitro*. Nevertheless, the ability to derive large numbers of myogenic cells starting from highly proliferative iPSCs opens doors for the application of powerful gene-editing techniques (e.g. TALEN and Zn finger nucleases [88]) to correct congenital muscle disorders by use of autologous cell therapy. Furthermore, use of iPSC technology or genetic engineering to create immortalized myoblast lines from patient biopsies [89] is expected to foster development of more predictive human muscle disease assays for screening of candidate drug, gene, and cell therapies.

Table 2.1 Cellular candidates for myogenic repair

Cell type	Positives	Negatives
Muscle SCs	-Can fill SC niche upon transplantation [78, 80, 81]	-Difficult to retain regenerative capacity following in vitro culture [78, 79]
MDSCs	-Can be expanded in vitro without loss of myogenic potential [90-92]	-Ability to aid in functional recovery in diseased states remains a question [93]
Mesoangioblasts	-Easy to access from blood and can be delivered systemically [94-96]	-Results are not repeatable between groups [97]
CD133$^+$ cells	-Allows for systemic delivery and can fill SC niche upon transplantation [84, 98]	-Difficult to expand in vitro [85, 98]
BMSCs/ASCs	-Readily available and easy to isolate [86, 99-101]	-Can lose myogenic lineage upon implantation in diseased states [102, 103] and lack ability to fill SC niche [104]
ESCs	-Cells have remarkable potential for regeneration and can be driven to SC fate [105-107]	-Ethical issues and the need for immunosuppression upon delivery [87]
iPSCs	-Cells can be driven to SC fate and allows for autologous cell therapy [87]	-Low differentiation efficiency and difficult to generate large cell numbers [87]

2.3.2. Engineering environments for therapeutic use

Advancement in biomaterial research has allowed bioengineers to control environments both *in vitro* and in scaffold technology to present optimal cues to control

cell fate and physiological events. Specifically, for use in cell culture, groups have created microenvironment characteristic of the SC niche in attempt to maintain regenerative capacity during expansion of isolated cells. Additionally, implantable co-delivery vehicles have been studied extensively and have shown promise in accelerating integration of myogenic cells into the host.

2.3.2.1. Engineering SC niche

As mentioned in section 2.3.1, the expansion of isolated SCs in normal tissue culture conditions results in the loss of the cell's regenerative capacity upon transplantation. It is suspected that this loss of "stemness" is due to the exposure of the cells to a micro-environment unnatural to the cell's normal niche. The niche, as described in section 2.1.1, is comprised of all local external cues, including cell-cell interactions, cell-ECM interactions, and soluble cues that regulate cellular fate [108]. One particularly intriguing aspect of the SC niche currently under investigation is mechanical stiffness. Recent work has identified the use of soft culture substrates (e.g. polyethylene glycol (PEG) hydrogels) with a stiffness mimicking that of natural skeletal muscle (~12 kPa) to show promise in the expansion of SCs [37]. When cultured on this hydrogels functionalized with laminin to encourage cell adhesion, SCs showed enhanced proliferation, self-renewal, and maintenance of Pax7 expression compared to rigid surfaces and those mimicking the stiffness of non-muscle tissues [37]. After a week of *in vitro* culture and expansion, the cells were able to fill the SC niche following intramuscular transplantation and contribute to continual rounds of regeneration. Additionally, collagen VI has recently been identified as a coating protein that provides niche-like local mechanical properties leading to enhanced proliferation and Pax7 expression of SCs [109]. A similar technique was utilized to differentiate both BMSCs

and ASCs into $MyoD^+$ and $myogenin^+$ myoblasts [110]. The artificial environment allowed differentiating stem cells to assemble focal adhesions efficiently, allowing better assembly of contractile proteins characteristic of myogenic cell types. Additionally, specific factors can aid in the development of an artificial niche setting, which will be discussed later (section 2.4.1.3).

2.3.2.2. In situ regeneration using engineered scaffolds

For therapeutic implantation use, especially in cases of VML, biological scaffolds have been utilized to deliver myogenic cells or support natural regeneration over a large area to rebuild lost tissue. Ideally, these engineered vehicles should stimulate myogenesis, angiogenesis, and neurogenesis in the damaged area while providing structural support [111, 112]. Implanted scaffolds should promote help regeneration by: 1) maintaining native tissue structure, 2) concentrating and retaining cells at the injury site, 3) protecting cells from the initial host immune response, 4) providing cues for cell adhesion, migration, and proliferation, 5) providing a tissue-characteristic microenvironment for delivered or infiltrating host cells, and 6) being biodegradable so the regenerated tissue is composed of native cellular and ECM material [111-113]. Groups have implemented a variety of techniques to support this *in situ* skeletal muscle regeneration using engineered materials in attempt to achieve functional muscle recovery.

Implantation of SCs, as mentioned in section 2.3.1, is an obvious candidate for muscle therapy. However, when these cells are transplanted alone they are unable to reconstitute large portions of muscle [111, 112]. Therefore, various bioresorbable synthetic polymer and naturally-derived scaffolds have been utilized to deliver SCs to damaged tissue, including micro-patterned poly(glycolic acid) [114], collagen hydrogels

[115], and hyaluronic acid hydrogels [80]. Of note, a unique approach has been reported recently which uses a hydrogel that can be injected and polymerized at the injury site to avoid invasive surgery. The study revealed that freshly isolated SCs implanted by this method not only resulted in functional recovery of the injured muscle, but also replenished the SC pool, with *in situ* injected cells comprising a fraction of the cells in the quiescent niche [80].

Although SCs display greater potential for myogenic repair following *in vivo* transplantation than cultured myoblasts, they are limited in number and may be an impractical cell source for use in human therapies [111]. Because of this, groups have utilized cultured SC-derived myoblasts, an expandable cell population, in conjunction with a scaffold to stimulate myogenesis for repair in a model of severe muscle damage. To aid in engraftment and cell viability, a porous alginate scaffold has been utilized to provide sustained and local release of the angiogenic growth factor VEGF and the myogenic growth factor IGF-1; factors that have been identified to aid in regeneration, vascularization, and reinnervation [116-118]. Delivery of the two growth factors dramatically enhanced participation of myoblasts in muscle regeneration. The scaffold with embedded cells and growth factors reduced muscle inflammation and fibrosis, improved formation of vasculature, and increased contractile function compared to implantation of the scaffold with only growth factors and the scaffold alone [111]. Furthermore, implantation of the functionalized alginate matrix alone, without a cellular component, was found to support tissue formation in the defect site by stimulating migration of the host cells [116].

Naturally-derived scaffolds such as decellularized ECM have shown promise in repairing various tissue types [119-121]. Natural scaffolds are typically degraded and

replaced with host site-specific cell types and ECM [120, 122]. Regeneration of host tissue may occur through recruitment of stem and progenitor cells [123]. Groups have attempted skeletal muscle repair using two types of natural scaffolds: (1) small intestinal submucosa (SIS) [121, 124, 125] and (2) decellularized skeletal muscle ECM (M-ECM), containing muscle-specific proteins and ECM components [125]. Both matrices were able to induce a constructive remodeling response, marked by scaffold degradation, vasculature formation, and myogenesis within the implant region, and showed no significant difference [125, 126]. Although promising, results suggest a greater pro-fibrotic response than myogenic response. When applied in a complex injury model, the natural scaffold proved unable to restore functional muscle and resulted in dense areas of collagenous tissue [126]. Biological scaffolds have been shown to increase regeneration through activation of the degeneration process. However, in cases of severe muscle damage, this action may lead to an increased wound healing response as opposed to activation of myogenesis, and ultimately result in unintended fibrosis.

2.3.3. Tissue-engineered muscle

For over two decades, bioengineering have focused their efforts on the development of biomimetic 3-dimensional (3D) cultures of skeletal muscle cells for studies of muscle physiology and disease as well as the potential for an onsite therapeutic. Compared to use of undifferentiated myogenic cells (alone or with scaffolds), implantation of biomimetic tissue-engineered muscle may offer several unique advantages including the ability to: 1) precisely design patient-specific muscle architecture, 2) significantly reduce mechanical overload at the injury site by using already functional tissue, 3) attain specific mechanical or metabolic properties by *in vitro* preconditioning, and 4) generate native-like SC niche within engineered muscle for

better protection from harsh injury environment [7]. The functionality, complexity, and physiological accuracy of these *in vitro* models of native muscle have progressed with development of advanced biomaterials as cell-carrying scaffolds, 3D culturing techniques, and bioreactors for application of biophysical and biochemical stimulation. Recent progress in human pluripotent stem cell technologies and in vitro maintenance of muscle stem cells has presented the field with new opportunities to develop contractile human muscle tissues for use in disease modeling and drug discovery studies. Engineered muscle constructs have also been considered for use in regenerative therapy, prompting the development of methods to promote implant engraftment and vascular and neuronal integration into the host muscle. In the next section, we will discuss in detail, methods allowing for the creation of these in vitro 3D skeletal muscle models.

2.4 Engineering skeletal muscle

Over the last 25 years, researchers in the field have developed a variety of methods for engineering of functional three-dimensional (3D) skeletal muscle tissues. This section will review procedures used by multiple groups in the field of skeletal muscle tissue engineering that involve generation of a myogenic cell pool, fabrication of 3D tissue constructs, structural and functional characterization *in vitro*, and implantation of tissue grafts *in vivo*.

2.4.1 Preparation of myogenic cell source

In vitro generation of tissues for use as therapeutic implants or screening models requires a large numbers of cells. Considering the myonuclei within myofibers are post-mitotic, the only suitable source of expandable primary myogenic cells is the satellite cell (SC) pool, a putative muscle stem cell source capable of myogenesis [2]. Unfortunately,

the percentage of SCs in adult muscle is relatively low, amounting to roughly 4% of the total muscle nuclei [127]. Therefore, the common paradigm in muscle tissue engineering is to isolate the resident muscle stem cells, stimulate their continuous proliferation while maintaining their purity and differentiation potential, and utilize them in engineered tissue formation.

2.4.1.1 Satellite cell isolation

Isolation of SCs from skeletal muscle has been achieved via two main routes, cellular outgrowth and whole tissue digestion. The outgrowth method involves gentle separation of myofibers from the extracellular matrix, physical trituration to separate individual muscle fibers, and subsequent seeding of the fibers onto protein-coated dishes. This method relies on maintaining SCs within their niche on the myofiber periphery and their activation following plating. SCs will initiate the process of myogenesis and ‘outgrow’ from the myofiber onto the dish. Depending on the micro-environment, the cells will continue to proliferate and commit down the myogenic pathway, yielding a population of myoblasts capable of generating myofibers [128]. Alternatively, whole muscle tissue can be extensively minced and fully digested to release the SCs from their home on the myofiber [129]. The digested solution can be strained to filter out the mixture of fragmented myofibers, resulting in a single cell suspension that can be plated and expanded.

A number of methods may be used to purify the myogenic, and specifically SC, population following extraction. Pre-plating is a simple strategy used to remove the population of fast-adhering cells, primarily fibroblasts, from the culture. Myogenic cells are re-suspended in a growth media following digestion and plated on non-coated tissue culture plastic; a surface in which fibroblasts, but not SCs, will attach [130]. After roughly

2 hours, the supernatant, consisting of a purified cell mixture, can be transferred to a different flask to encourage myogenic cell attachment [131, 132]. Myogenic cells with a higher SC fraction can be obtained using fluorescence-activated cell sorting (FACS) with antibodies against the extracellular domains of SC-specific membrane proteins [133]. For example`, the population of CD45-/CD31-/CD11b-/Sca1-/CD34+/integrin-α7+ cells from mouse muscle purified through two rounds of FACS was shown to contain 100% pure Pax7+ SCs that were capable of self-renewal and expansion following transplantation [81].

2.4.1.2 Myoblast cell culture

Traditional passaging of isolated SCs results in their rapid differentiation towards a myoblast phenotype [4, 81]. Myoblasts, typically expressing transcription factor MyoD, are in a proliferating state and, under particular environmental stimuli, can be induced to fuse and form multi-nucleated myotubes [2]. For tissue engineering purposes, these myogenic cells are maintained in a proliferative state *in vitro* in order to expand cell numbers prior to differentiation, at which point they become post-mitotic. Critical for the sustained growth of myoblasts are both the growth surfaces and media constituents used during culture.

Collagen I coated plates were among the first 2D culture substrates identified to be supportive of both myogenic cell growth [134] and robust differentiation into cross-striated, contractile myotubes [135]. Recent efforts have identified Matrigel as a superior candidate for myogenic attachment and expansion [131, 136]. Matrigel is a commercially-available protein cocktail primarily consisting of laminin and collagen IV; the two main constituents of muscle basal lamina matrix [137]. Compared to collagen I, muscle-derived cells cultured on Matrigel-coated flasks experienced enhanced

proliferation, expression of myogenic markers, and fusion capacity [136]. Laminin, alone, promotes myoblast growth as well, and stimulates cell locomotion [138]. To be discussed later, these results are likely attributable to outside-in integrin signaling due to binding between myoblasts and muscle-specific proteins.

In addition to protein-coated culture substrates, two media formulations are traditionally used for growth and differentiation of skeletal myoblasts. Generally, growth media contains high serum levels, typically 10-20% fetal bovine or calf serum, to stimulate cell proliferation by high doses of growth factors [130]. Identified as an inhibitor of myogenic differentiation, basic fibroblast growth factor (bFGF) is commonly used as a supplement to further encourage proliferation and prevent fusion events [134]. Likewise, epidermal growth factor (EGF) [139] and isoforms of platelet-derived growth factor [140] can also be supplemented to culture media to enhance myoblast growth. Sub-confluent cell culture (60-70% before cell passage) is another requisite condition to support cell proliferation and prevent spontaneous cell fusion events during expansion [141, 142]. Differentiation media is used to drive fusion of myoblasts to myotubes, which can be robustly achieved through use of low serum (e.g. 2% horse serum [134, 143]) or serum-free [144-146] media. In general, in high serum growth medium, myoblasts will express the inhibitor of DNA-binding/differentiation protein (Id), which prevents MyoD activation of downstream genes to trigger further myogenic differentiation [147]. Switching to low serum differentiation medium, significantly decreases Id expression and drives myoblast fusion into myotubes [148]. Additionally, specific growth factors, e.g. insulin-like growth factor 1 (IGF-1) or transforming growth factor-beta 1 (TGFβ-1) [130, 149], can be used to accelerate myotube formation.

2.4.1.3 Maintaining regenerative capacity in vitro

Maintenance of the SC niche within native muscle involves both physical and biochemical interactions with the abutting myofiber membrane and the basal lamina that collectively support the capacity of SCs to self-renew and repair damaged muscle [4]. As previously mentioned, it is imperative to mimic such an environment in vitro in order to retain the abilities for SCs to self-renew and contribute regeneration. Besides engineering physical stimuli, discussed in section 2.3.2.1, supplementation of biochemical factors can also simulate SC niche-like environment. Recently, SCs from aged donors have been shown to upregulate p38α/β mitogen-activated protein kinase activity, typically induced by stress-related pathways. Supplementation of an inhibitor of p38α/β, SB202190, in conjunction with the expansion on a laminin-coated PEG hydrogels, resulted in enhanced SC proliferation and Pax7 expression *in vitro* and improved regeneration of injured muscle *in vivo* [150]. Additionally, high-throughput screening in zebrafish was recently used to identify forskolin, an adenylyl cyclase activator, and BIO, a GSK3β inhibitor, as small molecule enhancers of myogenesis. Forskolin was further found to promote expansion of mouse SCs *in vitro*, while the combination of the two chemicals augmented muscle differentiation of human induced pluripotent stem cells (iPSCs) [151]. Remarkably, Fu et al. [152] have recently identified four cytokines present in pro-myogenic, T cell-conditioned media (IL-1α, IL-13, TNF-α, IFN-γ) that when supplemented during expansion of mouse SCs supported their functional phenotype (>80% $Pax7^+$ cells) for up to 22 passages. Following implantation, the expanded SCs displayed similar engraftment potential as freshly isolated cells and successfully integrated into the endogenous SC pool to aid muscle repair following secondary injury [152]. To our knowledge, this is the largest *in vitro* amplification of

mouse SCs (1x10^{18} fold) with maintained “stemness”. It remains to be studied if a similar cytokine cocktail can be identified for use with humans SCs.

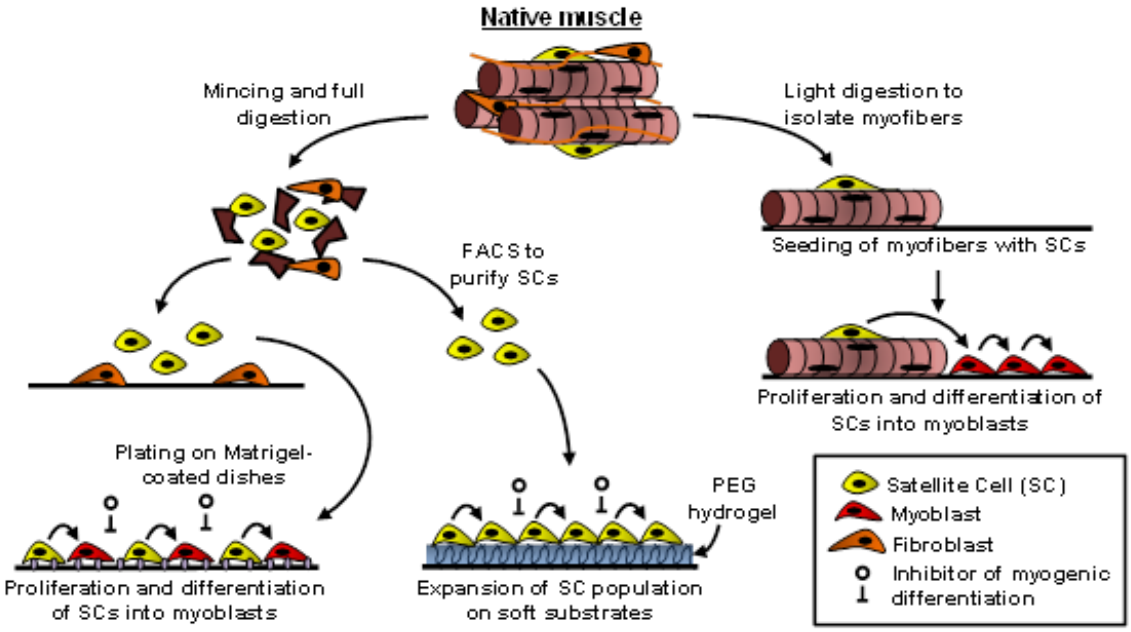

Figure 2.3 Methods to isolate and expand myogenic cells. Starting from whole native muscle, the tissue can be lightly enzymatically digested (right) to isolate and plate intact myofibers from which satellite cells (SCs) will outgrow, proliferate, and differentiate into myoblasts. Alternatively (left), native muscle can be fully digested to yield a suspension of mononuclear cells. These cells can be FACS sorted for extracellular markers or preplated to purify the SC population. The purified SCs can be either plated on Matrigel-coated dishes or on a soft, laminin-coated hydrogel substrate. Supplementation of culture media with differentiation inhibitors prevents cell fusion and allows SC expansion with preserved regenerative capacity.

2.4.2 Engineering functional muscle constructs

Formation of *in vitro* skeletal muscle tissues requires the exposure of myogenic cells to a 3D environment conducive to their growth, differentiation, and function [5]. Concurrent with advances in the field of tissue engineering, scaffolds and techniques for generating muscle constructs have evolved over the years as groups have aimed to optimize cell maturation, tissue structure, contractile function, *in vivo* survival, and regenerative ability [5]. In this section we will discuss various methods of generating and

culturing 3D constructs to optimize their structural organization and functional performance.

2.4.2.1 Generating 3D muscle

Engineering a biomimetic skeletal muscle tissue *in vitro* generally refers to the recreation of highly aligned and contractile myofibers within a 3D environment. Traditionally, there have been two approaches to develop such constructs. The first relies on the 'self-assembly' of differentiated myogenic cells into anchored cylindrical tissue bundles or free-floating planar tissue sheets as the cell monolayer is detached from a 2D surface. The second requires the initial or continuous presence of a supporting 3D matrix, where undifferentiated myogenic cells are either seeded into a polymer scaffold or encapsulated within a hydrogel and later induced to fuse and differentiate into myofibers. Both methodologies are still in use.

Self-assembly of *in vitro* muscle was first introduced by Strohman and colleagues in 1990 [153]. This method typically requires preparation of a protein-coated polydimethylsiloxane (PDMS) surface within a cell culture dish [14, 18, 21, 22]. The PDMS allows for the pinning of 'anchors' (e.g. silk sutures [18, 21, 22]), which act to secure the ends of the construct and provide passive tension to induce cellular alignment. To create more biomimetic systems, spinal cord explants [19], tendon structures [20], and engineered bone anchors [15] have also been used in attempt to establish neuromuscular or myotendinous junctions. Once the dish is prepared, a mixture of myogenic precursors (usually myoblast) and fibroblasts are seeded in a high serum growth medium to stimulate cell proliferation. The cells are grown into a confluent layer (4-7 days) and the media is switched to a low-serum differentiation medium to initiate myoblast fusion. After a few days, the dish is comprised of a population of

contracting, multi-nucleated myotubes and fibroblasts that will compact the cell layer inward resulting in gradual detachment from the dish. Once completely separated from the surface, the cellular composite will assemble around the anchors in the dish to create a cylindrical 3D tissue structure. This procedure can be further shortened by coating a hydrogel layer (e.g. fibrin) atop the PDMS surface to facilitate cell detachment [18]. Alternatively, myogenic cell monolayers can be detached via the use of thermo-responsive polymer coatings [154], however, unlike the anchored cylindrical tissues, the resultant free-floating cell sheets are not amenable to physiological testing.

Encapsulating cells in 3D scaffolds is the most commonly utilized method for skeletal muscle tissue engineering. Here, the primary (freshly isolated [8-10, 131, 132] or expanded [12, 13, 155]) or immortalized myogenic cells [11, 156, 157] are embedded into 3D synthetic polymer scaffolds [157] or natural hydrogels (fibrin, collagen I) [7-13]. For hydrogels, the cell/gel mixture is cast into a silicone tubing or PDMS mold coated in a pluronic solution to prevent cell adhesion. Cylindrical molds are typically used to generate a simple, cable-like tissue geometry, with porous felts at the ends of the mold that serve to anchor the hydrogel and provide passive tension for guiding unidirectional cell alignment [12]. For more complex planar tissue structures, mesoscopic hydrogel molding methods, in which soft lithography techniques are applied to precisely manufacture sub-millimeter PDMS posts [158], can be used to vary the local alignment of cells across a large tissue area [7, 8]. Once the cell/gel mixture is molded, the hydrogel is polymerized and the construct is placed in growth medium for a few days to increase cell number and density. During this period, fibroblasts present in the primary cell population will typically migrate to the periphery of the construct. Cell-mediated gel compaction will result in detachment of the construct from the mold and further

constriction along the free tissue boundaries [131]. Switching to differentiation medium will induce rapid fusion of myoblasts into myofibers followed by progressive structural and functional maturation. In general, under optimized conditions, the 3D encapsulation of myogenic cells in hydrogels has yielded engineered muscle constructs with higher total and specific force generation [5, 18, 131, 132] and more pronounced sarcomeric structures [131, 132] compared to use of scaffold-less approaches based on the 2D cell self-assembly. This might be attributed to enhanced myogenic fusion and larger myofiber size resulting from higher density of cell-cell contacts in 3D compared to 2D culture environment.

Due to a number of advantages, naturally derived hydrogels, fibrin and collagen I are the most commonly used biomaterials for the engineering of functional muscle [10]. In particular, they: 1) support uniform 3D cell seeding, 2) contain plentiful cell attachment sites that support cell-mediated gel compaction and spreading, leading to the formation of highly dense and aligned tissues, and 3) have appropriate mechanical compliance to withstand (but not impede) forceful muscle contractions [7]. Collagen I gels are formed through thermally induced polymerization following pH neutralization (i.e. addition of NaOH), while fibrin gels are formed through the cross-linking of fibrinogen and thrombin, with both gel types typically being supplemented with Matrigel for muscle engineering applications. Recently, in a direct comparison, engineered skeletal muscle tissues exhibited higher contractile forces when made using fibrin vs. collagen I gel [10]. This was attributed to stronger binding of integrins expressed by mature myotubes (α7, αV) to fibrin [159, 160] than collagen I (e.g. a collagen I-specific integrin α2 is not expressed in muscle [159]) which likely resulted in better transmission of contractile force between myofibers and the surrounding ECM. Furthermore, increased concentrations of Matrigel

and its associated basal lamina proteins, additionally enhanced muscle contractile function. As previously described, this was likely due to the enhanced interactions between α7β1 integrin and laminin, also shown to regulate force transmission in native muscle [161].

2.4.2.2 Maturation of engineered muscle in vitro

Once the engineered muscle is formed, it is cultured in conditions that promote myofiber maturation and survival. Exogenous biophysical and biochemical stimulations are traditionally applied to mimic natural environmental cues and encourage further cellular growth and have been reviewed in detail elsewhere [162, 163]. Mechanical stimulation, in the form of progressive or cyclic stretch to mimic developmental growth [164] and exercise [165, 166] respectively, has been proven to enhance alignment [164, 166], fusion [164, 166], myofiber hypertrophy [13], and force generation [165, 166] in engineered constructs. Electrical stimulation used to mimic neuronal input to muscle has also been shown to promote cell alignment, enhance fusion, improve maturation, and even guide fast-to-slow fiber type switching in engineered muscle [115, 167, 168]. Systems designed for exogenous electrical stimulation typically apply graphite, stainless steel, or platinum electrodes parallel to the engineered muscle within the culture dish to induce a field stimulus [115, 167-169].

2.4.3 In vitro assessment of engineered muscle

In vitro analysis of engineered muscle constructs involves both structural and functional evaluation to assess maturation level of the construct and predict its ability to repair tissue damage following implantation. With more emphasis on the development of screening assays using engineered tissues, these quality control *in vitro* assays can be adapted for higher throughput testing of drug effects on myogenic maturation, viability,

and regeneration. In this section, we will review the most common *in vitro* methodologies to evaluate engineered muscle structure, function, and potential for regeneration.

2.4.3.1 Muscle structure and morphology

Assessment of muscle morphology, structure, and protein expression via qualitative and quantitative immunohistology and western blot analysis are routinely used to evaluate myogenic maturation of *in vitro* engineered muscle and its resemblance to native tissue. Gross structure of engineered muscle can be evaluated by assessment of myofiber alignment [7, 9], density [9], and presence of various muscle and non-muscle cell types [10, 19, 20, 131, 132, 156] in longitudinal and transverse histological cross-sections. The percent of cells that underwent fusion can be quantified by counting a fraction of construct nuclei expressing myogenin [14, 131]. Myofiber diameter is commonly measured to evaluate cellular hypertrophy through analysis of transverse cross-sectional stainings [14, 131, 132, 155, 170, 171]. The fraction of myofibers expressing sarcomeres, muscle contractile units typically labeled by sarcomeric α-actinin (SAA) and myosin heavy chain (MyHC) antibodies, has been quantified to gauge myogenic differentiation [10, 131, 132, 155]. Additionally, the density and morphology of acetylcholine receptors have been identified through staining with bungarotoxin [8, 172]. Ideally, groups should report a direct structural comparison of engineered muscle to native neonatal muscle fascicles revealing similar myofibril appearance (SAA^+ sarcomeric units), basal lamina composition and distribution (collagen IV and laminin along periphery of myofibers), peripheral epimysial-like connective tissue layer ($vimentin^+$ fibroblasts), and quiescent SC pool ($Pax7^+$ cells).

2.4.3.2 Contractile function

Recording contractile force generation is considered one of the most valuable methods to dissect functional maturity of engineered muscle and its therapeutic potential *in vivo*. As freshly fused myotubes transition to mature myofibers and hypertrophy, their force generating capacity is augmented via both the increase in number of contractile units in the cross-section and the transition of MyHC isoforms from embryonic to adult [173]. First reviewed as early as 1999 [174], contractile force measurement in engineered muscle typically involves use of a custom testing platform. Several groups have developed such systems utilizing similar equipment configurations [10, 21, 22, 171]. Typically, a tissue sample is placed in a temperature-controlled bath that houses a pair of electrodes connected to a stimulator. One end of the sample is secured to a fixed anchor while a floating anchor links the other end of the sample to a force transducer. Following a field shock delivered by electrodes (~3-5 V/mm for maximum force [10, 132]), the muscle will undergo isometric contraction, pulling on the floating anchor and generating a force that will be recorded by the transducer. Assessment of contractile force in engineered muscle can be adapted for use in drug screening applications. A high throughput system, described in detail by Vandenburgh and colleagues [170], utilized a 96-microwell plate and a 'myoforce analysis device,' or MAD, to test the effects of various soluble factors on engineered muscle function [175]. In our recent study, the contractile responses of human engineered muscle ("myobundle") to statins, chloroquine, and clenbuterol were comparable to those in clinical reports [155], thus suggesting the utility of this system as a preclinical drug testing platform.

2.4.3.3 Calcium handling

Intracellular calcium handling is another critical parameter describing the maturity and functionality of the engineered muscle. Fluorescence recording of calcium-sensitive dyes (e.g., Fura-2, Rhod-2, Rhod-ff) and, more recently, genetically encoded calcium indicators (e.g. GCaMP) has been the classical method for measuring intracellular calcium transients in muscle cells. The GCaMP molecule, first developed by Nakai et al. [176], consists of fused permutated green fluorescent protein (GFP), calcium binding molecule, calmodulin, and M13, a peptide sequence from myosin light chain kinase. Binding of the free calcium to calmodulin causes a conformational shift of the molecule enabling rapid de-protonation of the GFP and bright fluorescence. The main advantage of these genetic indicators is the ability to perform cell type-specific, non-invasive, long-term calcium imaging *in vitro* and *in vivo* [155, 177, 178]. Usually, the system for intracellular calcium recordings requires the use of a sensitive photomultiplier tube or fluorescent camera, an adequate light source and filter set, and highly efficient light-collection optics. Amplitude of calcium transient determined from single-wavelength non-ratiometric measurement is usually expressed as the ratio between change in signal amplitude and baseline fluorescence, referred to as dF/F [132, 155]. Recent studies in human engineered muscle have shown good correlation between dF/F calcium signals measured non-invasively by lentivirally expressed GCaMP6 [178] and corresponding amplitudes of contractile force for both twitch and tetanus contractions under a variety of pharmacological conditions [155].

2.4.4 Implantation of engineered muscle in vivo

Determining the potential of tissue engineering therapies for skeletal muscle injury and disease will require well-designed animal studies to examine the therapeutic

efficacy of engineered muscle grafts *in vivo*. Ideally, engineered muscle implants would rapidly integrate into the host neurovascular system, restore function of the damaged muscle, and be able to self-regenerate to ensure long-term survival, maturation, and be resistant to injury [5]. Implantation methods have evolved over recent years to effectively recreate clinically relevant skeletal muscle defects and enable real-time monitoring of implant viability and function.

Surgical implantation methods (Figure 2.4) are chosen based on critical endpoints of the particular study or to recreate a specific disease condition of relevance to pathology. Advanced surgical techniques have also been applied to improve implant survival and integration. Subcutaneous implantation is a simple surgical method that exposes grafts to vascular beds beneath the animal skin and is employed to evaluate the ability of engineered muscle to vascularize and survive [157, 179]. Intramuscular implantations create more realistic models of corrective surgery and aim to assess engineered muscle's ability to integrate with host musculature and contribute to its contractile function. In some of these procedures, tissue construct is placed either alongside the hindlimb muscle [157, 180] or within a small void left by excising portion of the muscle [14, 80] or abdominal wall [156]. More drastic surgical procedures are needed to model volumetric muscle loss (VML) where the damage of more than 20% of muscle volume hinders the natural repair process and leads to scar accumulation [17, 24, 181].

Dorsal skin-fold window chambers offer intriguing possibilities for engineered tissue implantation studies as it enables non-destructive, real-time monitoring of the implant survival and vascularization in live animals. Originally described for studies of tumor vascularization [182], the method involves removal of the front skin layer to

expose the rearward-facing subcutaneous tissue. Implants can be laid against this tissue, covered by a glass top, and secured within a chamber sutured to the skin to lock its position and prevent contamination. When combined with intravital microscopy, researchers can track real-time vascular growth and use fluorescent indicators of function to monitor implant viability. Moreover, the implant and underlying skin can be readily explanted for *ex vivo* functional and histological assessment.

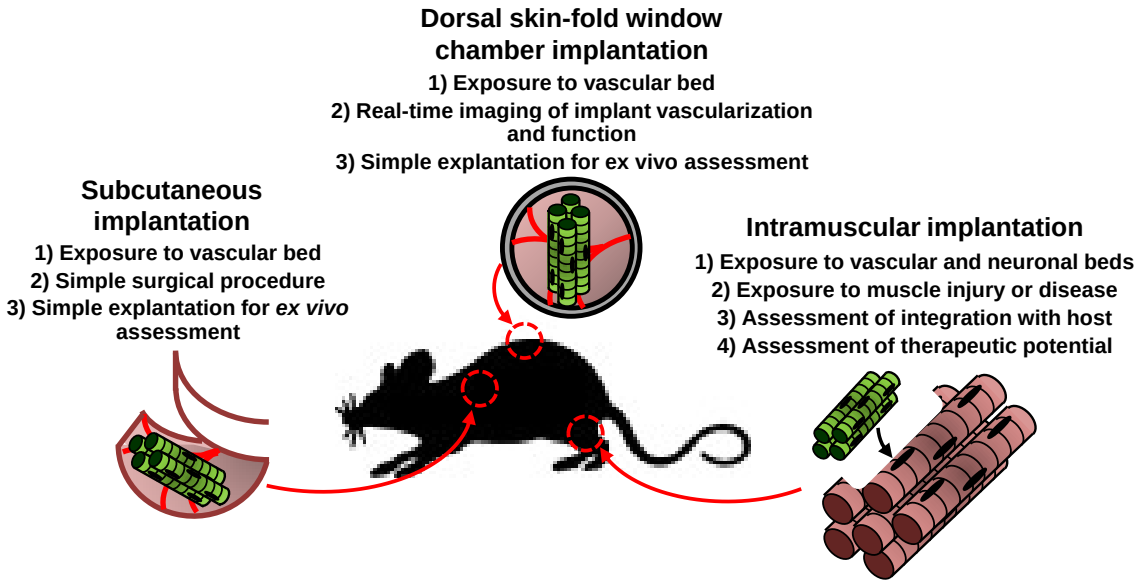

Figure 2.4 Methods for implantation of engineered muscle. Three animal implantation methods (subcutaneous, intramuscular, and dorsal skin-fold window chamber) along with their main advantages.

3. Identification of the roles of cellular source and culture condition in muscle myogenesis and function

3.1 Rationale and experimental plan

In recent years, our lab has optimized various parameters of skeletal muscle engineering (also referred to as *muscle bundles*), including tissue geometry [8], hydrogel composition [10], micro-fabrication process [7, 9], and biochemical supplementation [9], in attempt to improve contractile function, myofibril alignment, and expression of acetylcholine receptors. Building on this work, we set to further elucidate the effects of cellular composition and culture conditions on the function, structure, and cellular heterogeneity of engineered skeletal muscle. We utilized primary neonatal rat SCs as a highly proliferative, and easily accessible cell type [127] to generate cylindrical tissue constructs, named “engineered muscle bundles”. The effects of freshly-isolated (FI) cells, used in earlier work [7-10], and the adherent fraction (AF) of the FI cells that attaches to a Matrigel-coated flask were assessed. In addition, we evaluated the effects of static [7-10] and dynamic culture conditions on engineered muscle structure and functional performance. We hypothesized that the use of FI or AF cells will influence the maintenance of the SC pool and myogenic events. Previous studies in 2D cultures have reported that FI cells better retain self-regenerative capabilities compared to cultured and expanded cells [78, 80]. Therefore we expected to observe better retention of SCs with the undifferentiated FI cells and more robust fusion events when using AF cells. Furthermore, we expected that dynamic culture would promote survival of muscle cells within the interior of the relatively large muscle construct via improved diffusion of oxygen and nutrients [183]. These hypotheses were tested by systematically comparing use of FI and AF cells under static and dynamic culture (total of 4 groups) for the effects

on engineered muscle morphology, contractile function, maturity, cellular composition, and fusion events. Furthermore, skeletal muscle tissues engineered under optimal conditions were structurally and functionally compared to native neonatal muscle.

3.2 Methods

3.2.1 Myogenic cell preparation

Skeletal muscle tissue was isolated from the lower hind limbs of 2-3-d-old Sprague-Dawley rats and all connective tissue and fat were carefully removed. The tissue was digested in 1 mg/mL collagenase (Worthington) and 2% dispase ((v/v) BD) dissolved in Wyles solution (137 mM NaCl, 5 mM KCl, 21 mM HEPES, 0.7 mM Na2HPO4, 100 mM glucose, and 0.1 mg/mL BSA) for 1 h at 37°C on a rocker. The isolated cells were resuspended in growth medium (Dulbecco's modified Eagle's medium (DMEM), 10% (v/v) fetal bovine serum, 50 unit/mL penicillin G, 50 ug/mL streptomycin, 5 ug/mL gentamicin) and preplated for 2 h at 37°C to reduce fraction of fast-adhering fibroblasts. These freshly isolated cells (*Freshly-Isolated* (FI)) where either used directly to create engineered muscle, or were plated onto Matrigel-coated (1% (v/v), BD) flasks in growth media at ~50,000 cells/cm^2. Plated cells were washed in PBS after 24 hr and growth media was replenished. At 36 hr following initial plating, the adherent cells (*Adherent Fraction* (AF)) were detached by 2% dispase (v/v, BD) and used for generation of engineered muscle [132]. Non-adherent cells (*Non-adherent Fraction* (NAF)) that did not attach during the initial 24 hr of platting were also used to engineer muscle tissues.

3.2.2 Fabrication of engineered muscle

Engineered muscle bundles were formed within polydimethylsiloxane (PDMS) molds containing semi-cylindrical wells (1.25 cm long, 3 mm diameter) cast from 3D-

machined Teflon masters. PDMS molds were coated with 0.2% (w/v) pluronic (P3000MP, Invitrogen) to prevent hydrogel adhesion and two Velcro felts (2mm x 4mm) were pinned at ends of the wells to anchor the hydrogel. The cell/hydrogel mixture (10 million cells/mL, 2x growth medium, 4mg/mL bovine fibrinogen (F8630, Sigma), Matrigel (20% (v/v)), and thrombin (0.2 unit/mg fibrinogen, T4648, Sigma)) was injected into the PDMS wells and polymerized at 37°C for 45 min before addition of growth medium. The formed bundles were either cultured at static or dynamic (rocked at 0.4 Hz, -30º to +30º tilt) conditions for 2 weeks. After 4 days of culture, growth medium was replaced by differentiation medium (DMEM, 3% (v/v) horse serum, 50 unit/mL penicillin G, 50 ug/mL streptomycin, 5 ug/mL gentamicin) to promote differentiation of the myogenic cells into myofibers. Degradation of fibrin was inhibited by 1 mg/mL aminocaproic acid (A2504, Sigma) added to culture media. Cell-mediated hydrogel compaction generated passive tension between anchored hydrogel ends resulting in uniaxial cell alignment.

3.2.3 Immunostaining analysis

Engineered muscle bundles were fixed in 2% formaldehyde overnight on a rocker at 4ºC. Samples were treated using a blocking solution (0.5% Triton-X, 5% chicken serum in Ca^{+}/Mg^{+} PBS) overnight on a rocker at 4ºC. Primary antibody solutions (listed in Table 3.1) at 1:15 - 1:200 dilution were applied in blocking solution overnight on a rocker at 4ºC. Samples were then washed 3 times in 0.1% Triton-X and incubated in secondary antibody (1:200 dilution in blocking solution) with DAPI and/or Alexa Fluor® 488-conjugated phalloidin (Invitrogen) overnight on a rocker at 4ºC. Fluorescence images were acquired on an inverted confocal microscope (Zeiss LSM 510) at 20-40x magnification. For staining of transverse cross-sections, the samples were submerged in optimal cutting temperature (OCT) compound (Electron Microscopy Sciences), snap-

frozen in liquid nitrogen, sliced (10-50 µm thick) perpendicular to bundle's long axis, and mounted on glass slides, followed by blocking and application of antibodies. Images were acquired at different magnifications either parallel or perpendicular to the bundle's long axis. For quantitative analyses of nuclear stains, we utilized a custom ImageJ (Fiji) program that identifies areas stained for DAPI, transcription factor (Pax7, MyoD, myogenin), or proliferation marker (Ki67), and, based on the median nucleus size for a given magnification, designates and automatically counts identified nuclei. Nuclear count is then manually verified by user. Myofiber area density in the engineered muscle bundles was quantified from longitudinal confocal sections acquired at 10-40 µm bundle depth and 20x magnification by calculating the percentage of bundle area positively stained for F-actin [132]. These images were also used to manually measure myofiber diameter by LSM Image Browser (Zeiss). Specific primary and secondary antibodies are found in Table 3.1 and 3.2.

Table 3.1 Primary antibody list for chapter 3

Primary Epitope	Dilution	Supplier	Catalog no.
Pax7	1:15	Developmental Studies Hybridoma Bank	Pax7-s
MyoD	1:200	BD Pharmingen	554130
myogenin	1:200	Santa Cruz Biotechnology	sc-576
sarcomeric α-actinin	1:200	Sigma	a7811
vimentin	1:400	Sigma	v6630
Ki67	1:200	Abcam	ab15580
mCadherin	1:200	Abcam	ab65157
Laminin	1:300	Abcam	ab11575
Collagen IV	1:300	Abcam	ab6586

Table 3.2 Secondary antibody list for chapter 3

Secondary Epitope	Dilution	Supplier	Catalog no.
Alexa Fluor 488 Phalloidin	1:200	Life Technologies	A12379
Alexa Fluor 594 Chicken Anti-Mouse IgG	1:200	Life Technologies	A21201
Alexa Fluor 594 Chicken Anti-Rabbit IgG	1:200	Life Technologies	A21442
Alexa Fluor 647 Chicken Anti-Mouse IgG	1:200	Life Technologies	A21463
Alexa Fluor 488 Phalloidin	1:400	Life Technologies	A21200
Alexa Fluor 594 Chicken Anti-Mouse IgG	1:200	Life Technologies	A12379

3.2.4 Assessment of contractile function

Force generating capacity of engineered muscle was assessed at 2 weeks of culture using a custom-made setup described in detail elsewhere [10]. Specifically, engineered muscle bundles were loaded into a system containing a sensitive optical force transducer, a computer-controlled linear actuator (ThorLabs, Inc), platinum field electrodes, and a heated 37°C chamber. One end of the bundle was pinned to a stationary PDMS ledge in the chamber while the other was pinned onto a floating PDMS platform that was secured to the transducer. Samples were stimulated (10 ms, 3V/mm pulses) and isometric twitch contraction (response to a single pulse) and tetanic contraction (response to a 40 Hz, 1 sec duration pulse train) were recorded in bundles that were stretched to 110% of their culture length. Specific contractile force of a muscle bundle was determined by dividing its force of contraction with the cross-sectional muscle area measured at the center of the bundle.

3.2.5 Statistics

Results are presented as mean ± SEM. Statistically significant effects of culture type (static vs. dynamic) or cell source (AF vs. FI) were evaluated by two-way ANOVA with post hoc Tukey's tests to determine significant differences ($p < 0.05$) among individual groups using GraphPad Prism (GraphPad Software, Inc.). Levels of significance are noted in text, figures, or figure captions.

3.3 Results

3.3.1 Effects of culture and cell source on muscle area

After 2 weeks of culture, engineered muscle using both freshly-isolated (FI) and adherent fraction (AF) cells contained myofibers dispersed along the periphery of the bundle (Figure 3.1). Consistent with previous reports, the engineered tissue compacted during culture, reducing the total cross-sectional area up to 4 fold by 2 weeks [8, 10]. This bundle compaction was found to be dependent on both the cell source (FI vs. AF) ($p < 0.0001$) and culture method (static vs. dynamic) ($p < 0.0001$) (Figure 3.1B). Viable muscle area was measured as the area of F-actin positive staining within the cross-section of the muscle. Dynamic culture had a significant effect ($p < 0.0001$) on muscle area compared to static culture while cell source did not ($p = 0.087$) (n = 6-9 bundles) (Figure 3.1C). Muscle fraction (muscle area divided by total area) was also significantly affected by culture ($p < 0.0001$) as dynamic culture (FI: 0.44 ± 0.04, AF: 0.40 ± 0.05) resulted in bundles consisting of a greater percent of muscle fibers than static culture (FI: 0.066 ± 0.002, AF: 0.089 ± 0.01) (n = 6-9 bundles) (Figure 3.1D).

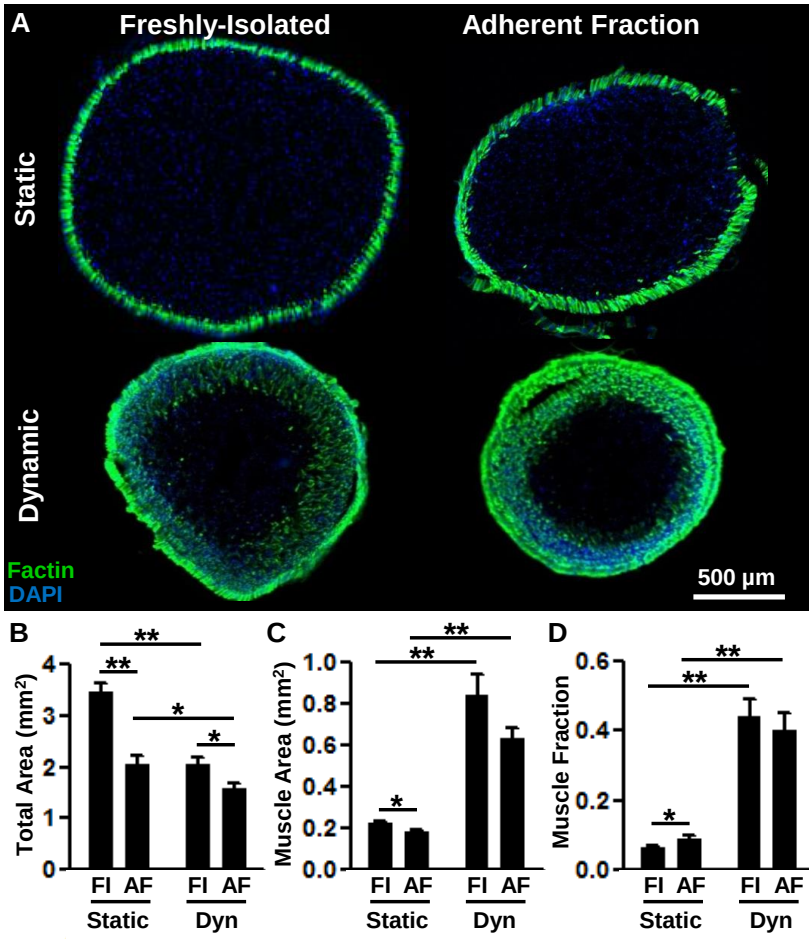

Figure 3.1 Cross-sectional analysis on engineered muscle. (A) Cryo-sectioned bundles made from freshly-isolated (FI) and adherent fraction (AF) cells cultured both in static and dynamic (Dyn) conditions stained for muscle content (Factin) and nuclei (DAPI). (B-D) Quantification of (B) total bundle area, (C) muscle area (f-actin^{+} area), and (D) muscle area fraction (muscle area per total area). $p^{*} < 0.05$ and $p^{**} < 0.001$ (n = 6-9 bundles per group).

3.3.2 Effects of culture and cell source on contractility

Force testing revealed that all groups were able to generate both twitch and tetanic (40 Hz) contractions (Figure 3.2A) up to 30 mN. Dynamic culture (FI: 14.52 ± 1.55 mN (twitch) and 19.75 ± 2.01 mN (tetanus); AF: 17.83 ± 1.00 mN (twitch) and 28.80 ± 0.93 mN (tetanus)) resulted in significantly greater twitch ($p < 0.0001$) and tetanus ($p < 0.0001$) force generation than static culture (FI: 2.04 ± 0.32 mN (twitch) and 2.95 ± 0.35 mN (tetanus); AF: 3.09 ± 0.26 mN (twitch) and 4.21 ± 0.42 mN (tetanus)) (n = 6-9

bundles) (Figure. 3.2B). Interestingly, cell source only affected absolute tetanic force generation (p = 0.0006) as the AF was significantly stronger than the FI group. Specific force calculations (force per muscle area) revealed that both dynamic culture (p < 0.0001) and cell source (p = 0.0004) had significant affects as dynamic culture of AF cells yielded the strongest muscle (43.39 ± 3.82 mN/mm^2) (n = 6-9 bundles) (Figure. 3.2B).

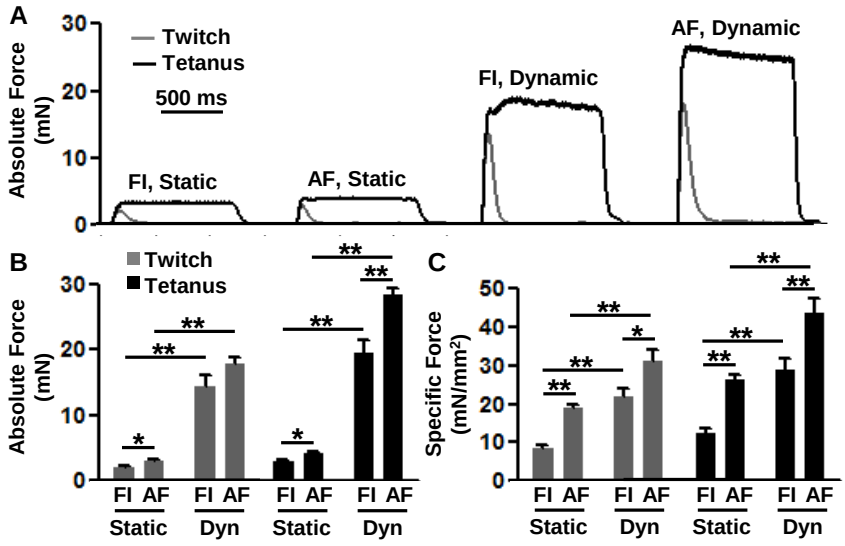

Figure 3.2 Contractile force generation of engineered muscle. (A) Active force traces of bundles made from freshly-isolated (FI) and adherent fraction (AF) cells cultured both in static and dynamic (Dyn) conditions induced by twitch (10 ms pulse) and tetanic (40Hz) electrical stimulation. (B-C) Quantification of (B) absolute and (C) specific force (force per muscle area). Error bars denote mean ± SEM. *P < 0.05 and **P <0.001 between groups designated by line. N = 6-9 bundles per group.

3.3.3 Effects of culture and cell source on hypertrophy and fusion

Myofiber hypertrophy (diameter), a marker of myogenic maturity, was quantitatively analyzed from confocal images within the muscle region of all groups (n = 4-6 bundles, 3-5 locations per bundle, 5-20 myofibers per location) (Figure 3.3A). Results revealed that both cell source (p = 0.0005) and culture (p < 0.0001) had significant effect on myofiber diameter as dynamic culture and AF cells yielded the

greatest hypertrophy (FI: static: 9.81 ± 0.36 µm, dynamic: 11.94 ± 0.49 µm; AF: static: 11.14 ± 0.59 µm, dynamic: 15.56 ± 0.65 µm) (Figure 3.3B).

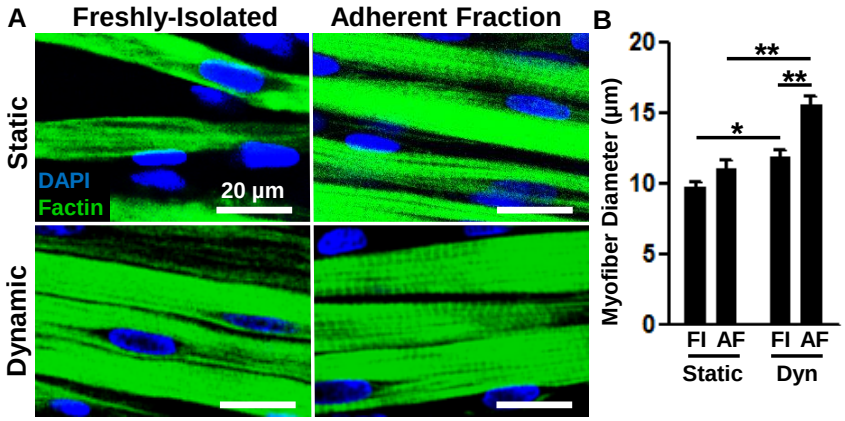

Figure 3.3 Quantification of myofiber hypertrophy. (A) Confocal images of representative myofibers in bundles made from freshly-isolated (FI) and adherent fraction (AF) cells cultured both in static and dynamic (Dyn) conditions. (B) Quantification of myofiber diameter from images. Error bars denote mean ± SEM. **P* <0.05, ***P* <0.001 between groups designated by line. N = 4-6 bundles per group, 3-5 locations per bundle, 5-20 myofibers per location.

To determine the effect of culture and cell source on fusion efficiency, engineered muscle at 2 weeks were fixed and stained for the transcription factor myogenin (MyoG), a marker of myonuclei and myogenic differentiation (Figure 3.4A). The greater amount of $MyoG^+$ cells indicates enhanced fusion events and may result in hypertrophy; as muscle growth is supported through addition of myonuclei [173]. Quantitative analysis of confocal images of the muscle area within engineered muscle revealed significantly greater $MyoG^+$ cell percentage ($MyoG^+$ cells/total nuclei) in AF vs FI ($p < 0.0001$) in both static and dynamic conditions (Figure 3.4B), as culture condition had no effect ($p = 0.58$) (n = 4-6 bundles, 3-5 locations per bundle). To determine myonuclei density, the amount of $MyoG^+$ cells per myofiber area (f-$actin^+$ area) was calculated (Figure 3.4C). Again, myonuclei density was significantly affected by cell source ($p < 0.0001$) and not culture condition ($p = 0.61$), as AF was greater than FI (n = 4-6 bundles, 3-5 locations per bundle).

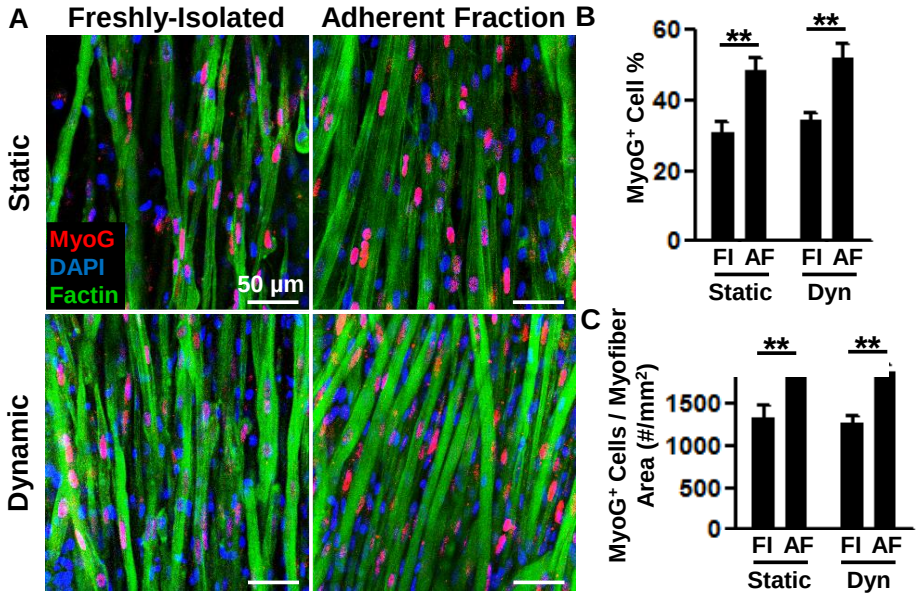

Figure 3.4 Fusion efficiency in engineered muscle. (A) Confocal images within the muscle region in bundles made from freshly-isolated (FI) and adherent fraction (AF) cells cultured both in static and dynamic (Dyn) conditions stained for myonuclei marker myogenic (MyoG). (B-C) Quantification of (B) MyoG$^+$ cell percentage and (C) density (cells per muscle area). Error bars denote mean ± SEM. ***P* <0.001. N = 4-6 bundles per group, 3-5 locations per bundle.

3.3.5 Retention of satellite cells

Satellite cells (SCs) are required for skeletal muscle regeneration [2] and growth [173] and may be an important feature for regenerative capacity in engineered muscle. Therefore, the ability of each group to maintain a SC pool was assessed by quantifying the percent and density of Pax7$^+$ cells, a common marker of satellite cells (n = 4-6 bundles, 3-5 locations per bundle) (Figure 3.5). Pax7$^+$ cells were found in all groups (Figure 3.5A) and the percentage of Pax7$^+$ cells (Pax7$^+$ cells/total nuclei) depended on both cell source (p = 0.045), culture (p = 0.0004), and their interaction (p = 0.017), with the greatest percentage found in dynamically cultured AF cells (14.37 ± 1.14 %) (Figure 3.5B). Calculation of satellite cell density (Pax7$^+$ cells per muscle area (f-actin$^+$ area)) revealed a significant impact of culture (p = 0.0018) and the interaction of cell source

and culture (p = 0.013) (Figure 3.5C). Under dynamic conditions, AF cells were able to maintain significantly greater SC percentage and density than FI cells.

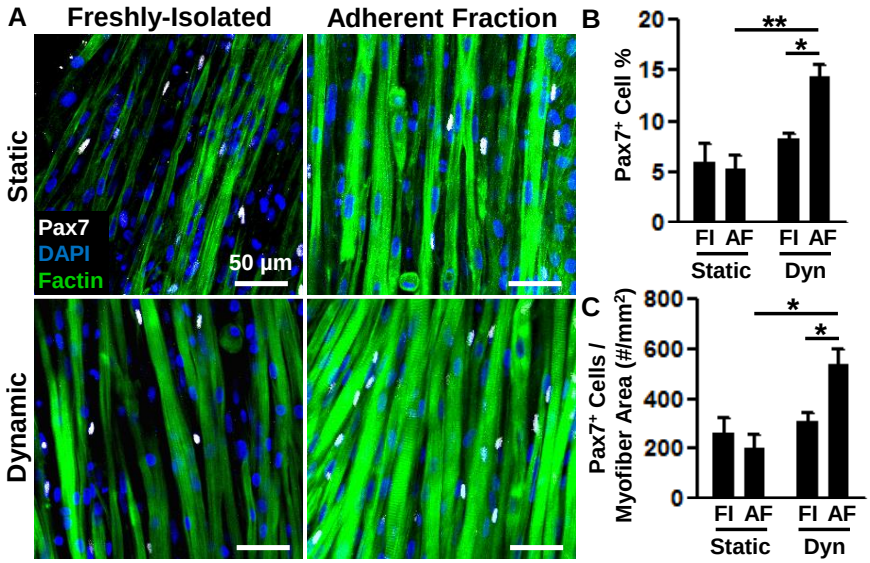

Figure 3.5 Maintenance of satellite cell pool. (A) Confocal images within the muscle region in bundles made from freshly-isolated (FI) and adherent fraction (AF) cells cultured both in static and dynamic (Dyn) conditions stained for satellite marker Pax7. (B-C) Quantification of (B) $Pax7^+$ cell percentage and (C) density (cells per muscle area). Error bars denote mean ± SEM. *P <0.05, **P <0.001 between groups designated by line. N = 4-6 bundles per group, 3-5 locations per bundle.

3.3.6 Cellular dynamics during fusion events

To better explore the cellular dynamics within the engineered muscle, myogenesis was assessed at early time-points (2, 3, and 4 days) in dynamically cultured bundles using FI and AF cells (n = 5 bundles, 4-8 locations per bundle to analyze). Engineered muscle was stained for key myogenic markers (Pax7, MyoD, and myogenin (MyoG)), and a cell proliferation marker (Ki67) (Figures 3.6 and 3.7).

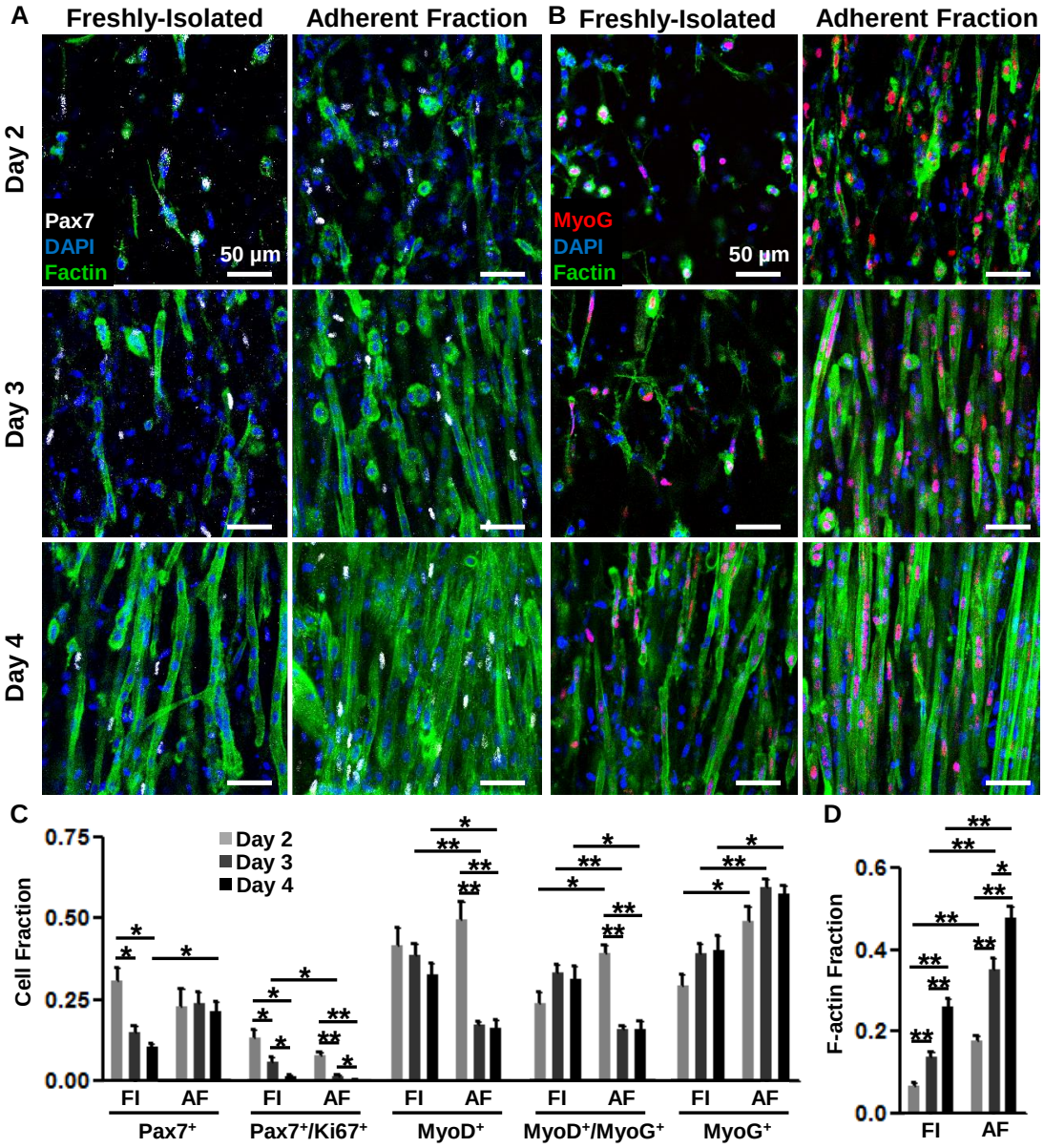

Figure 3.6 Cellular dynamics within engineered muscle during fusion. (A-B) Confocal images within the muscle region in bundles made from freshly-isolated (FI) and adherent fraction (AF) cells cultured dynamically stained for (A) satellite cell marker, Pax7, and (B) myonuclei marker, myogenin (MyoG), at day 2, 3, and 4. (C) Quantification of cell fraction within engineered muscle stained for key myogenic markers (Pax7, MyoD, and MyoG) and Ki67 (N = 5 bundles per group, 4-8 locations per bundle). (D) F-actin, or myofiber, density at day 2, 3, and 4 (N = 10 bundles per group, 4-8 locations per bundle). Error bars denote mean ± SEM. **P* <0.05, ***P* <0.001.

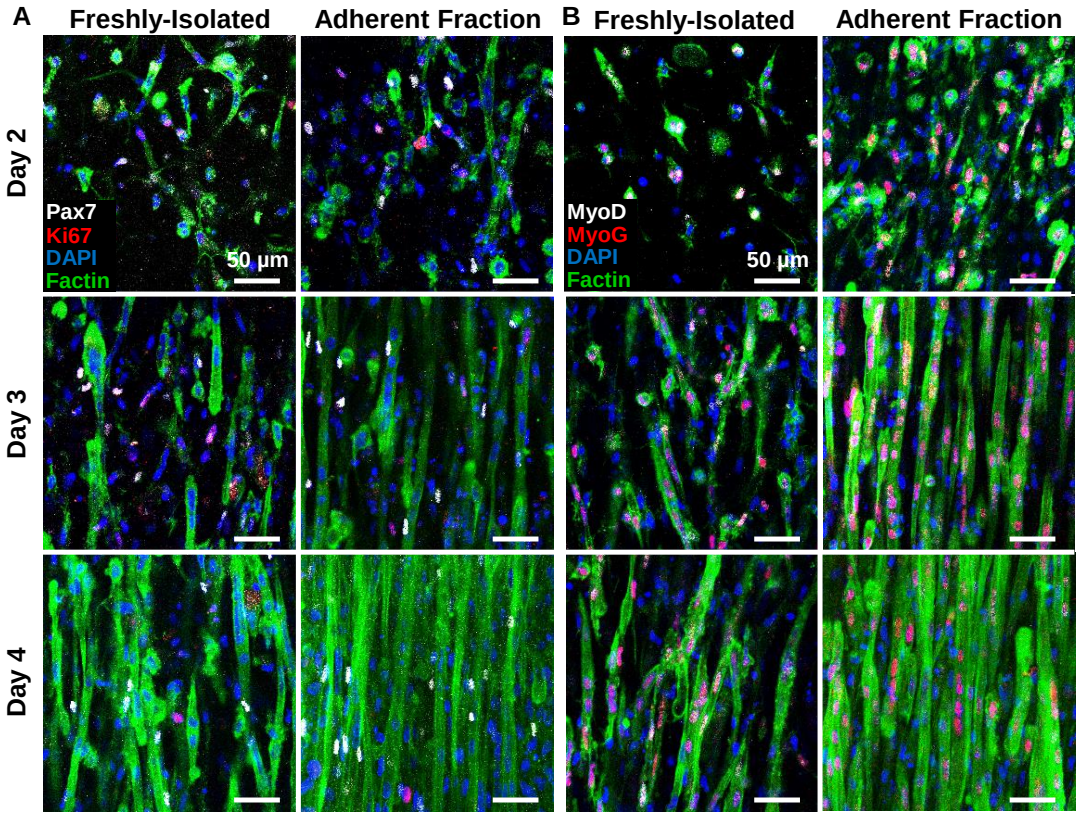

Figure 3.7 Co-expression of myogenic markers within engineered muscle during fusion. (A-B) Confocal images within the muscle region in bundles made from freshly-isolated (FI) and adherent fraction (AF) cells cultured dynamically stained for (A) satellite cell marker, Pax7, and, proliferation marker, Ki67, and (B) marker of myogenic differentiation, MyoD, and mature myonuclei marker, myogenin (MyoG).

Quantitative analysis of $Pax7^+$ cell fraction, a population consisting of quiescent or activated satellite cells, reveals that there was a greater percentage of positive cells at day 2 using FI (30.7 ± 4.3%) than AF cells (23.0 ± 5.6%). However, the pool within FI muscle significantly decreases by day 3 (15.1 ± 2.1%) and 4 (10.5 ± 1.1%) (Figure 3.6A&C). Interestingly, this decline of $Pax7^+$ cells did not occur in engineered muscle using AF cells as the pool stays consistent till day 4 (day 3: 24.1 ± 3.4%, day 4: 21.5 ± 2.7%) (Figure 3.6A&C) resulting in a significantly greater percentage compared to FI cells at day 4. Co-staining for Ki67 reveals a significant drop in proliferating cells $Pax7^+$

cells in both groups suggesting that nearly all $Pax7^+$ cells are quiescent by day 4 (Figure 3.6C and 3.7A).

MyoD expression levels, a marker for activated satellite cells and more differentiated precursor cells [2], were high at day 2 for both groups (FI: 42.0 ± 5.3%, AF: 49.7 ± 5.6%) (Figure 3.6C and 3.7B). These values experienced a steady decline in the FI group over the next two days and a significantly drop within the AF group to values significantly lower than those of the FI group (Figure 3.6C and 3.7B). Co-expression of MyoD with myogenin, a mature marker of myogenic differentiation, marks precursors primed for fusion or newly fused myonuclei. In FI muscle, this population of cells was significantly less prevalent at day 2 (24.5 ± 3.4%) compared to AF muscle (40.1 ± 2.3%) and peaked at day 3 (33.9± 2.9%) (Figure 3.6C and 3.7B). Similar to MyoD expression dynamics in AF muscle, co-expressing cells peaked at day 2 and significantly dropped by day 3 and 4 (Figure 3.6C and 3.7B). Tracking myogenin expression, found in mature precursors and fully-differentiated myonuclei [2], revealed a significantly lower percentage at day 2 in FI (29.6 ± 3.9%) compared to AF (50.0 ± 4.3%) cells (Figure 3.6B&C). This population undergoes a steady increase in both cases, as AF bundles still contained a significantly higher pool at day 4 (FI: 40.8 ± 4.6%, AF: 58.7 ± 2.3%) (Figure 3.6B&C). The dynamics of cellular expression in both groups suggests differentiation of myogenic precursors as there is an observed transition from MyoD to myogenin expression. Differentiation appears to be more sudden for AF cells as MyoD expression experiences a more abrupt decline.

To further analyze the early dynamics of muscle formation, myofiber formation was tracked through calculations of f-$actin^+$ area within the muscle layer in the engineered muscle (Figure 3.6A-B&D and 3.7A&B) (n = 10 bundles, 4-8 locations per

bundle) at day 2, 3, and 4. In both cases, using FI and AF cells, we observed rapid increases in f-actin density with significant jumps every day up to day 4. Furthermore, accelerated formation was observed when using AF cells, as at day 2, 3, and 4, myofibers appeared at significantly greater density compared to FI cells (Figure 3.6A-B&D and 3.7A&B). In addition to a more rapid formation of myofibers, there also appeared to be more rapid maturation using AF cells, as by day 4, there was already sarcomere formation marked by striated sarcomeric α-actinin expression (Figure 3.8).

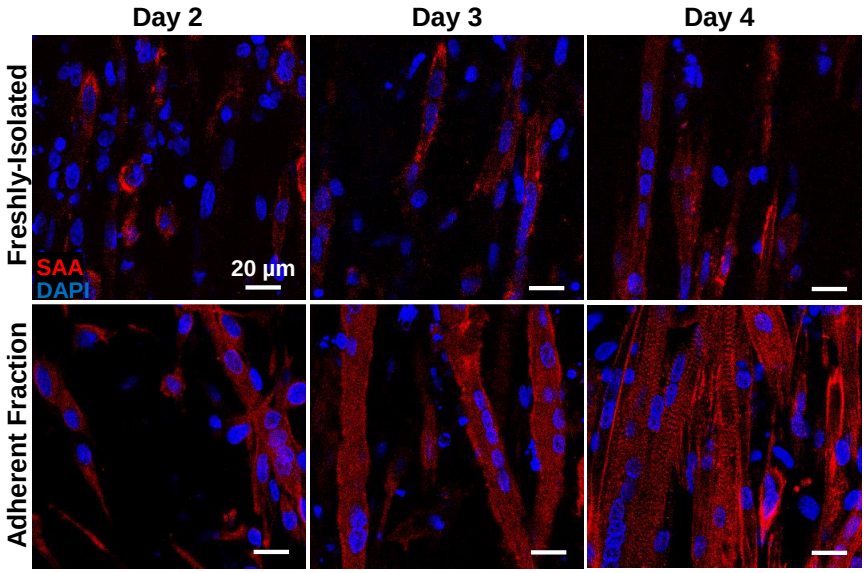

Figure 3.8 Early formation of sarcomeres within engineered muscle. Representative images of sarcomeric structruces (marked by sarcomeric α-actinin (SAA)) within myofibers in engineered muscle bundles made from freshly-isolated and adherent fraction cells cultured dynamically at day 2, 3, and 4 days.

Tracking bundle diameter from day 2 to 4 (n = 4 bundles per group), significant compaction was observed at these early time-points when using both FI and AF cells. Furthermore, significantly greater compaction was noticed at both day 2 and 4 when using AF compared to FI cells (Figure 3.9A&B). A significant factor in bundle compaction is the layer of fibroblasts located on the periphery of the bundle [184]. Confocal imaging

for the presence of fibroblasts at early time-points suggests more rapid formation of a high-density fibroblast layer when using AF cells (Figure 3.10).

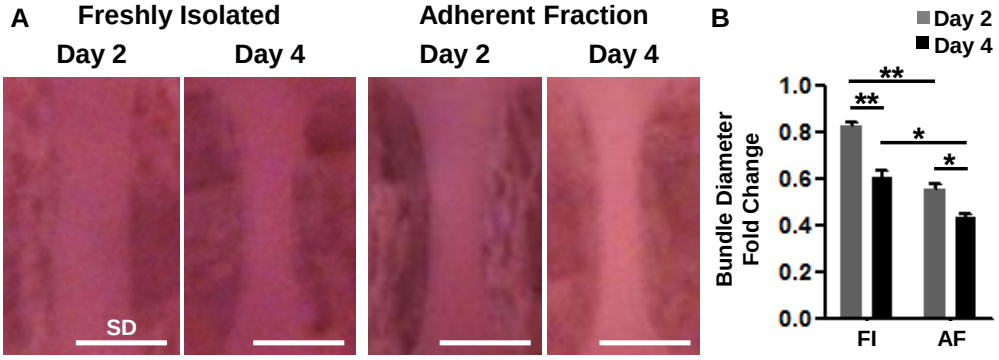

Figure 3.9 Early compaction of dynamically cultured bundles. A) Representative images of bundles made from freshly-isolated (FI) and adherent fraction (AF) cells cultured at dynamic conditions at day 2 and 4 (SD: starting diameter at day 0). B) Quantification of compaction expressed as fold change of bundle diameter. Error bars denote mean ± SEM. *P < 0.05 and **P <0.001 between groups designated by line. N = 4 bundles per group.

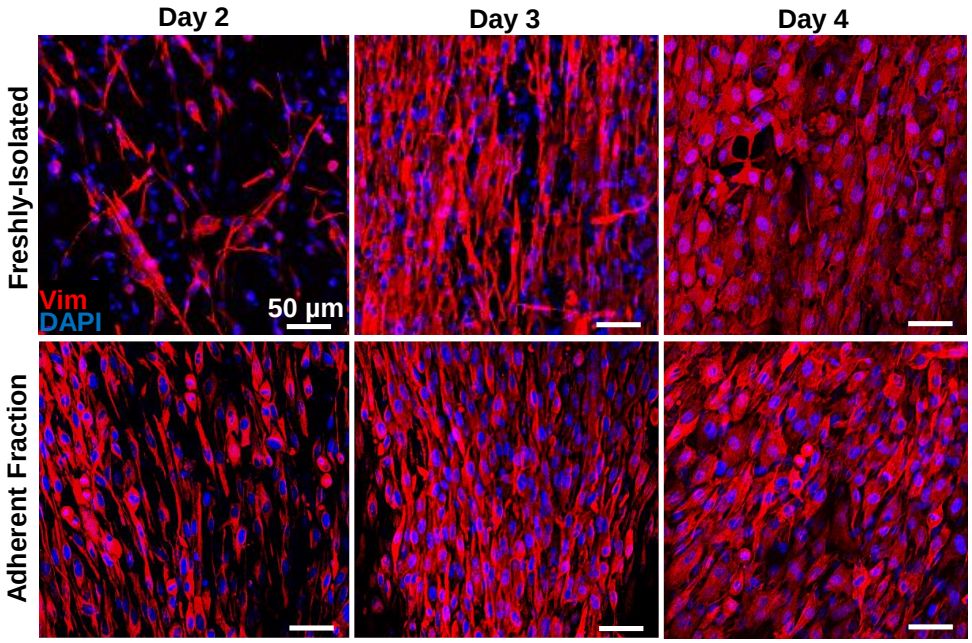

Figure 3.10 Exterior layer of fibroblasts in engineered muscle during fusion. Representative images of fibroblasts (marked by vimentin (Vim)) on the exterior of the engineered muscle bundles made from freshly-isolated and adherent fraction cells cultured dynamically at day 2, 3, and 4 days.

3.3.7 Structural characteristics of engineered muscle

Due to the greatest functionality and SC retention in AF bundles cultured dynamically, that group was considered to be the most optimal method and chosen for greater characterization. The initial cell input, characterized through immunofluorescence, consisted primarily of $Pax7^+/MyoD^+$ activated SCs and a small fraction of $myogenin^+$ precursors, but no evidence of endothelial or smooth muscle cells (Figure 3.11).

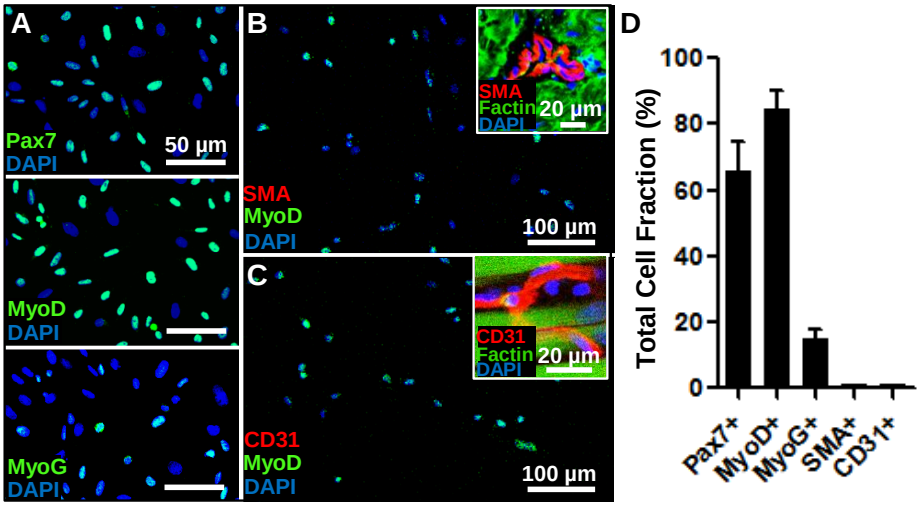

Figure 3.11 Input cell population for engineering of skeletal muscle bundles. (A) Representative immunostaining of $Pax7^+$, $MyoD^+$, and myogenin $(MyoG)^+$ cells. (B-C) No α-smooth muscle actin $(SMA)^+$ smooth muscle cells (A) or $CD31^+$ endothelial cells (B) were present in the cell isolates. Insets, positive controls for SMA and CD31 antibodies showing a blood vessel in adult rat cardiac muscle (B) and capillaries in native neonatal rat skeletal muscle (C). (D) Quantified fractions of myogenic ($Pax7^+$, $MyoD^+$, $MyoG^+$) and vasculogenic (SMA^+, $CD31^+$) cells used for engineering of skeletal muscle (N = 3 cell isolations). Stainings suggest that cell population consists primarily of activated satellite cells (SCs), a proliferative population of $Pax7^+/MyoD^+$ cells that can either commit to a myoblast fate ($Pax7^-/MyoD^+$) or revert to the quiescent state ($Pax7^+/MyoD^-$) characteristic of homeostatic native muscle. Error bars denote mean ± SEM.

After 2 weeks of 3D culture, engineered bundles consisted of a peripheral layer of $vimentin^+$ fibroblasts that resembled the epimysial connective tissue layer encasing the myofibers of neonatal hindlimb muscle (Figure 3.12). The interior of both engineered and native neonatal muscle contained densely packed, highly aligned, multinucleated,

and cross-striated myofibers surrounded by a basal lamina-like matrix consisting of laminin and collagen IV (Figure 3.12). Within the basal lamina, $Pax7^+$ SCs were found residing within a native-like niche, closely abutting myofiber sarcolemma (Figure 3.12). Overall, the 3D organization of the engineered muscle bundle highly resembled that of a native muscle fascicle, while lacking higher-order structures including multi-fascicle organization, tendons, and neurovascular bed.

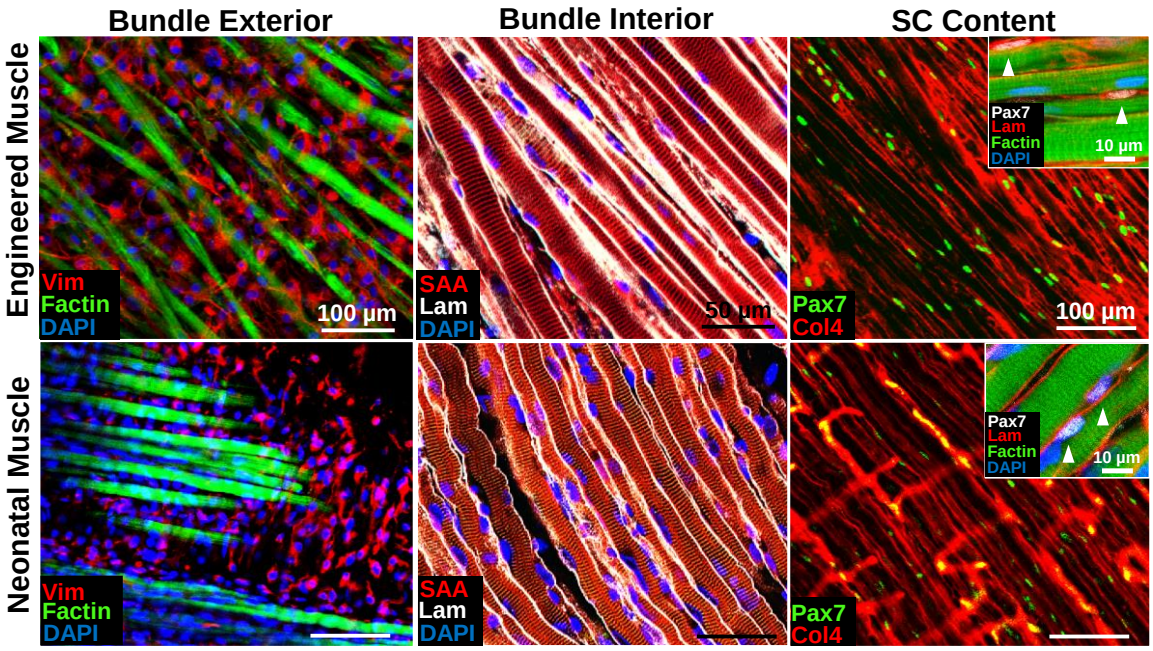

Figure 3.12 Structural characterization of engineered muscle. Confocal images comparing the fibroblast periphery, myofibril structures, and satellite cell pool in engineered muscle and neonatal rat soleus muscle. Insert: image of SC in apparent niche.

3.3.8 Maturation of engineered muscle

In natural muscle, post-natal growth and hypertrophy is supported by creation of new myonuclei via secondary fusion of SCs with myofibers [173]. We therefore quantified the temporal changes in myofiber size and SC density at 1, 2, and 4 weeks of culture and found significant increase in myofiber diameter (1 wk: 8.73 ± 0.33 µm, 2 wk: 14.9 ± 0.87 µm, 4 wk: 22.2 ± 1.33 µm) accompanied by decreases in SC number per

100 µm of myofiber length (1 wk: 1.22 ± 0.12, 2 wk: 0.75 ± 0.05, 4 wk: 0.52 ± 0.02) (Figure 3.13A,B&C) indicative of a functioning SC pool and continuous myogenesis. After 4 weeks of culture, these parameters achieved values intermediate between those of neonatal and adult rat muscle tissues (Figure 3.13C).

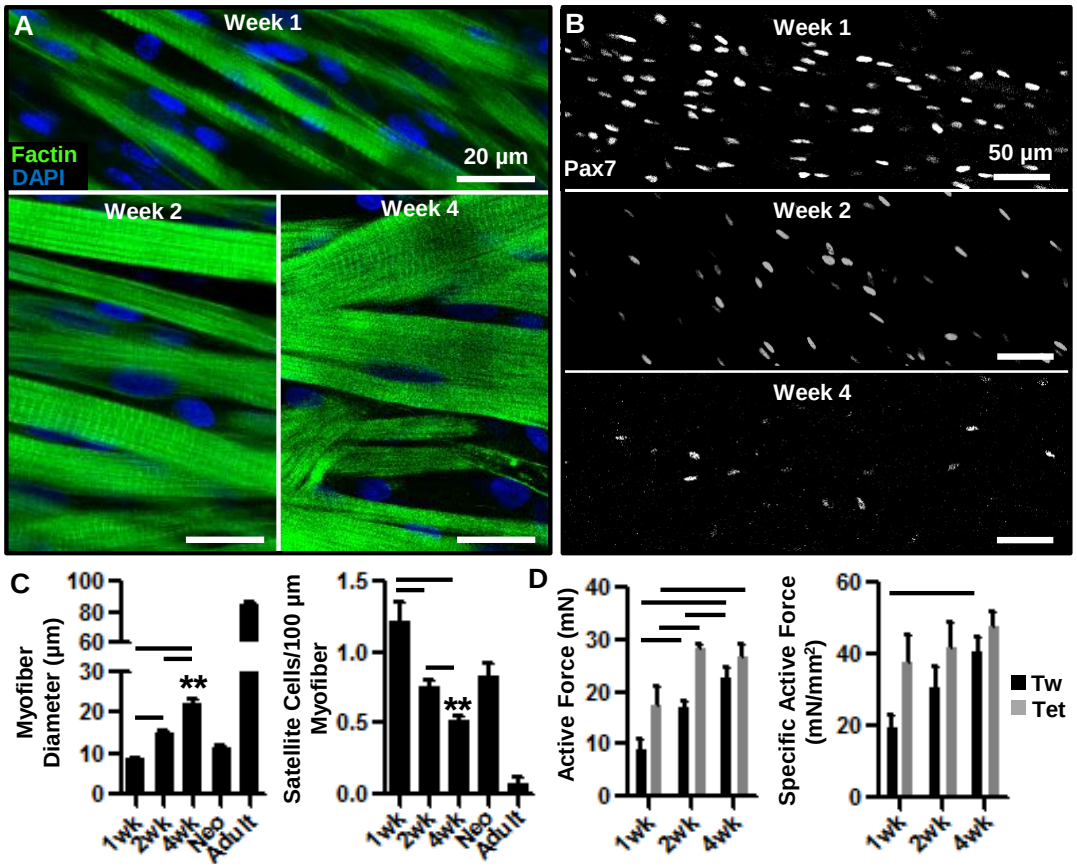

Figure 3.13 Maturation of engineered muscle. (A-B) Representative images of the steady increase in myofiber diameter (A) and decrease in Pax7^{+} SC number (B) within engineered muscle bundles over 4 week (wk) culture. (C) Average myofiber diameter and SC number per 100 µm myofiber length at 1, 2, and 4 wk of culture compared to native neonatal (neo) and adult soleus muscles. (D) Absolute and specific (force per area) twitch and tetanus (40 Hz) amplitudes in engineered bundles at 1, 2, and 4 wk of culture. Error bars denote mean ± SEM. **P < 0.01 between 4 wk bundle and native muscles, P < 0.01 between denoted groups. N =4-10 samples per group, 8-10 images per sample.

In response to electrical stimulation, engineered muscle bundles generated strong twitch contractions that with increase in stimulus frequency fused into a more forceful tetanic contraction (Figure 3.14A). As characteristic of native muscle [185],

lengthening of engineered muscle yielded a biphasic increase in the amplitude of active (contractile) force and a monotonic increase in passive tension (Figure 3.14B).Contractile force generating capacity of engineered muscle also increased with time of culture (1 wk: 8.83 ± 2.3 and 17.27 ± 3.6 mN, 2 wk: 17.08 ± 1.1 and 28.39 ± 0.92 mN, 4 wk: 22.79 ± 2.1 and 26.75 ± 2.3 mN (twitch and tetanus), Figure 3.13D), attaining values more than an order of magnitude higher than those previously reported for other engineered muscle tissues [9, 10, 14, 18, 21, 156, 180, 186]. Specific tetanic force per unit muscle cross-sectional area of 47.9 ± 4.1 mN/mm2 in 4-week engineered bundles surpassed values reported for native neonatal rat soleus muscle (44 mN/mm2) [185]. Moreover, passive tension during 4-week culture did not change significantly (Figure 3.14C), yielding high active-to-passive force ratios of ~10-15 (Figure 3.14D), characteristic of neonatal skeletal muscle [185, 187] and, to our knowledge, unmet in previous tissue engineering studies.

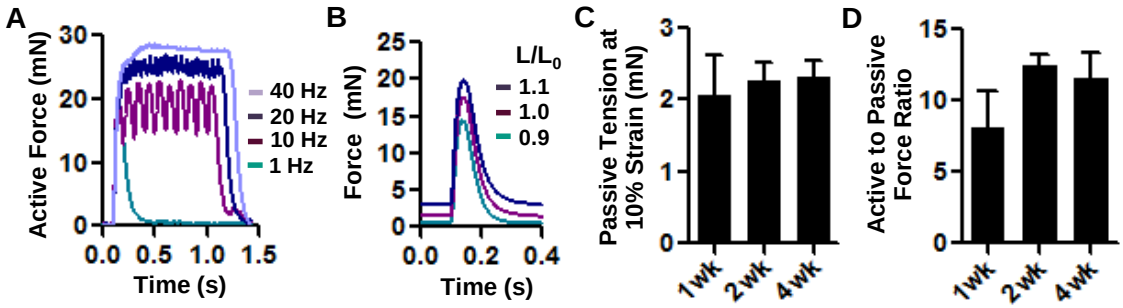

Figure 3.14 Functional characterization of engineered muscle bundles. (A) Representative active force traces in 2-week (wk) old engineered muscle bundles showing increase in active force amplitude and generation of tetanic contraction at increased frequency of electrical stimulation. (B) Representative twitch force traces in 2-week old engineered muscle bundles showing changes in active twitch and passive tension amplitudes with increase in engineered muscle length L (relative to initial length L_0). (C) Amplitude of passive tension at 10% strain (L/L_0=1.1). (D) Ratio of active tetanus force to passive tension amplitudes at 10% strain. Error bars denote mean ± SEM. N = 4-10 bundles per group.

3.4 Discussion

The goal in this chapter was to explore the roles of cellular input (FI vs. AF) and culture method (static vs. dynamic) on contractility and myogenesis in attempt to develop an optimal culturing procedure to engineer muscle constructs with superior function and myogenic maturity while maintaining the presence of satellite cells (SCs). The optimal engineered muscle was then compared to natural neonatal muscle in order to assess the physiological-accuracy of the model.

3.4.1 Optimizing cell source and culture conditions

Reports have identified the effect of culture on SC function and characteristics, revealing that FI SCs are able to retain self-regenerative capabilities better than cultured cells which undergo differentiation [78, 80]. Thus, adding undifferentiated SCs may provide a potential benefit when attempting to reconstitute the SC niche within the engineered muscle. However, as researchers look towards methods for gene and protein delivery and cellular expansion, there are benefits of working with myogenic cells in culture. Further, freshly-isolated cell populations include many non-myogenic cells types leading to variability in projected function, evidence by the formation of sparse myofibers in engineered muscle using the non-adherent fraction of FI cells (Figure 3.15). Therefore, the ability of the fraction of cells which adhere to a Matrigel-coated flask (adherent fraction (AF)), and, following gentle disassociation, are used to create engineered muscle following culture was tested.

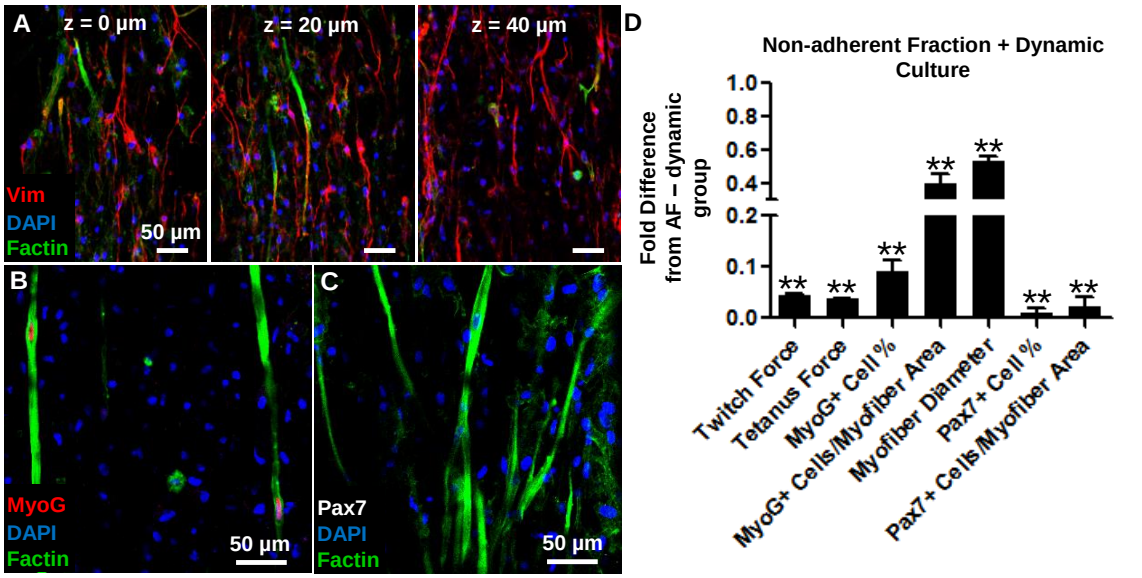

Figure 3.15 Characterization of engineered muscle from non-adherent cell fraction cultured dynamically. (A) Z-stack of vimentin^{+} (Vim) fibroblast alignment and distribution from the periphery of the bundle. (B-C) Confocal images within muscle layer stained for (B) myogenin^{+} (MyoG) myonuclei, (C) Pax7^{+} satellite cells, and f-actin^{+} myofibers. (D) Fold difference between engineered muscle derived from the non-adherent fraction of cells compared to adherent fraction (AF) cells both cultured under dynamic conditions. ***P* <0.001 compared to AF-dynamic group. N = 3 bundles for non-adherent group, 3-5 locations per bundle.

Dynamic culture has been introduced in the field of tissue engineering in attempt to increase oxygen and nutrient diffusion, enhance waste removal, and apply shear forces within a 3-dimensional construct [183]. Reported effects of dynamic culture include not only increased cell survival and distribution [188] but also changes in cellular expression and behavior [188-190]. In the study, a simple method of incubation on a rocking system (0.4 Hz, -30º to +30º tilt) was utilized to introduce fluid shear to a suspended engineered muscle construct.

3.4.1.1 Effects on engineered muscle compaction

Over 2 weeks of engineered muscle culture, cells within the fibrin hydrogel will migrate, proliferate, differentiate, and fuse, depending on cell type and external stimuli, remodeling the hydrogel scaffold. In our system, we commonly observe migration of

fibroblasts to the periphery of the bundle surrounding myofibers formed from fused myogenic precursors. This external layer of fibroblasts may assemble due to durotaxis towards the greater tension on the surface of the construct [132, 191] or enhanced migratory properties of the cell type as it seeks more favorable oxygen and nutrient concentrations. Hydrogel compaction, attributed to fibroblast contraction during migration [184, 192], creates passive tension in the system and results in myofibril alignment. Both dynamic culture and the AF cells increased total bundle contraction at 2 weeks (Figure 3.1A&B). Given the reported effects of shear stress in enhancing fibroblast migration [193] and proliferation [194], the result of dynamic culture on compaction can be expected and confocal images of bundle periphery at 2 weeks suggest greater density with dynamic culture (Figure 3.16). Further, as shown in Figure 3.10, there was a more rapid accumulation of fibroblasts at the periphery when using AF cells resulting in accelerated compaction compared to FI cells. The 48 hours in culture may have resulted in fibroblast proliferation and an increase in cell surface proteins to enhance mobility.

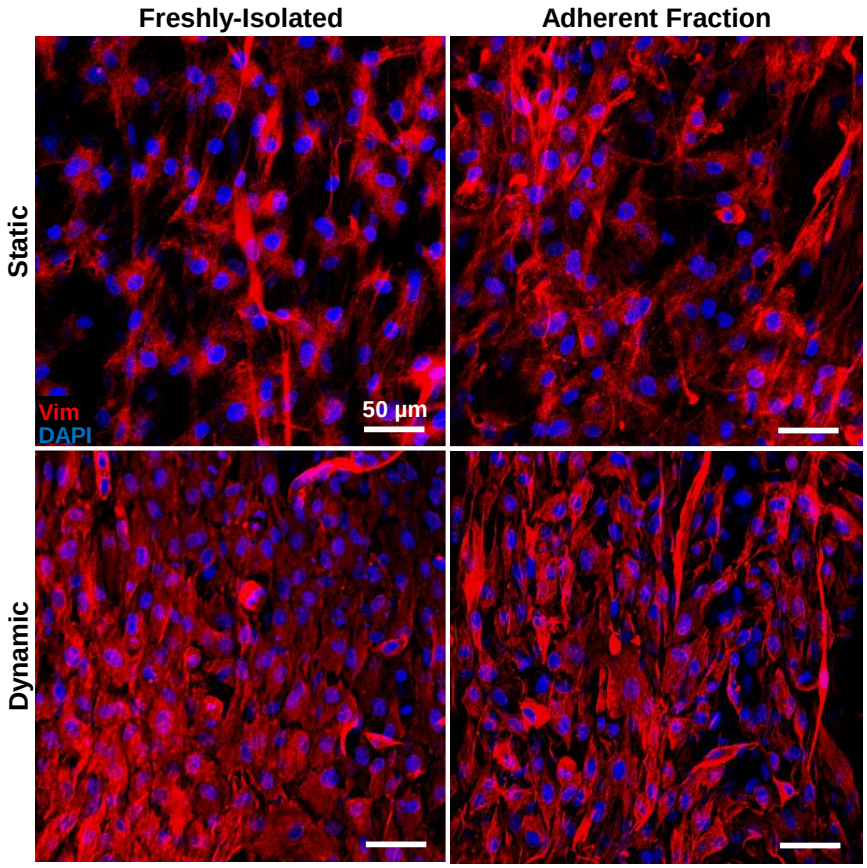

Figure 3.16 Peripheral fibroblast layer in engineered muscle. Representative confocal images of engineered muscle periphery at 2 weeks showing density and distribution of vimentin^{+} (Vim) fibroblasts for each group.

As expected, dynamic culture resulted in a significant increase in viable muscle area and fraction compared to static culture (Figure 3.1C&D). Static results are consistent with prior reports of relatively large engineered muscle [10], demonstrating only a thin layer of musculature on the exterior of the bundle. Dynamic culture was able to significantly increase the muscle layer and create tissues with substantial amounts of viable myofibers. With the increase of muscle, the increase in absolute twitch and tetanic force was expected as there are more healthy myofibers contributing to contraction (Figure 3.2A&B). However, dynamic culture also had a significant effect on specific force, a parameter of individual myofiber integrity and maturity. Furthermore, the use of

AF cells resulted in significant increase in absolute and specific forces without affecting muscle area, again suggesting enhancement of individual myofiber performance. Additively, dynamic culture and the use of AF cells in our engineered muscle constructs result in absolute forces approaching 30 mN, an order of magnitude higher than those previously reported for other engineered muscle tissues [9, 10, 14, 18, 21, 156, 180, 186], and specific forces comparable to native neonatal muscle [185].

3.4.1.2 Effects on myofiber maturity

A key indicator of individual myofiber maturity is cellular hypertrophy, or fiber diameter. As expected, similar trends in myofiber diameter as with specific forces was observed, as both dynamic culture and the use of AF cells resulted in significant increases in cell size (Figure 3.3). Extensive studies of myofiber hypertrophy have shown that it is resultant of increase protein synthesis caused by either accumulation of myonuclei, nutrient uptake, and/or the stimulation of specific pathways [195, 196]. Quantitative analysis of myonuclei within the engineered muscle following 2 weeks of culture, showed significant impact of the use of AF cells in both myogenin^{+} cell percentage and density (cells/fiber area) (Figure 3.4). These results suggests increased fusion efficiency within the engineered system when using AF cells, potentially attributed to myogenic differentiation or increased expression of adhesion proteins following culture, yielding a cellular pool more primed for fusion events. Dynamic culture, however, did not show any effect on myonuclei accumulation, suggesting it may not impact fusion efficiency within the engineered muscle. Therefore, it can be postulated that the applied fluid shear provided myofibers with sufficient nutrients, shown to increase cell survival (Figure 3.1), to support hypertrophy [197]. Further, as shear is known to enhance of insulin-like growth factor 1 (IGF-1) signaling in various cell types [198, 199], dynamic

culture may also stimulate common myogenic hypertrophic pathways downstream of IGF-1 [195, 196].

3.4.1.3 Maintaining a satellite cell population and tracking early fusion events

As described in detail in section 2.1, $Pax7^+$ SCs are necessary for muscle growth [200] and regeneration [201], thus making $Pax7^+$ cell retention a crucial parameter. Since FI cells avoid myogenic differentiation with culture, it was expected that there would be greater SC density at 2 weeks. Surprisingly, in dynamic culture, engineered muscle using AF cells were able to retain almost twice as many $Pax7^+$ cells compared to the FI group (Figure 3.5). To better understand the cellular dynamics within the engineered muscle, and to unveil how $Pax7^+$ cells are maintained, early time-points during myogenic fusion events (day 2, 3, and 4) were examined. As expected, the use of FI cells introduced a greater percentage of $Pax7^+$ at day 2 than AF cells (Figure 3.6). However, this population experienced a significant drop by day 3 and 4 in the FI group, a trend not experienced when using AF cells. By day 4, engineered muscle using AF cells retained twice as many $Pax7^+$ cells compared to FI cells. Additionally, at this time, the large majority of $Pax7^+$ cells lacked expression of Ki67 in both groups, suggesting transition to a quiescent state (Figure 3.7).

Expression of more mature myogenic markers, MyoD and myogenin, were also tracked during fusion events (Figure 3.6 and 3.7). As expected, AF cells introduced a greater population of more differentiated cells at day 2 and, based on a significant drop in MyoD expressing cells by day 3, underwent accelerated differentiation compared to FI cells which experienced a slower transition from MyoD to myogenin expression (Figure 3.6 and 3.7). As a result, the AF group was able to support rapid fusion events and myofiber formation (Figure 3.6D), as a significantly greater amounts of f-$actin^+$ cell

density compared to the FI group at day 2, 3, and 4 was observed. In addition, the use of AF cells resulted in accelerated myofibril maturation evidenced by earlier formation of contractile sarcomeric structures (Figure 3.8).

3.4.1.4 Formation of the satellite cell niche

The cellular dynamics observed during early time-points within the engineered muscle suggest that SC maintenance may rely on the rapid formation of myofibers, providing a niche for SC survival. The SC niche, critical for maintaining SC regenerative function, consists of the host myofiber and a laminin-rich basal lamina [202]. Key adhesion proteins associated with the SC niche are α7β1 integrin, expressed by the satellite cell for attachment to laminin [202], and m-Cadherin, expressed by both the satellite cell and myofiber for mutual binding [202, 203]. Even though using FI cells provide a greater percentage of $Pax7^+$ cells initially, the AF cells consisted of a heterogeneous myogenic population more favorable for retaining the $Pax7^+$ pool. AF cells cultured on Matrigel introduced a population that was able to retain Pax7 expression, due to potential linkage between the laminin in the protein cocktail and α7β1 integrin expressed by the SC [136, 204], and, based on MyoD and myogenin levels at day 2 (Figure 3.6 and 3.7), a population of more mature precursors. The more differentiated cells, following gentle disassociation with dispase in attempt to preserve cell surface proteins, underwent rapid fusion events creating immature multi-nucleated myotubes, known to express m-Cadherin in developing muscle [205, 206]. These events, coupled with the presence of laminin within the hydrogel matrix (Figure 3.12), may have contributed to enhanced sites for more undifferentiated $Pax7^+$ cells to dock, as by day 4, $Pax7^+$ cells already abut myofibril surfaces expressing m-Cadherin (Figure 3.17). All such events are further supported through the accelerated compaction seen in

AF gels under dynamic conditions, increasing cell to cell contacts. The use of FI cells, however, created an environment that experienced a delay of myofiber formation and a decrease in SC maintenance, potentially resultant of differentiation of dysfunction of SCs due to lack of homing locations [207]. All-in-all, it is suggested through our work that the formation of the satellite cell niche in engineered muscle requires rapid an environment and cellular source that enables rapid fusion of myogenic cells allowing undifferentiating SCs an opportunity to home and mature.

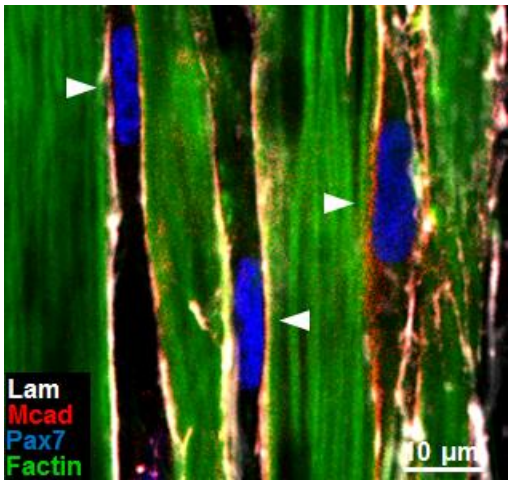

Figure 3.17 Pax7^{+} cells homed to myofibers at day 4. Confocal images showing Pax7^{+} (blue) nuclei abutted to f-actin^{+} myofibers expressing m-Cadherin (Mcad) surrounded in laminin (Lam). White arrows indicate locations of m-cadherin expression and the adhesion of the myofiber and Pax7^{+} cell.

3.4.2 Comparing optimized constructs to native muscle

One of the overarching goals of tissue engineering is to create constructs that accurately model native organs in both structure and function and can recreate natural tissue processes. To validate the engineered tissue as a credible representation of natural muscle structure, the architecture and composition of AF-derived engineered muscle cultured dynamically for 2 weeks was directly compared to that of neonatal rat muscle (Figure 3.12). Confocal microscopy showed the exterior of the bundles to be

sheathed in a layer of vimentin^{+} fibroblasts, characteristic of native muscle epimysium, a layer of connective tissue encompassing bundles of myofibers. Both native muscle and our bundles' interior consisted of densely packed, highly aligned, multinucleated, and cross-striated myofibers surrounded in basal lamina consisting of muscle-specific ECM proteins (laminin and collagen IV). Localized to the basal lamina are resident muscle stem cells, or SCs, marked by expression of Pax7. Figure 3.12 reveals that in our constructs, SCs are homed to their natural niche, beneath the basal lamina on the periphery of myofibers. The temporal changes in myofiber size and SC density at 1, 2, and 4 weeks were quantified to evaluate the ability of the engineered muscle to undergo continued myogenesis and post-natal muscle growth (Figure 3.13). Differentiation of SCs during 4-week culture contributed to myofiber hypertrophy, a process characteristic of the natural process [173]. Along with the structural maturation, contractile capacity of engineered muscle increased beyond specific force values measured in neonatal rat muscle, reaching contractile force amplitude (~30 mN) 10-100 times higher than previously achieved [9, 10, 14, 18, 21, 156, 180, 186].

3.5 Summary and Implications

The described work reveals significant benefits of the use of an adherent myogenic cell fraction and dynamic culture towards the development of a skeletal muscle construct capable of replicating the function, structure, and cellular heterogeneity of natural muscle using both neonatal and adult cell sources. Furthermore, crucial requisites for the maintenance of satellite cells in engineered muscle *in vitro* we discovered, as constituents of their natural niche played a critical role in Pax7^{+} cell retention. The methods and findings presented can be applied to create more accurate models of skeletal muscle for use in studies of function and regeneration and potentially

clinical applicable replacements; serving as the foundation for the following two chapters.

4. Assessing the ability of neonatal-derived engineer muscle to respond to injury in vitro and survive following in vivo implantation

4.1 Rationale and experimental plan

In response to common acute injury, native muscle shows a remarkable capacity for self-repair [201, 208] mediated by rapid SC activation and myogenesis to rebuild damaged myofibers [1, 201, 209]. Development of tissue-engineered muscle capable of self-repair, a feat previously not accomplished in the field, would open doors to studying physiology and pathology of muscle regeneration in vitro and increase efficacy of tissue engineering therapies for muscle repair *in vivo*. In chapter 3, we demonstrated that engineered muscle bundles retain a SC pool that contributes to continued myogenesis with time of culture. In this chapter, we studied the self-repair capacity of the engineered muscle using a novel *in vitro* regeneration assay in which myofibril disruption was induced via application of cardiotoxin (CTX) and the recovery from injury was subsequently monitored by live imaging, force tests, and immunostainig. To reveal the roles of SCs in engineered muscle regeneration, we expanded the myogenic cells using varying concentrations of bFGF, engineered muscle bundles with vayring SC density, and further studied their regenerative response after injury with cardiotoxin.

We further studied the ability of engineered muscle bundles to survive, vascularize, and continually function *in vivo*. Thus far, implanted *in vitro* engineered muscle tissues have not been able to recreate the structural and force generating properties of native muscle, while implantation of committed myogenic cells has led to cell death and the inability to engraft or support continued regeneration [78-80]. By contrast, undifferentiated, freshly isolated muscle stem cells, known as satellite cells

(SCs), can home to the resident host niche, undergo myogenic commitment, and regenerate host muscle upon implantation [78, 80, 81]. Our hypothesis was that for optimal therapy, engineered muscle should fully recreate the cellular heterogeneity of native muscle and consist of both force-generating, differentiated myofibers and a functioning SC pool to allow further maturation and regeneration *in vivo*. To assess the fate of engineered muscle constructs in vivo, we transduced cells with genetic indicator of calcium concentration, GCaMP3 (section 2.4.3.3), and implanted them in dorsal window chambers in nude mice (section 2.4.4). This allowed us to non-destructively in real time image the ingrowth of vessels from the host into the implanted tissue as well as GCaMP-reported calcium transients, reflective of muscle function. Furthermore, differentiated engineered muscles and those containing only undifferentiated myogenic cells were compared for their abilities to vascularize and function *in vivo*.

4.2 Methods

4.2.1 Cell isolation and culture

Muscle tissue was harvest and myogenic precursors were isolated using the same method described in 3.2.1. Cells used for implantation studies were exposed to a GCaMP3, a genetic indicator of intracellular calcium, lentivirus driven by a CMV promoter for 24 h following initial cell seeding (Figure 4.3A&B). When expanding the myogenic pool, in attempt to vary the SC population, cells were cultured on 1% Matrigel-coated dishes in an expansion media (F10 Nutrient Mixture and 20% FBS) and supplemented with rat recombinant bFGF (R&D Systems) at 0, 2.5, 5, and 10 ng/mL concentrations. The expanded cells were passaged up to 5 times and quantified for the presence of myogenic cells ($Pax7^+$, $MyoD^+$, and $MyoG^+$). During passaging and prior to engineered muscle formation, the cells were detached by 2% dispase (v/v).

4.2.2 Engineered muscle formation

Large single muscle bundles were generated as described in 3.2.2 using the adherent cell fraction (AF) under dynamic culture conditions. For implantation studies, a smaller tri-bundle mold (7 mm long, 2 mm diameter) was developed in a similar method as described 3.2.2. In the tri-bundle system, laser-cut Cerex® frames (9 mm x 9 mm, 1 mm wide rim) were positioned around the 3 wells to enable hydrogel attachment and facilitate construct handling and implantation. Likewise, the implanted tri-bundle muscle constructs were generated using AF cells and cultured dynamically for either 2 or 14 days. Constructs cultured for 2 days and only exposed to growth media comprise the undifferentiated group (UnD) and constructed cultured for 14 days and exposed to differentiation media comprise the pre-differentiated group (PreD).

4.2.3 In vitro regeneration assay

Following 2 weeks of *in vitro* culture, differentiated engineered muscle bundles were exposed to 0.2 µM cardiotoxin (CTX, Cardiotoxin from *Naja mossambica mossambica*, Sigma) for 6 hours on a rocker at 37°C. The injured bundles were washed 3x in differentiation medium to rid the environment of toxin. Bundles were assessed for contractile function, described in section 4.2.8, and structural composition, described in section 4.2.9, immediately after CTX administration and following culture in differentiation media for 5 or 10 days (and up to 15 days in chapter 3) (Figure 4.1). Specifically, SC dynamics were tracked using the SC marker, Pax7, proliferation marker, Ki67, activated SC marker, MyoD, and mature myonuclei marker, myogenin.

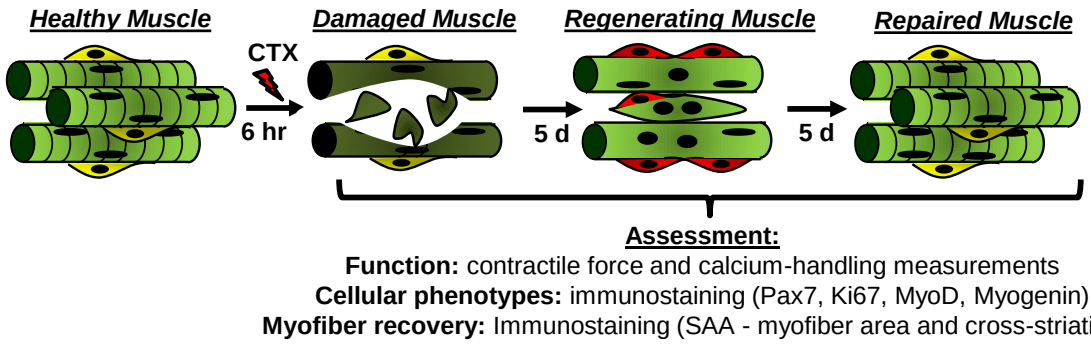

Figure 4.1 In vitro assessment of engineered muscle regeneration. Cardiotoxin (CTX) is applied for 6 hours (hr) to induce myofiber fragmentation and response to injury was assessed by evaluating muscle function, cellular makeup, and myofiber recovery at 6 hours, 5 days, and 10 days post injury.

4.2.4 Implantation of engineered muscle bundles

All animal experiments were approved by the Duke University ACUC. Nude mice (~10 weeks of age; 22-30 g) were anesthetized by intraperitoneal injection of ketamine (100 mg/kg) and xylazine (10 mg/kg). Using aseptic technique, the dorsal skin was attached to a temporary "C-frame" at the center of the back. The skin was perforated in three locations to accommodate the screws of the chamber, and a circular region (~12 mm) of the forward-facing skin (i.e., cutis, subcutis, retractor and panniculus carnosis muscles, and associated fascia) was dissected away to accommodate the window proper. The forward and rearward pieces of the titanium dorsal skinfold chamber were assembled together from opposite sides of the skin, and a Cerex® frame with tri-bundle muscle constructs was laid perpendicular (verified under microscope) to the intact panniculus carnosis muscle of the rearward-facing skin (Figure 4.3F&G), providing a source of microvessels for vascularization. A sterile cover glass was placed over the window and engineered tissue while superfusing with sterile saline solution. The chamber was then secured with suture and the “C-frame” was removed. Post-

operatively, the mouse was injected subcutaneously with buprenorphine (1 mg/kg) painkiller and let to recover on a heating pad.

4.2.5 Intravital imaging of blood vessels

Intravital recordings were performed in anesthetized mice on d 2, 5, 7, 9, 12, and 14 post-implantation (PI). Mice were anesthetized by nose cone inhalation of isoflurane and positioned on a heating pad under a microscope objective. Hyperspectral brightfield image sequences (10 nm increments from 500 – 600 nm) were captured at 5x magnification using a tunable filter (Cambridge Research & Instrumentation, Inc.) and a DVC camera (ThorLabs), as previously described [182]. A custom MATLAB (MathWorks) script [210] was applied to create maps of total hemoglobin concentration (Figure 4.2). Obtained maps were further processed using local contrast enhancement in ImageJ (FIJI) and thresholded to binary images to identify vessel area and calculate blood vessel density (BVD, total area of blood vessels per bundle area).

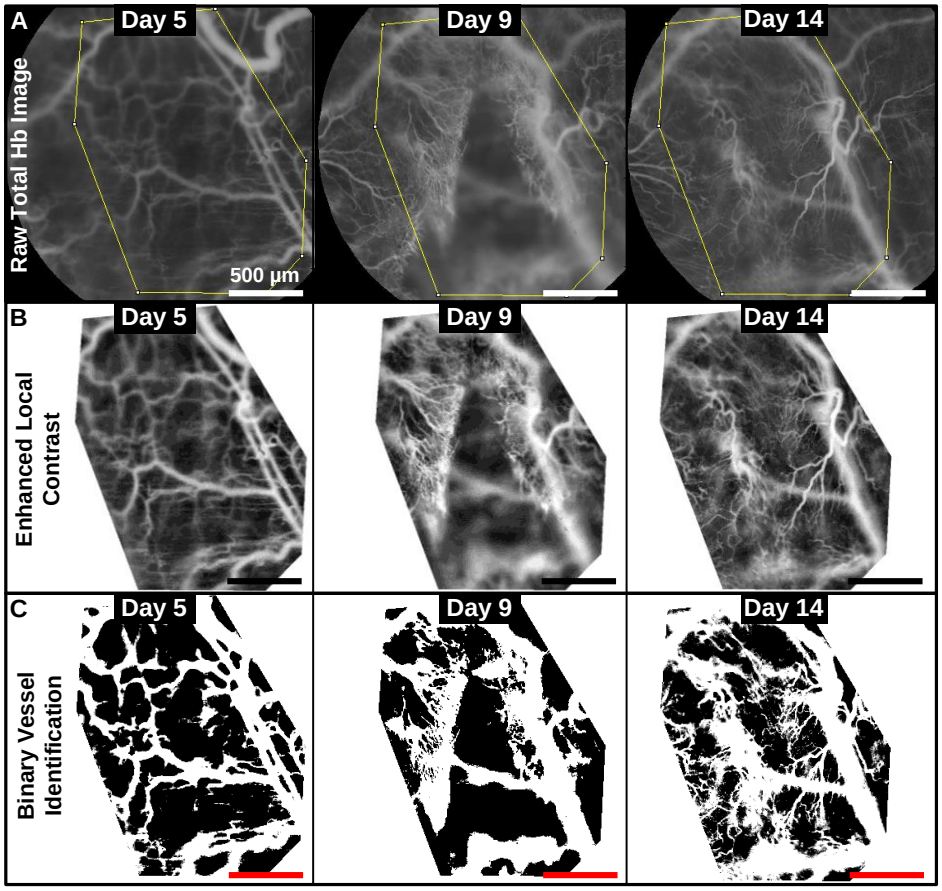

Figure 4.2 Method for calculating blood vessel density in implanted engineered muscle bundles. (A) Consistent regions of interests (ROIs) were identified within raw intravital images of total hemoglobin concentration for the same implanted bundle at different time points (days) post implantation. Using ImageJ (FIJI) software, local contrast was enhanced (B) and blood vessels were identified following conversion of the enhanced into binary images (C). From these images, the blood vessel density (i.e., total vessel area per bundle area) was measured in blind fashion.

4.2.6 Intravital imaging of intracellular Ca^{2+} transients

Intravital imaging of spontaneous Ca^{2+} transients was performed immediately after vessel imaging with mice still anesthetized. Fluorescent gCaMP3 signals in implanted bundles were video-imaged through a FITC-filter using a fast fluorescent camera (Andor; at 16 µm spatial and 20 ms temporal resolution). Amplitudes of spontaneous Ca^{2+} transients were determined using the Solis software (Andor) by

averaging relative fluorescence intensity (ΔF/F) from three ~400x400 μm^2 regions within each bundle (Figure 4.3C) [9].

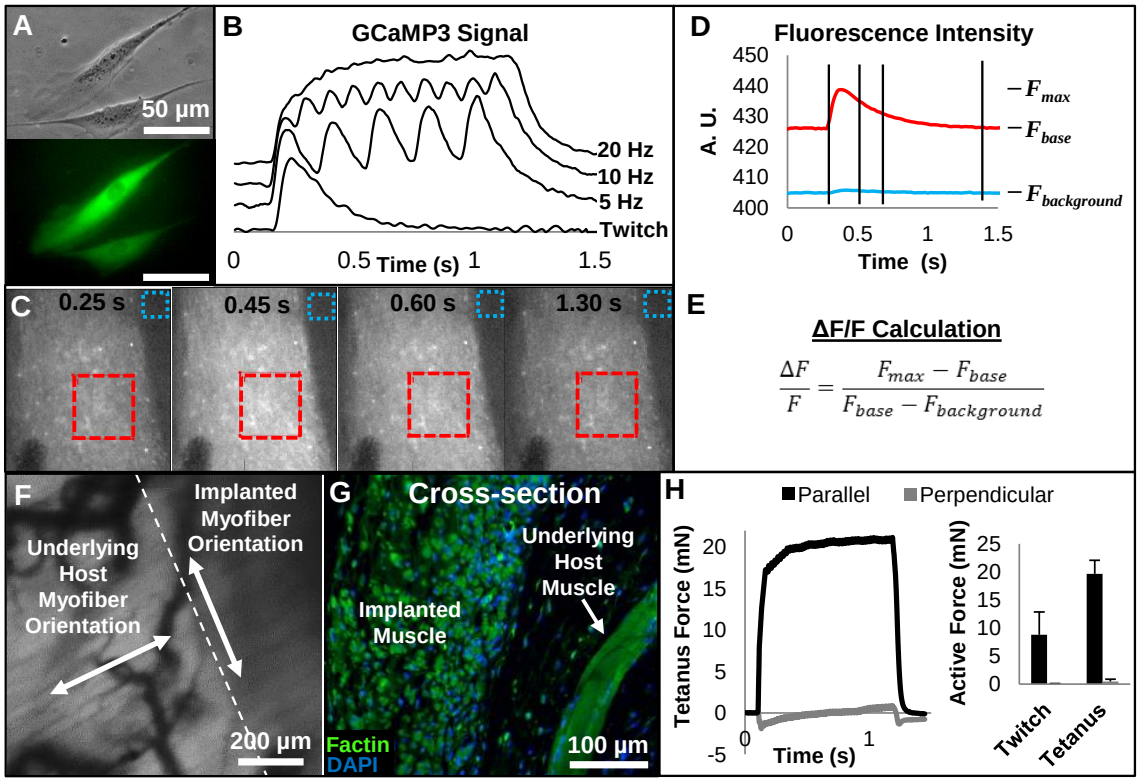

Figure 4.3 Measurements of intracellular calcium transient and contractile force generation in implanted engineered muscle bundles. (A) Representative brightfield and fluorescent images of myogenic cells transduced with GCaMP3 virus prior to assembly into a muscle bundle. (B) Representative GCaMP3 traces from an engineered muscle bundle at various stimulation frequencies. The traces are progressively shifted upwards for improved clarity. (C) Select time snapshots of recorded GCaMP3 fluorescence from an explanted muscle bundle during application of an electrical stimulus. (D) Averaged fluorescence traces from the red square region within the muscle bundle and blue square region (background) outside of the bundle shown in (C). Vertical lines denote times of the snapshots shown in (C). (E) ΔF/F signal amplitude is calculated using the shown formula. (F) Representative brightfield image of an engineered muscle bundle implanted perpendicular to the direction of underlying host muscle fibers within a dorsal window chamber. (G) 2 week (wk) post-implantation, transverse cross-section of implanted muscle overlaying longitudinal section of host muscle confirms that two muscles remain perpendicular to each other. (H) Representative tetanus force traces and average active forces of control host muscle without implant, measured parallel and perpendicular to host myofiber orientation. Note that in the direction perpendicular to host myofiber orientation (and along the orientation of implanted muscle bundles), the active force generated by the host muscle is negligible. Error bars denote mean ± SEM. N = 3 mice.

4.2.7 In vitro and ex vivo measurements of Ca^{2+} transients

Electrically-induced GCaMP3 Ca^{2+} transients were imaged in engineered muscle bundles after 2 and 14 d of *in vitro* culture and in muscle explants 1 and 2 weeks PI. Engineered muscle constructs were transferred into a custom chamber mounted on an inverted fluorescence microscope (Nikon), placed in 37°C Tyrode's solution (135 mM NaCl, 5.4 mM KCl, 1.8 mM CaCl, 1 mM MgCl, 0.33 mM NaHPO, 5 mM HEPES, 5 mM glucose), and electrically stimulated (10 ms pulse, 3 V/mm). Induced GCaMP3 signals were recorded using a fast fluorescent camera Andor iXon 860 EMCCD (24 μm spatial and 20 ms temporal resolution) and analyzed as described for intravital assessment. Kinetics of Ca^{2+} transients were also characterized as previously described [10].

4.2.8 In vitro and ex vivo force measurements

Force generating capacity of *in vitro* engineered muscle was assessed as described in section 3.2.4. To measure the force of explanted tissues, the whole tissue was harvested from the chamber. The excised tissue was placed with the engineered tissue parallel to the force transducer and the underlying native tissue perpendicular (Figure 4.3H)

4.2.9 Immunostaining

Cultured cells and engineered tissues were fixed and stained as described in section 3.2.3. Explanted tissues used for cross-sectional staining were embedded in paraffin, sectioned (5 μm), washed with xylene, rehydrated, microwaved 5 times for 3 minutes in a citrate buffer solution (90% H2O, 8% 100mM Sodium Citrate, 2% 100mM Citric Acid), and immunostained. Additional primary antibodies used in this chapter are described below (Table 4.1).

Table 4.1 Additional primary antibodies used in chapter 4

Primary Epitope	Dilution	Supplier	Catalog no.
CD31	1:300	Abcam	ab28364
vWF	1:200	Abcam	ab6994
GFP	1:300	Abcam	ab6556

4.2.10 Nucleus counting image analysis

To automate nuclear counting, we used a custom MATLAB software developed by Dr. Nima Badie. The program allows user-thresholding of DAPI or transcription factor (Pax7, Ki67, MyoD, myogenin) staining and, based on the median size of nuclei for the given magnification, designates and counts identified nuclei. The program outputs the processed images with identified nuclei for the user to verify.

4.2.11 Analysis of myofiber and blood vessel alignment

Orientation of muscle fibers (marked by expression of GFP or F-actin) and blood vessels (marked by expression of CD31) was quantified in engineered muscle implants and native muscle from confocal images acquired at 20x magnification using a previously described image intensity gradient algorithm [158, 211]. Local feature orientation was calculated within 25x25 pixel (11x11 μm) subregions (Figure 4.12B) in which myofibers or blood vessels were present and standard vessel angle deviation and absolute mean fiber angle difference between myofiber and vessel directions were calculated by averaging subregion data over the entire (450x450 μm) image. Four images were analyzed per each muscle sample.

4.2.12 Statistics

Results are presented as mean ± SEM. Statistical significances among different groups were evaluated by unpaired t-test or one-way ANOVA with post hoc Tukey's test using GraphPad Prism (GraphPad Software, Inc.). $P<0.05$ was consider statistically significant. Different levels of significance were noted in figures and figure captions.

4.3 Results

4.3.1 Evaluation of homeostatic state of engineered muscle

The temporal changes in cell proliferation and expression of key myogenic transcription factors (Pax7, MyoD, and myogenin (MyoG)) during *in vitro* culture (Figure 4.4) was monitored to ensure the quiescent state of $Pax7^+$ SCs. At early stages of engineered muscle formation (day 2), a large majority of $Pax7^+$ cells (~75%) were activated and proliferating as evidenced by their expression of Ki67 (Figure 4.4A&B). Simultaneously, the vast majority of early fusing cells or newly-formed, multinuclear myotubes expressed MyoD, either without or with MyoG (Figure 4.4C&D). By culture day 14, the cells expressing MyoD alone virtually disappeared and all myonuclei in the engineered muscle expressed MyoG, either alone (~80%) or together with MyoD (Figure 4.4D). The ~20% $MyoG^+/MyoD^+$ myonuclei located at the periphery or within existing myofibers indicated cells that were either primed for fusion or recently fused. By culture day 14, $Pax7^+$ cells (Figure 4.4A) remained in relatively high numbers (~20% of all cells) and, as expected, did not co-express MyoG. Virtually all of the $Pax7^+$ cells were also $MyoD^-$ and quiescent, with only a small fraction (~1.5%) expressing Ki67, suggesting that the engineered muscle attained a differentiated, homeostatic state. The presence of $MyoD^+$ cells in the homeostatic engineered muscle (Figure 4.4D) suggested the existence of continuous cell growth and hypertrophy as revealed in chapter 3.

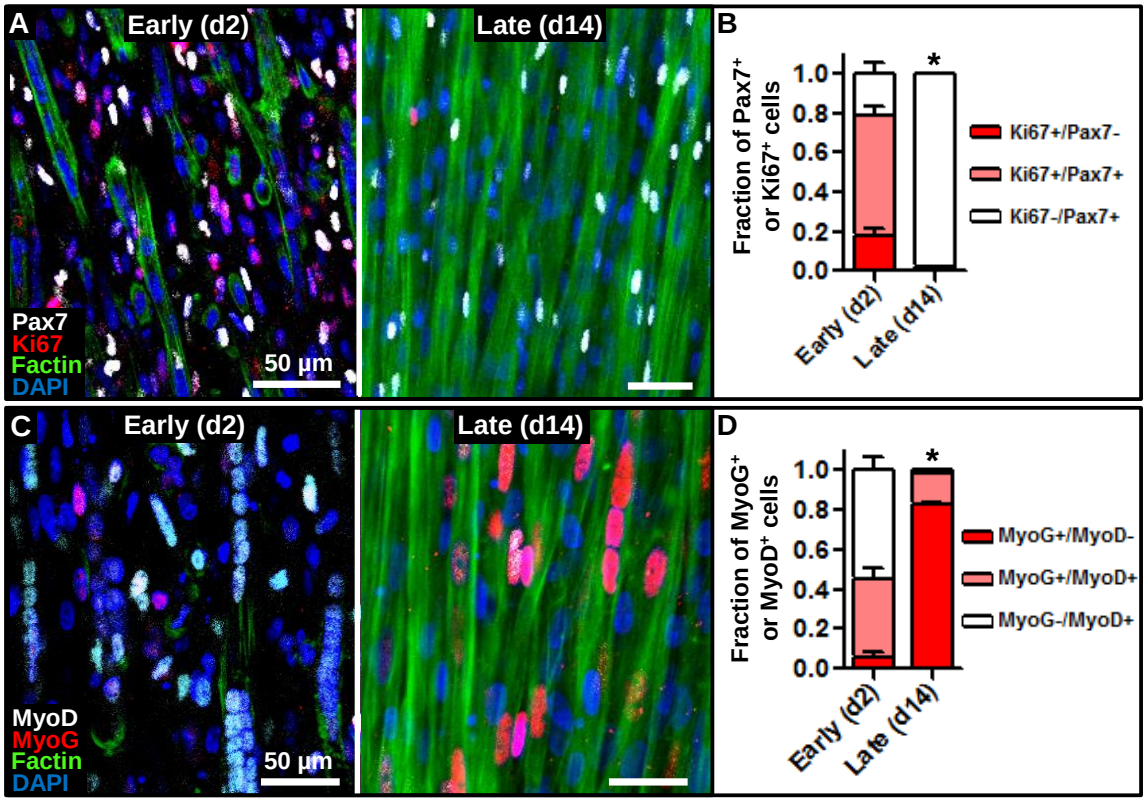

Figure 4.4 Acquisition of homeostatic cell composition within engineered muscle bundles. (A) Representative images of Pax7 and Ki67 expression inside the engineered muscle bundles at early fusion (2d) and late post-differentiation (14d) times during in vitro culture. (B) Quantified fractions of $Pax7^+$ and/or $Ki67^+$ cells at 2 and 14 days of culture. Note a homeostatic shift to a non-proliferative quiescent muscle phenotype at 14d of culture. (C) Representative MyoD and myogenin (MyoG) expression inside the engineered muscle bundles at 2 and 14 days of culture. Note that abundant expression of MyoD in early fusing myofibers at culture day 2 is significantly decreased with the formation of mature myofibers by day 14. (D) Quantified fractions of $MyoD^+$ and/or $MyoG^+$ cells demonstrate switch to a mature, differentiated muscle phenotype. Error bars denote mean ± SEM. N = 3-6 bundles per group. *P<0.05 compared to corresponding early time-point for each group.

4.3.2 Response of engineered muscle to in vitro injury

To further investigate the SC function within the engineered muscle, a cardiotoxin (CTX)-injury assay was utilized to assess whether the SCs can support muscle self-repair *in vitro*. Homeostatic, 2-week old engineered muscle was exposed to 0.2 μM CTX for 6 h and allowed to recover for 10 days. Consistent with *in vivo* reports [212], the CTX exposure resulted in immediate fragmentation of myofibers, cell death, and disruption of

contractile elements leading to a 4-fold decrease in contractile force generation (Figure 4.5). In response to injury, SCs in the engineered muscle underwent robust activation and proliferation such that by 5 days post-injury, initially decreased $Pax7^+$ and $MyoD^+$ cell numbers significantly increased beyond those present in the pre-injury muscle accompanied by a significant rise in the percentage of proliferating SCs ($Ki67^+/Pax7^+$) (Figure 4.5A&B). By 10 days post-injury, numbers of $Pax7^+$, $Ki67^+/Pax7^+$, and $MyoD^+$ cells decreased while the number of $MyoG^+$ myonuclei, myofiber density, and % cross-striated myofibers increased to near pre-injury levels (Figure 4.5A&B). The progressive regrowth, differentiation, and sarcomerogenesis of engineered muscle fibers resulted in steady recovery of both twitch and tetanic force generation, which by 10 days post-CTX injury reached the near pre-injury levels (Figure 4.5A&B). Of note, the overall time-course of *in vitro* recovery was comparable with *in vivo* regeneration of native muscle [1, 212, 213].

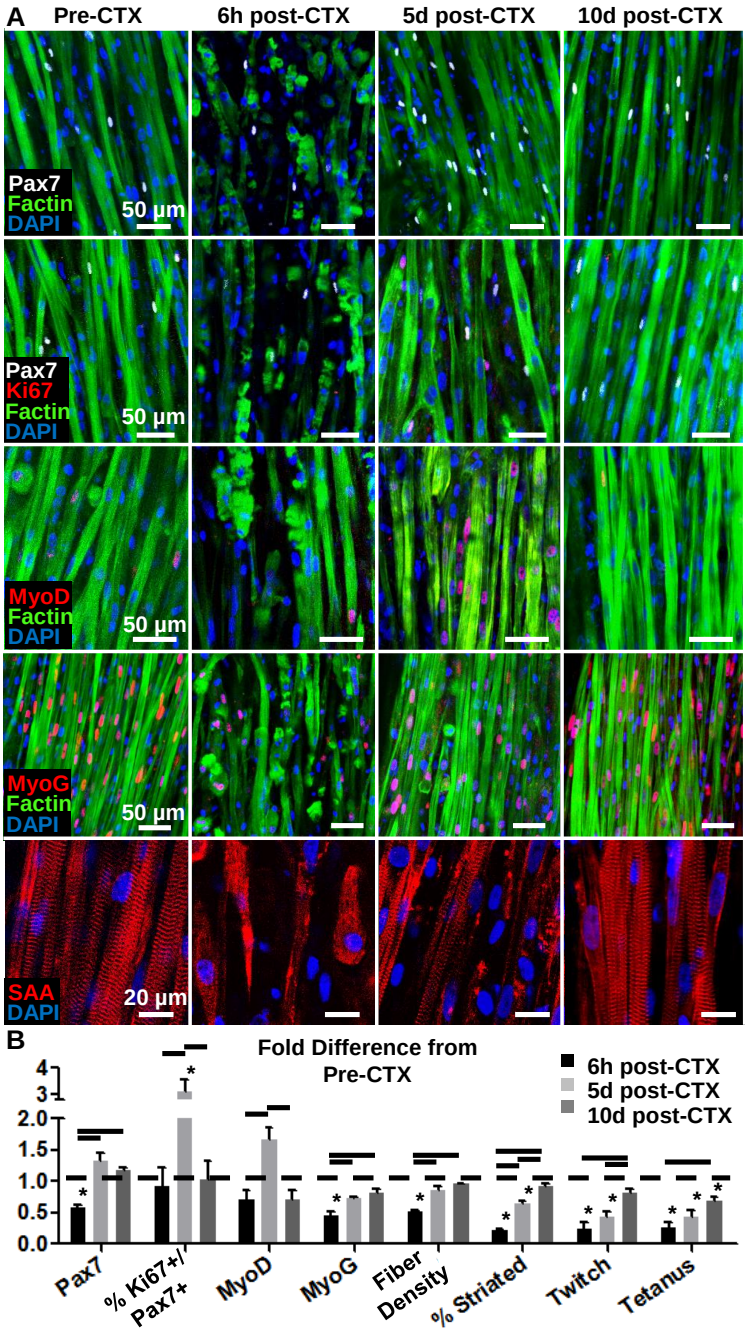

Figure 4.5 Regenerative response of engineered muscle to in vitro cardiotoxin (CTX) injury. (A) Representative images of engineered muscle structure, $Pax7^{+}$ and $myogenin^{+}$ (MyoG) cells, and sarcomeric structures (SAA) with time post-CTX injury (induced at 14 d of culture). (B) $Pax7^{+}$, $Ki67^{+}/Pax7^{+}$ (% of $Pax7^{+}$), $MyoD^{+}$, and myogenin $(MyoG)^{+}$ cell density, myofiber density, % cross-striated myofibers and twitch and tetanus force amplitudes shown relative to pre-injury levels at 6 h, 5 d, and 10 d post CTX addition. Error bars denote mean ± SEM. N = 3-5 samples per group, 6-10 images per sample. *$P < 0.05$ compared to 2 week healthy controls; $P < 0.05$ between denoted groups.

4.3.3 Expansion of neonatal cells to maintain SC pool and enhance function

To further elucidate the roles of SCs in *in vitro* regeneration of engineered muscle, we expanded isolated cells under different conditions to vary final fractio of $Pax7^+$ SCs. Specifically, we expanded SCs on Matrigel-coated dishes [136] in the presence of Ham's F-10 medium supplemented with bFGF [134, 143] (a potent mitogen and inhibitor of myogenic differentiation [214]) at 0, 2.5, 5, and 10 ng/mL. Under this protocol, neonatal myogenic cells can be rapidly expanded (via 5 passages) by 1000-fold in 9-12 days (Figure 4.6A). The highest $Pax7^+$ + $MyoD^+$ cell fraction was obtained for bFGF concentrations ≥ 5 ng/ml (Figure 4.4B). Notably, myogenic expansion in the presence of 5-10 ng/ml bFGF also reduced the fraction of $Pax7^+$ cells to ~40% of that present at passage 0 (P0, Figure 4.6B).

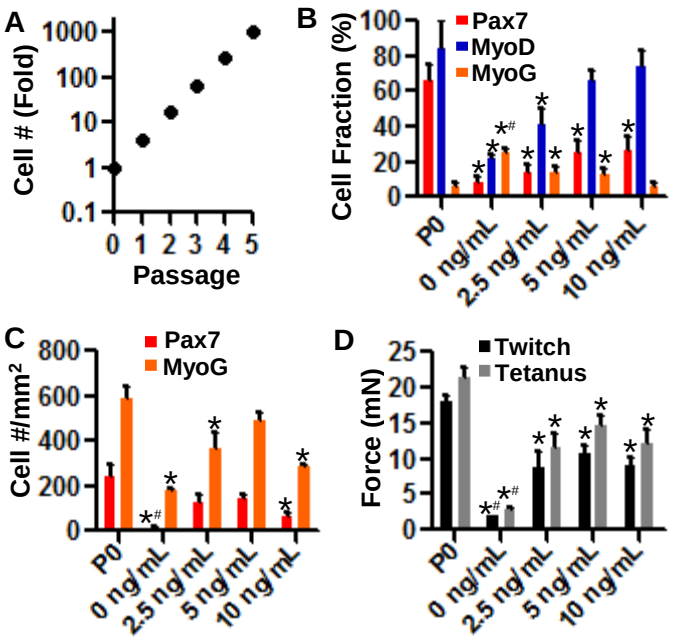

Figure 4.6 Expansion of neonatal myogenic cells in bFGF supplemented media. (A) Increase in cell number with passaging (at 70% confllluence). (B) Total fraction of $Pax7^+$, $MyoD^+$, and $MyoG^+$ cells at passage 0 (P0) and 5 in the presence of 0, 2.5, 5, 10 ng/mL bFGF. Average time needed for 5 passages: bFGF=0 ng/mL, 15d; 2.5 ng/mL, 12d; 5 ng/mL, 10d; 10 ng/mL, 9d. (C-D) $Pax7^+$ and $MyoG^+$ cell density (C) and twitch and tetanus force amplitude (D) in 2-week

muscle bundles made of P0 and P5 cells. Error bars denote mean+SEM. N = 6-8 per group. *P < 0.05 compared to P0. $^{\#}P$ < 0.05 compared to all other groups.

To further screen the effects of the bFGF-based cell expansion on engineered muscle properties, the bundle volume and cell number was reduced 4-fold without loss of force generating capacity. Muscle bundles made from the cells expanded in 5 ng/ml bFGF contained the highest percentage of cross-striated myofibers (Figure 4.7A), the most Pax7^{+} SCs and MyoG^{+} myofibers (Figure 4.6C and 4.7B) , and generated the highest contractile forces (Figure 4.6D) compared to all other bFGF groups. These structural and functional parameters were by 20-40% lower than those measured in bundles made of P0 cells (Figure 4.6C&D). Taken together, a 1000-fold expansion of freshly isolated neonatal cells yielded a potent myogenic cell population able to generate highly functional engineered muscle tissues.

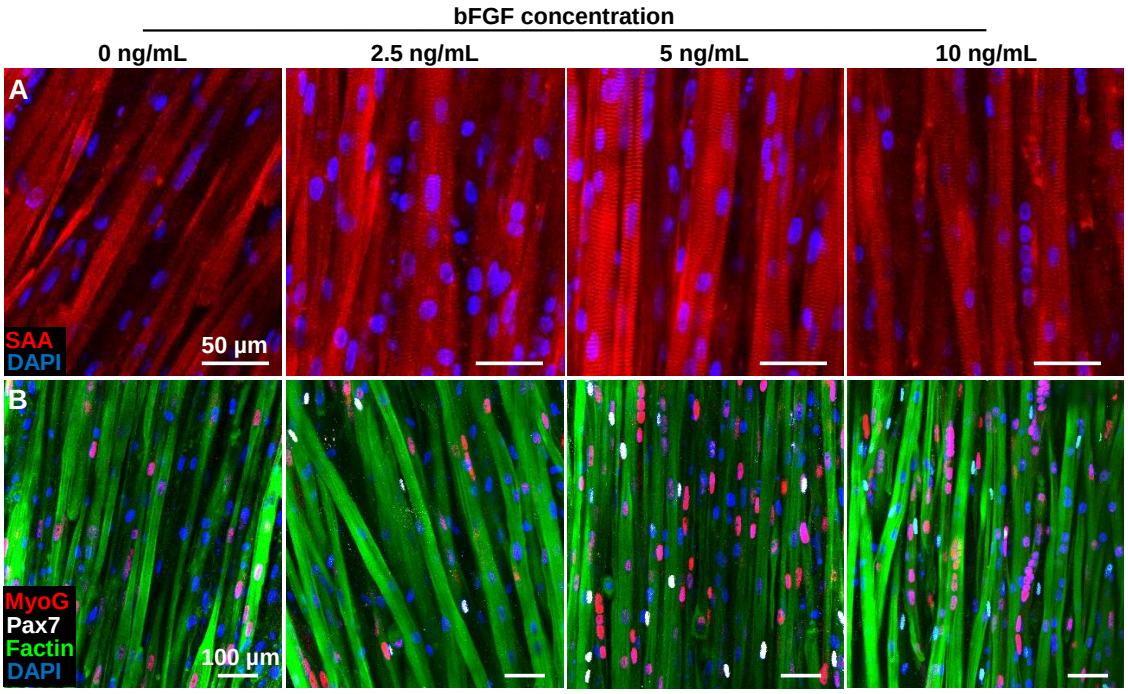

Figure 4.7 Engineered muscle from myogenic cells expanded in bFGF. (A-B) Representative images of (A) myofibers marked with sarcomeric α-actinin (SAA) and (B) the satellite cells (Pax7^{+}) and myonuclei (MyoG^{+}) in engineered muscle formed from myogenic cells expanded in 0, 2.5, 5, and 10 ng/mL bFGF for 5 passages.

4.3.4 Effect of Pax7^{+} SCs on in vitro regeneration

In order to confirm that self-repair capacity is correlated to the presence of Pax7^{+} SCs, engineered muscle bundles made from bFGF-passaged cells were tested in the CTX-injury assay as described in Section 4.2.2. Similar to the results with non-expanded (P0) SCs (Figure 4.5), expanded SCs showed the ability to activate in response to CTX injury with best myofiber regeneration found in bundles derived from cells expanded in 5 ng/mL bFGF (Figure 4.8). Pooling individual groups over multiple isolations, we plotted Pax7^{+} cell density against the increase in force 5 days post-CTX compared to immediately following injury (Figure 4.8). From the plot, it becomes clear that there is a relationship between SC number and regenerative potential within the engineered bundles.

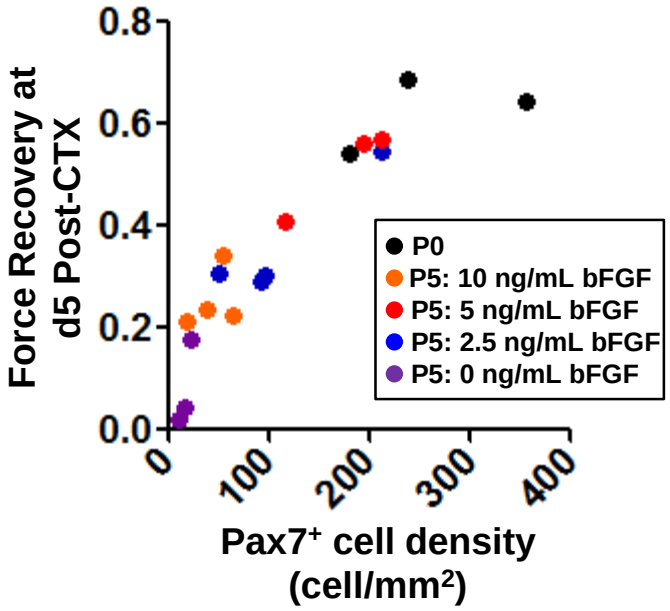

Figure 4.9 SCs and regeneration. Dependence of tetanic force recovery recorded 5 days post-CTX injury on Pax7^{+} cell density prior to injury shown for bundles made of P0 and P5 neonatal myogenic cells (expanded in various bFGF concentrations). Legend denotes corresponding color to P0 and P5 cells cultured in differing bFGF concentration. Each dot represents the mean of 1-3 bundles per 1 isolation.

4.3.5. Vascularization of implanted engineered muscle

In order to assess the ability of the engineered muscle to survive and vascularize *in vivo*, 2-week pre-differentiated (PreD) bundles were implanted into a dorsal skinfold window chamber in nude mice [182]. For this purpose, smaller 3-bundle constructs anchored within a single 9x9 mm square Cerex® frame that fit within the window chamber (Figure 4.10A) were generated. As a comparison group, undifferentiated (UnD) muscle bundles cultured for only 2 d without switching to differentiation media that contained sporadically fusing myotubes and high numbers of $Pax7^+$ and $Ki67^+$ cells (Figure 4.11) were implanted. Placing the engineered muscle between the thin panniculus carnosus muscle layer of the dorsal skin and a cover glass window allowed us to non-destructively, in live animals, track angiogenesis and perfusion of the muscle implant in real time. With time post implantation (PI), initially avascular muscle bundles underwent rapid invasion by host blood vessels (Figure 4.10B, yellow pseudo-colored region) at a rate that was greater in PreD than in UnD muscle implants, which showed apparent saturation of vessel ingrowth by 14 d PI (Figure 4.8C). Importantly, all ingrown capillary networks appeared functional and perfused by host blood flow (evident from red blood cell motion) as early as 7 d PI. Interestingly, while asynchronous spontaneous twitches recorded at 2 week PI had no apparent effect on the blood flow through ingrown capillaries, occasionally observed spontaneous tetanic contractions appeared to transiently restrict blood perfusion. Immunostaining analysis (Figure 4.10D) further revealed randomly oriented vessel networks at the periphery of implanted muscle, while within the implant interior the ingrown capillaries co-aligned with surrounding myofibers to a degree (4.97 ± 1.8°) characteristic of native neonatal muscle (Figure 4.12). In addition, in transverse cross-sections, endothelialized vessel lumens were found

throughout the full thickness of the implants (Figure 4.10E). In agreement with intravital imaging analysis, cross-sectional lumen density in both PreD and UnD implant regions increased between 1-week (PreD: 170 ± 11 per mm^2, UnD: 75 ± 10 per mm^2) and 2-week (265 ± 30 per mm^2, UnD: 175 ± 18 per mm^2) PI and was significantly higher in PreD implants (Figure 4.10F). From cross-sectional immunostainings, the average rate of vascular ingrowth in PreD muscle bundles was 18.9 ± 2.1 vessels/mm^2/d. Further, mean lumen diameter increased with time PI, and after 2 weeks amounted to 7.1 ± 0.2 µm, similar to values measured in native hindlimb muscle (Figure 4.13).

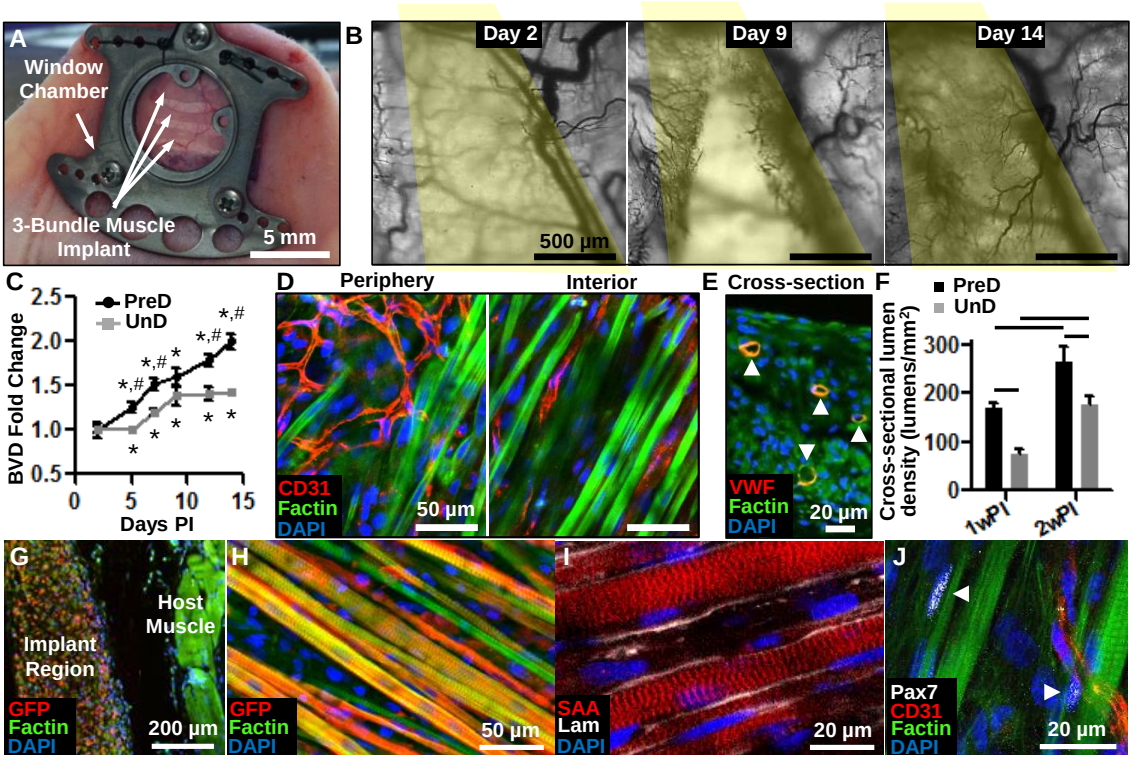

Figure 4.10 Vascular integration of implanted engineered muscle. (A) Implanted muscle patch within the dorsal skin-fold window chamber. (B) Images of total hemoglobin at d 2, 9, and 14 in window chamber (yellow = implant region). (C) Fold change in blood vessel density (BVD) in the implant region of pre-differentiated (PreD) and undifferentiated (UnD) bundles with time PI. (D) Vessel organization at the periphery and interior of muscle implant. CD31 labels endothelial cells. (E) Cross-section of the muscle implant showing lumens of ingrown blood vessels (arrowheads); VWF, Von Wilenbrand factor. (F) Increase of cross-sectional BVD from 1 week (wk) PI to 2 wk PI. Error bars denote mean ± SEM. N = 8-12 per group. *P < 0.05 from value at d 2, $^{\#}P$ < 0.05 between PreD and UnD groups at same time-point, P < 0.05 between denoted

groups. (G) Cross-section of implant region (GFP-positive myofibers) and underlying host muscle. (H-I) Longitudinal section of implanted bundle showing aligned and cross-striated myofibers (H) embedded in laminin matrix (I). (J) Pax7^{+} satellite cells (arrowheads) are found at the periphery of implanted myofibers.

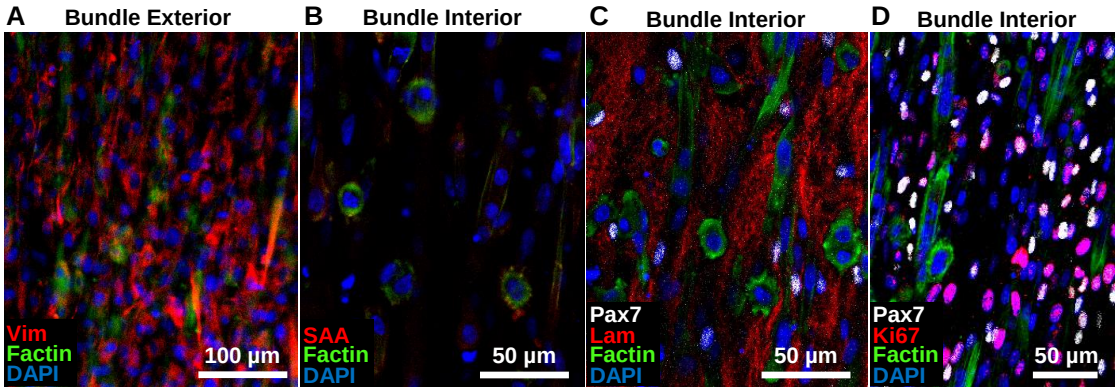

Figure 4.11 Structural characterization of 2-day old undifferentiated engineered (UnD) muscle bundles. (A) Vimentin (Vim)$^{+}$ fibroblasts were predominantly found at the exterior of the bundle. (B-C) Non-fused or newly fusing myogenic cells as well as short immature myotubes were found within the interior of bundle (B), along with Pax7^{+} cells and a laminin (Lam)-rich matrix (C). (D) Undifferentiated myogenic cells inside the bundle were highly proliferative, as evident by the abundant expression of Ki67.

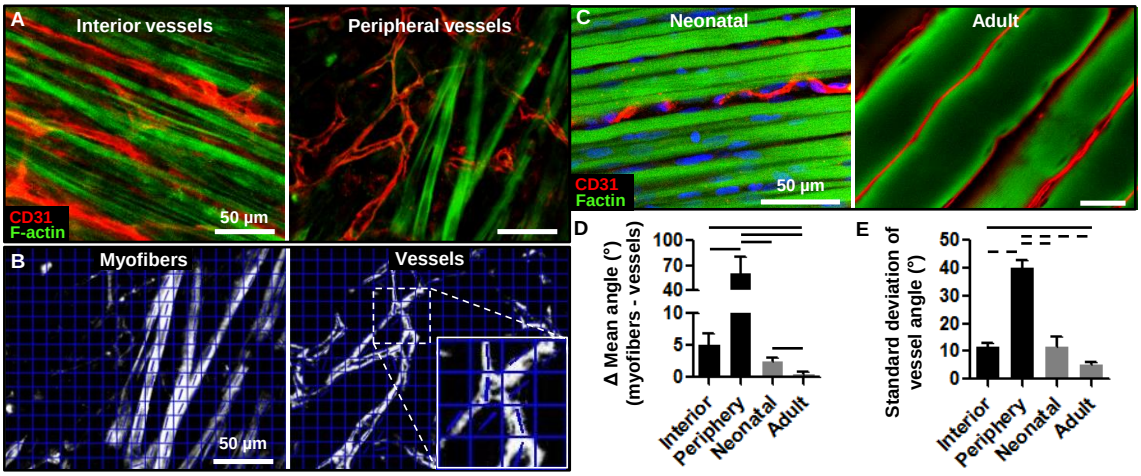

Figure 4.12 Vascular organization in implanted engineered muscle bundles. (A) Representative images of CD31^{+} blood vessels and GFP^{+} myofibers in the interior and periphery of the pre-differentiated (PreD) muscle bundles at 2 week (wk) post-implantation (PI). (B) Processed panel A (right) showing separated green and red channels with local myofiber and vessel directions quantified within individual 25x25 pixel (11x11 μm) regions. The close-up inset shows mean direction (angle) of alignment within each pixel denoted by a thin line. (C) Representative images of CD31^{+} vessels in the interior of neonatal and adult muscle. (D) Standard deviations of vessel alignment within the interior and periphery of the 2wk PI bundles and native muscles. (E) Mean angle differences between average myofiber and vessel directions of alignment. Error bars denote mean ± SEM. N = 4-8 samples per group, 8-10 images per

sample, $P<0.05$ and $P<0.001$ between groups denoted by solid and dashed horizontal lines, respectively.

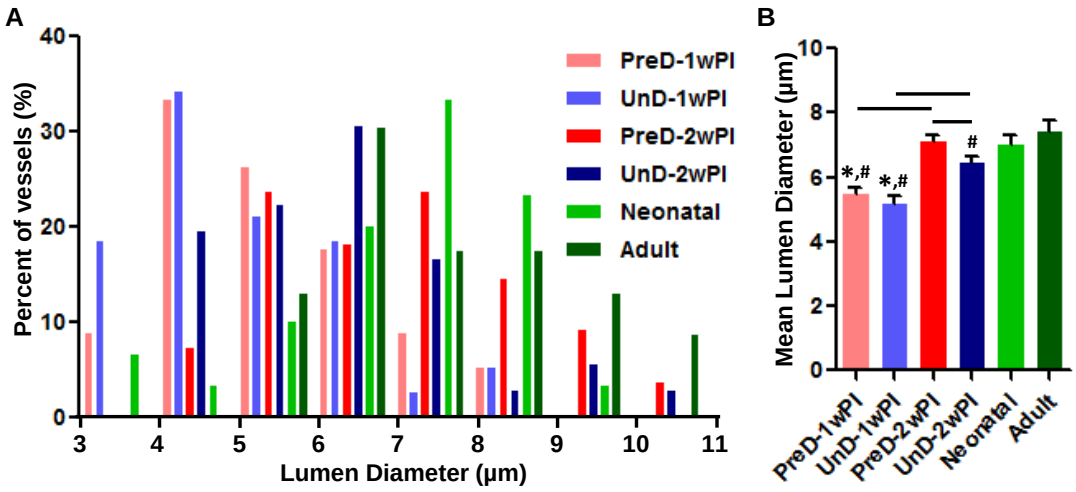

Figure 4.13 Capillary lumen diameters in implanted engineered muscle bundles. (A) Histogram distribution of lumen diameters within the implanted pre-differentiated (PreD) and undifferentiated (Und) engineered muscle at 1 (1wPI) and 2 weeks (2wPI) post-implantation (PI) as well in neonatal and adult hind limb muscles. Capillary lumen diameters were measured from cross-sectional images immunostained with F-actin and Von Willebrand Factor (example shown in Figure 3E). (B) Mean lumen diameters in 6 studied groups. Error bars denote mean ± SEM. N = 50-70 lumens per group. $^{*}P < 0.001$ compared to neonatal values, $^{\#}P < 0.05$ compared to adult values, and $P < 0.05$ between groups denoted by horizontal lines.

4.3.6 Myogenesis in implanted engineered muscle

After 2 weeks *in vivo*, implanted PreD muscle bundles (identified by GFP^{+} staining for GCaMP3) remained separated from the underlying host muscle and appeared to maintain pre-implantation volume and a structure consisting of aligned cross-striated myofibers surrounded by basal lamina proteins (Figure 4.10I). Importantly, the implanted myofibers remained abutted by $Pax7^{+}$ satellite cells at 2 week PI, suggesting continued myogenic capacity of engineered muscle *in vivo* (Figure 4.10J). Compared to pre-implantation values (i.e., 2 weeks *in vitro* culture (IVC)), PreD bundles at 1 week PI had less cross-striated myofibers (-40.0 ± 7%); however, by 2 week PI, virtually all myofibers exhibited cross-striations (Figure 4.14A&B) while the PreD myofiber diameter became significantly increased (+40.7 ± 5% relative to IVC). Control

UnD muscle bundles that prior to implantation showed only sporadic myofiber formation (Figure 4.11), underwent significant myogenesis over 2 weeks PI; however, their myofiber organization, alignment, diameter, and percent of cross-striated myofibers remained inferior to those of the PreD implants (Figure 4.14 and 4.15).

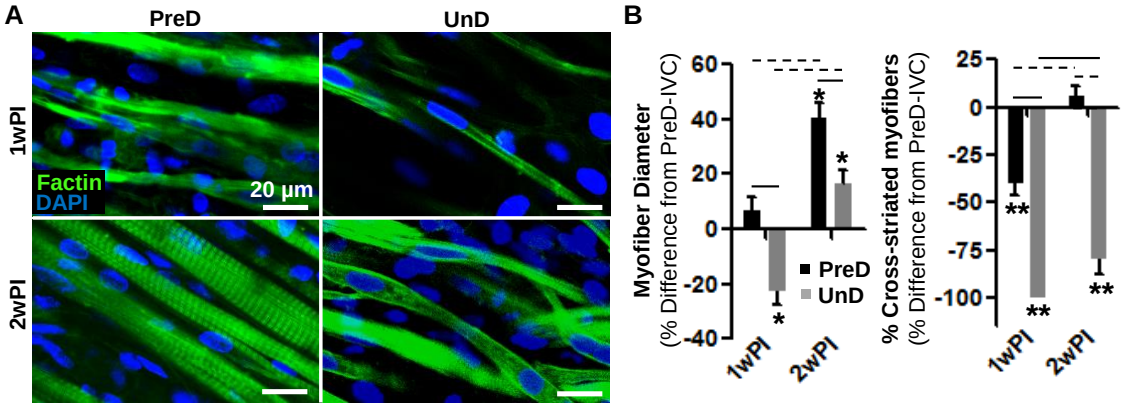

Figure 4.14 Myogenesis and structural differentiation of implanted engineered muscle bundles. (A) Representative images of myofibers within implanted pre-differentiated (PreD) and undifferentiated (UnD) muscle bundles at 1 (1wPI) and 2 weeks (2wPI) post-implantation. (B) Changes in myofiber diameter and percent of cross-striated myofibers relative to values in PreD bundles cultured for 2 week in vitro (PreD-IVC). Error bars denote mean ± SEM. N = 8-12 bundles (10-20 measurements per bundle) per group; **P*<0.05 and ***P*<0.001 compared to PreD-IVC values; P<0.01 and P<0.001 between groups denoted by solid and dashed horizontal lines, respectively.

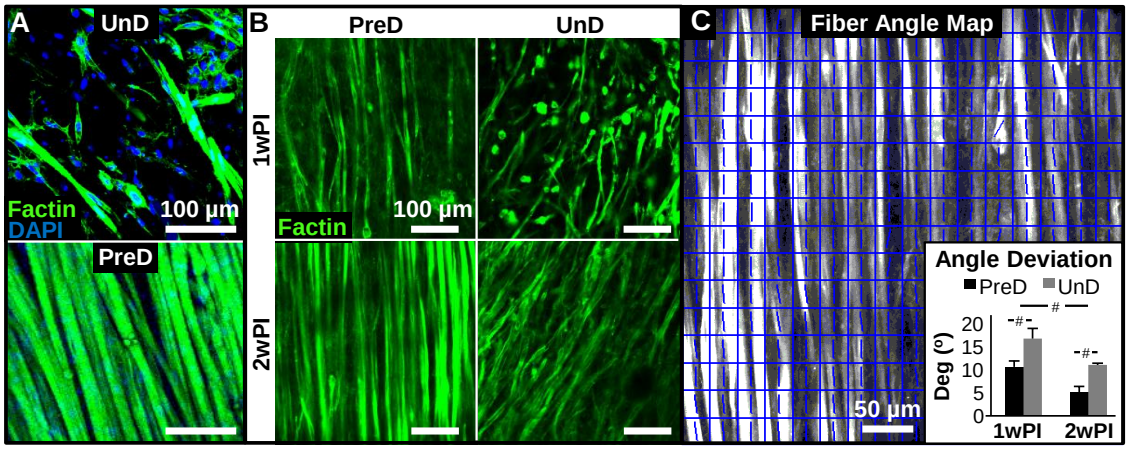

Figure 4.15 Myofiber alignment in pre-differentiated and undifferentiated implanted engineered muscle bundles. (A) Representative images of myofibers in undifferentiated (UnD) and pre-differentiated (PreD) engineered muscle bundles prior to implantation. (B) Representative images of myofiber alignment in PreD and UnD bundles at 1 (1wPI) and 2 weeks (2wPI) post-

implantation. (C) Example map of local myofiber directions within 25x25 pixel (11x11 μm) regions in a PreD bundle. Inset, average local angle deviation from mean myofiber direction (in units of deg). Note more uniform unidirectional alignment (smaller angle deviation) in PreD vs. UnD group. Error bars denote mean ± SEM N = 4 bundles per group, $^{\#}P < 0.01$.

4.3.7 Function of implanted engineered muscle

To non-destructively monitor viability and functionality of the engineered muscle *in vivo*, intracellular Ca^{2+} sensor GCaMP3 [177] was lentivirally-transduced in isolated myogenic cells which allowed recording of spontaneous and electrically-induced Ca^{2+} transients in muscle implant by measuring GCaMP3 fluorescence (ΔF/F, Figure 4.3A-E). Intravital GCaMP3 fluorescence movies during spontaneous twitching of implanted muscle (Figure 4.16A) revealed that after an initial lag period of ~7 d, the PreD muscle implants exhibited a steady increase in Ca^{2+} transient amplitude (Figure 4.16B). The UnD implants, with limited functionality at 2 days PI, also exhibited a steady increase in spontaneous activity and amplitude of Ca^{2+} transients (Figure 4.16B). Measurements of electrically-induced Ca^{2+} responses in explanted muscle showed that at 2 weeks PI, both PreD and UnD muscle bundles displayed significantly greater Ca^{2+} transient amplitudes compared to their IVC and 1 week PI counterparts (Figure 4.16C). Kinetics of GCaMP3 Ca^{2+} transients were not significantly changed between 1 and 2 weeks PI and were comparable between the two implant groups (Figure 4.17A).

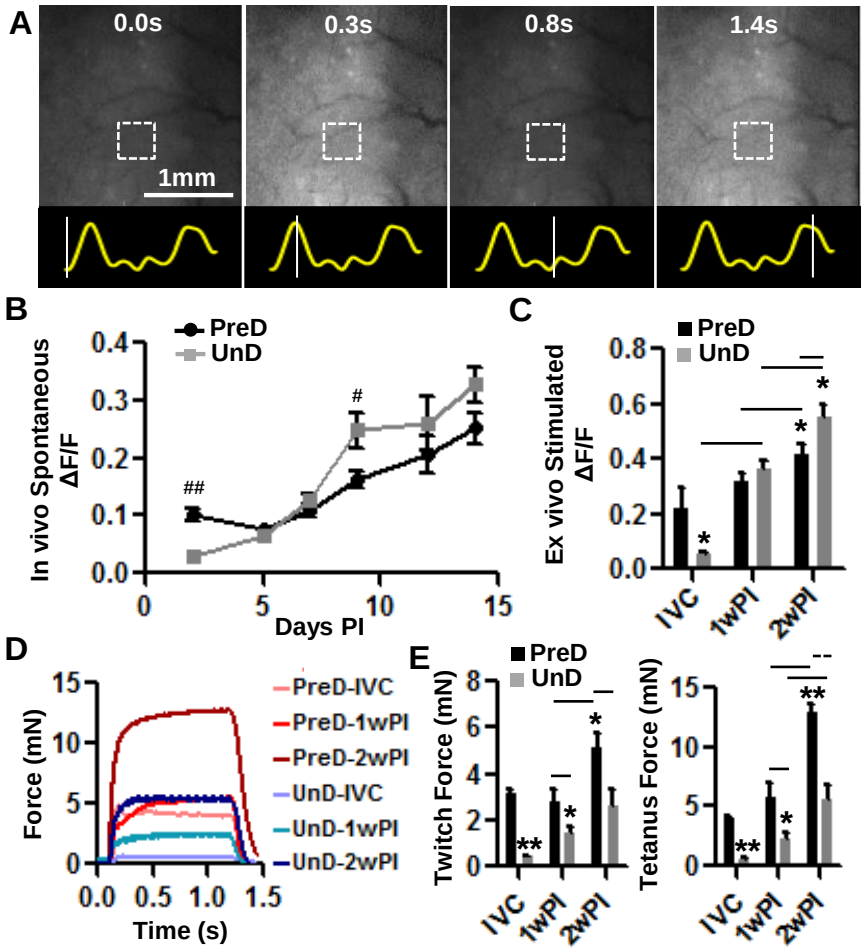

Figure 4.16 Calcium transients and force generation of implanted engineered muscle. (A) Representative intravital snapshots of a GCaMP3 movie recorded during spontaneous activity of an implanted muscle bundle. Traces below panels show time course of GCaMP3 signal from a small bundle region (square) with lines denoting the snapshot times. Average amplitudes of in vivo spontaneous (B) and ex-vivo electrically-induced (C) GCaMP3 transients in implanted PreD and UnD engineered muscle with time PI. IVC, 2 week (wk) of in vitro culture, prior to implantation. Representative tetanus force traces (D) and quantified (E) twitch and tetanus force amplitudes for PreD and UnD muscle cultured in vitro (IVC) or explanted at 1 wk PI and 2 wk PI. Error bars denote mean ± SEM. N = 6-12 bundles per group. $^{\#}P < 0.05$ and $^{\#\#}P < 0.001$ between PreD and UnD group at same time-point; $^{*}P < 0.05$ and $^{**}P < 0.001$ compared to PreD IVC group; $P < 0.05$ and $P < 0.001$ between groups identified by horizontal solid and dashed lines, respectively.

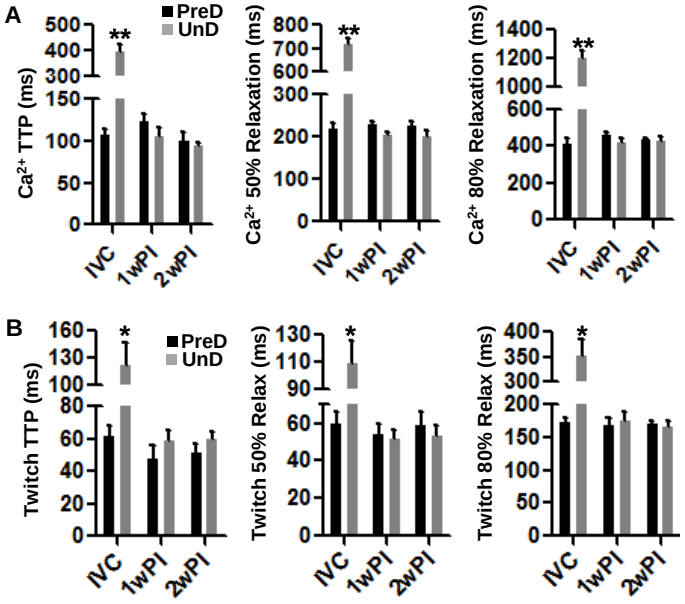

Figure 4.17 Kinetics of electrically-induced calcium transient and twitch force responses in engineered muscle bundles. (A-B)Time-to-peak (TTP), 50% relaxation, and 80% relaxation times of (A) recorded GCaMP3-calcium transients and (B) measured twitch forces during 1 Hz electrical stimulation in pre-differentiated (PreD) and undifferentiated (UnD) in vitro (IVC) patches and patches explanted at 1 (1wPI) and 2 weeks (2wPI) post-implantation. Error bars denote mean ± SEM. N = 6-10 bundles per group. ***P*<0.0001 and **P*<0.05 compared to all other groups.

Since the implanted engineered muscle underwent robust vascular integration with the host dorsal skin, it could not be separated from the skin without being damaged. Therefore, to eliminate host contribution to the measured contractile force, engineered muscle bundles were implanted in the direction perpendicular to that of the host panniculus carnosus muscle layer (Figure 4.3F-H). Functional measurements in 1 and 2 weeks explants revealed robust contractile force responses in both UnD and PreD groups (Figure 4.16D). Specifically, implanted engineered UnD muscle steadily increased its force generating capacity *in vivo*, and after 2 weeks PI reached values similar to those measured in the PreD group prior to implantation (Figure 4.16E). The implanted PreD muscle showed no enhancement in contractile force generation during first week PI; however, its force generating capacity significantly increased by 2 weeks

PI, reaching tetanus amplitudes 3.2-fold higher than the pre-implantation values. This significant increase in the absolute contractile force amplitude was associated with a ~3.8-fold increase in specific force, which at 2 weeks PI averaged 65.7 ± 8.9 mN/mm^2. Similar to Ca^{2+} transients, the kinetics of force generation in muscle implants did not significantly change between 1 and 2 weeks PI and was comparable between the two implant groups (Figure 4.17B). Overall, measurements of both Ca^{2+} transient and active force generation suggested that in addition to robust vascularization, implanted engineered muscle underwent significant enhancement of contractile function *in vivo*, beyond what was achievable *in vitro*.

4.4 Discussion

The optimization of the myogenic cell source and culture conditions in chapter 3 allowed us to engineer 3D skeletal muscle tissues with structure, cellular composition and force generating capacity characteristic of native neonatal muscle. In this chapter, we further examined the functionality of satellite cell (SC) pool in engineered muscle bundles and assessed the potential of bundle implants to survive, vascularize, and undergo continued myogenesis *in vivo*.

4.4.1 Characterization of satellite cell pool

To our knowledge, this was the first described maintenance of a functional SC pool in engineered [9, 10, 14, 18, 21, 156, 180, 186]. The goal of this section was to explore if following muscle differentiation, the SCs would attain a homeostatic quiescent state but remain capable of supporting a robust regenerative response in the case of injury [1, 202]. In section 3.3.8, we noticed that over 4 weeks in culture SCs incorporate into myofibers, increasing the myonuclei number to mature the muscle (Figure 3.13). These results put in question the ability of the SCs to find a steady niche which in

necessary the cell to undergo a proper response to regeneration [1, 40]. Similar to results in section 3.3.6, a vast majority of SCs after the bundle formation were proliferating as evidenced by co-expression of Pax7 and Ki67 (Figure 4.4A-B). It is also clear that the myogenic population has yet to commit to differentiation, marked by their expression of MyoD and little expression of MyoG (Figure 4.4C-D). However, by day 14 in culture, the SC pool shifted from a proliferative to a quiescent state, losing Ki67 expression, and most of the myogenic precursors fully differentiated into a myonuclei fate, gaining MyoG and losing MyoD expression (Figure 4.4). At this point, it is clear that the myogenic population in the engineered tissue is at a relatively homeostatic state, consisting of either committed, post-mitotic myonuclei or quiescent SCs. In addition to their non-proliferative state, SCs in natural muscle are marked by the specific niche constituents. As mentioned in section 3.3.7, these cells are found beneath muscle-specific proteins found in the natural basal lamina of the tissue (Figure 3.12). Further, as revealed in Figure 4.18, which illustrates the formation of the SC niche in our engineered muscle, the SCs also express m-Cadherin, a link between the stem cell and the myofiber. M-Cadherin, a reliable marker of a quiescent satellite [1], is critical for cell

division activation in the regenerative response [215].

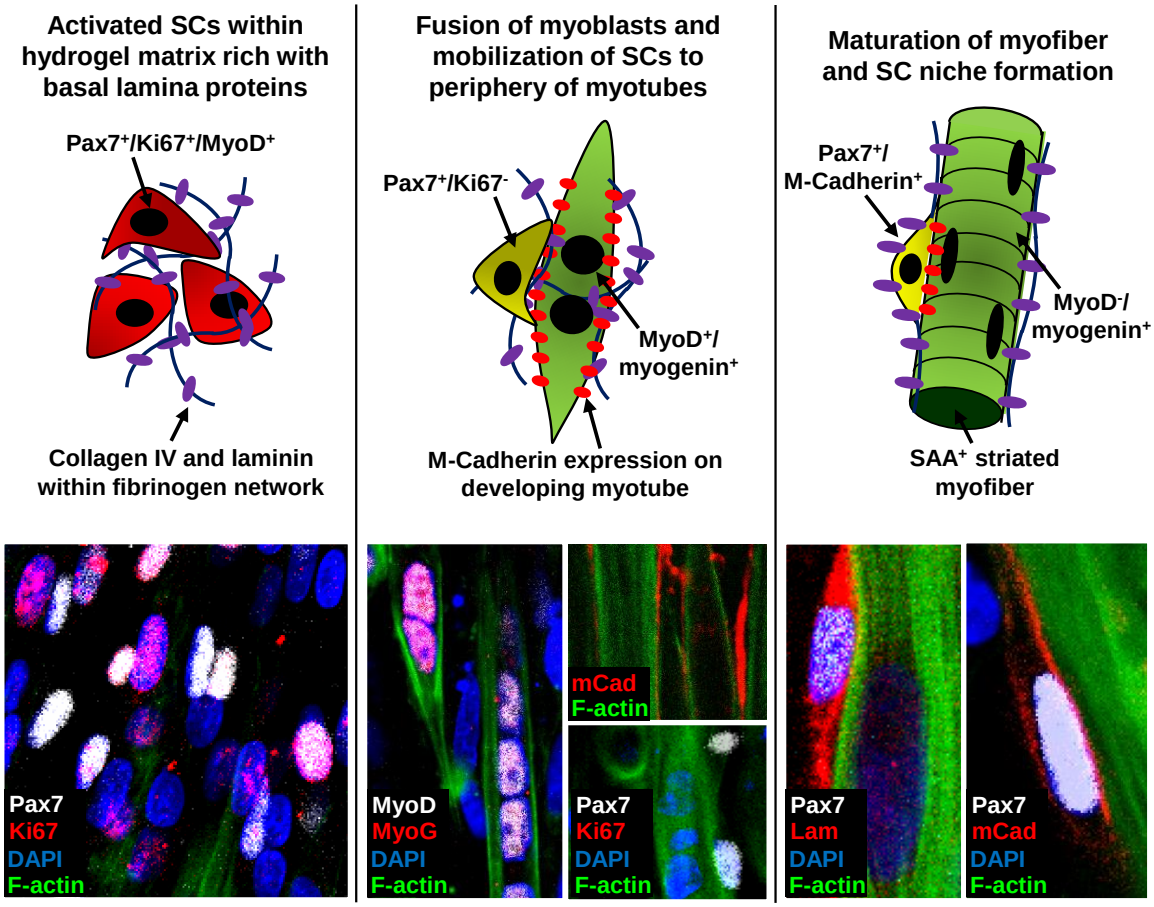

Figure 4.18 The formation of SC niche within engineered muscle tissue. Left, activated SCs, when embedded in a myoconductive 3D environment, will rapidly fuse. Middle, a subset of the cells will home to the membrane of the developing myotubes, link to M-cadherin, and cease to proliferate. Right, with time, the SCs will further build their niche on the mature myofiber by homing beneath the basal lamina, expressing m-Cadherin (mCad), and becoming quiescent.

4.4.2 In vitro regeneration of engineered bundles in response to CTX injury

After verifying that the SCs within in our engineered muscle were capable of forming an anatomical niche, we assessed their regenerative capacity by injuring muscle bundles with cardiotoxin (CTX). CTX injury is utilized frequently *in vivo* to activate and study the regeneration cascade in skeletal muscle [37, 80, 81]. As expected [212], CTX caused significant myofiber fragmentation and death and a decline in functional output

(Figure 4.5). SCs, which remained present in the tissue following injury, underwent a significant spike in number by day 5 post injury. The response was consistent with *in vivo* findings which report SC expansion starting as soon as 12 hours after injury and elevated $Pax7^+$ cell numbers lasting for approximately 7 days [213, 216]. Also similar to the natural process [213, 216], SC numbers reverted back down to healthy levels with little to no Ki67 expression at 10 days post-CTX. MyoD, which is not found in homeostatic muscle, marks either activated SCs or newly fused myogenic precursors [2]. In natural muscle, MyoD expression begins to peak at 2 days post-injury during SC proliferation, remains elevated for 7 days, and then disappears as differentiation is complete [213, 216, 217]. Our immunostaining results show a similar time course with transient MyoD expression at 5 days and limited expression at healthy and 10 days post-CTX (Figure 4.5). Of note, it is clear from the staining that $MyoD^+$ cells are either on the periphery of myofibers, marking activated SCs, or centrally-located within a myofiber, marking a newly-fused myonuclei.

Maturation following regeneration can be assessed through myogenin expression, growth of myofibers, and the reformation of sarcomeric structures. Myogenin expression marks committed myoblasts or fully-differentiated myonuclei. The marker begins to rise after 3 days in natural muscle and undergoes a steady increase until day 7 [213, 216, 217]. During this period, a portion of the expanding SC pool is differentiating into myogenic cells primed for fusion to restore the myonuclei lost during injury; thus gaining myogenin [2]. Within our engineered muscle, we see a similar progression as $myogenin^+$ cells, which are significantly lost upon CTX, steadily increase in number up to day 10 post-CTX (Figure 4.5). As mentioned, the addition of new myonuclei enables enhanced protein synthesis within the myofibers and enables the regrowth of these

contractile cells [173]. The extension of the fibers is through a process known as myofibrillogenesis, in which intermediate “premyofibrils” sprout to elongate the cell parallel to the long axis, normally occurring upon the onset of regeneration [218, 219]. These transient filaments are then replaced as the mature, actin-myosin contractile apparatus, or sarcomere, is formed in a process known as sarcomerogenesis [220]. The restoration of the sarcomere, which upon completion results in the striated pattern of myosin and actin, is initiated roughly 4 days following injury [218-220]. In our system we see evidence of both myofibrillogenesis and sarcomerogenesis. Parallel to the increase in mature myonuclei, myofibers undergo a stable regrowth and elongation, restoring healthy fiber density by day 5 post-CTX. At this time, however, the contractile properties of the engineered tissue are not recovered. It is not until a high percent of the myofibers within the regenerating tissue contain sarcomeric structures when the injured muscle is able to generate forces approaching healthy levels.

These results, to our knowledge, for the first time describe engineered muscle constructs capable of self-repair mimicking that of native skeletal muscle. The model has potential to facilitate systematic studies of SC fate during muscle growth, exercise, injury, or disease [1, 58].

4.4.3 Importance of satellite pool for in vitro regeneration

Following the observation of a natural SC response to injury, we wanted to evaluate engineered muscle regenerative capacity with the use of expanded cells. Through assessment of passaging methods we sought to 1) identify optimal conditions for future work with adult cells, a source in which expansion is necessary [127], and 2) vary the amount of SCs in our engineered muscle to determine the influence of the pool on regeneration. We employed an expansion protocol to control the extent of myogenic

differentiation and induce proliferation with the supplementation of bFGF ranging from 0 to 10 ng/mL [2, 134]. As expected [134, 152], increased concentration of bFGF for 5 passages (P5) resulted in greater retention of $Pax7^+$ and total myogenic cells ($MyoD^+$). However, compared to P0, even under optimal conditions (10 ng/mL), the maintenance of $Pax7^+$ cells was significantly lower at P5 in monolayer culture (Figure 4.6B). As previously reported, this can be expected with the expansion of myogenic cells as regeneration capacity, and Pax7 expression, is lost [78, 81, 150].

The implementation of expanded cells into engineered muscle resulted in functional and structural differences depending on the bFGF exposure. Interestingly, even though we recorded the greatest amount of $Pax7^+$ cells in culture in the 10 ng/mL group, it was the 5 ng/mL groups that reported the greatest retention of these cells in 3D (Figure 4.6C and 4.7B). Additionally, 5 ng/mL constructs also contained the greatest amount of mature $myogenin^+$ cells (Figure 4.6C and 4.7B), had the highest instance of striated myofibers (Figure 4.7A), and generated the most force (Figure 4.6D). Similar to the work using freshly isolated and the adherent fraction of myogenic cells, we see a case in which a less differentiated myogenic population results in reduced maintenance of SCs. It is clear that the importance of early fusion events in dictating SC retention can be applied to these results as well. Even though maintenance of $Pax7^+$ cells in culture is necessary, as seen in the 0 ng/mL group, a mixed population of SCs and mature myogenic cells are ideal for initiating fusion events and the subsequent homing of SCs. Further, as discussed previously and shown in Figure 3.9 and 3.10, a fibroblast population is crucial to induce early compaction, again enhancing fusion by increasing cell-cell contact. The $MyoG^+$ cell density, force production, and noticeable enhanced myofiber density in 5 ng/mL bFGF-derived bundles suggest greater fusion potential of

these cells and supports the claim that enhanced fusion leads to better retention of SCs, as shown in Figure 3.6.

4.4.4 Implantation of engineered muscle

To explore the fate of engineered muscle *in vivo*, we combined GCaMP3 transduction with dorsal window chamber studies in live mice and non-invasively monitored the ability of implanted engineered muscle to spontaneously contract, generate Ca^{2+} transients, and undergo blood perfusion over a 2 week period post-implantation (PI). The tissues were explanted at 1 and 2 weeks PI at which point functional and histological assessments were made. Besides simply observing if our pre-differentiated, tissue-engineered construct could survive *in vivo*, we wanted to compare its effectiveness as an on-site therapeutic with the implantation of undifferentiated myogenic cells.

4.4.4.1 Vascularization of implanted tissue

Implanted engineered muscle, showing no evidence of vascular cells at the time of implantation became progressively infiltrated with host blood vessels and, as evidenced by video-imaging, actively perfused with readily discernible blood cells by 7 days PI. By day 14, the vessel density within the PreD muscle implant (265 ± 30 vessels per mm^2) was comparable to that previously reported for implanted tissue-engineered muscle with pre-formed vascular structures [156] demonstrating that purely angiogenic vessel ingrowth was sufficient to support the *in vivo* survival and function of small size avascular engineered muscles used in our study. On the other hand, successful survival of large engineered muscles implants will likely require the development of novel methods for *in vitro* fabrication of highly aligned, functional, and pre-vascularized skeletal muscle tissues. Related, our preliminary data demonstrate that simple co-encapsulation

of myogenic and endothelial cells may significantly impair contractile function of engineered muscle, suggesting that angiogenic vessel ingrowth rather than simple vasculogenesis may be a desired mode of engineered muscle vascularization, compatible with the formation of biomimetic muscle architecture and function *in vitro*.

4.4.4.2 Benefit of pre-differentiated muscle implant

Previously, various cell-based approaches have been explored for treatment of muscle injury or disease [1]. Specifically, implanted freshly isolated SCs were found to fuse to existing myofibers, rescue contractile function, and, by homing to the host niche, enhance muscle capacity for endogenous self-repair [78, 80, 81]. Still, without development of more efficient methods for their expansion *in vitro* [37, 221], implanted SCs may not be able to undergo timely myogenesis to successfully repair large muscle loss [24] . Implanting readily expandable myoblasts or pre-differentiated myofibers may accelerate *in vivo* myogenesis, while co-delivery of growth factors may improve cell survival and engraftment [111], however, without SCs, such strategies are likely to provide a limited support for future regenerative events [37, 78, 80]. In this section, we compared the post-implantation fate of PreD muscle constructs consisting of differentiated myofibers and functional SCs with UnD constructs consisting of undifferentiated, proliferative myogenic cells. We found that PreD implants not only exhibited superior structural and functional maturation, evidenced by larger myofiber diameter, percent cross-striations, and contractile force (Figure 4.14 and 4.16D&E), but also attracted significantly more neovessel ingrowth than UnD implants (Figure 4.10C&F), possibly due to the increased metabolic demand of more functional myofibers [222]. Although these studies utilized a small implant size inadequate for therapeutic muscle replacement, they suggest potential benefits of implanting a functional

engineered muscle in which mature myofibers provide niche-like environment for SCs compared to sole use of undifferentiated myogenic cells.

4.4.4.3 Continued functional and structural maturation of implanted muscle

Despite a steady increase in vascularization (Figure 10C), the amplitude of spontaneous Ca^{2+} transients in engineered muscle implants started to steadily increase (and correlate with vascular ingrowth [223]) only after an initial lag period of 1 week (Figure 4.16B). Furthermore, the percentage of cross-striated fibers in PreD implants at 1 week PI was decreased compared to the pre-implantation values (Figure 4.14A). This adaptation period may have resulted from potential tissue damage caused by initial hypoxia upon implantation into the dorsal window chamber and/or disruption of cell-matrix interactions caused by increased fibrinolysis (in the absence of the antifibrinolytic supplement amino-caproic acid present *in vitro*) [10]. Nevertheless, by 2 weeks PI, continuous vascularization, myogenesis, and differentiation of the PreD implants led to a ~3-fold increase in force generating capacity compared to pre-implantation values (Figure 4.16E) yielding specific contractile forces of ~70 mN/mm^2. This *in vivo* recovery of the engineered muscle function and structural organization followed a similar time-course to that observed *in vitro* upon CTX-induced injury. Along with the maintenance of aligned, cross-striated myofiber architecture (Figure 4.10I) and satellite cell pool (Figure 4.10J), vascularized engineered muscle implants in our study, for the first time to our knowledge, exhibited structure, contractile function, and myogenic capacity representative of post-neonatal skeletal muscle.

4.5 Summary and Implications

In this chapter, we reported the ability of our neonatal-derived engineered skeletal muscle model to recapitulate the regenerative *in vitro* and vascularize and

mature upon *in vivo* implantation. The capability of the SCs within the constructs to respond to injury through activation, proliferation, and differentiation to stimulate muscle regrowth was, to our knowledge, the first demonstration of 3D muscle tissue regeneration in an *in vitro* setting. Further, while initially avascular, these engineered muscle tissues underwent robust vascularization and perfusion, and exhibited continued myogenesis and improved contractile function *in vivo*, all of which were significantly enhanced by myogenic pre-differentiation of tissue constructs in culture. Together, these results lay a foundation for novel *in vitro* and *in vivo* studies of skeletal muscle function, regeneration, and vasculogenesis and provide a blueprint for future engineering of 3D functional human muscle microtissues for drug and toxicology studies [224, 225].

5. Engineering highly functional muscle tissues derived from adult cell isolates capable of self-repair and survival in vivo.

5.1. Rationale and experimental plan

The goal of this chapter was to transition from the use of neonatal to adult rodent cells to better model potential therapeutic scenarios expected to predominantly use adult cell sources. Isolating adult myogenic cells presents greater challenges as the SC percentage is reduced in mature compared to neonatal tissue [173] (Figure 3.13C) and muscle has a diminished capacity for regeneration [38, 150]. For any clinical applications, isolated SCs would require significant expansion that is known to negatively impact their self-renewal and myogenicity [37, 78, 80]. We thus systematically optimized conditions to enhance the maintaince of the SC pool in culture and within engineered muscle and, supplementat additional cues to enhance the regenerative capacity of engineered muscle. Our hypothesis was that maximizing the number and function of satellite cells in adult-derived engineered muscle tissues would optimally support their myogenesis, functional maturation, and self-repair potential.

First, optimized conditions for neonatal myogenic cell expansion determined in section 4.3.3 were applied to generate adult-derived tissue and the regenerative capactiy of such constructs was evaluated. As the baseline regenerative potenital of adult-derived bundles was expected to be less than that of their neonatal counterparts we also applied previously identified soluble factors during cellular expansion to further limit SC differentation [152] and enhance SC number prior to engineered muscle formation. In parallel, we attempted to promote the activity of SCs following injury with supplementation of pro-regenerative soluble factors [226-228] or immune system cells

(i.e. macrophages [27]). To increase the throughput of our studies, we modified the regeneration assay, introduced in section 4.2.3, to incorporate a real time indicator of calcium concentration, GCaMP6, and used a live-cell imaging system to non-invasively monitor recovery following injury. Mechanisms of injury response in this system were further studied by assessment of cellular proliferation, apoptosis, and paracrine signaling as described in chapter 4.

Finally, we assessed the fate of adult-derived engineered muscle tissues in dorsal window chamber implantation model by a non-destructive, real-time monitoring of implant vascularization and function, as described in 4.2.4. We hypothesized that regenerative adult-derived muscle constructs harboring population of macrophages will be better suited for *in vivo* vascularization and survival. Specifically, as implanted constructs in window chambers undergo an initial period of ischemia that results in functional loss (Figure 4.16) and myofibril destruction (Figure 4.14A), we expected that the self-regenerative capacity of constructs optimized *in vitro* will enhance their chances for *in vivo* survival until onset of perfusion through ingrown capillaries.

5.2 Methods

5.2.1 Myogenic cell preparation

Skeletal muscle tissue was isolated from the lower hind limbs of adult Sprague-Dawley rats (~10 weeks old) using the method described in Section 3.2.1 with a digestion time of 3 hours. Myogenic cells used for *in vitro* regeneration assay and implantation studies were transduced by a lentivirus in which GCaMP6 expression was driven by a MHCK7 promoter for 24 h following initial cell seeding. Adult myogenic cells were expanded for up to 5 passages in 5 ng/mL bFGF or, in attempt to enhance SC yield, in a cocktail of 4 rat recombinant growth factors: Tnfα (10 μM, R&D Systems),

IFNγ (10 µM, R&D Systems), IL-1α (5 µM, R&D Systems), and IL-13 (5 µM, R&D Systems). Expanded cells were quantified for the presence of myogenic cells ($Pax7^+$, $MyoD^+$, $Ki67^+$, and $MyoG^+$).

5.2.2 Bone marrow-derived macrophage isolation and differentiation

Bone marrow-derived macrophages (BMDMs) were derived from the in vitro differentiated bone marrow monocytes using methods adapted from published mouse protocols [52, 229, 230]. Specifically, following the removal of the hindlimb muscle used for myogenic cell isolation, each lower leg was cleared of surrounding tissue, sectioned above the knee, washed twice in 70% EtOH and once in PBS, before two cuts were made in tibia at the knee and at the junction of the fibula. The cuts exposed the bone marrow which was flushed out with BMDM media using a 20 gauge needle. Following disassociation of the marrow, it was strained and plated onto non-tissue culture plastic petri dishes at a density of 1 leg/150 cm^2. BMDM media consisted of high glucose DMEM, 20% FBS, and 30% media (LCCM) condition during 5-day culture of L929 cell line in high glucose DMEM with 10% FBS. A key component of LCCM is macrophage colony-stimulating factor (M-CSF) which drives the differentiation of monocytes towards a macrophage phenotype i*n vitro* [53]. The bone marrow-derived cells were cultured for 7 days in BMDM media to allow differentiation with additional media being added at day 3. Differentiation of adherent cells was confirmed through staining with macrophage-specific antibody CD68. After 7 days in culture, differentiated BMDMs were washed twice in warm PBS and dissociated with 0.05% Trypsin before mixing with myogenic cells and making of co-cultured engineered bundles. All muscle bundles with incorporated BMDMs were cultured in a media containing 30% LCCM to maintain cell survival.

Isolation of bone marrow-derived mesenchymal stem cells (BM-MSCs) was performed using similar methods as described above for BMDMs. However, bone marrow cells, upon removal, were subjected to a low glucose DMEM medium with 10% FBS and seeded onto tissue culture plastic as described in literature [231]. MSCs were identified using a Thy-1, or CD90, antibody [232]. Similar to BMDMs, BM-MSCs were washed twice in warm PBS and dissociated with 0.05% Trypsin before being used in engineered muscle.

5.2.3 BMDM polarization

Macrophage polarization techniques were utilized to achieve pro- and anti-inflammatory phenotypes. The described procedure of macrophage differentiation in 5.2.2 was used to derive the non-polarized M0 phenotype [52, 53]. Following differentiation into M0 macrophages, we subjected the cells to specific soluble factors to induce polarization into the pro-inflammatory, M1, or anti-inflammatory, M2,macrophages. Rat recombinant IFNγ (50 ng/mL, R&D Systems) and lipopolysaccharide (LPS, 100 ng//mL, Sigma) were used to induce M1 and IL-10 (10 ng/mL, R&D Systems) was used to induce M2 polarization, respectively [52, 233]. The introduction of polarized BMDMs into the engineered tissues was accomplished by two methods. The first method involved the polarization of the BMDMs in 2D culture prior to the incorporation of the cells into the muscle constructs. The second method polarized the BMDMs once already embedded in the tissue. This was achieved by making the constructs with M0 BMDMs and subjecting the constructs to polarizing factors after 10 days of 3D culture. In each case, cells were exposed to IFNγ and LPS or IL-10 for 24-48 hours.

5.2.4 Engineered muscle formation and culture

All engineered muscle constructs in this section were generated in smaller, 2-bundle molds (7 mm long, 2 mm diameter) to enable higher throughput studies. All engineered muscle bundles were cultured under dynamic conditions as described in 3.2.2 and had a density of 15 million cells/mL. Frames with bundles were removed from molds 2 days following bundle formation and left to free float in media thereafter. For co-cultured bundles, BMDMs or BM-MSCs were added to the myogenic population at a ratio of 1:6. For paracrine studies, one bundle in a well contained both muscle cells and BMDMs and the other contained just muscle cells. LCCM was supplemented to all culture media at 30%.

5.2.3 Real-time in vitro regeneration assay

In order to track functional regeneration in live bundles, myogenic cells were transduced with MHCK7-GCaMP6 virus prior to bundle formation. At day 10 of culture, bundles were injured by applying 0.2 μM CTX for various durations. Functional and histological assessments, described in 4.2.3, were performed at 5, 10, and 15 days post-CTX along with measurements of cross-sectional myofiber area, cell proliferation, and apoptosis. Every 2-3 days of culture, GCaMP6-reported calcium transients in electrically stimulated muscle bundles were imaged in sterile conditions using Andor camera attached to a Nikon microscope placed within a gas and temperature controlled live imaging chamber. The muscle bundles were exposed to a train of stimuli (10 ms duration, 1 Hz, 100 V) and each bundle was recorded for 2 seconds to capture at least one calcium transient. A MATLAB script was created to recognize the bundle area in the stimulation movies and calculate dF/F, as described in Figure 4.3D. “Severe” injury of a

bundle was induced by exposing it to CTX until 75% of dF/F was lost (~5-7 hours), while "mild" injury involved 50% loss of signal after ~3-4 hours of CTX exposure.

5.2.4 Cellular proliferation assay

In order to track cumulative cell proliferation in muscle bundles, the modified thymidine analog, EdU (10 µM), was supplemented every day into the media following CTX injury. The EdU kit (ThermoFisher) includes a fluorophore capable of detecting the EdU once it has incorporated into newly synthesized DNA.

5.2.4 Supplementation of pro-regenerative and anti-apoptotic factors

Rat recombinant proteins were supplemented every day to engineered muscle at their working concentrations: IGF-1 (20 ng/mL, R&D Systems), IL-10 (20 ng/mL, R&D Systems), and granulocyte colony-stimulating factor, G-CSF (10 ng/mL, Peprotech). The anti-apoptotic factor Q-VD-OPh (1 µM, Sigma), a pan-caspase inhibitor, was supplemented daily up to 10 days after CTX injury.

5.2.5 Quantitative RT-PCR

Total RNA was extracted from monolayers or engineered bundles using the RLT lysis buffer provided in RNeasy mini kits (Qiagen). Total RNA (1-2 µg per 20µl reaction) was reverse transcribed using SuperScript™ II Reverse Transcriptase (Invitrogen). Quantitative PCR was carried out on CFX384 Real-Time PCR system (Bio-Rad) using Sso-Fast EvaGreen Supermix (Bio-Rad) according to the manufacturer's instructions. Relative expression levels were normalized to GAPDH and calculated using the $2^{-\Delta Ct}$ method. All primers were purchased from Invitrogen and are listed in Table 5.1.

Table 5.1 QT-PCR primer list

Gene	Forward	Reverse
CASPASE-3	5'-GGAGCTTGGAACGCGAAGAA	3'-ACACAAGCCCATTTCAGGGT
TNF	5'-CCCCCATTACTCTGACCCCT	3'-CCCAGAGCCACAATTCCCTT

5.2.6 Immunostaining

Cultured cells and engineered tissues were fixed and stained as described in section 3.2.3. Additional primary antibodies used in this section are listed below (Table 5.2). Methods described in section 3.2.3 for the quantitation of nuclear staining and myofiber area were also used in this chapter.

Table 5.2 Additional primary antibodies used in Section 5

Primary Epitope	Dilution	Supplier	Catalog no.
CD68	1:200	Abcam	Ab31630
CD206	1:200	Abcam	Ab64693
CD86	1:200	Abcam	Ab53004
iNOS	1:200	Novus	NB300-605
Cleaved Caspase-3	1:200	Cell Signaling	Asp175

5.2.7 Implantation of adult-derived engineered muscle bundles

All animal experiments were approved by the Duke University ACUC. Prior to surgery, nude mice (~10 weeks of age; 22-30 g) were anesthetized by intraperitoneal injection of ketamine (100 mg/kg) and xylazine (10 mg/kg). Specific surgical techniques associated with the dorsal window chamber implantation can be found in section 4.2.4. Post-operatively, the mouse was injected subcutaneously with buprenorphine (1 mg/kg) painkiller and let to recover on a heating pad.

5.2.8 Intravital imaging of blood vessels and intracellular Ca^{2+} transients

Intravital recordings were performed in anesthetized mice on day 2, 5, 7, 9, 12, and 15 post-implantation (PI). Mice were anesthetized by nose cone inhalation of isoflurane and positioned on a heating pad under a microscope objective. Detailed descriptions of intravital blood vessel and Ca^{2+} imaging are found in sections 4.2.5 and 4.2.6 and Figures 4.2 and 4.3.

5.2.9 In vitro and ex vivo functional testing

In vitro and *ex vivo* force and Ca^{2+} transient measurements were performed using the same methods described in detail in sections 3.2.4, 4.2.7, and 4.2.8. *In vitro* functional testing of engineered muscle occurred at day 10 of 3D culture, prior to CTX injury, and 5, 10, and 15 days post-injury. *Ex vivo* functional testing was performed following explantation of engineered muscle at days 5, 10, and 15 post-implantation.

5.3 Results

5.3.1 Formation of adult-derived engineered muscle

Based on the results with neonatal cells in section 4.3.3, myogenic cells were isolated from adult rat hindlimb muscles, expanded on Matrigel-coated flasks for 5 passages in the presence of 5 ng/ml bFGF, and used to form bundles. After 2 weeks of dynamic culture, the adult-derived engineered muscle bundles had overall structure similar to that of neonatal-derived muscle (Figure 5.1A) and consisted of highly aligned, $MyoG^{+}$ cross-striated myofibers surrounded by laminin-rich matrix and a pool of $Pax7^{+}$ SCs (Figure 5.1B&C). Compared to neonatal-derived bundles, adult-derived bundles exhibited smaller cross-sectional muscle area (Figure 5.1B). While fewer myofibers generated less total contractile force, the specific forces of adult- and neonatal-derived

bundles were comparable (~100 mN/mm^2, Figure 5.1C).

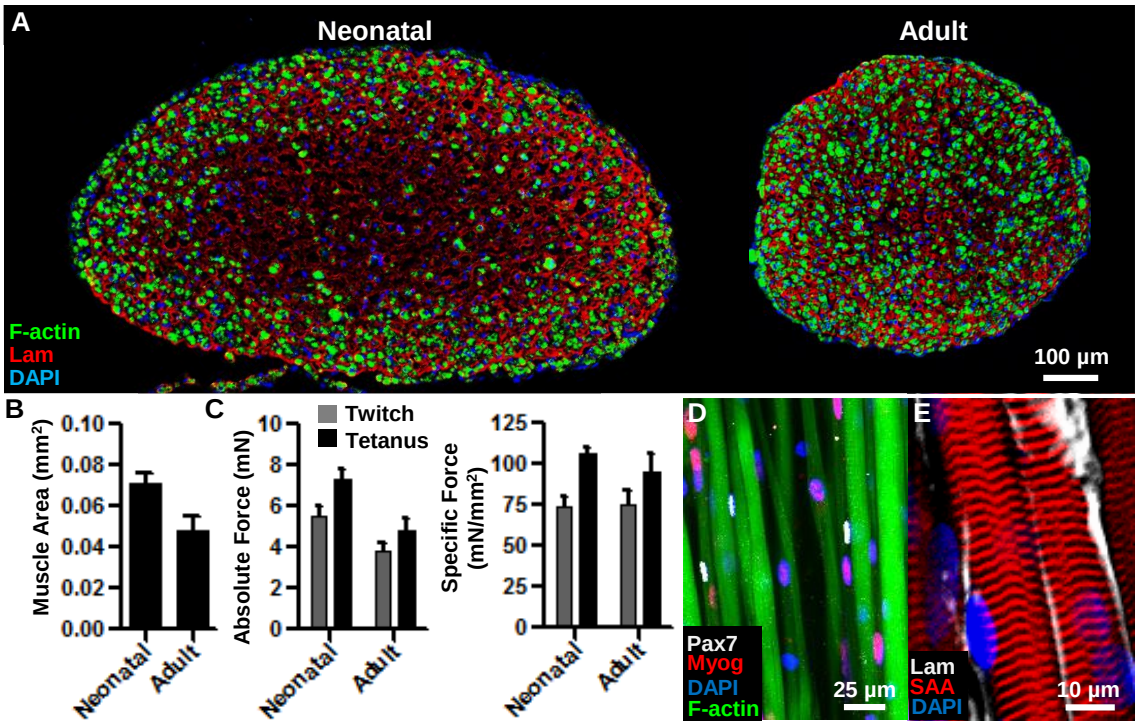

Figure 5.1 Adult-derived engineered muscle. (A) Cross-sectional images of neonatal- and adult-derived muscle showing myofibers and ECM protein laminin (lam). (B-C) Quantified (B) muscle area and (C) absolute and specific twitch and tetanus forces. (D-E) Confocal images showing (D) maintained Pax7$^+$ SC pool and (E) cross-striated myofibers (marked by sarcomeric α-actinin) within a basal lamina in adult bundles. Error bars denote mean + SEM. N = 6-8 isolations.

5.3.2 Regenerative ability of adult-derived constructs following CTX injury

To assess the regenerative ability of the adult-derived constructs, we utilized the same assay in section 4.3.2 involving the application of CTX to induce myofiber damage. Similar to the results of the neonatal-derived tissues (Figure 4.5A), CTX created an environment of fragmented myofibers (Figure 5.2A) and disrupted sarcomeric structures (Figure 5.2B). However, unlike the neonatal-derived muscle, the constructs were unable to recover myofiber area, myonuclei count, or sarcomeres at 5 or 10 days post-injury (Figure 4.2).

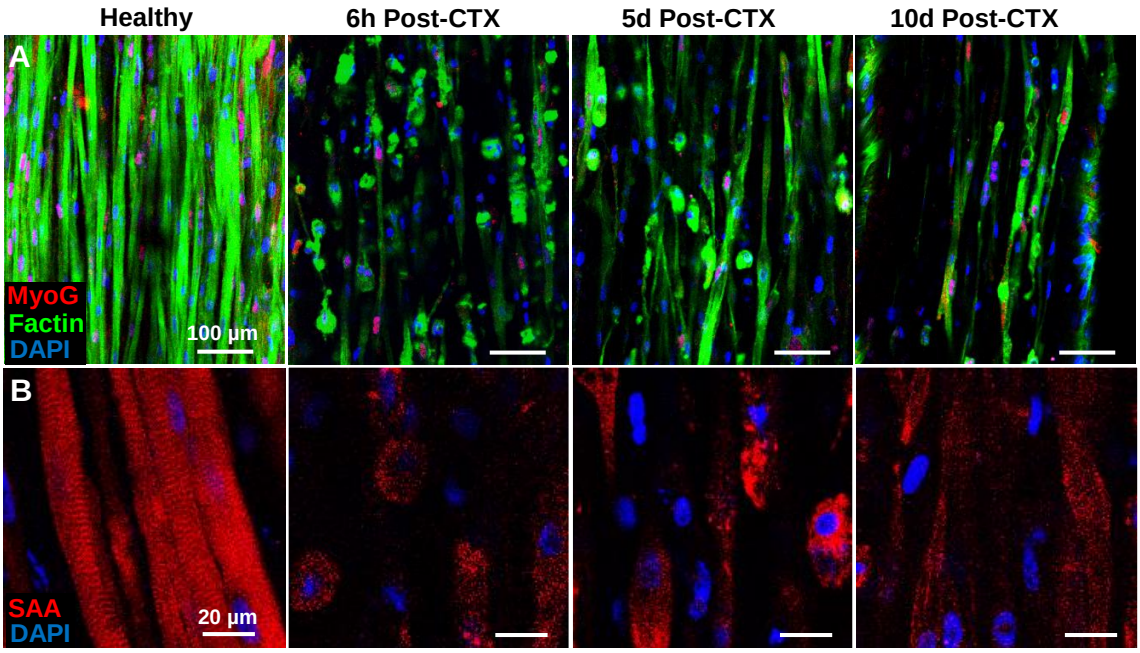

Figure 5.2 Adult-derived engineered muscle regenerative response. (A-B) Representative images of (A) myofibers and myonuclei, marked by myogenin (MyoG), and (B) sarcomeres, marked by sarcomeric α-actinin (SAA), in adult-derived engineered muscle in a healthy state and 6 hours, 5 days, and 10 days following CTX administration.

To reveal the reasons for the lack of regenerative response in adult-derived bundles, we compared the myogenic profile of the neonatal and adult cells following 5-passage expansion in 5 ng/mL bFGF. We found little difference between the fractions of $Pax7^+$ (neonatal: 0.25 ± 0.07, adult: 0.23 ± 0.04), $MyoD^+$ (neonatal: 0.66 ± .07, adult: 0.61 ± .11), or $MyoG^+$ (neonatal: 0.13 ± 0.03, adult: 0.14 ± 0.02) in the two cell populations (Figure 5.3A). However, after 14 days of 3D culture, adult-derived bundles exhibited lower $Pax7^+$ cell density (63.67 ± 5.8 cells/mm^2) compared to neonatal-derived bundles (147.65 ± 17.9 cells/mm^2) (Figure 5.3B). This drop in SC number was accompanied with a significant drop in $MyoG^+$ myonuclei content (Figure 5.3B). Plotting the dependence of force recovery at 5 days post-injury on $Pax7^+$ cell density prior to injury in adult bundles (Figure 5.3C), revealed their inferior regenerative capacity compared to neonatal bundles, which correlated with their lower SC numbers. Even at

similar densities of Pax7$^+$ cells, adult SCs appeared less capable of supporting functional recovery compared to neonatal SCs (Figure 5.3C).

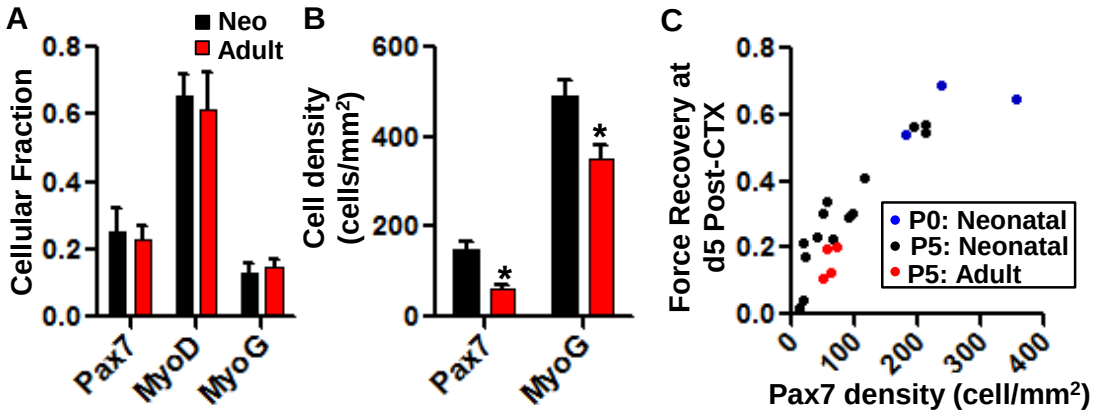

Figure 5.3 SC pool and regenerative ability in adult-derived muscle. (A) A comparison of Pax7$^+$, MyoD$^+$, and myogenin$^+$ (MyoG) fractions in neonatal and adult myogenic cells expanded for 5 passages using 5 ng/mL bFGF. (B) Pax7$^+$ and myogenin$^+$ (MyoG) cell density in neonatal- (Neo) and adult-derived engineered muscles following expansion in 5 ng/mL bFGF. (C) Dependence of force recovery on Pax7$^+$ cell density at 5-days post-CTX in P0 and P5 (various bFGF concentrations) neonatal engineered muscle and P5 adult-derived engineered muscle using 5 ng/mL bFGF. Each dot represents the mean of 1-3 bundles per 1 isolation.

5.3.3 Attempt to enhance SC maintenance within engineered muscle bundles

One approach to enhance the regenerative capacity of adult-derived engineered muscle would be to increase the Pax7$^+$ cell density regarding that the P0 neonatal cells that yielded the most regenerative bundles contained highest fraction of Pax7$^+$ SCs (Figure 4.6B&C). We thus utilized a recently published protocol which identified soluble growth factors (GFs) from T-cell conditioned media which significantly enhanced the maintenance and proliferation of SCs in culture, namely Tnfα (10 μM), IFNγ (10 μM), IL-1α (5 μM), and IL-13 (5 μM) [152]. Application of this growth factor cocktail during cell expansion increased the Pax7$^+$ and MyoD$^+$ cell fractions to 0.64 ± .04 and 0.92 ± .06, respectively. Further, the combination of growth factors significantly enhanced proliferation evidenced by increased Ki67$^+$ cell fractions (bFGF: 0.61 ± .07, GFs: 0.92 ±

.06) and total cell number at day 3 (bFGF: 844 ± 91, GFs: 4488 ± 349) at P5 (Figure 5.4C&D).

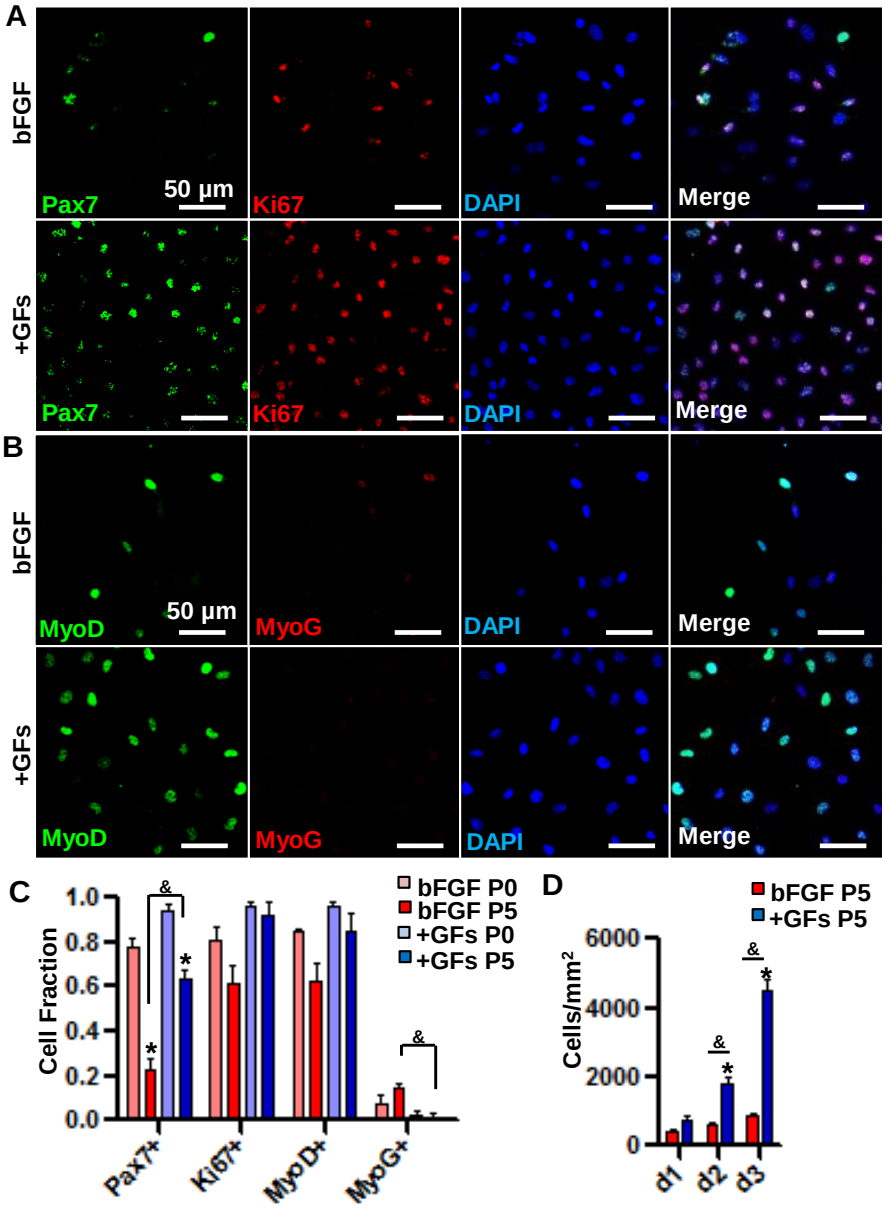

Figure 5.4 Enhanced retention of myogenic cells with regenerative potential using specific growth factors. (A-B) Representative staining for myogenic markers Pax7, MyoD, and myogenin (MyoG) and proliferation marker Ki67 in adult-derived cells cultured with bFGF and a cocktail of 4 growth factors (+GFs; IL1α, IL13, TNFα, IFNγ) at passage 5. C) Quantified expression of markers at passage 0 (P0) and 5 (P5). n = 2 isolations (2 coverslips/isolation and 4 images/coverslip); *, P<0.05 relative to P0; &, P<0.05 between groups at same passage. D) Quantified cell densities at each day during 3-day culture at P5. n = 2 isolations (2 wells/day and 3 images/well); *, P<0.05 relative to previous day; &, P<0.05 between groups at same day.

Interestingly, despite having high Pax7^{+} and MyoD^{+} fractions after expansion, the GF-treated cells yielded poor myofiber formation within engineered muscle (Figure 5.5A) including appearance of short mono-nucleated myotubes (Figure 5.5B). Furthermore, we found a limited SC pool within the engineered muscle (Figure 5.5B&C). Compared to adult-derived engineered muscles made of cells expanded without the 4 growth factors, these constructs had inferior function (twitch: 0.62 ± .08, tetanus: 0.60 ± .12 of control) and regeneration capacity (Figure 5.5C).

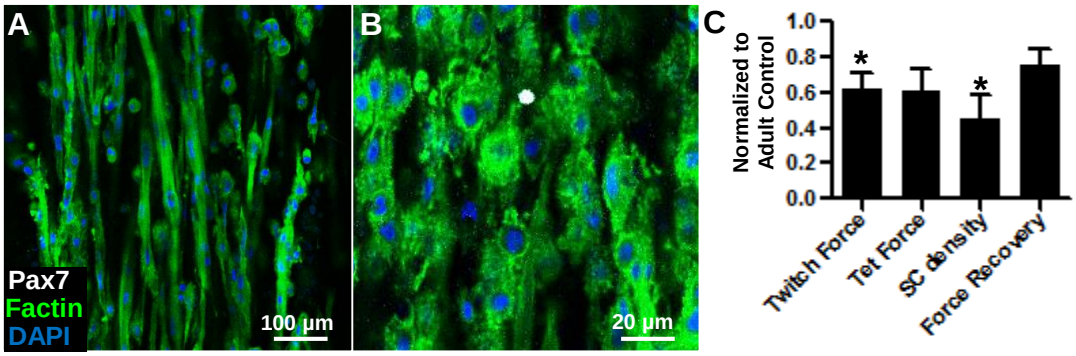

Figure 5.5 Engineered muscle from growth factor expanded cells. (A-B) Images of myofibers and the SC pool (Pax7) within 10-day old engineered muscle formed from growth factor expanded adult myogenic cells showing (A) disarrayed and (B) short, mono-nucleated fibers. C) Plot comparing twitch and tetanus (tet) force, SC density, and twitch force recovery at 5 days post-CTX compared to the adult control condition (5 ng/mL bFGF passaged cells). N = 4-6 bundles, *, P<0.05 relative to control.

5.3.4 Supplementation of pro-regenerative factors following CTX injury

Concurrent with the attempts to increase SC maintenance, we screened various factors for their ability to enhance regeneration of adult-derived muscles by transducing the cells with GCaMP6 indicator [178], followed by the bundle fabrication and differentiation, CTX application, and live monitoring of calcium transients during recovery from injury. To enable increased GCaMP expression in cells without compromising calcium-dependent myogenic differentiation, we replaced originally used CMV promoter [234], with a muscle-specific MHCK7 promoter [235] that was active only in fused

myofibers but not in undifferentiated myoblasts (Figure 5.6A). At high viral concentrations, bundles made of MHCK7-GCaMP6 transduced cells, but not CMV-GCaMP6 transduced cells exhibited same forces of contraction as untransduced controls (Figure 5.6B). Similar to control bundles, the MHCK7-GCaMP6 transduced bundles contained cross-striated myofibers, a $Pax7^+$ SC pool, and an outer coat of $vimentin^+$ fibroblasts that lacked gCaMP6 labeling (Figure 5.6C-E). Figure 5.6F shows an example of an electrically-induced calcium transient in an MHCK7-GCaMP6 transduced bundle recorded on a microscope within the live imaging setup.

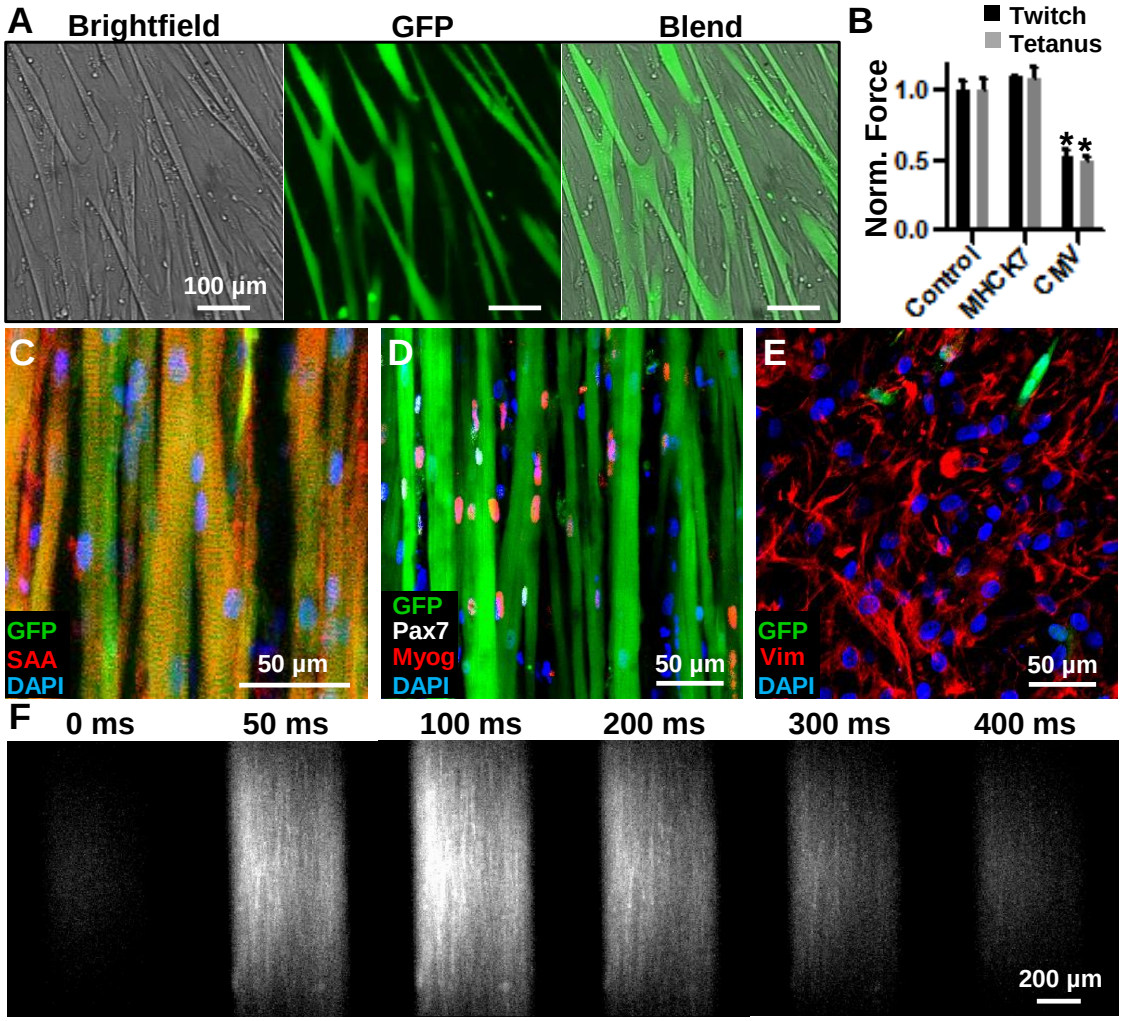

Figure 5.6 MHCK7 promoter in engineered muscle. (A) Brightfield and GFP images of MHCK7-GFP transduced myogenic cells in 2D culture showing high GFP expression in fused myotubes but not surrounding myoblasts. B) Normalized twitch and tetanus forces in engineered muscle made of cells transduced with high concentration of MHCK7-GFP and CMV-GFP viral particles normalized to control engineered muscle (no viral transduction). C-E) Confocal images of MHCK7-GCaMP6 engineered muscle revealing (C) sarcomeric α-actinin $(SAA)^{+}$ cross-striations in GFP^{+} myofibers, (D) the presence of $Pax7^{+}$ satellite cells on the myofiber periphery and (E) GFP^{-} fibroblasts at bundle periphery verifying muscle specificity of MHCK7 promoter. F) Electrically-stimulated calcium transient recorded from MHCK7-GCaMP6 transduced engineered muscle within the live cell imaging system.

We used the described live imaging system to screen various soluble factors that could promote regeneration of adult-derived engineered muscle following injury, including IGF-1 [228], IL-10 [227], and G-CSF [226]. GCaMP6 recordings pre-CTX and 6

hours, 2, 5, 7, 10, 12, and 15 days post-CTX injury revealed that even though the addition of some of these factors transiently increased calcium transient amplitude at a few time-points (G-CSF: 2d, and 5d post-CTX, IGF-1: 7d and 10d post-CTX), overall, they did not support functional recovery of muscle bundles (Figure 5.7A). Fifteen days post-injury, all groups showed significant loss of bundle diameter and muscle mass.

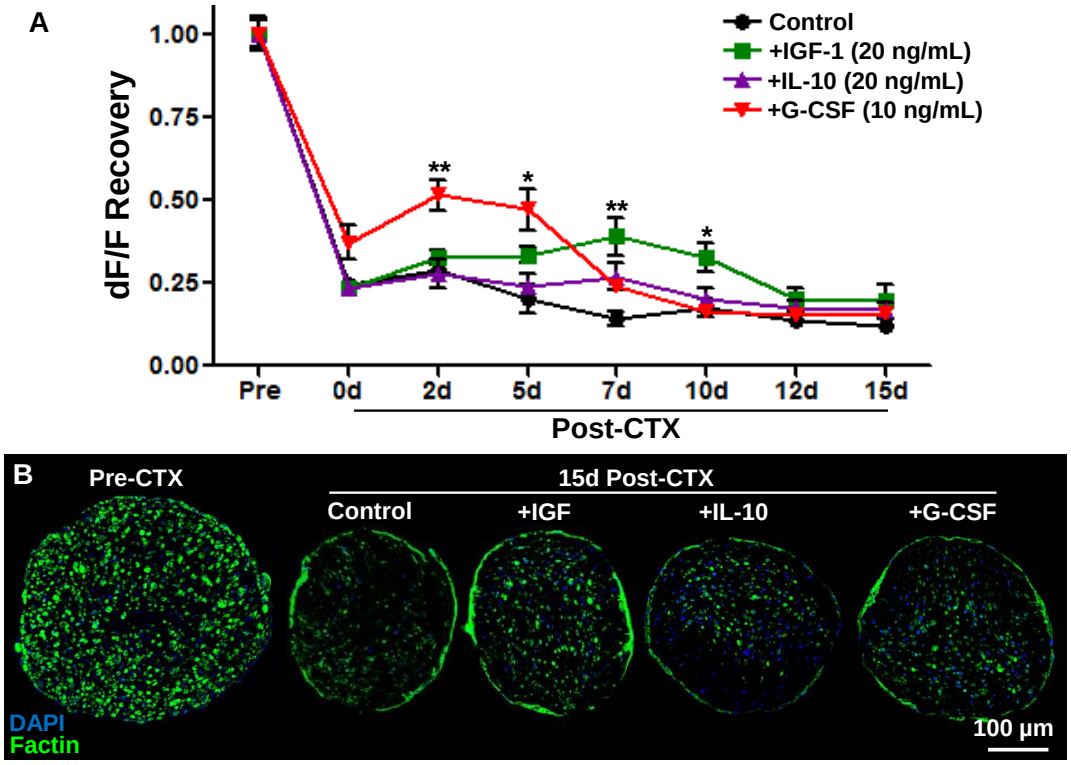

Figure 5.7 Effect of pro-regenerative factors on engineered muscle following injury. (A) dF/F (Ca^{2+} transient amplitude) values from electrically-stimulated bundles at different times post-injury with and without (control) supplemented factors. (B) Bundle cross-sections (myofibers marked by F-actin) pre-CTX and 15 days post-CTX administration. N = 2-3 isolations (6-8 bundles per isolation) per group. *, P<0.05 compared to control.

5.3.5 Incorporation of bone marrow-derived macrophages into engineered muscle

As an alternative to adding individual soluble factors, which may only have specific roles in particular aspects of regeneration, we explored a cell-based pro-regenerative strategy by supplementing bundles with bone marrow derived

macrophages (BMDMs, Fig. 5.8A) that in an appropriate temporal fashion may secrete multiple factors to enhance muscle recovery from injury (section 2.1 and 2.2). Consistent with previous reports [52], we obtained cells that ubiquitously expressed the common macrophage marker CD68 (Figure 5.8B). These cells were considered to be of a M0 phenotype, as they were not exposed to polarizing factors. We prepared muscle-BMDM constructs in which presence of macrophages did not adversely affect overall bundle structure (Figure 5.8C), myofiber formation (Figure 5.8D), SC maintenance (Figure 5.8E&F), or contractile function (Figure 5.8F).

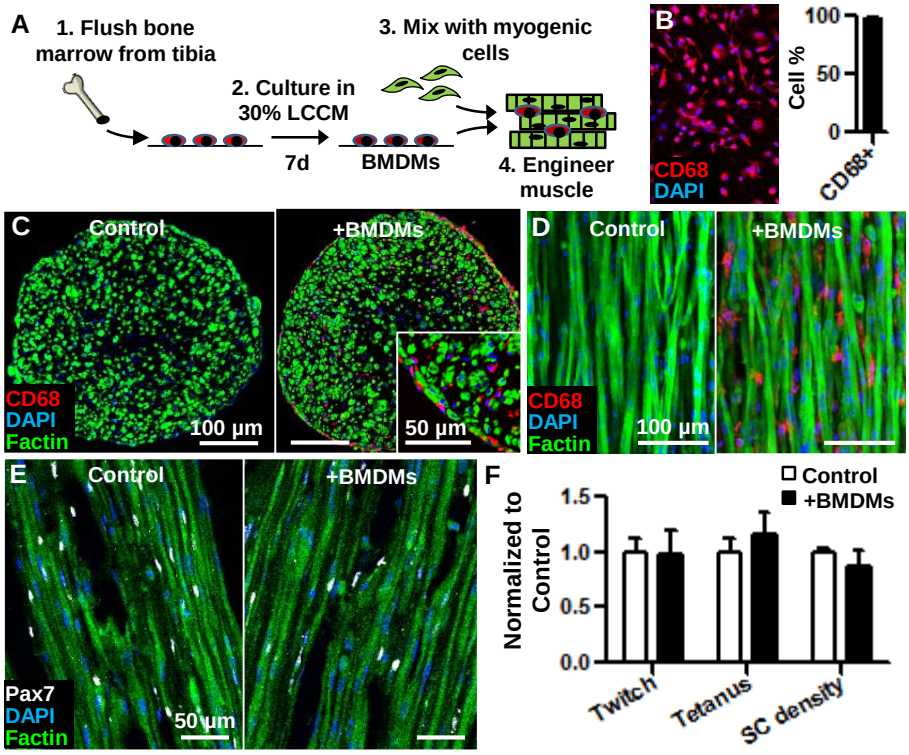

Figure 5.8 Structure and function of bone marrow-derived macrophage (BMDM)-muscle co-cultured engineered bundles. (A) Schematic of the isolation and differentiation of BMDMs and their use in engineered muscle. B) Virtually all BMDMs express CD68 after 7 days of differentiation. C) Cross-sectional and (D) longitudinal confocal images revealing the presence of $CD68^{+}$ BMDMs within the engineered muscle. E) Representative images of $Pax7^{+}$ cells in the sections from control (Cnt) and muscle-BMDM constructs. F) Normalized force generation (Twitch and Tetanus) and SC density (cells/mm^2) in co-cultured vs. control bundles. N = 8 - 12 bundles.

5.3.6 Regenerative capacity of muscle-BMDM constructs following CTX injury

To test the regenerative capacity of muscle-BMDM constructs we utilized our live imaging CTX assay. As a negative control, we used muscle bundles where BMDMs were replaced by MSCs derived from rat bone marrow [231] as described in section 5.2.2. The bundles were exposed to CTX until ~75% of the live-imaged GCaMP6 signal was lost (control: 24 ± 2%, +BMDMs: 23 ± 1%, +MSCs: 2 of pre-CTX level), and were followed 15 days thereafter. As shown in Fig. 5.10A, while calcium transient amplitude in control bundles steadily decreased with time post-injury, muscle-BMDM bundles showed progressive recovery of the signal toward pre-injury levels. Specifically, by 15 days post-injury, muscle-BMDM bundles recovered Ca^{2+} transient amplitudes to 85 ± .4% of pre-injury levels, while signal in muscle-only bundles further deteriorated to 12 ± 1% of pre-injury values (Figure 5.9B). The muscle-MSC constructs experienced significantly larger recovery of dF/F signal compared to the control group by 7 days post-CTX (41 ± 6% of pre-CTX values). However, their dF/F signal steadily decreased thereafter to reach 28 ± 3% of pre-CTX levels at 15 days post-injury.

Consistent with Ca^{2+} transient results, twitch and tetanic force production of the muscle-BMDM bundles steadily improved over the 15 day period (twitch: 5d: 0.31 ± .09, 10d: 0.57 ± .08, 15d: 0.82 ± .05, tetanus: 5d: 0.30 ± .08, 10d: 0.45 ± .03, 15d: 0.71 ± .08 relative to pre-CTX values) while it decreased in the muscle-only group (twitch: 5d: 0.11 ± .02, 10d: 0.09 ± .02, 15d: 0.03 ± .01, tetanus: 5d: 0.12 ± .03, 10d: 0.08 ± .01, 15d: 0.004 ± .005 relative to pre-CTX values) (Figure 5.9C). Despite some transient recovery of Ca^{2+} transient amplitude, force generation was found to steadily decrease in the muscle-MSC. At 15 days post-CTX, the addition of MSCs did result in significantly

greater tetanic force production compared to control; however, both twitch and tetanic forces were significantly less than those of the muscle-BMDM bundles (Figure 5.9C).

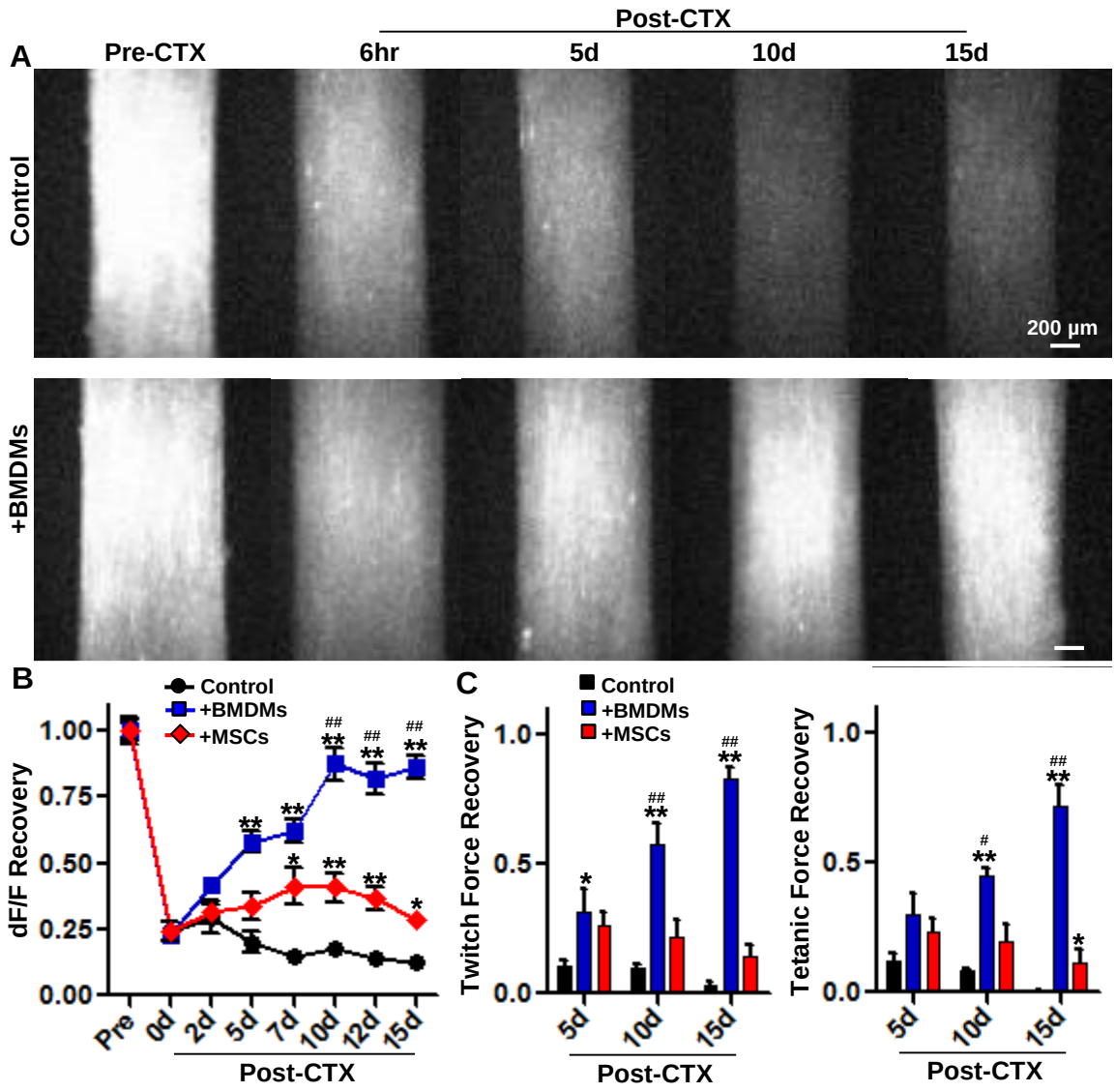

Figure 5.9 Functional recovery of muscle-BMDM constructs following CTX injury. (A) Peak dF/F signals before (pre-CTX) and at different times after the injury (post-CTX) in adult-derived engineered muscle without (control) and with BMDMs (+BMDMs). B-C) Quantified recovery of dF/F (B) and contractile function (C) relative to pre-CTX levels. n = 5-7 isolations (4-8 bundles/isolation). *P<0.05; **P<0.01 vs. control at same time point. $^{\#}$P<0.05; $^{\#\#}$P<0.01 vs. +MSC group at same time point.

As expected from functional results, analysis of cross-sectional staining (Figure 5.10A) revealed recovery of myofibers in muscle-BMDM but not muscle-only bundles. As

the muscle-only group continued to degenerate following injury, the muscle-BMDM constructs steadily increased in myofiber area, myofiber number, and total nuclei number, reaching respectively 67± 11%, 79 ± 8%, and 71 ± 4% of pre-injury levels by post-injury day 15 (Fig. 5.10B-D).

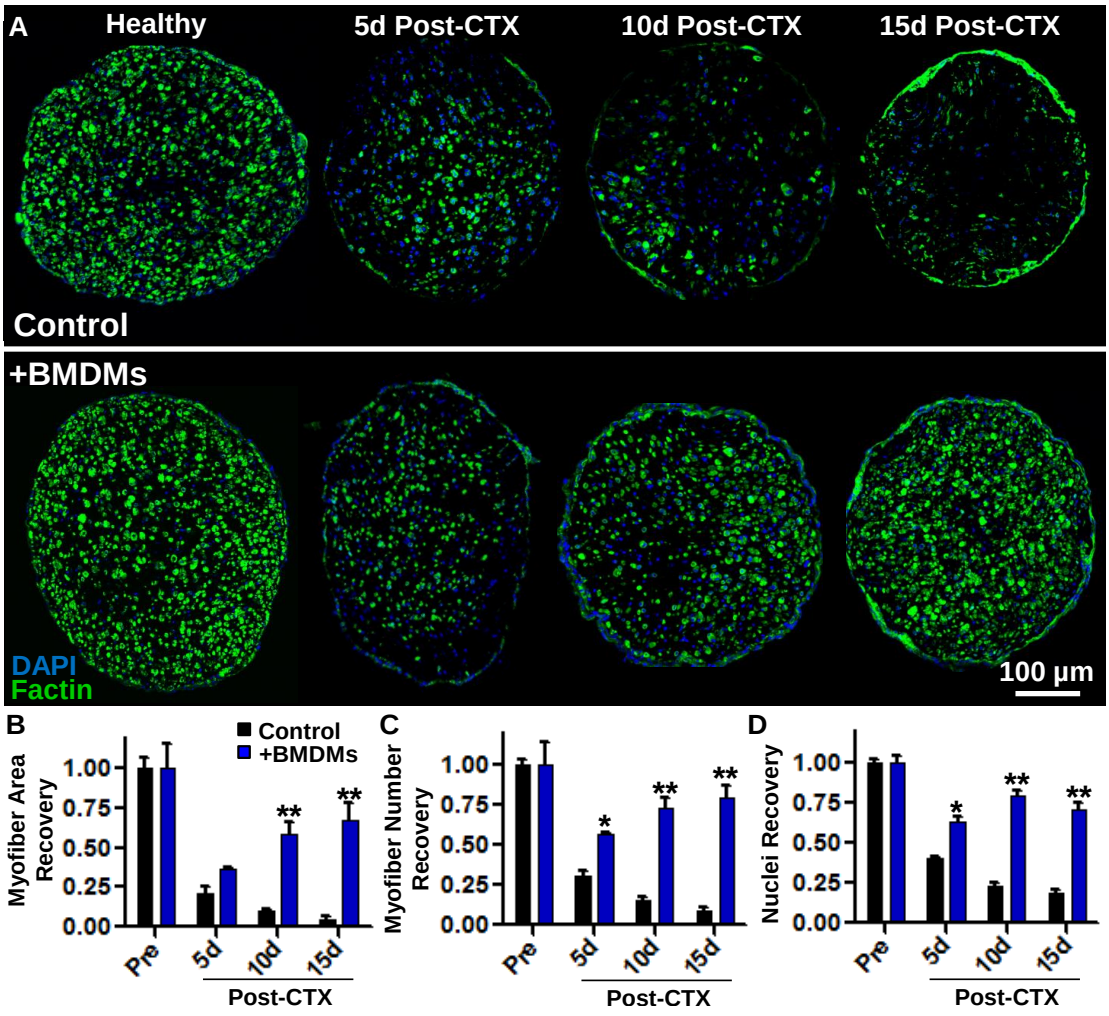

Figure 5.10 Structural recovery of muscle-BMDM constructs following CTX injury. (A) Cross-sections of engineered muscle bundles pre-CTX and at 5, 10, and 15 days post-CTX injury (myofibers labeled with F-actin). B-D) Quantified recovery of (B) myofiber area, (C) myofiber number, and (D) total nuclei number over 15 days post-injury compared to pre-CTX levels. n = 3-5 isolations (4-8 bundles/isolation). *, P<0.05; **, P<0.01 vs. control at same time-point.

Moreover, from longitudinal staining, we found that similar to the muscle-only controls, exposure of muscle-BMDM bundles to CTX resulted in severe myofiber

fragmentation (Figure 5.11A). Unlike in muscle-only controls (Figure 5.2), this was followed by rebuilding of myofibers during 15-day recovery period. During this period, BMDMs remained intermixed with myofibers while maintaining constant numbers relative to pre-injury levels (Figure 5.11B). Additionally, the regrowth of myofibers is concurrent with the reformation of sarcomeric structures (Figure 5.11C).

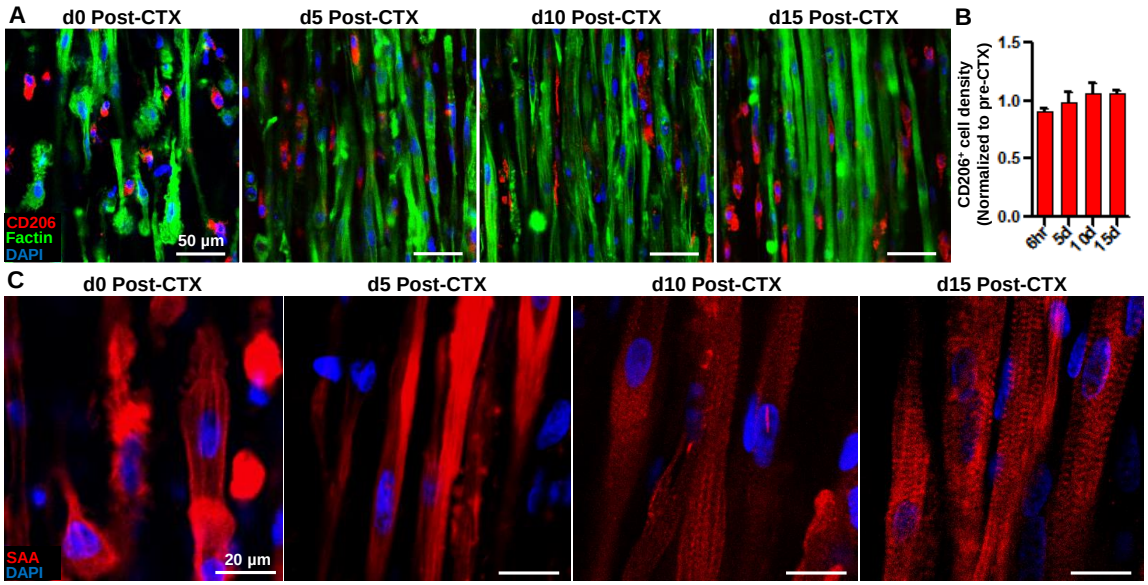

Figure 5.11 The regrowth of myofibers in muscle-BMDM constructs after CTX injury. (A) Representative images of regenerating myofibers and BMDMs (labeled by CD206) following CTX-induced injury. B) Quantified density of $CD206^+$ cells within the interior muscle layers during regeneration normalized to pre-CTX levels. C) Representative images of sarcomeric reformation in muscle-BMDM bundles following CTX injury. Error bars denote mean ± SEM.

5.3.7. Mechanisms of BMDM-induced in vitro regeneration

We then set to better understand the process leading to the drastic improvement of the regenerative response of muscle bundles supplemented with BMDMs. Considering the effect of macrophages on in vivo SC activation, proliferation, and differentiation [27], we first examined the early stages of regeneration and observed populations of $Pax7^+/Ki67^+$ and $MyoD^+$ cells in both the muscle-only and muscle-BMDM bundles (Figure 5.12A&B) at 5 days post-CTX. Specifically, in muscle-only bundles

Pax7$^+$ Ki67$^+$ and MyoD$^+$ cell fractions ($^+$nuclei/total nuclei) increased 1.38 ± .26, 2.93 ± .66, and 1.98 ± .32 fold, respectively, compared to pre-injury levels (Figure 5.12C) and this early regenerative process appeared to be further amplified in the muscle-BMDM constructs to 2.20 ± .28, 5.21 ± .79, and 3.39 ± .54 fold, respectively, compared to pre-CTX levels (Figure 5.12C). These results signified the initiation of repair events in adult-derived engineered muscle regardless of the addition of BMDMs.

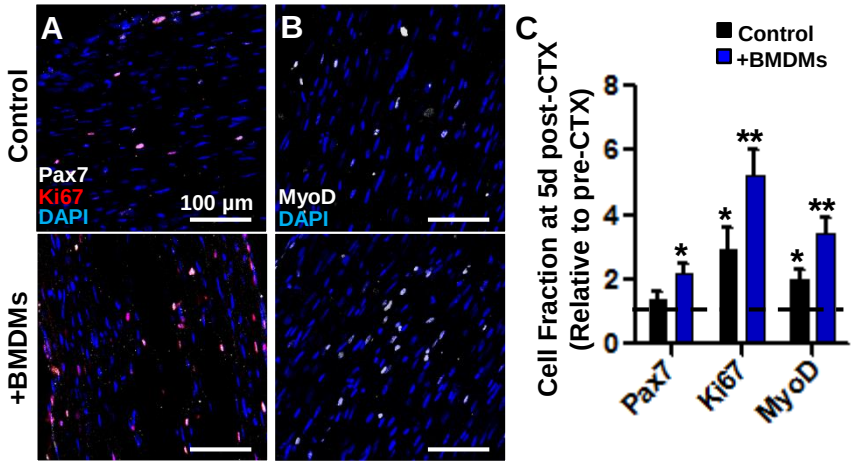

Figure 5.12 Early myogenic responses in adult-derived engineered muscle after CTX injury. (A-B) Longitudinal sections showing activated SCs, marked by (A) Pax7 and Ki67 as well as myoblasts marked by (B) MyoD at 5 days post-CTX in engineered muscle without (top) and with BMDMs (bottom). (C) Plot of the fold change in fraction of Pax7$^+$, Ki67$^+$, and MyoD$^+$ cells at 2 and 5 days post-CTX relative to pre-CTX levels. N = 3 isolations (1 bundle per group per isolation). *, P<0.05; **, P<0.01 compared to pre-CTX levels.

To further assess regenerative process, we tracked cell proliferation by supplementing EdU into the media every day following injury, cumulatively marking cells that had undergone proliferation. An initially high density of EdU$^+$ cells at 2 days post-injury in both groups (muscle-only: 102 ± 7, muscle-BMDM: 92 ± 5 cells/mm^2) (Figure 5.13A&B) was followed by a steady decline in the muscle-only group (5d: 26 ± 2, 10d: 10 ± 2, 15d: 4 ± 1 cells/mm^2) and an increase and leveling of EdU$^+$ cell density in the BMDM group (5d: 137 ± 9, 10d: 168 ± 15, 15d: 147 ± 6 cells/mm^2) out to 15 days post-CTX (Figure 5.13A&B). The EdU$^+$ labeled nuclei either resided in myofibers at 10 days

post-CTX (Figure 5.13C) or were co-expressed in MyoD$^+$ (Figure 5.13D) but not vimentin$^+$ cells (Figure 5.13E) at 5 days post-CTX, suggesting that the majority of the proliferative cells post-injury were myogenic.

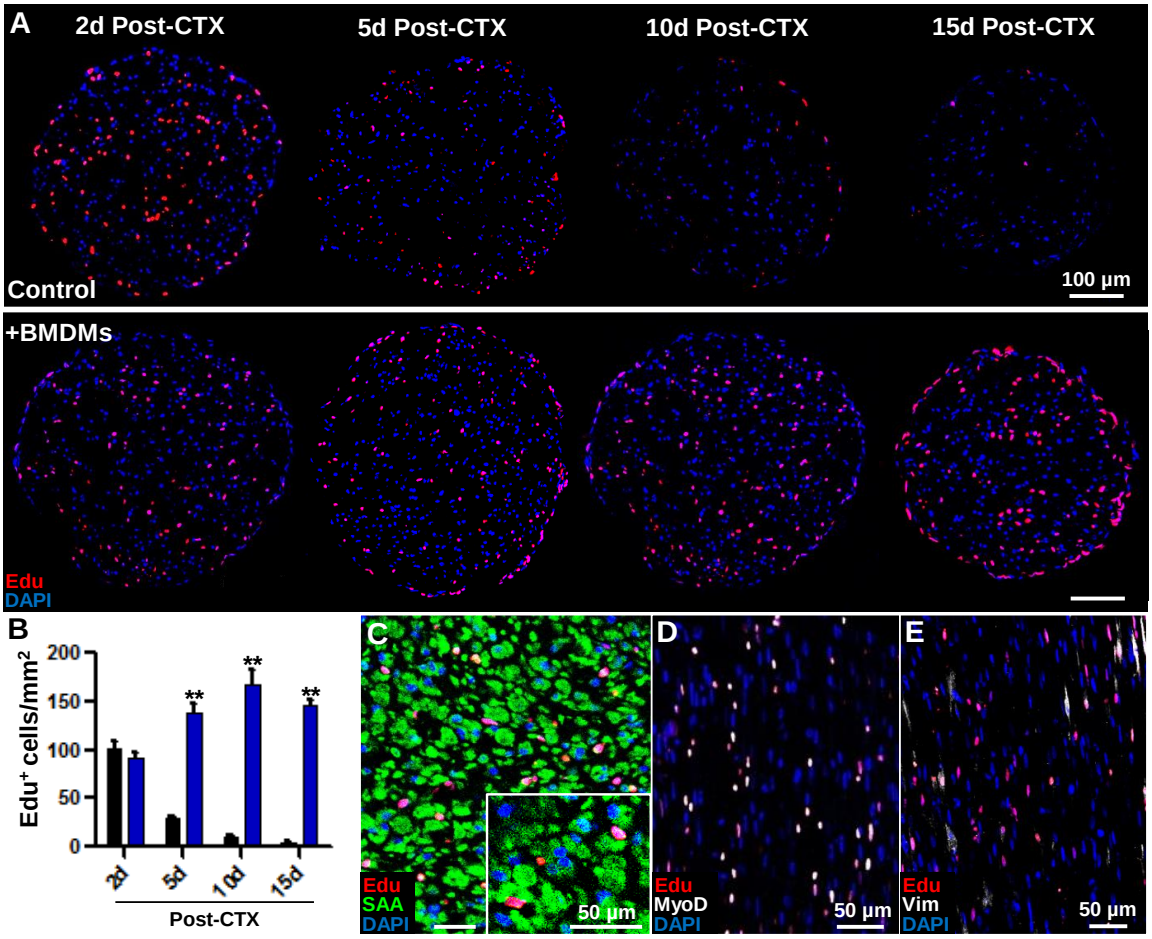

Figure 5.13 Cell proliferation during *in vitro* muscle bundle regeneration in response to CTX injury. (A) Representative staining of EdU$^+$ cells in the cross-sections of the adult-derived engineered muscle bundles without (control) and with BMDMs. B) Quantified EdU$^+$ cell densities over the time-course of regeneration. C-E) Representative images showing EdU$^+$ cells (C) associated with myofibers at d10 post-CTX, marked by SAA, (D) co-labelled with MyoD at d5 post-CTX, and (E) absent from vimentin$^+$ (Vim) cells at d5 post-CTX. n=3 isolations (2 bundles per time-point per isolation), **, P<0.01 vs. muscle-only (control) group at same time-point.

The capacity for SCs to proliferate following CTX injury in muscle-only bundles suggested that the inability to regenerate may not be associated with limited SC function. This led us to assess the role of BMDMs in preventing cellular degeneration,

rather than stimulating regeneration, following injury. As mentioned in section 2.2, in many diseases of muscle atrophy, the propensity of myofiber apoptosis is enhanced and typically contributed to activity of caspase-3 pathway [76]. PCR results showed significant increase in caspase-3 gene expression immediately after injury in both conditions in our system (control: 2.19 ± 0.35, +BMDM: 1.80 ± 0.14 compared to pre-CTX) (Figure 5.14A). Expression remained elevated in the muscle-only condition (2d: 1.81 ± 0.34, 5d: 2.46 ± 0.22, 10d post-CTX: 2.50 ± 0.74 compared to pre-CTX) yet reverts back to healthy levels with the addition of BMDMs (2d: 1.02 ± 0.01, 5d: 1.37 ± 0.08, 10d post-CTX: 1.27 ± 0.16 compared to pre-CTX) (Figure 5.14A). Quantification of activated (cleaved) caspase-3 area relative to total nuclei using image analysis revealed significantly higher levels in the muscle-only group (2d: 13.2 ± 1.3, 5d: 33.4 ± 5.9, 10d post-CTX: 24.1 ± 3.4 μm^2/cell) compared to the muscle-BMDM group (2d: 5.91 ± .45, 5d: 2.43 ± 5.9, 10d post-CTX: 2.71 ± .55 μm^2/cell) (Figure 5.14B). Importantly, the ratio significantly rose without the presence of BMDMs and decreased with their addition at early time-points following injury (Figure 5.14B). Representative images showed the differences in cleaved-caspase-3 expression and myofiber area in the muscle cross-section (Figure 5.14C).

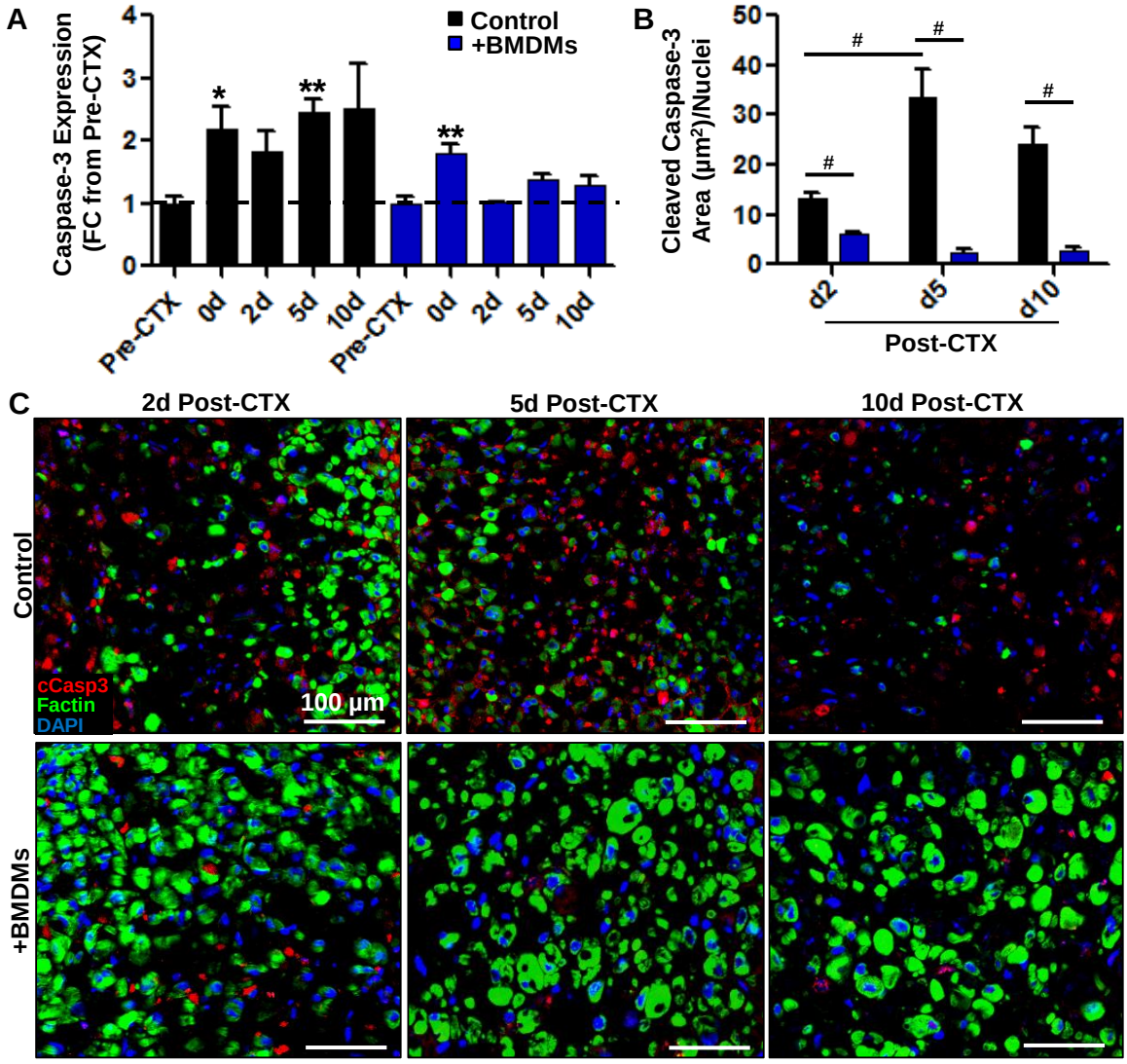

Figure 5.14 Caspase activity in engineered muscle bundles following CTX injury. (A) Fold change of caspase-3 gene expression in engineered muscle at 0, 2, 5, and 10 days post-injury relative to healthy conditions (pre-CTX) and in bundles without (control) and with BMDMs. B-D) (B) Quantified fraction of cleaved caspase-3 area over myofiber area and representative (C) longitudinal and (D) cross-sectional staining of cleaved caspase-3 (cCasp3) and myofibers, marked with F-actin, at (C-D) 2 and (D) 5 days post-injury. n=3 isolations (1-2 bundles per time-point per isolation). *P<0.05, **P<0.01 compared to pre-CTX levels. $^{\#}$P<0.05 between groups designated by line.

To recreate the beneficial, anti-apoptotic effect of BMDMs within adult-derived engineered muscle, we applied a pan-caspase inhibitor Q-VD-OPh [236]. Real-time recording of dF/F following injury showed the effect of the inhibitor to rescue signal in the

adult-derived engineered muscle resulting in a steady increase over time post-injury (0d: 0.24 ± .03, 2d: 0.49 ± .06, 5d: 0.57 ± .09, 7d: 0.60 ± .07, 10d: 0.66 ± .10, 12d: 0.78 ± .09, 15d post-CTX: 0.84 ± .08 relative to pre-CTX) (Figure 5.15A&B). Force measurements at 15 days post-CTX revealed the Q-VD-OPh aided force recovery (twitch: 0.70 ± .10, tetanus: 0.63 ± .08 compared to pre-CTX); values significantly greater than the control group (Figure 5.15C). Quantification of cleaved caspase-3 area per nuclei and EdU^+ cell density at 5 days post-CTX showed significant decreases in caspase-3 activity (0.31 ± .10 relative to control) and significant increases in cell proliferation (2.91 ± .31 relative to control) at early time-points with the addition of the inhibitor (Figure 5.15D). Representative images at day 2 and 5 post-CTX revealed an attenuation of apoptotic events (Figure 5.15E) in the presence of Q-VD-OPh and greater muscle area within the bundles (Figure 5.15F).

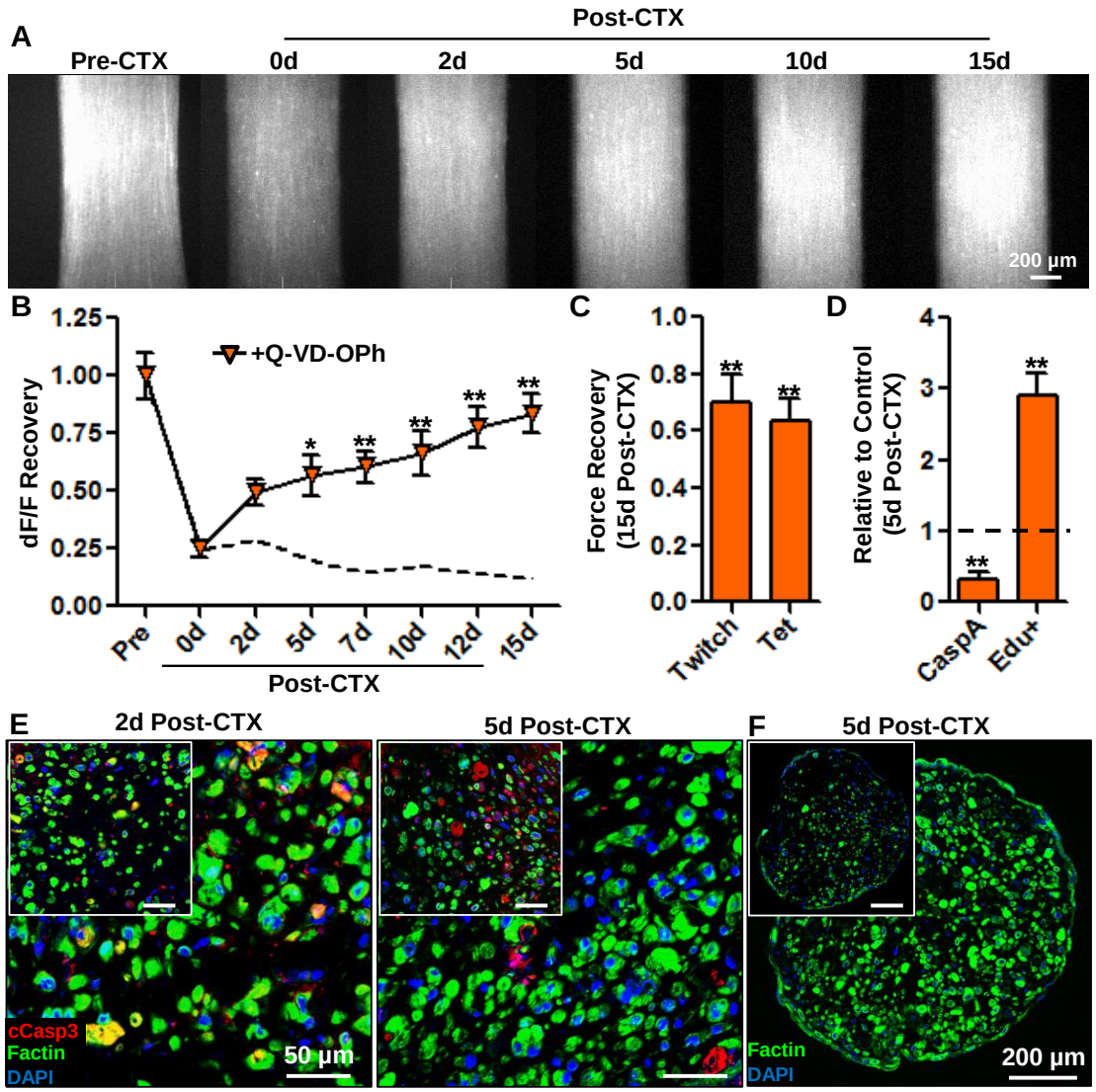

Figure 5.15. Effects of Q-VD-OPh on regeneration following CTX injury. (A) Peak dF/F signals in health (pre-CTX) and injured adult engineered muscle supplemented with pan-caspase inhibitor Q-VD-OPh over 15 days. (B) Quantified recovery of dF/F following injury (dashed line represents control group). (C) Recovery of twitch and tetanus force at 15 days post-CTX with supplementation of Q-VD-OPh. (D) Values of cleaved caspase-3 (cCasp3) area per nuclei and EdU^{+} cell density relative to the control group at 5 days post-CTX. (E-F) Representative staining of (E) cCasp3 and myofibers at 2 and (F) 5 days post-CTX in the Q-VD-OPh group (inset: control group at same time-point). Error bars denote mean ± SEM. N = 2 isolations (4-8 bundles per time-point). **P<0.01 compared to control group at same time-point.

5.3.8. Assessing paracrine effects of BMDMs within engineered muscle following injury

To determine if the anti-apoptotic effects following injury were mediated through paracrine signaling, we performed a shared media assay by forming a muscle-BMDM and a muscle-only (control) bundle on the same frame and cultured them in the same well. The study will be referred to as “paracrine” in which “para-control” and “para-BMDM” will designate the bundle without and with BMDMs. Following severe CTX injury, quantification of dF/F for 15 days revealed the inability for recovery in either of the bundles, even the para-BMDM bundle (Figure 5.16A). Active force measurements at 15 days post-CTX showed a significant drop in contractile function (para-control: twitch: 0.040 ± 0.005, tetanus: 0.039 ± 0.004, para-BMDM: twitch: 0.073 ± 0.012, tetanus: 0.071 ± 0.013 compared to pre-CTX) (Figure 5.16B). Additionally, quantification of cross-sectional muscle area revealed a steady degeneration of myofibers over time post-injury in both groups (para-control: 5d: 0.32 ± 0.07, 10d: 0.21 ± 0.03, 15d: 0.09 ± 0.01, para-BMDM: 5d: 0.38 ± 0.08, 10d: 0.26 ± 0.05, 15d post-CTX: 0.15 ± .02 compared to pre-CTX) (Figure 5.16C&D).

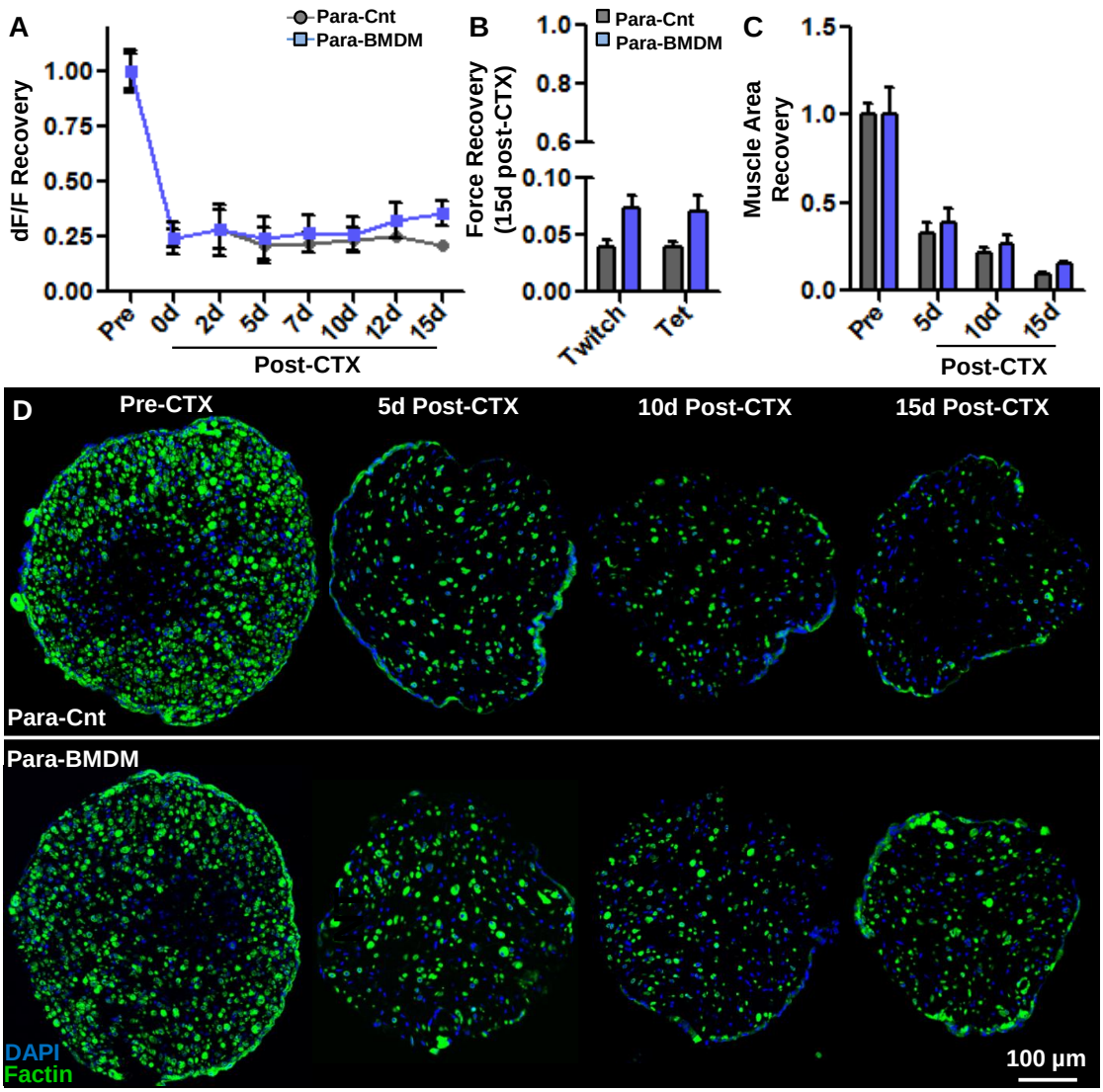

Figure 5.16 In vitro regeneration of engineered muscle bundles in paracrine system following severe CTX injury. (A-C) Plots of (A) dF/F recovery over time post-injury, (B) force generation at 15 days post-CTX, and (C) muscle area recovery at 5, 10, and 15 days post-CTX in para-control (cnt) and para-BMDM bundles. D) Representation images of muscle area, marked by F-actin, at time-points following injury. Error bars denote mean ± SEM. N = 3 isolations (1-4 bundles per group per time-point).

In order to determine if the detrimental effects on regeneration in the paracrine system were dependent on severity of injury, we employed a “mild” injury on the bundles (~50% drop in dF/F). Tracking changes in dF/F revealed the inability of the control group to recover signal and degeneration by day 15 post-CTX (0.39 ± 03 relative to pre-CTX)

(Figure 5.17A). However, with mild injury (para-control: 0.51 ± .03, para-BMDM: 0.52 ± .07 compared to pre-CTX), both paracrine bundles recovered significantly better than the muscle-only construct, reaching 0.81 ± 0.04 (para-control) and 0.89 ± 0.05 (para-BMDM) of pre-CTX values at day 15 post-CTX (Figure 5.17A). The significant difference in dF/F recovery was associated with significant increases in twitch (control: 0.12 ± .04, para-control: 0.73 ± .12, para-BMDM: 0.86 ± 0.09 compared to pre-CTX) and tetanus force (control: 0.11 ± .05, para-control: 0.68 ± .15, para-BMDM: 0.76 ± 0.08 compared to pre-CTX) recovery at the 15 day time-point (Figure 5.17B). Additionally, quantification of muscle area over the time-course of regeneration revealed a steady regrowth in both paracrine groups, reaching 0.73 ± 0.10 (para-control) and 0.76 ± .09 (para-BMDM) compared to pre-CTX values (Figure 5.17C&D). Adversely, the muscle-only group experienced a steady decrease in muscle mass over time in this mild injury setting, reducing to 0.16 ± 0.03 of its pre-CTX value by day 15 post-CTX (Figure 5.17C&D).

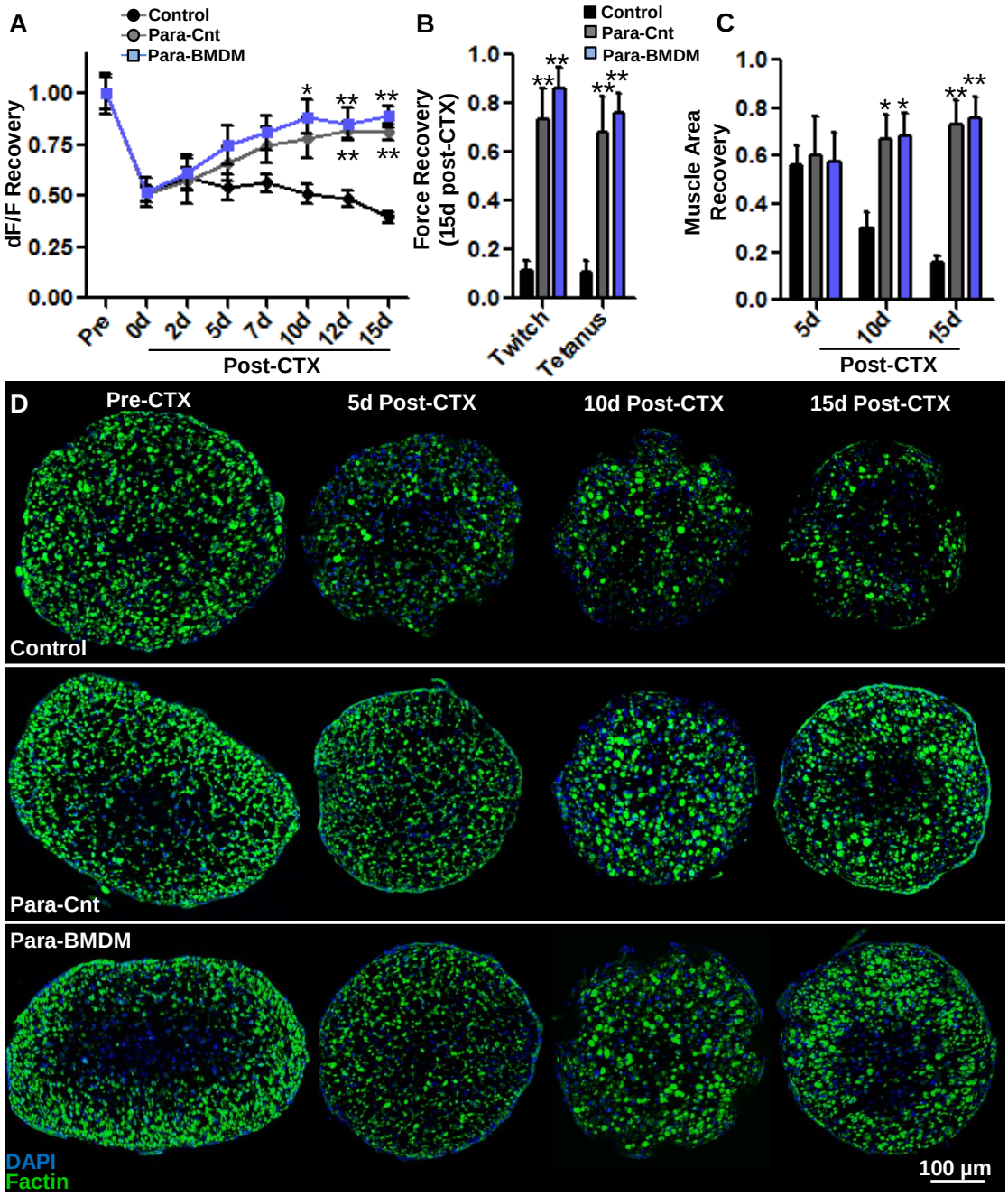

Figure 5.17 In vitro regeneration of engineered muscle bundles in paracrine system following mild CTX injury. (A-C) Plots of (A) dF/F recovery, (B) force generation at 15 days post-CTX, and (C) muscle area recovery post-CTX in control, para-control (cnt), and para-BMDM bundles in a mild injury setting. (D) Representative images of muscle area, marked by F-actin, at time-points following injury. Error bars denote mean ± SEM. N = 3 isolations (1-3 bundles per group per time-point). *, P<0.05, **, P<0.01 compared to control at same time-point (marks made below symbols in A correspond to Para-Cnt group).

To assess whether the enhanced regenerative events in the paracrine bundles following mild injury were associated with apoptosis, we assessed caspase-3 activity at early time-points. Cross-sectional staining of cleaved-caspase-3 revealed the occurrence of apoptosis 2 days post-CTX for all groups (Figure 5.18A&B). However, from day 2 to 5 post-CTX, the caspase levels significantly increased in the control group (2d: 16.38 ± 1.78, 5d post-CTX: 36.44 ± 4.53 μm^2/nuclei) and decreased in both paracrine groups (para-control: 2d: 10.58 ± 1.49, 5d post-CTX: 5.28 ± 1.18, para-BMDM: 2d: 8.11 ± 2.65, 5d post-CTX: 2.44 ± 1.16 μm^2/nuclei) to a level significantly less than the control (Figure 5.18A&B).

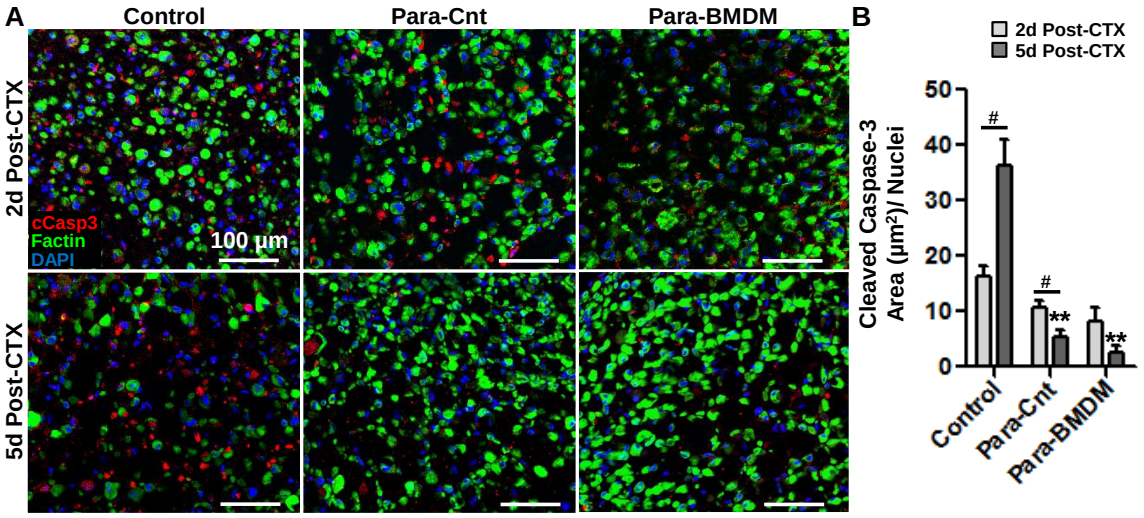

Figure 5.18 Cleaved-caspase-3 activity following mild CTX injury in paracrine muscle bundles. (A) Representative cross-sectional staining of cleaved-caspase-3 (cCasp3) and myofibers, marked with F-actin, following mild damage in control (muscle-only) and paracrine without (Para-Cnt) and with (Para-BMDM) BMDMs (Para-BMDM), groups. B) Quantified fraction of cleaved-caspase-3 area over myofiber area. Error bars denote mean ± SEM. N=3 isolations (1-2 bundles per time-point per isolation). *P<0.05 compared to control at same time-point, $^{\#}$P<0.05 between groups designated with line.

5.3.9 Effect of macrophage phenotype for regeneration following CTX injury

As mentioned in section 2.1, pro-inflammatory M1 and anti-inflammatory M2 macrophage phenotypes play separate roles in muscle regeneration [27]. Due to this distinction, we wanted to test whether adding polarized M1 or M2 BMDMs would have

an effect on *in vitro* regeneration compared to non-polarized M0 BMDMs used in previous sections. As described in section 5.2.3, IFNγ + LPS and IL-10 [52, 233] were supplemented in monolayer culture for 2 days following M-CSF-driven differentiation into BMDMs to induce M1 and M2 polarization, respectively (Figure 5.19A). PCR for M1 and M2 markers following the 2 days in culture revealed higher expression of pro-inflammatory marker TNFα and reduced expression of anti-inflammatory genes Arg1, Mrc1, and IL10 in M1-treated BMDMs compared to M0 (Figure 5.19B). On the contrary, M2 polarization triggered the reduction of TNFα and increased expression of anti-inflammatory markers (Figure 5.19B) compared to M0. Staining for common markers of M1 and M2 macrophages, iNOS and CD206 respectively, resulted in strong expression of each following their corresponding polarization (Figure 5.20C). M0 macrophages, as expected, did also stain positively for anti-inflammatory CD206 (Figure 5.19C) [237].

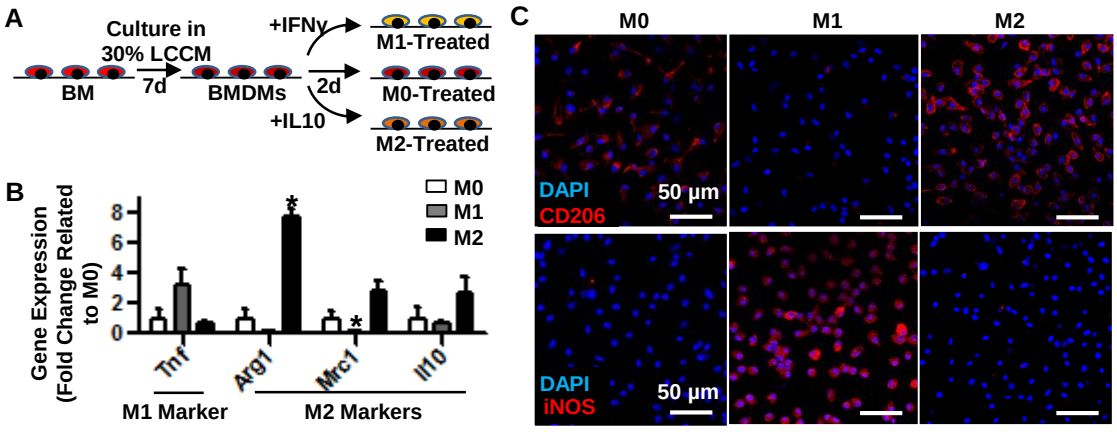

Figure 5.19 Bone marrow-derived macrophage polarization. (A) Schematic of polarization technique to coax cells towards M1 (IFNγ + LPS) or M2 (IL10) phenotypes. (B) Quantified gene expression of M1 and M2 markers from all groups. (C) Representative staining for M2 marker (CD206) and M1 marker (iNOS) in polarized and non-treated BMDMs. N = 2 isolations; *P<0.05 relative to M0-treated group.

Polarized BMDMs were incorporated into 3D engineered muscle and cultured for 10 days. Gene expression at this point reported a shift back towards M0 levels (Figure 5.20A) in comparison to 2D expression levels (Figure 5.19A). As an alternative to 2D

macrophage polarization before formation of bundles, we also polarized the cells while in 3D culture just prior to injury. Supplementation of IFNγ + LPS into the media at 3D culture day 9 xx for 1-2 days resulted in significant upregulation of pro-inflammatory genes (TNFα and iNOS) and significant down-regulation of anti-inflammatory genes (Mrc1, Arg1, and IL10) (Figure 5.20B). M2 polarization cased a significant upregulation of Arg1 but otherwise had minor effects on gene expression (Figure 5.20B). Staining of the engineered muscle revealed greater CD206 expression in bundles containing M0 and M2 BMDMs and greater iNOS expression in the M1-treated bundles (Figure 5.20C).

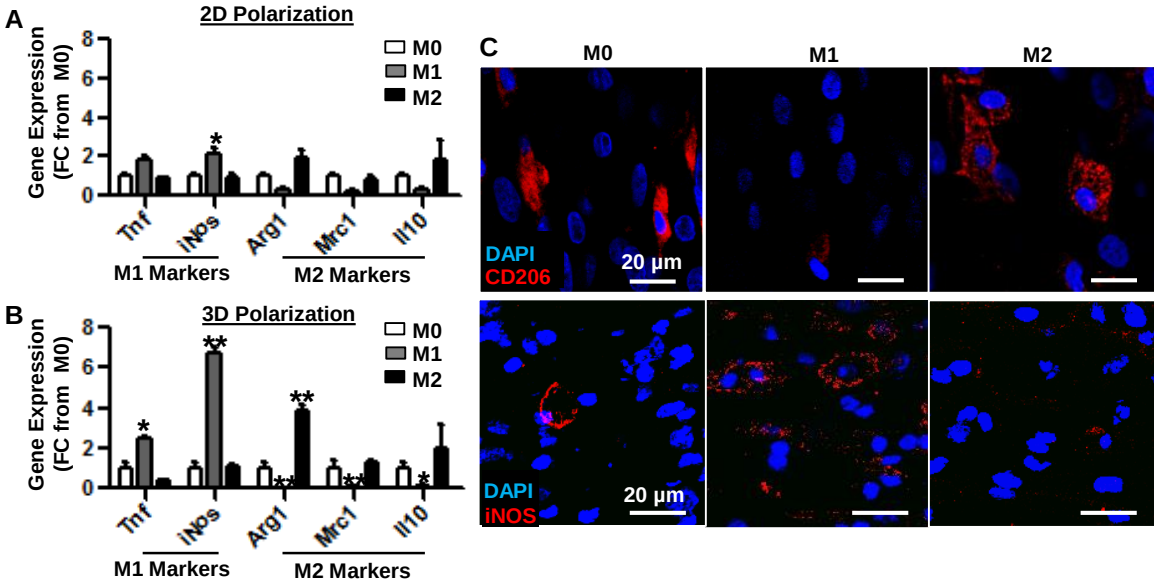

Figure 5.20 Expression of polarization markers within engineered muscle. (A-B) Quantified gene expression of M1 and M2 markers in engineered tissues with M0, M1, and M2 BMDMs added or polarized using 2 methods: (A) prior to bundle formation in 2D culture and (B) within bundles in 3D culture. (C) Representative stainings for M2 marker (CD206) and M1 marker (iNOS) in engineered muscle with M0 BMDMs or following 3D polarization into M1 and M2 phenotypes. N = 2 isolations; *P<0.05, **P<0.01 relative to M0 group.

Following 3D polarization, we assessed roles of BMDM phenotype on response of engineered muscle to CTX injury. BMDM polarization did not have an effect on pre-injury function (Figure 5.21A) or significantly affect dF/F recovery following CTX administration compared to the M0 group (Figure 5.21B). Likewise, active twitch and

tetanus force recovery 5, 10, and 15 days post-CTX was comparable to those of the non-polarized M0 group (Figure 5.21C). M2-treated BMDMs did significantly improve tetanic force recovery at 10 and 15 days post-CTX compared to the M1-treated group, however (Figure 5.21D). Overall, trends reported for dF/F and force recovery suggested improved recovery with the use of M2 vs. M1 BMDMs.

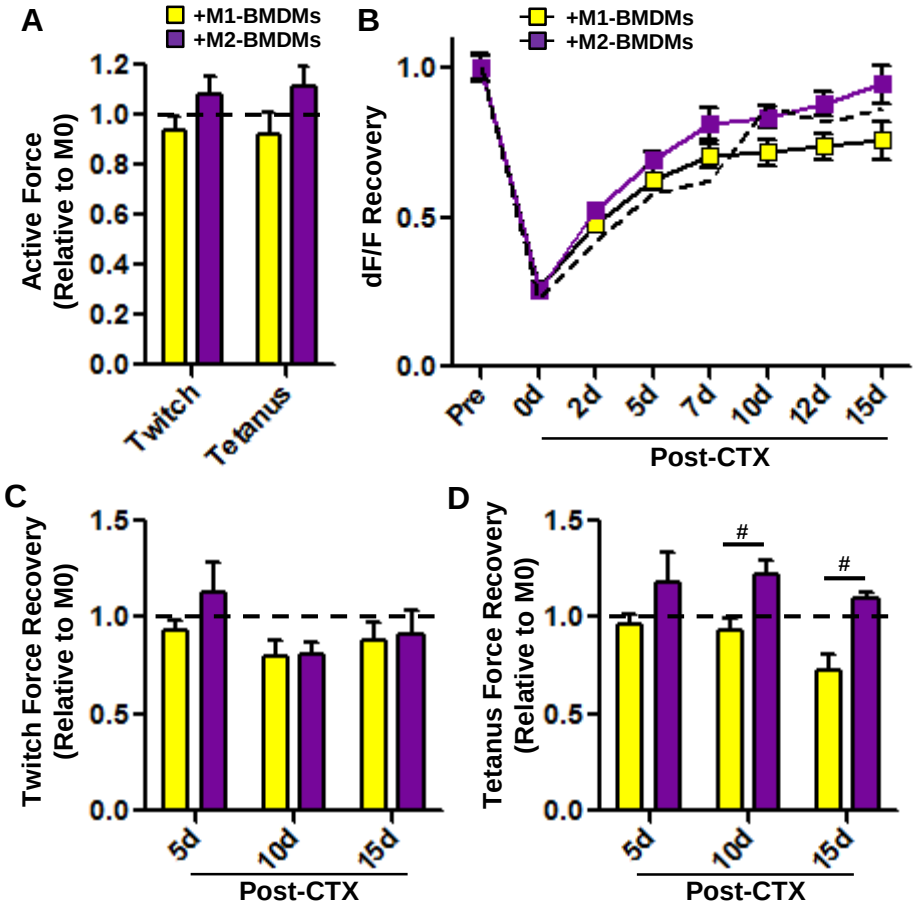

Figure 5.21 Effect of BMDM polarization on functional recovery following CTX injury. (A) Relative force from engineered tissues with polarized M1 and M2 BMDMs compared to M0 pre-CTX injury. (B) dF/F recovery following injury (dashed line represents M0 values). (C-D) Quantified (C) twitch and (D) tetanus force recovery relative to M0 at 5, 10, and 15 days post-CTX. Error bars denote mean ± SEM. N=3 isolations (1-2 bundles/group/isolation). $^{\#}P < 0.05$ between designated groups.

To assess the effects of BMDM phenotype on muscle structure following injury, we analyzed cross-sectional muscle areas (Figure 5.22A). The M1 group exhibited

decreased muscle area at both day 5 and 10 post-CTX compared to M0 group (Figure 5.22B) and at all time-points compared to M2 group (Figure 5.22B). From EdU assay (Figure 5.22C), while neither M1 nor M2 group differed from M0 group, the M1 bundles showed enhanced EdU^+ cell density compared to M2 bundles at day 5 and 10 post-CTX (Figure 5.22D).

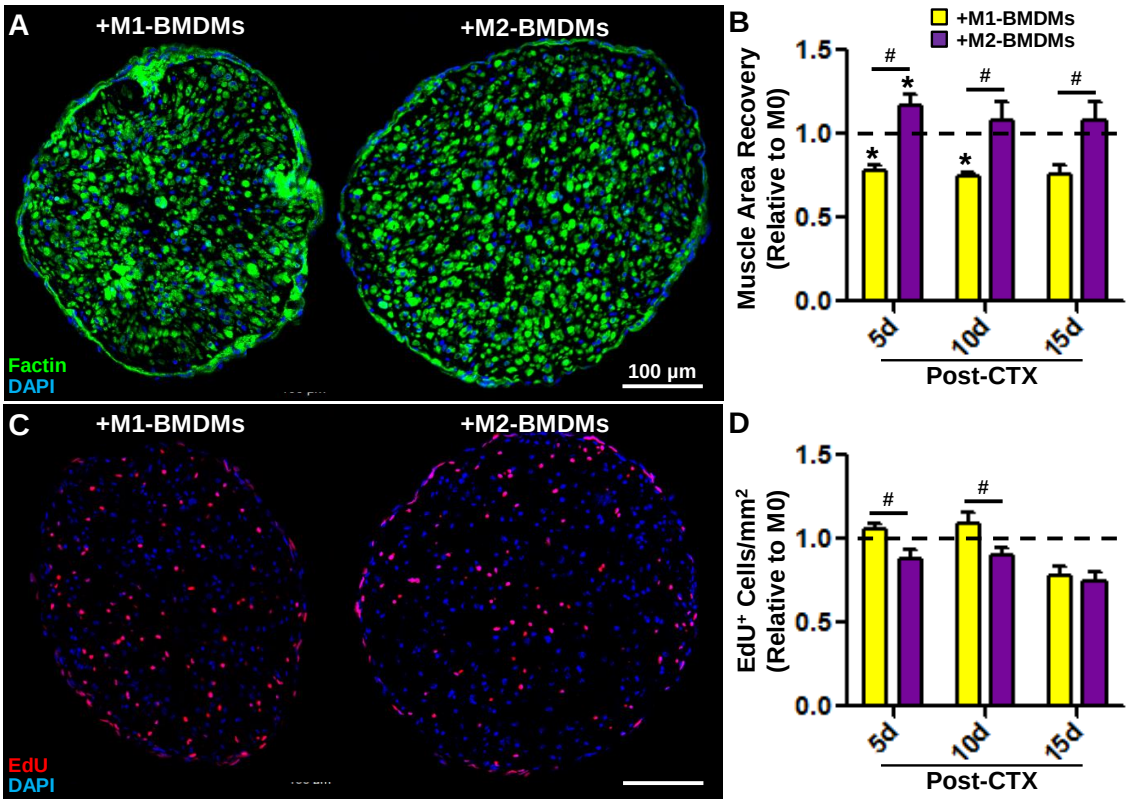

Figure 5.22 The effect of BMDM polarization on structural recovery following CTX injury. (A-B) (A) Representative cross-sectional staining for muscle area at 15 days post-CTX and (B) quantified recovery shown as the percent different from the M0 BMDM group. (C-D) (C) Representative cross-sectional staining for EdU at 15 days post-CTX and (D) quantified EdU^+ cell density shown as the percent different form the M0 BMDM group. Error bars denote mean ± SEM. N = 3 isolations (2-4 bundles per time-point). *P<0.05 compared to M0-BMDM group at same time-point.

5.3.10. Roles of BMDMs in implanted muscle survival, vascularization, and function

Similar to our studies using neonatal-derived muscle, we implemented dorsal window chamber surgery in conjunction with GCaMP transduction to enable real-time, *in*

vivo monitoring of both vascularization and function in control (muscle-only) and muscle-BMDM (M0, M1, M2) tissues. In addition, at 5, 10, and 15 days post-implantation (PI), the constructs were explanted and underwent *ex vivo* functional testing and histological assessment.

5.3.10.1 Effect of M0 BMDMs on engineered muscle vascularization following implantation

Using window chamber model we observed enhanced vessel ingrowth from the host tissue into engineered muscle containing M0 BMDMs compared to the muscle-only control (Figure 5.23A). Quantification of blood vessel density showed a steady increase in vasculature in the M0 BMDM group from day 2 post-implantation (PI) onward (d5: 1.03 ± .04, d7: 1.20 ± .04, d10: 1.44 ± .04, d12: 1.76 ± .06, 2.00 ± .08 fold increase from day 2 PI) and significantly greater ingrowth compared to muscle-only after day 10 PI (d5: 1.06 ± .03, d7: 1.08 ± .03, d10: 1.12 ± .05, d12: 1.23 ± .06, 1.25 ± .07 fold increase from day 2 PI) (Figure 5.23B). From cross-sectional stainings (Figure 5.23C), muscle-BMDM implants exhibited significantly higher lumen density compared to the control group starting at day 10 PI (control: 5dPI: 32.4 ± 7.3, 10dPI: 73.9 ± 5.3, 15dPI: 111.2 ± 8.7 lumens/mm^2, +BMDMs: 5dPI: 38.2 ± 9.8, 10dPI: 124.2 ± 4.4, 15dPI: 200.5 ± 14.5 lumen/mm^2) (Figure 5.23D).

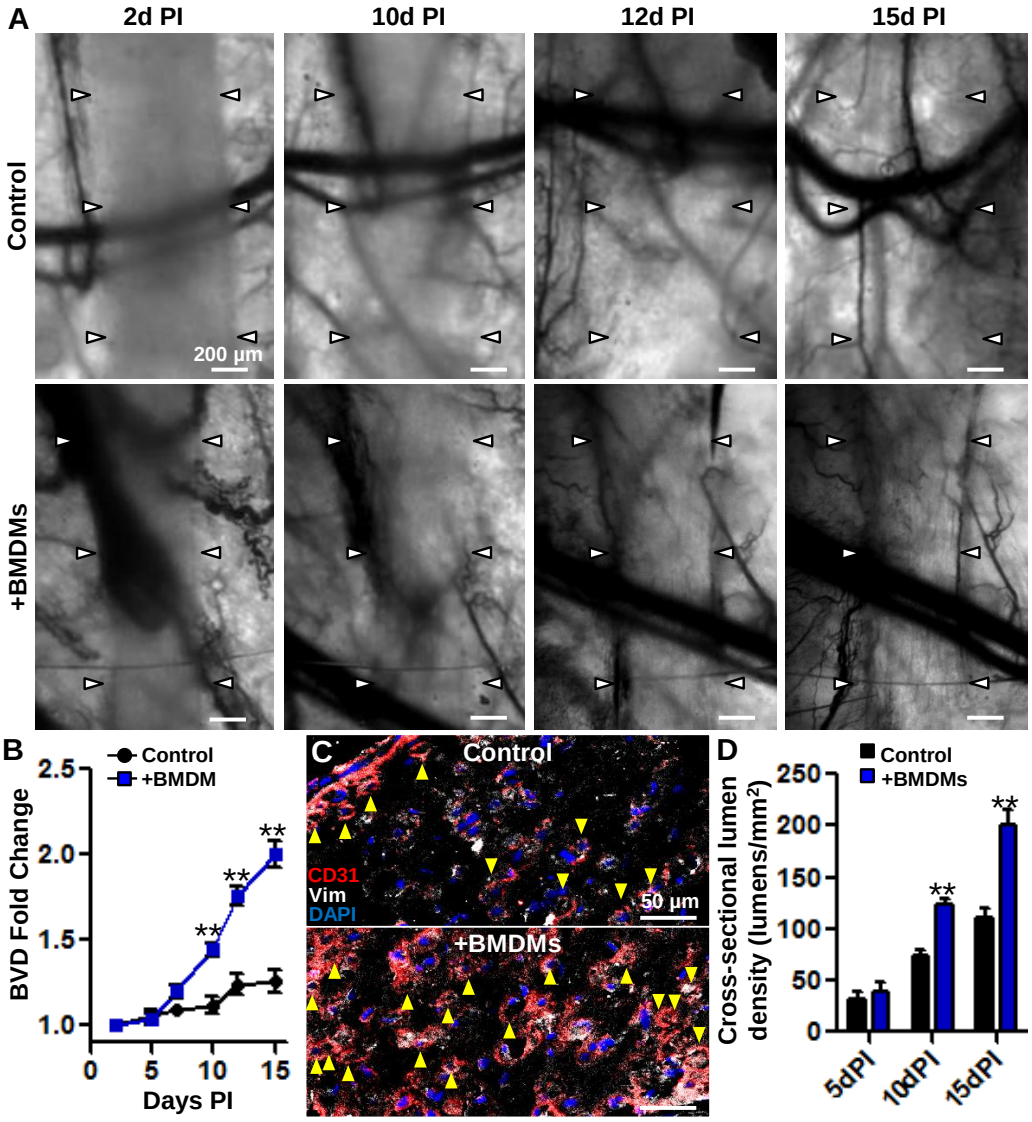

Figure 5.23 Vascularization of implanted adult-derived engineered muscle bundles. (A) Representative intravital images of vascular ingrowth into control (muscle-only, top) and muscle-BMDM (bottom) constructs (white arrows specificy implant boundary). (B) Quantification of blood vessel density (BVD) change over 15 days post-implantation (PI). (C-D) (C) Representative cross-sectional staining of vessel lumens (yellow arrowheads) at day 15 PI and (D) quantified lumen density with time PI. Error bars denote mean ± SEM. N = 8-16 bundles for intravital recordings and 4-6 bundles for lumen density (2 bundles/mouse). ***P*<0.01 compared to control.

5.3.10.2 Effect of M0 BMDMs on engineered muscle function and survival following implantation

Intravital imaging of GCaMP6-reported Ca^{2+} transients (Figure 5.24A) revealed that the BMDM implants (10d: 0.98 ± 0.13, 12d: 1.23 ± 0.16, 15d PI: 1.31 ± 0.23) had

significantly higher transient amplitude starting at day 10 PI compared to control (10d: 0.98 ± 0.11, 12d: 0.44 ± 0.12, 15d PI: 0.42 ± 0.08) (Figure 5.24B). Consistent with intravital studies, electrically-induced Ca^{2+} transients in muscle explants (Figure 5.24C&D) exhibited higher amplitudes in the BMDM group (twitch: 1.49 ± 0.29, tetanus: 4.11± 0.39) compared to control (twitch: 0.56 ± 0.22, tetanus: 1.72 ± 0.36) at 15 days PI, which was associated with higher contractile force generation (Figure 5.24E&F). Importantly, the addition of BMDMs resulted in a significant increase in twitch and tetanic force from 5 to 15 days PI and no statistically significant change in the muscle-only implants (Figure 5.25D).

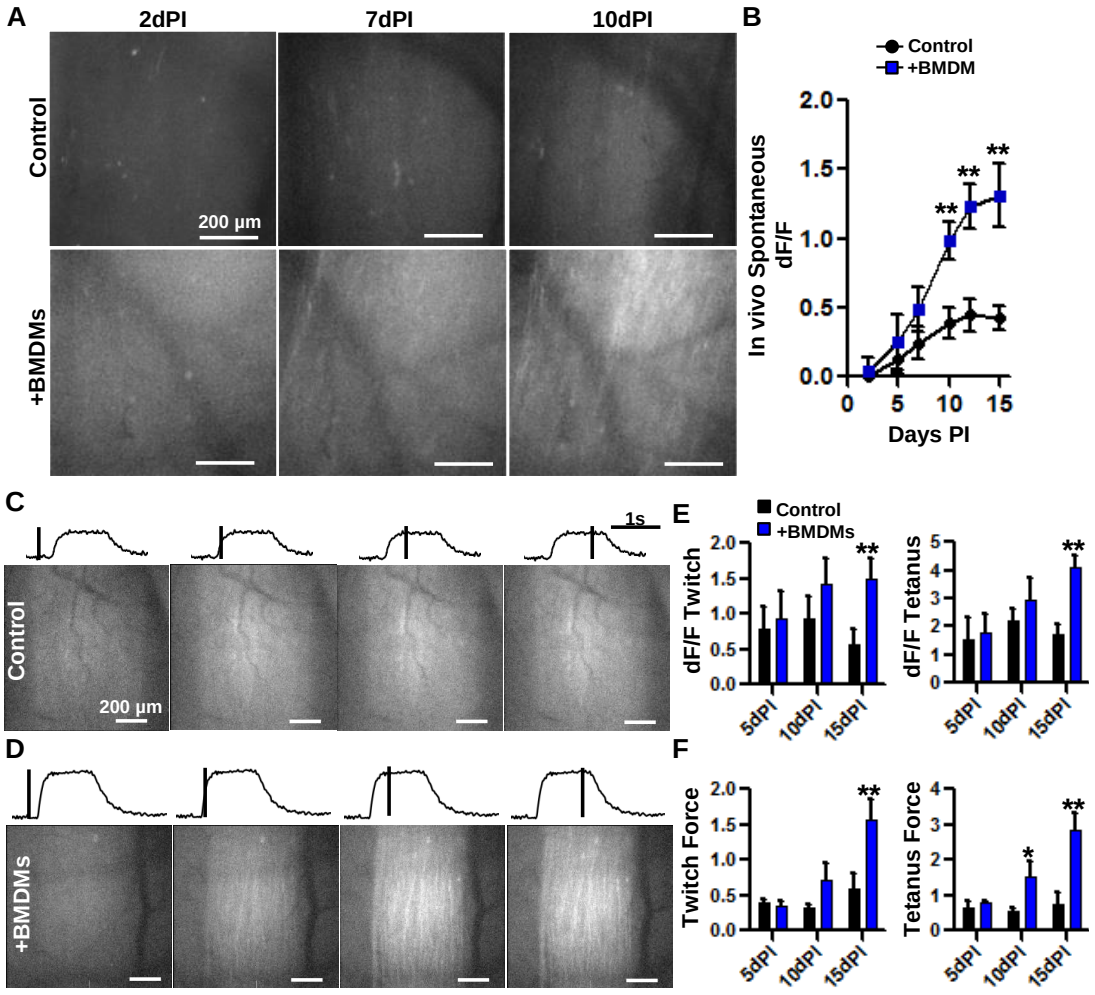

Figure 5.24 Function of adult-derived engineered muscle implants. (A) Representative images of peak spontaneous gCaMP6 signals in implanted engineered muscle without (control) and with M0 BMDMs at various times PI. (B) Quantified peak in vivo spontaneous dF/F amplitude over time PI. (C-D) Representative images of GCaMP signaling during electrically-induced tetanic contraction of explanted engineered muscle (C) without and (D) with BMDMs. (E) Quantified electrically-induced dF/F during twitch and tetanus stimulation in explanted engineered muscle at day 5, 10, and 15 PI. (F) Quantified active twitch and tetanus force in explanted muscle at day 5, 10, and 15 PI. Error bars denote mean ± SEM. N = 8-16 bundles. *P < 0.05, ***P* < 0.01 vs. control at same time-point

From immunostaining analysis (Figure 5.25A), by 15 days PI, the muscle-BMDM bundles appeared to contain more myofibers compared to the control (Figure 5.25B). When compared to pre-implantation state, both groups showed significant loss in myofiber area by day 5 PI, which was gradually recovered over the following 10 days in the BMDM group (5d: 0.36 ± .05, 10d: 0.58 ± .05, 15d PI: 0.81 ± .09 compared to pre-

implantation values) but not in muscle-only group (5d: 0.33 ± .05, 10d: 0.43 ± .09, 15d PI: 0.37 ± .08 compared to pre-implantation values).

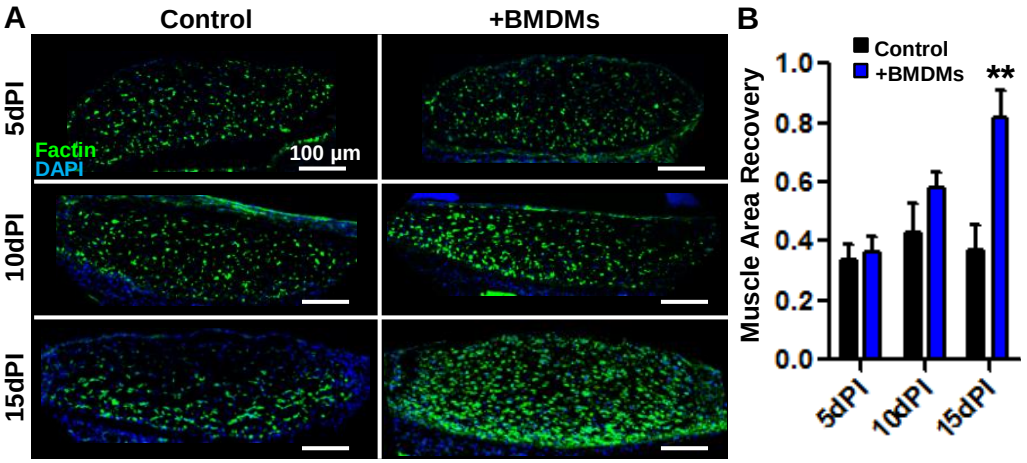

Figure 5.25 Survival of adult-derived engineered muscle following implantation. (A) Representative cross-sectional images of implanted control and BMDM containing muscle bundles, stained with F-actin, shown at day 5, 10, and 15 PI. (B) Cross-sectional myofiber area relative to pre-implantation values. Error bars denote mean ± SEM. N = 4-12 bundles per time-point. **P < 0.01 vs. control at same time-point.

5.3.10.4 Effect of BMDM polarization on survival, vascularization, and function of engineered muscle implants

Similar to use of M0 BMDMs, muscle implants containing M1 and M2 macrophages exhibited a steady ingrowth of blood vessels (Figure 5.26A) and increase in vessel density (M1 d5: 1.04 ± .08, d7: 1.20 ± .08, d10: 1.35 ± .09, d12: 1.59 ± .12, 1.75 ± .16 fold; M2 d5: 1.04 ± .03, d7: 1.21 ± .08, d10: 1.56 ± .08, d12: 1.94 ± .10, 2.05 ± .13 fold compared to day 2 PI) (Figure 5.26B). Furthermore, at 15 days PI, the M1 BMDM containing bundles generated similar twitch (0.87 ± .04) but significantly lower tetanic forces (0.61 ± .09) compared to M0 group (Figure 5.26C), while M2 bundles maintained relatively steady force production (twitch: 0.89 ± .05, tetanus: 1.02 ± 0.12) (Figure 5.26C). This was associated with lower myofiber density found in M1 compared to M2 implants (0.79 ± .06 vs. 1.05 ± .04 relative to M0) (Figure 5.26D&E).

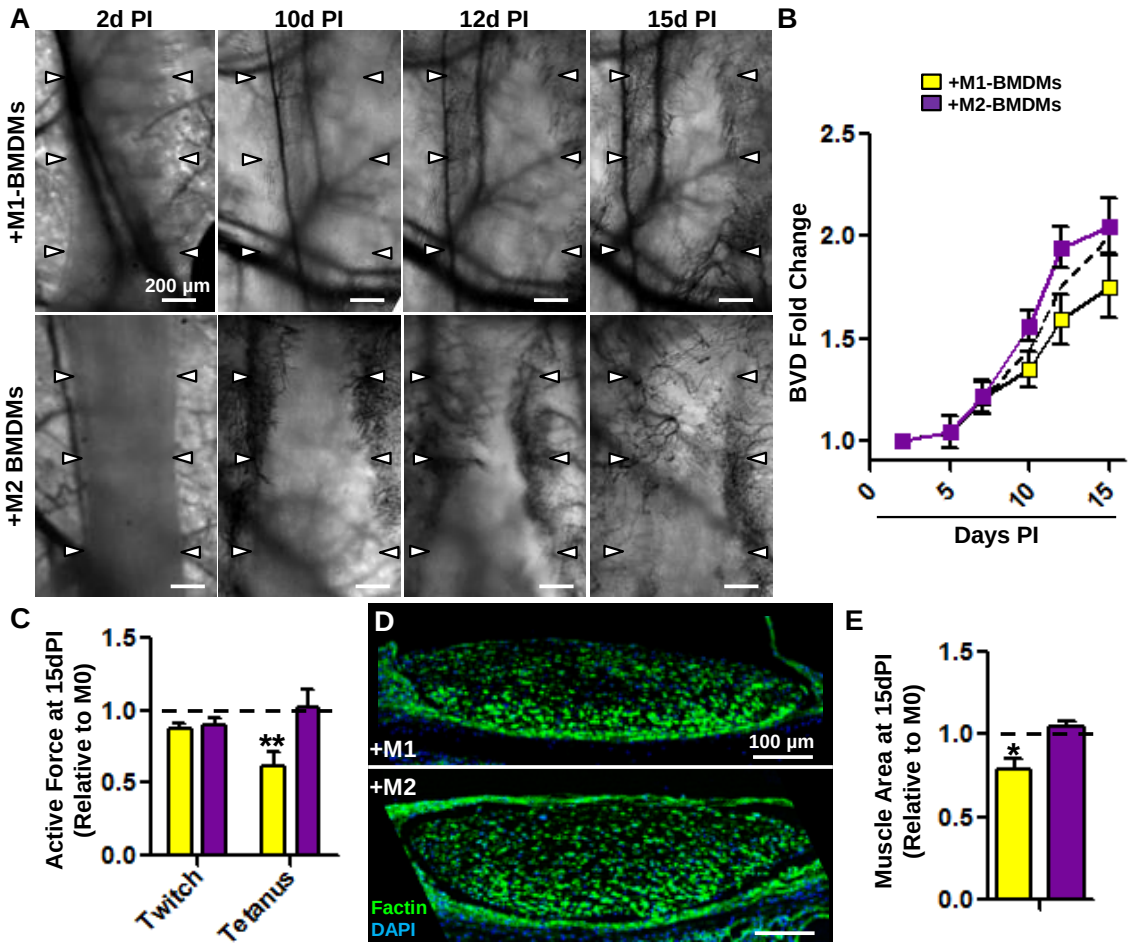

Figure 5.26. Effect of BMDM polarization on vascularization, function, and survival of engineered muscle implants. (A) Representative intravital images of vascular ingrowth into constructs containing polarized M1 (top) and M2 (bottom) macrophages (white arrows specify bundle boundary). (B) Quantification of blood vessel density (BVD) post-implantation (PI) (dashed line represents M0 group). (C) Quantification of twitch and tetanic force at day 15 PI relative to M0 group. (D-E) (D) Representative cross-sectional images of muscle implants at 15 day PI and (E) quantification of myofiber cross-sectional area relative to that of M0 group. Error bars denote mean ± SEM. N = 4-6 mice per time-point, 2 bundles/mouse. **P < 0.01 vs. M0 at same time-point.

5.4 Discussion

In this chapter, to increase translational value of our work, we utilized adult myogenic cells, which compared to neonatal cells are known to be less proliferative, abundant, and regenerative [40, 127]. Engineering of highly functional and regenerative muscle tissues with the improved ability to survive and vascularize *in vivo* was

accomplished by the addition of bone marrow derived macrophages as a pro-regenerative and pro-angiogenic constituent of the adult-derived muscle constructs.

5.4.1 Generation of adult-derived engineered muscle

The future use of tissue-engineered muscle for *in vitro* testing or regenerative therapies would require a significant number of adult-derived cells. Thus we developed methods for utilization of adult rat myogenic cells to lay a foundation for the future work with adult human cells. As SCs from adult muscle [173] require *in vitro* expansion before potential applications, we optimized expansion conditions under a specific bFGF concentration to obtain engineered muscles with robust myofiber formation and the functional properties mimicking those of neonatal engineered muscle (Fig. 5.1) Unlike neonatal-derived constructs, however, the adult-derived tissues did not attain the capacity for self-repair (Figure 5.2), which we attributed to their significantly reduced SC pool compared to neonatal constructs (Figure 5.3).

We therefore expanded the adult myogenic cells (Figure 5.3A) in the presence of inflammation-related growth factors (GFs) shown recently by Fu et al. [152] in murine cells to maintain a high $Pax7^+$ cell fraction during 20-passage expansion without loss of myogenic potential *in vitro* or *in vivo*. Similar to that study, the GF protocol resulted in [152] significantly increased $Pax7^+$ fraction and proliferative potential of expanded cells to levels comparable with those of P0 neonatal cells. However, the resulting muscle bundles showed significantly inferior function, SC pool, and regenerative potential compared to the control adult-derived bundles (Figure 5.5). This result was similar to our findings with passaged neonatal cells when a higher bFGF concentration yielded more SCs in monolayers but less in 3D (Figure 4.6B&C). One likely reason for the lack of SC retention when using the GF-expanded cells could be the limited capacity for occurrence

of early fusion events. In chapter 3 we showed that even though freshly-isolated myogenic cells are expected to be more regenerative [80], they had less propensity for fusion compared to the adherent fraction and thus were not able to create a niche-like environment for SC homing (Figure 3.6). Importantly, the GF-expanded cells had a significantly lower fraction of myogenin^{+} cells, marking myoblasts that are primed to fusion and myotube formation (Figure 5.4C), as well as MyoD^{-} cells, which in our experience represent a fibroblast population necessary for early compaction of 3D tissues and enhancement of cell-cell contacts and fusion (Figure 3.9 and 3.10). Additionally, the treated cells may have experienced epigenetic changes resulting in inhibited myogenic differentiation, suggested by a large number of mono-nucleated fibers found in the bundles (Figure 5.5B). In contrast, P0 neonatal cells which have similar numbers of Pax7^{+} cells in culture, yet are still capable of rapid fusion, were not exposed to factors inhibiting differentiation. These results emphasize the concept that an ideal mixture of activated and committed myogenic cells exists to yield the most functional and regenerative engineered muscle tissues and uncover potential negative effects of myogenic inhibitors for (immediate) engineered muscle formation. Although the murine GF-expanded cells were reported to undergo differentiation and the formation of myotubes in 2D [152], our system relies on this process occurring at a rapid rate upon introduction into the engineered construct.

5.4.2 Enhancing the regeneration of adult-derived muscle

Even at similar SC densities to those of neonatal-derived muscle constructs, the adult-derived tissues were inferior in their ability to functionally recover from CTX injury (Figure 5.3C). As observed in studies of SC populations in aged mice, this may be due to increased p38α/β mitogen-activated protein kinase (MAPK) activity causing defective

function [4]. Supplementing three pro-regenerative factors[178, 235] IGF-1, IL10, or G-CSF, all recently reported to enhance muscle regeneration *in vivo* [226-228], did not improve this inadequate self-repair capacity (Figure 5.7), potentially because these factors mostly enhance one aspect of the regeneration process, such as SC activation and proliferation [226] or differentiation into functional muscle [228]. Additionally, the therapeutic action of different GFs in native muscle may occur indirectly via the effects on non-myogenic muscle cells (e.g. vascular cells, neurons, fibro/adipocyte progenitors) or the recruitment and stimulation of the resident and blood-derived immune system cells [227, 228]. The actions of macrophages, in particular, aid in the activation and proliferation of SCs and subsequent differentiation into mature muscle [27, 238].

5.4.3 Effect of bone marrow-derived macrophages on regeneration

Macrophages incorporated into our system were derived from bone marrow (BMDMs) due to a large yield of this protocol and potential scalability for future clinical applications. Crucial to the differentiation of non-polarized M0 BMDMs was the presence of M-CSF in culture medium [55] which resulted in nearly 100% $CD68^+$ cells (Figure 5.8B) [52]. The M0 BMDMs have been reported to induce myogenic cell proliferation *in vitro* [56, 57] and *in vivo* [52] and are more plastic than polarized pro-inflammatory M1 or anti-inflammatory M2 macrophages [239, 240]. The use of the more plastic M0 BMDMs could allow environmentally induced shift from M1 to M2 phenotype to occur and aid recovery from injury. While polarized macrophages can shift back to the non-polarized state with the depletion of cytokines in the media and become alternatively polarized (e.g. M1 to M2) in the presence of specific factors, both of these processes take days to occur [239, 240]. Of importance, incorporating the numbers of M0 BMDMs into engineered muscle that had no deteriorating effect on SC retention or function (Figure

5.8), still yielded remarkable structural and functional recovery upon CTX injury (Figures 5.9&5.10). The macrophage phenotype proved to be critical to the regenerative response as bone marrow-derived MSCs were incapable of eliciting similar repair.

5.4.4 Understanding the mechanisms behind BMDM-induced regeneration

Analysis of SC activity in muscle-only and muscle-BMDM constructs following injury suggested the ability of SCs to respond appropriately through cellular proliferation and increases in Pax7, Ki67, and MyoD cell populations (Figures 5.12 and 5.13). However, the continual decline in function (Figure 5.9), cellular mass (Figure 5.10B&C), nuclei count (Figure 5.10D), and proliferating cell pool (Figure 5.13) occurring beyond the introduction of injury, made it clear that muscle degeneration was transpiring with the lack of BMDMs present. The events suggested apoptosis within the injured engineered muscle, a process commonly associated with CTX-induced injury *in vivo* [241]. Cleaved Caspase-3, a protein responsible for apoptosis through DNA fragmentation in myofibers *in vivo* [242-244] and *in vitro* [245], was present at high levels out to 10 days post-injury in the muscle-only condition. Although Caspase-3 was upregulated immediately upon injury in muscle-BMDM constructs (Figure 5.14A), this is consistent with injury models *in vivo* [246] and is known to stimulate proliferation in surrounding cells via paracrine actions [247]. BMDMs attenuated Caspase-3 expression by 2 days and cleaved-Caspase-3 presence by 5 days post-injury (Figure 5.14A-C). Highlighting the importance of the anti-apoptotic effect of BMDMs, administration of a commercially available pan-caspase inhibitor, Q-VD-OPh [248], for 10 days following injury significantly enhanced the regenerative ability in muscle-only bundles (Figure 5.15).

Shared media experiments in which regeneration within muscle-only and muscle-BMDM bundles was dependent on the extent of injury, identified that anti- and pro-

regenerative extrinsic stimuli are acting in the system (Figures 5.16 and 5.17). One factor which may be a significant effector is tumor necrosis factor-α (TNFα). For one, TNFα and its receptor (TNFR1) is a major extrinsic apoptotic pathway upstream of Caspase-3 [249]. In skeletal muscle, increases in circulating and local TNFα concentrations are associated with aging [250] and disease [251] and are linked to increased apoptotic events and sarcopenia [250, 252]. Importantly, adult muscle is more susceptible to TNFα-induced apoptosis, linked to age-related differences in TNFα-induced NF-κB activation [253] and a greater propensity of cross-talk between extrinsic and intrinsic apoptotic pathways [252]. TNFα is immediately upregulated in the engineered muscle upon injury (Figure 5.27), consistent with *in vivo* findings [251, 254] as the factor is known to stimulate the immune response and initiate regeneration [27]. *In vivo* suppression of TNFα occurs as anti-inflammatory macrophages attenuate pro-inflammatory factors, including TNFα [27]. Without external stimuli, TNFα is known to self-regulate in instances of cell damage, increasing its secretion in an autocrine manner [255]. This continued propagation of the pro-apoptotic cytokine could explain the steady upregulation of TNFα and Caspase-3 over a 5 and 10 day span, respectively, and the subsequent spread of apoptotic events (Figures 5.14 and 5.27). Furthermore, as neonatal cells are less susceptible to apoptosis through this pathway, their ability to undergo the regenerative response may be less affected by the stimuli [252, 253].

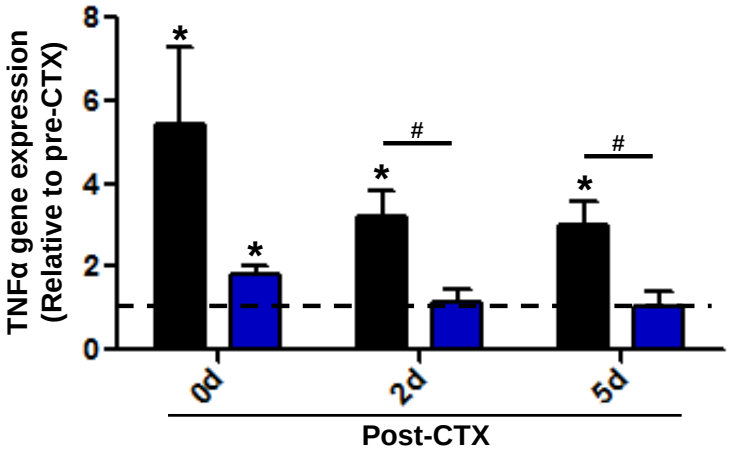

Figure 5.27. TNFα gene expression following injury. Plot of quantitative RT PCR results showing TNFα gene expression at 0, 2, and 5 days post-CTX relative to pre-CTX levels. Error bars denote mean ± SEM. N = 3-4 isolations. *P<0.05 compared to pre-CTX expression at same time-point, #P<0.05 between groups designated with line.

The addition of BMDMs could affect apoptosis in a few ways. Previous studies report that BMDMs are capable of preventing apoptosis in SCs and myotubes through cell-cell contact-dependent signaling [56, 57]. As seen in Figure 5.28A, BMDMs within the engineered tissues do come in contact with regenerating myofibers which could aid in their survival and prevent autocrine increases in TNFα or other pro-apoptotic factors. However, considering the pro-regenerative paracrine effects in mild injury, it is more likely that BMDMs aid through cytokine release. Bone marrow-derived cells have been reported to secrete cell survival factors to limit apoptosis, including Akt and eNOS [256]. More specific to our system, BMDMs may offer suppression of TNFα-induced apoptosis. As the BMDMs within the engineered muscle resemble the M2 phenotype (Figures 5.20 and 5.21) and M-CSF-exposure tends to drive differentiation in that direction [237], the cells may support the down-regulation of TNFα through secretion of anti-inflammatory factors such as IL-6 and IL-10 [27, 257]. Phagocytic events occurring following injury (Figure 5.28B) are also linked to the subsequent promotion of anti-inflammatory cytokine release and down-regulation of pro-inflammatory factors including TNFα [258]. In the

shared media setting, it could be expected that severe injury would result in too high of concentrations of TNFα for BMDMs to have an effect consistent with findings in chronic inflammatory diseases [250-252, 254].

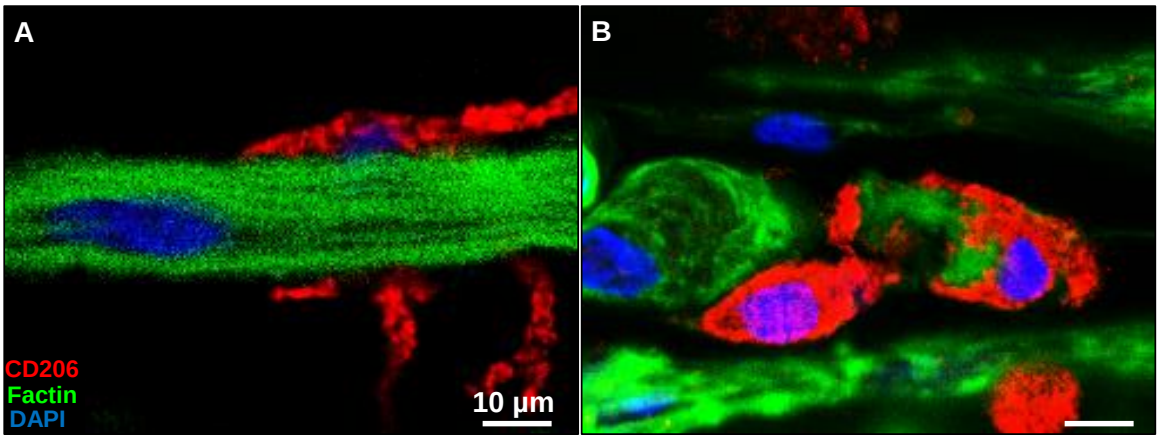

Figure 5.28. BMDMs contribution during regeneration. (A-B) CD206^{+} macrophages appearing to (A) be in cell-cell contact with a distraught myofiber at day 5 post-CTX and (B) participate in phagocytosis.

5.4.5 Effect of BMDMs polarization on regeneration following CTX injury

The addition of polarizing cytokines to stimulate pro- (M1) and anti-inflammatory (M2) phenotypes proved efficient in 2D monolayer and 3D engineered muscle culture (Figures 5.19 and 5.20). As functional results following the CTX injury revealed marginal differences in response compared to non-polarized M0, the general trend suggested enhanced repair in the presence of anti-inflammatory BMDMs (Figure 5.21). The varied results may stem from the negative effects of pro-inflammatory factors early in the regenerative process evidenced by significantly greater muscle loss in the M1-BMDMs constructs compared to M2 (Figure 5.22). Cell death may again be associated with TNFα expression which was upregulated in M1 and decreased in M2 polarization prior to injury (Figure 5.20) and commonly secreted and attenuated by the two phenotypes, respectively [27]. The significantly higher amount of EdU^{+} cells in the M1 vs. M2

condition at early time-points (Figure 5.22D) supports this claim as TNFα and other pro-inflammatory cytokines are stimulants of SC proliferation [27]. The ability of M1-BMDMs to ultimately support regeneration may suggest a shift from pro- to anti-inflammatory phenotype during the regeneration process. The transition could have occurred due to the withdrawal of polarizing cytokines, as reported in a non-injury condition (Figure 5.20A) and literature [239, 240]. Alternatively, events of phagocytosis [258] or environmental cues associated with M1 to M2 transition, including IGF-1 expression [45], may have triggered the conversion.

Of further interest was the tendency of the M0 BMDMs to exhibit anti-inflammatory properties when in co-culture with muscle cells as suggested by gene expression (Figures 5.19 and 5.20). As mentioned, M-CSF exposure results in a more M2-like phenotype without the presence of polarized factors [237]. An intriguing possibility is the adaptation of M0-BMDMs to a tissue-resident macrophage phenotype while in the engineered muscle. Muscle-resident macrophages are commonly M2-like and respond immediately to injury by attenuating the pro-inflammatory response [49] and aiding in apoptotic cell clearance through phagocytosis [50]. It would be of future interest to compare the characteristics of the BMDMs in our engineered muscle to the muscle-resident population in natural muscle. Optimized conditions to induce recreation of the resident macrophage niche could further enhance regeneration and may contribute towards other therapeutic venues.

5.4.6 Effect of BMDMs on in vivo vascularization, function, and survival of engineered muscle

The ability of adult-derived engineered muscle to integrate, function, and survive in an *in vivo* setting was assessed through the use of the window chamber implantation

method described in chapter 4. Without the presence of BMDMs, muscle-only implants underwent marginal increases in vascular density and GCaMP activity over 15 days *in vivo* and experienced minimal changes in contractile force or muscle area (Figures 5.23, 5.24, and 5.25). On the contrary, the BMDMs significantly enhanced vascular ingrowth and *in vivo* GCaMP activity when incorporated into the implants and resulted in greater vessel density, electrically-stimulated dF/F measurements, active force generation, and muscle area at 15 days PI compared to the muscle-only group (Figures 5.23, 5.24, and 5.25). Importantly, the BMDMs inspired increases in all these values over time suggesting a steady maturation or recovery process occurring within the implant.

The neonatal implantation studies highlighted the detrimental effects as a result of initial ischemic conditions. This result led us to associate the ability to survive and mature *in vivo* with the regenerative capacity to overcome the initial cellular stress. Similarly, we observed greater *in vivo* success with adult muscle-BMDM implants, also capable of *in vitro* self-repair. It was evident that *in vitro* regeneration was attributed to the anti-apoptotic effects of BMDMs, however it is not known if the cells are contributing to *in vivo* survival through a similar mechanism. In ischemia, skeletal muscle cells typically experience necrosis rather than apoptosis [259]. Unlike CTX-induced damage *in vitro*, the muscle-only implants did not experience continual degeneration indicating that apoptosis may not be occurring *in vivo*. This suggests that the ability of BMDMs to stimulate angiogenesis [33, 34, 233, 260] may have a greater influence on *in vivo* health than the anti-apoptotic effects associated with regeneration following CTX-induced injury. Supporting this claim is the observed association of functional increases with enhanced vascular density in the muscle-BMDM implants. Further, this is consistent with reports of myofiber maturation following increased nutrient supply in ischemic muscle *in*

vivo [261]. However, maintained survival attributed to BMDM localization within the implant could have triggered angiogenic events due to increased metabolic activity as proposed when comparing pre- vs. undifferentiated muscle constructs [222].

Similar to our work *in vitro*, we assessed the impact of polarized BMDMs on success *in vivo*. As with SC activity, events of neo-vascularization are coordinated through actions of both M1 and M2 phenotypes [260]. Traditionally, pro-inflammatory M1 cells initiate angiogenesis and the migration of vessels and anti-inflammatory M2 cells support the stabilization of the vascular network [260]. Our results showed steady vascular ingrowth in both settings (Figure 5.26A&B). Although not significant, anti-inflammatory BMDMs tended to induce greater vessel density in the implant region than pro-inflammatory. This is consistent with recently reported results of enhanced angiogenesis with the implantation of M2 vs M1 macrophages [233]. M2-BMDMs did not differ from the use of M0-BMDMs in active force generation or muscle area at 15 days PI. However, the use of M1-BMDMs resulted in significant decreases in both tetanic force amplitude and musculature. Overall, the results of BMDM polarization on *in vivo* implantation coincide with the results of *in vitro* regeneration. In both conditions, anti-inflammatory BMDMs seem more efficient in restoring musculature and functional following insult. It was proposed *in vitro* that the anti-inflammatory response contributed to a reduction in apoptotic events. Whether this is the same case *in vivo* and M2-BMDMs prevent cellular loss or if anti-inflammatory response is inducing enhanced vasculature, as previously reported [233], is still in question.

All-in-all, it is clear that the introduction of BMDMs supports implant success *in vivo*. The presence of the immune cell type encouraged increases in vasculature formation and function over time PI. Introducing macrophages into engineered tissues

prior to implantation may lead to a new paradigm in the field. As seen in Figure 5.29, $CD68^+$ macrophages from the host are recruited to the implant region in both muscle-only and BMDM conditions by day 15 PI. Localization of the BMDMs in the implant prior to implantation likely accelerates the beneficial effects of the immune response resulting in greater cell survival and function.

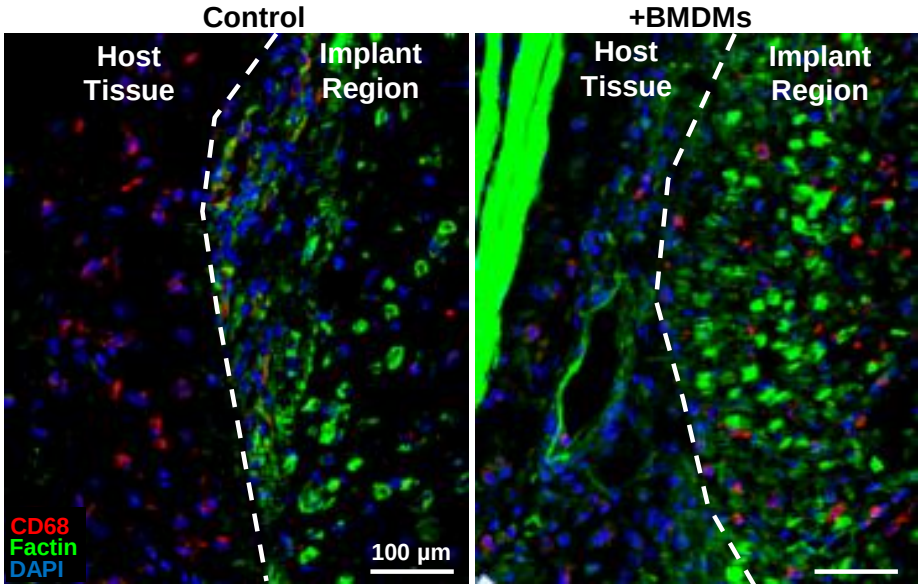

Figure 5.29. Invasion of macrophages following implantation. Representative cross-sectional images showing high number of $CD68^+$ cells in the host tissue surrounding the engineered muscle implant at 15 days PI. Of note, $CD68^+$ cells are present within the muscle-BMDM implant.

5.5 Summary and Implications

In this chapter, we reported the ability to construct adult-derived engineered muscle tissue and identified the ability of BMDMs to support its regenerative ability and function as an implant. Using an expanded adult myogenic population, we were able match the structure and force generating ability of neonatal muscle under the same condition. However, we revealed the inability of engineered tissues to respond to injury *in vitro*, unlike their neonatal counterpart. After failed attempts to enhance SC density and activity within the tissue, we discovered the remarkable benefits of the addition of

BMDMs to the 3D construct. BMDMs proved valuable in preventing apoptotic events and supporting the proliferation of SCs, the reformation of muscle, and recovery of function following injury. Inhibitor and shared media studies suggested that the mechanism governing the effect of BMDMs was upstream of cleaved caspase-3 activity and an extrinsic signal. Based on these results and gene expression data, we suspected that BMDMs may be involved in attenuating the TNFα-induced apoptosis pathway in our model. Using polarized M1 and M2 BMDMs, we revealed the benefit of anti-inflammatory macrophages in supporting *in vitro* regeneration events. Finally, we applied the muscle-BMDMs to an *in vivo* setting using the dorsal window chamber implantation method. BMDMs proved beneficial in inducing vasculature ingrowth and enhancing muscle area and contractile function over time *in vivo*. The anti-inflammatory phenotype again proved more successful for implant survival. Together, these results can applied to further study adult models of muscle regeneration, growth, and disease *in vitro* and *in vivo*. Importantly, the muscle-BMDM system can be studied more extensively to unravel specific molecular pathways increases regenerative potential of muscle which may eventually lead to more effective therapeutics.

6. Summary

Skeletal muscle tissue engineering presents a unique opportunity to create 3D tissues that recapitulate developmental, regenerative, and disease-related events in an *in vitro* setting. Researchers are able to isolate specific cellular components, control culture environment, and assess functional and structural results more efficiently than with animal studies. Further, methods can be applied to human isolates to enable drug screening and therapeutic testing in a non-invasive, patient-specific manner. Moreover, implantation studies using engineered constructs lay the foundation work for future procedures involving the replacement of large tissues. Identifying methods to enhance implant integration into the host, survival, and maturation may eventually lead to optimized structures capable of rapid and efficient contribution to natural function. In this thesis we were able to progress the field of tissue engineering, presenting methods to engineer biomimetic skeletal muscle constructs capable of accurate modeling of native tissue structure, function, growth, and regeneration. We also reported studies identifying optimal methods applying to *in vivo* survival and functional maturation of engineered-tissues upon implantation. Through our work, we also developed tools to enable non-invasive, real-time recording of cellular viability and function *in vitro* and *in vivo*.

Initial *in vitro* work began with the creation of constructs capable of recreating the cellular composition, structure, and force generating abilities of natural muscle using neonatal myogenic cells isolates. We identified that selecting the adherent fraction of the isolated cells and culturing the tissue under dynamic conditions generated the most optimal tissue. The engineered muscle contained highly-aligned, contractile myofibers and a $Pax7^+$ SC pool, was comprised of skeletal muscle-specific ECM proteins, and able to generate forces comparable to aged-matched native muscle. With increased time in

culture, the muscle demonstrated the capacity to undergo hypertrophy and functional maturation. Important to our work was the identification of processes that enabled SC maintenance within our engineered tissue. Tracking myogenesis at early time-points, we were able to witness the necessity of rapid myofiber formation to create a niche-like environment to home SCs and preserve their quiescence.

For the first time, we were able to recreate the SC's contribution to muscle regeneration in a 3D environment *in vitro*. We tracked the cellular activity during activation, proliferation, and differentiation as the SC pool regenerative actions resulted in the functional and cellular recovery following injury. Using methods to control SC density, we were able to show the importance of the cellular pool in stimulating muscle regrowth in our system. When transitioning to adult muscle isolates, we incorporated the optimized methods from our neonatal work in attempt to generate adult-derived engineer muscle also capable of modelling regeneration. However, even with a retained SC pool, the adult tissues proved unable to survive following induced injury. Using a real-time, *in vitro* regeneration assay we screened for therapeutics that could aid in recovery in these constructs. Through this assessment, we identified the remarkable benefit of bone marrow-derived macrophages (BMDMs) to contribute to regenerative events.

BMDMs were initially added due to their role in natural regeneration to stimulate SC activation, proliferation, and differentiation [27]. Interestingly, in our system we identified that BMDMs were most crucial in preventing continued apoptotic events occurring in the injured adult muscle. Studies revealed the ability of SCs to respond to injury without and with the presence of BMDMs. However, in muscle-only constructs, pro-apoptotic stimuli induced the steady degeneration of cells past that of initial insult. BMDMs prevented apoptotic events and allow SCs to fulfill their contribution to functional

and cellular recovery. The effect of a pan-caspase inhibitor to enable regeneration without the presence of BMDMs furthered stressed the importance of anti-apoptotic mechanisms in our system. Shared media studies and work with polarized BMDMs phenotypes further suggested that extrinsic signaling was responsible for the induction of apoptosis and may be contributed to pro-inflammatory TNFα. TNFα-induced apoptosis, upstream of caspase-3, is commonly associated with muscle degeneration [251-254]. Gene expression data revealing the attenuation of the pro-inflammatory cytokine in muscle-BMDM constructs further strengthened the prospect of its effect in engineered muscle regeneration.

Throughout the thesis, we also assessed the ability of neonatal- and adult-derived engineered muscle to survive *in vivo*. To enable real-time, non-invasive monitoring of the implants we designed a novel system combining the dorsal widow chamber model with GCaMP transduction. This method allowed for intravital imaging of vascular ingrowth and cellular function marked by Ca^{2+} transients. Neonatal muscle proved capable of integrating into the vasculature network of the host and, upon recovery from initial insult, steady functional improvement and cell growth. Within our neonatal studies, we also revealed the benefit of pre- compared to un-differentiated muscle implants in inducing angiogenesis, providing initial structure, and increasing force generating abilities. Transitioning to adult-derived engineered muscle implantation, we revealed the advantages associated with the addition of BMDMs in the tissue once again. The BMDMs encouraged more rapid vascularization and functional improvements compared to the muscle only control. Additionally, we exhibited promotion of these events using anti- vs. pro-inflammatory cell types. In all, these results lay direction a strong foundation for future implantation studies.

7. Future Applications

While the work reported in this dissertation contributes to the tissue engineering and muscle regeneration fields, it also suggests additional questions and applications that could be explored in future studies. In particular, our system could be applied to create regenerative human-derived muscle tissue, used to thoroughly investigate the interaction between macrophages and myogenic cells during regeneration, and implemented into more advanced and clinically-relevant implantation models.

An obvious transition of the rodent work presented in this dissertation is towards the engineering of regenerative human-derived muscle. Our group has reported the ability to generate human muscle constructs from patient biopsies capable of contractile response to electrical and chemical stimuli; however, the tissues lack the ability for self-repair [155]. Specific strategies identified in this work would be implemented to retain a functional SC pool in the human system. Following isolation, culture with inflammatory growth factors (GFs: TNFα, IL-13, IL-1β, and IFNγ [152]) identified to enhance $Pax7^+$ cells in monolayers during expansion would be used to generate a starting population of SCs prior to engineered muscle formation. If unsuccessful, other protocols to enhance proliferation and self-renewal of SCs could also be attempted, including the use of different media supplements (SB202190 [150], forskolin/BIO [151], or LY364947 [262]), ECM coatings (fibronectin [263] or collagen VI [109]), and/or hypoxia [264]. Alternatively, iPSC technology could be used to generate human myogenic cells using a protocol to induce conditional expression of Pax7 [87] that will not require invasive extraction of muscle tissue. Upon the formation of engineered muscle, rapid fusion events proved critical for $Pax7^+$ cell retention in the rodent work. To drive immediate formation of myofibers in the human system, we would implement administration of cytokines

inducing myogenic differentiation (IGF-1 or TGFβ [2]), the addition of contractile fibroblasts to enhance cell-cell interactions, and/or the withdrawal of culturing factors prior to use to avoid negative effects on fusion. If consistent with rodent results, adult human-derived engineered muscle may require the addition of macrophages to obtain regenerative potential. Two methods would be attempted to generate the immune cell source for incorporation into muscle constructs, 1) isolation of circulating monocytes from patient blood [265] and 2) derivation of monocytes from human iPSCs using reported protocols [266].

The generation of a regenerative human muscle could contribute significantly to advancements in personalized therapeutics associated with inefficient repair in cases of injury [24], age [150], or other myopathies [58]. The real-time, *in vitro* regeneration assay could be scaled down for application as a 96-well high-throughput system [224] to strengthen its utility as a screen. Additionally, a reporter generated by CRISPR/Cas9-mediated incorporation of a florescent protein cassette into the genomic local of Pax7 [267] could be utilized to specifically track SC dynamics in real-time following injury. Such a system would be able to identify patient-specific small molecule effectors of self-repair and comprehensive study of human SCs in response to various stimuli and environments.

Future studies will need to be performed to gain a more comprehensive mechanistic understanding the anti-apoptotic effects of BMDMs on myogenic cells during regeneration. TNFα was proposed as the effector molecule in the system, serving as an extrinsic signal to induce downstream caspase activity deduced through results from shared media experiments, gene expression, and the effect of pan-apoptotic inhibitors. Cytokine profiles will need to be evaluated through an enzyme-linked

immunosorbert assay (ELISA) to confirm the enhanced release of the TNFα protein following severe injury of muscle-only constructs. Further, antibodies targeting TNFα and its receptor (TNFR1) will be used in attempt neutralize the effect of the stimulus in muscle-only constructs following injury. If antibodies prove successful, clinically-used TNF-inhibitors for rheumatoid arthritis, including infliximab, adalimumab, etanercept, golimumab, and certolizumab-pegolb [268], will be screened to identify potential therapeutics.

The specific mechanism in which BMDMs inhibit apoptosis will also need to be evaluated. Our shared media experiments suggested a paracrine effect of BMDMs and therefore two pathways will be explored: 1) cytokine release and 2) exosomal transfer. ELISA will be used to identify upregulated cytokines in conditioned media following CTX injury of muscle-BMDM constructs. Identified factors will be screened alone, or in combination, to assess whether they can stimulate regeneration in muscle-only bundles following severe injury. In the event of successful regeneration, QT-PCR will be applied to assess the effect of the specific factors on gene expression related to apoptosis with particular focus on the TNFα pathway. Exosomes, microvesicles carrying messenger RNA, micro-RNA, and cytokines, are known to regulate cellular behavior through cell-to-cell transfer of functional RNA constructs and growth factors stimulating transcription [269]. Although much less investigated than cytokines, recent work has identified muscle-derived, either from resident progenitors [270] or differentiated myofibers [271], and MSC-derived [272] exosomes to contribute and enhance regeneration. Macrophage-derived exosomes, the largest portion of circulating microvesicles [273], to our knowledge, have yet to be explored for their roles in muscle repair. Exosomes will be isolated from conditioned media following severe injury of muscle-BMDM constructs

using ultra-centrifugation methods. The purified vesicles will be applied to muscle-only bundles following injury to determine whether they can stimulate regeneration. If successful, exosomal miRNA will be isolated and screened using a miRNA assay to identify specific sequences responsible for the effect. Additionally, the effect of BMDMs on muscle repair will be assessed *in vitro* using injury modalities to better represent *in vivo* environments. These will include necrosis-stimulating $BaCl_2$ administration and the use of hypoxic culture to simulate ischemia [274].

Lastly, our *in vivo* work provides a foundation for many future implantation studies. The ability of engineered muscle tissues to serve for volumetric muscle loss therapy [17, 24, 181] will need to be explored. We have developed an implantation model in which muscle bundles are inserted into the biceps femoris of a nude mouse following excision of ~40% of the tissue. Intra-muscular placement of the implant would enable assessment of functional integration, a process that cannot be studied in the window chamber model. Importantly, innervation of the engineered tissue could be assessed through GCaMP transduction of the implant and subsequent neuronal stimulation. Induced-GCaMP signal would confirm the capacity of the implant to function via integration into the neuromuscular system of the host. Additionally, the introduction of BMDMs into the engineered muscle could enable study of the role of macrophages in re-innervation post-injury. In peripheral and central nervous system repair, anti-inflammatory macrophages are considered to have beneficial effects on neural regrowth as pro-inflammatory cells contribute to neuronal damage, however, effects following muscle injury are still unknown [275-277]. Although initial implantation studies should target clinically-relevant replacement of small muscles (e.g. craniofacial reconstruction), methods to scale-up implant volume should be explored. Pre-vascularization techniques

utilizing endothelial cells to create existing vessel networks within the muscle implants may expedite the vascularization process. Upon implantation, rather than host vasculature migrating into full thickness of the engineered tissue, rapid anastomosis could link the existing vessel network to the host's blood supply. Considering the *in vitro* limitations of developing large tissues, such a technique could be used in implantation of multiple small tissues to facilitate rapid vascularization and prevent hypoxia-induced cell death during large volume repair. Finally, the window chamber implantation method described within the dissertation could be applied to human-derived engineered muscle. The ability to track vascularization and function through intravital imaging would allow us to assess real-time effects of therapeutics or drugs on engineered human muscle in an *in vivo* environment. Additionally, in this setting, intravenous injections of drugs and/or muscle-specific, adeno-associated viruses would result in their vascular delivery into the implanted human muscle tissue in a clinically-relevant fashion.

References

[1] H. Yin, F. Price, M.A. Rudnicki, Satellite cells and the muscle stem cell niche, Physiological reviews, 93 (2013) 23-67.

[2] S.B. Charge, M.A. Rudnicki, Cellular and molecular regulation of muscle regeneration, Physiological reviews, 84 (2004) 209-238.

[3] A.S. Brack, T.A. Rando, Intrinsic changes and extrinsic influences of myogenic stem cell function during aging, Stem cell reviews, 3 (2007) 226-237.

[4] B.D. Cosgrove, A. Sacco, P.M. Gilbert, H.M. Blau, A home away from home: challenges and opportunities in engineering in vitro muscle satellite cell niches, Differentiation; research in biological diversity, 78 (2009) 185-194.

[5] M. Juhas, N. Bursac, Engineering skeletal muscle repair, Current opinion in biotechnology, (2013).

[6] N. Bursac, M. Juhas, T.A. Rando, Synergizing Engineering and Biology to Treat and Model Skeletal Muscle Injury and Disease, Annual review of biomedical engineering, 17 (2015) 217-242.

[7] W. Bian, N. Bursac, Engineered skeletal muscle tissue networks with controllable architecture, Biomaterials, 30 (2009) 1401-1412.

[8] W. Bian, M. Juhas, T.W. Pfeiler, N. Bursac, Local tissue geometry determines contractile force generation of engineered muscle networks, Tissue engineering. Part A, 18 (2012) 957-967.

[9] W. Bian, N. Bursac, Soluble miniagrin enhances contractile function of engineered skeletal muscle, FASEB journal : official publication of the Federation of American Societies for Experimental Biology, 26 (2012) 955-965.

[10] S. Hinds, W. Bian, R.G. Dennis, N. Bursac, The role of extracellular matrix composition in structure and function of bioengineered skeletal muscle, Biomaterials, 32 (2011) 3575-3583.

[11] C. Rhim, C.S. Cheng, W.E. Kraus, G.A. Truskey, Effect of microRNA modulation on bioartificial muscle function, Tissue engineering. Part A, 16 (2010) 3589-3597.

[12] J. Shansky, M. Del Tatto, J. Chromiak, H. Vandenburgh, A simplified method for tissue engineering skeletal muscle organoids in vitro, In vitro cellular & developmental biology. Animal, 33 (1997) 659-661.

[13] C.A. Powell, B.L. Smiley, J. Mills, H.H. Vandenburgh, Mechanical stimulation improves tissue-engineered human skeletal muscle, Am J Physiol Cell Physiol, 283 (2002) C1557-1565.

[14] S. Carosio, L. Barberi, E. Rizzuto, C. Nicoletti, Z. Del Prete, A. Musaro, Generation of eX vivo-vascularized Muscle Engineered Tissue (X-MET), Scientific reports, 3 (2013) 1420.

[15] K.W. VanDusen, B.C. Syverud, M.L. Williams, J.D. Lee, L.M. Larkin, Engineered Skeletal Muscle Units for Repair of Volumetric Muscle Loss in the Tibialis Anterior Muscle of a Rat, Tissue engineering. Part A, (2014).

[16] Y. Shandalov, D. Egozi, J. Koffler, D. Dado-Rosenfeld, D. Ben-Shimol, A. Freiman, E. Shor, A. Kabala, S. Levenberg, An engineered muscle flap for reconstruction of large soft tissue defects, Proceedings of the National Academy of Sciences of the United States of America, 111 (2014) 6010-6015.

[17] B.T. Corona, C.L. Ward, H.B. Baker, T.J. Walters, G.J. Christ, Implantation of in vitro tissue engineered muscle repair constructs and bladder acellular matrices partially restore in vivo skeletal muscle function in a rat model of volumetric muscle loss injury, Tissue engineering. Part A, 20 (2014) 705-715.

[18] Y.C. Huang, R.G. Dennis, L. Larkin, K. Baar, Rapid formation of functional muscle in vitro using fibrin gels, J Appl Physiol, 98 (2005) 706-713. Epub 2004 Oct 2008.

[19] L.M. Larkin, J.H. Van der Meulen, R.G. Dennis, J.B. Kennedy, Functional evaluation of nerve-skeletal muscle constructs engineered in vitro, In vitro cellular & developmental biology. Animal, 42 (2006) 75-82.

[20] L.M. Larkin, S. Calve, T.Y. Kostrominova, E.M. Arruda, Structure and functional evaluation of tendon-skeletal muscle constructs engineered in vitro, Tissue engineering, 12 (2006) 3149-3158.

[21] R.G. Dennis, P.E. Kosnik, 2nd, Excitability and isometric contractile properties of mammalian skeletal muscle constructs engineered in vitro, In vitro cellular & developmental biology. Animal, 36 (2000) 327-335.

[22] R.G. Dennis, P.E. Kosnik, 2nd, M.E. Gilbert, J.A. Faulkner, Excitability and contractility of skeletal muscle engineered from primary cultures and cell lines, Am J Physiol Cell Physiol, 280 (2001) C288-295.

[23] F. Mourkioti, N. Rosenthal, IGF-1, inflammation and stem cells: interactions during muscle regeneration, Trends in immunology, 26 (2005) 535-542.

[24] N.J. Turner, S.F. Badylak, Regeneration of skeletal muscle, Cell and tissue research, 347 (2012) 759-774.

[25] G.R. Coulton, J.E. Morgan, T.A. Partridge, J.C. Sloper, The mdx mouse skeletal muscle myopathy: I. A histological, morphometric and biochemical investigation, Neuropathology and applied neurobiology, 14 (1988) 53-70.

[26] J.M. McClung, J.M. Davis, J.A. Carson, Ovarian hormone status and skeletal muscle inflammation during recovery from disuse in rats, Experimental physiology, 92 (2007) 219-232.

[27] J.G. Tidball, S.A. Villalta, Regulatory interactions between muscle and the immune system during muscle regeneration, American journal of physiology. Regulatory, integrative and comparative physiology, 298 (2010) R1173-1187.

[28] S.E. Chen, E. Gerken, Y. Zhang, M. Zhan, R.K. Mohan, A.S. Li, M.B. Reid, Y.P. Li, Role of TNF-{alpha} signaling in regeneration of cardiotoxin-injured muscle, Am J Physiol Cell Physiol, 289 (2005) C1179-1187.

[29] N. Al-Shanti, A. Saini, S.H. Faulkner, C.E. Stewart, Beneficial synergistic interactions of TNF-alpha and IL-6 in C2 skeletal myoblasts--potential cross-talk with IGF system, Growth factors, 26 (2008) 61-73.

[30] T.J. Hawke, D.J. Garry, Myogenic satellite cells: physiology to molecular biology, J Appl Physiol, 91 (2001) 534-551.

[31] M.D. Grounds, J.D. White, N. Rosenthal, M.A. Bogoyevitch, The role of stem cells in skeletal and cardiac muscle repair, The journal of histochemistry and cytochemistry : official journal of the Histochemistry Society, 50 (2002) 589-610.

[32] X.D. Zhou, M.M. Xiong, F.K. Tan, X.J. Guo, F.C. Arnett, SPARC, an upstream regulator of connective tissue growth factor in response to transforming growth factor beta stimulation, Arthritis and rheumatism, 54 (2006) 3885-3889.

[33] D. Scholz, S. Thomas, S. Sass, T. Podzuweit, Angiogenesis and myogenesis as two facets of inflammatory post-ischemic tissue regeneration, Molecular and cellular biochemistry, 246 (2003) 57-67.

[34] A. Wagatsuma, Endogenous expression of angiogenesis-related factors in response to muscle injury, Molecular and cellular biochemistry, 298 (2007) 151-159.

[35] R. Schofield, The relationship between the spleen colony-forming cell and the haemopoietic stem cell, Blood cells, 4 (1978) 7-25.

[36] A. Mauro, Satellite cell of skeletal muscle fibers, The Journal of biophysical and biochemical cytology, 9 (1961) 493-495.

[37] P.M. Gilbert, K.L. Havenstrite, K.E. Magnusson, A. Sacco, N.A. Leonardi, P. Kraft, N.K. Nguyen, S. Thrun, M.P. Lutolf, H.M. Blau, Substrate elasticity regulates skeletal muscle stem cell self-renewal in culture, Science, 329 (2010) 1078-1081.

[38] I.M. Conboy, M.J. Conboy, A.J. Wagers, E.R. Girma, I.L. Weissman, T.A. Rando, Rejuvenation of aged progenitor cells by exposure to a young systemic environment, Nature, 433 (2005) 760-764.

[39] S.A. Villeda, K.E. Plambeck, J. Middeldorp, J.M. Castellano, K.I. Mosher, J. Luo, L.K. Smith, G. Bieri, K. Lin, D. Berdnik, R. Wabl, J. Udeochu, E.G. Wheatley, B. Zou, D.A. Simmons, X.S. Xie, F.M. Longo, T. Wyss-Coray, Young blood reverses age-related impairments in cognitive function and synaptic plasticity in mice, Nature medicine, 20 (2014) 659-663.

[40] S.D. Gopinath, T.A. Rando, Stem cell review series: aging of the skeletal muscle stem cell niche, Aging cell, 7 (2008) 590-598.

[41] P. Mourikis, R. Sambasivan, D. Castel, P. Rocheteau, V. Bizzarro, S. Tajbakhsh, A critical requirement for notch signaling in maintenance of the quiescent skeletal muscle stem cell state, Stem cells, 30 (2012) 243-252.

[42] Y. Gao, T.Y. Kostrominova, J.A. Faulkner, A.S. Wineman, Age-related changes in the mechanical properties of the epimysium in skeletal muscles of rats, Journal of biomechanics, 41 (2008) 465-469.

[43] E. Rigamonti, P. Zordan, C. Sciorati, P. Rovere-Querini, S. Brunelli, Macrophage plasticity in skeletal muscle repair, BioMed research international, 2014 (2014) 560629.

[44] S.J. Forbes, N. Rosenthal, Preparing the ground for tissue regeneration: from mechanism to therapy, Nature medicine, 20 (2014) 857-869.

[45] J. Tonkin, L. Temmerman, R.D. Sampson, E. Gallego-Colon, L. Barberi, D. Bilbao, M.D. Schneider, A. Musaro, N. Rosenthal, Monocyte/Macrophage-derived IGF-1 Orchestrates Murine Skeletal Muscle Regeneration and Modulates Autocrine Polarization, Molecular therapy : the journal of the American Society of Gene Therapy, 23 (2015) 1189-1200.

[46] V. Horsley, K.M. Jansen, S.T. Mills, G.K. Pavlath, IL-4 acts as a myoblast recruitment factor during mammalian muscle growth, Cell, 113 (2003) 483-494.

[47] L.C. Davies, S.J. Jenkins, J.E. Allen, P.R. Taylor, Tissue-resident macrophages, Nature immunology, 14 (2013) 986-995.

[48] M. Brigitte, C. Schilte, A. Plonquet, Y. Baba-Amer, A. Henri, C. Charlier, S. Tajbakhsh, M. Albert, R.K. Gherardi, F. Chretien, Muscle resident macrophages control the immune cell reaction in a mouse model of notexin-induced myoinjury, Arthritis and rheumatism, 62 (2010) 268-279.

[49] A. Mantovani, S.K. Biswas, M.R. Galdiero, A. Sica, M. Locati, Macrophage plasticity and polarization in tissue repair and remodelling, The Journal of pathology, 229 (2013) 176-185.

[50] P.M. Henson, D.A. Hume, Apoptotic cell removal in development and tissue homeostasis, Trends in immunology, 27 (2006) 244-250.

[51] L. Bosurgi, A.A. Manfredi, P. Rovere-Querini, Macrophages in injured skeletal muscle: a perpetuum mobile causing and limiting fibrosis, prompting or restricting resolution and regeneration, Frontiers in immunology, 2 (2011) 62.

[52] P.F. Lesault, M. Theret, M. Magnan, S. Cuvellier, Y. Niu, R.K. Gherardi, J.P. Tremblay, L. Hittinger, B. Chazaud, Macrophages improve survival, proliferation and migration of engrafted myogenic precursor cells into MDX skeletal muscle, PloS one, 7 (2012) e46698.

[53] C.A. Gleissner, I. Shaked, K.M. Little, K. Ley, CXC chemokine ligand 4 induces a unique transcriptome in monocyte-derived macrophages, Journal of immunology, 184 (2010) 4810-4818.

[54] D.A. Hume, K.P. MacDonald, Therapeutic applications of macrophage colony-stimulating factor-1 (CSF-1) and antagonists of CSF-1 receptor (CSF-1R) signaling, Blood, 119 (2012) 1810-1820.

[55] J.A. Hamilton, Colony-stimulating factors in inflammation and autoimmunity, Nature reviews. Immunology, 8 (2008) 533-544.

[56] B. Chazaud, C. Sonnet, P. Lafuste, G. Bassez, A.C. Rimaniol, F. Poron, F.J. Authier, P.A. Dreyfus, R.K. Gherardi, Satellite cells attract monocytes and use macrophages as a support to escape apoptosis and enhance muscle growth, The Journal of cell biology, 163 (2003) 1133-1143.

[57] C. Sonnet, P. Lafuste, L. Arnold, M. Brigitte, F. Poron, F.J. Authier, F. Chretien, R.K. Gherardi, B. Chazaud, Human macrophages rescue myoblasts and myotubes from apoptosis through a set of adhesion molecular systems, Journal of cell science, 119 (2006) 2497-2507.

[58] A. Sacco, F. Mourkioti, R. Tran, J. Choi, M. Llewellyn, P. Kraft, M. Shkreli, S. Delp, J.H. Pomerantz, S.E. Artandi, H.M. Blau, Short telomeres and stem cell exhaustion model Duchenne muscular dystrophy in mdx/mTR mice, Cell, 143 (2010) 1059-1071.

[59] A.E. Emery, Duchenne muscular dystrophy--Meryon's disease, Neuromuscular disorders : NMD, 3 (1993) 263-266.

[60] B. Mokri, A.G. Engel, Duchenne dystrophy: electron microscopic findings pointing to a basic or early abnormality in the plasma membrane of the muscle fiber, Neurology, 25 (1975) 1111-1120.

[61] D.J. Blake, A. Weir, S.E. Newey, K.E. Davies, Function and genetics of dystrophin and dystrophin-related proteins in muscle, Physiological reviews, 82 (2002) 291-329.

[62] T.A. Rando, M.H. Disatnik, Y. Yu, A. Franco, Muscle cells from mdx mice have an increased susceptibility to oxidative stress, Neuromuscular disorders : NMD, 8 (1998) 14-21.

[63] J.D. Porter, S. Khanna, H.J. Kaminski, J.S. Rao, A.P. Merriam, C.R. Richmonds, P. Leahy, J. Li, W. Guo, F.H. Andrade, A chronic inflammatory response dominates the skeletal muscle molecular signature in dystrophin-deficient mdx mice, Human molecular genetics, 11 (2002) 263-272.

[64] C. Delaporte, M. Dehaupas, M. Fardeau, Comparison between the growth pattern of cell cultures from normal and Duchenne dystrophy muscle, Journal of the neurological sciences, 64 (1984) 149-160.

[65] G. Jasmin, C. Tautu, M. Vanasse, P. Brochu, R. Simoneau, Impaired muscle differentiation in explant cultures of Duchenne muscular dystrophy, Laboratory investigation; a journal of technical methods and pathology, 50 (1984) 197-207.

[66] H.M. Blau, C. Webster, G.K. Pavlath, Defective myoblasts identified in Duchenne muscular dystrophy, Proceedings of the National Academy of Sciences of the United States of America, 80 (1983) 4856-4860.

[67] A. Goyenvalle, J.T. Seto, K.E. Davies, J. Chamberlain, Therapeutic approaches to muscular dystrophy, Human molecular genetics, 20 (2011) R69-78.

[68] H. Abdel-Hamid, P.R. Clemens, Pharmacological therapies for muscular dystrophies, Current opinion in neurology, 25 (2012) 604-608.

[69] F.S. Tedesco, G. Cossu, Stem cell therapies for muscle disorders, Current opinion in neurology, 25 (2012) 597-603.

[70] C.E. Nelson, C.H. Hakim, D.G. Ousterout, P.I. Thakore, E.A. Moreb, R.M. Castellanos Rivera, S. Madhavan, X. Pan, F.A. Ran, W.X. Yan, A. Asokan, F. Zhang, D. Duan, C.A. Gersbach, In vivo genome editing improves muscle function in a mouse model of Duchenne muscular dystrophy, Science, 351 (2016) 403-407.

[71] M. Tabebordbar, K. Zhu, J.K. Cheng, W.L. Chew, J.J. Widrick, W.X. Yan, C. Maesner, E.Y. Wu, R. Xiao, F.A. Ran, L. Cong, F. Zhang, L.H. Vandenberghe, G.M. Church, A.J. Wagers, In vivo gene editing in dystrophic mouse muscle and muscle stem cells, Science, 351 (2016) 407-411.

[72] C. Long, L. Amoasii, A.A. Mireault, J.R. McAnally, H. Li, E. Sanchez-Ortiz, S. Bhattacharyya, J.M. Shelton, R. Bassel-Duby, E.N. Olson, Postnatal genome editing partially restores dystrophin expression in a mouse model of muscular dystrophy, Science, 351 (2016) 400-403.

[73] M.J. Tisdale, Cachexia in cancer patients, Nature reviews. Cancer, 2 (2002) 862-871.

[74] M.A. Ruegg, D.J. Glass, Molecular mechanisms and treatment options for muscle wasting diseases, Annual review of pharmacology and toxicology, 51 (2011) 373-395.

[75] W.A. He, E. Berardi, V.M. Cardillo, S. Acharyya, P. Aulino, J. Thomas-Ahner, J. Wang, M. Bloomston, P. Muscarella, P. Nau, N. Shah, M.E. Butchbach, K. Ladner, S. Adamo, M.A. Rudnicki, C. Keller, D. Coletti, F. Montanaro, D.C. Guttridge, NF-kappaB-mediated Pax7 dysregulation in the muscle microenvironment promotes cancer cachexia, The Journal of clinical investigation, 123 (2013) 4821-4835.

[76] A. Dirks, C. Leeuwenburgh, Apoptosis in skeletal muscle with aging, American journal of physiology. Regulatory, integrative and comparative physiology, 282 (2002) R519-527.

[77] B.K. Pedersen, M.A. Febbraio, Muscles, exercise and obesity: skeletal muscle as a secretory organ, Nature reviews. Endocrinology, 8 (2012) 457-465.

[78] D. Montarras, J. Morgan, C. Collins, F. Relaix, S. Zaffran, A. Cumano, T. Partridge, M. Buckingham, Direct isolation of satellite cells for skeletal muscle regeneration, Science, 309 (2005) 2064-2067.

[79] J.R. Beauchamp, J.E. Morgan, C.N. Pagel, T.A. Partridge, Dynamics of myoblast transplantation reveal a discrete minority of precursors with stem cell-like properties as the myogenic source, The Journal of cell biology, 144 (1999) 1113-1122.

[80] C.A. Rossi, M. Flaibani, B. Blaauw, M. Pozzobon, E. Figallo, C. Reggiani, L. Vitiello, N. Elvassore, P. De Coppi, In vivo tissue engineering of functional skeletal muscle by freshly isolated satellite cells embedded in a photopolymerizable hydrogel, FASEB journal : official publication of the Federation of American Societies for Experimental Biology, 25 (2011) 2296-2304.

[81] A. Sacco, R. Doyonnas, P. Kraft, S. Vitorovic, H.M. Blau, Self-renewal and expansion of single transplanted muscle stem cells, Nature, 456 (2008) 502-506.

[82] B. Zheng, B. Cao, M. Crisan, B. Sun, G. Li, A. Logar, S. Yap, J.B. Pollett, L. Drowley, T. Cassino, B. Gharaibeh, B.M. Deasy, J. Huard, B. Peault, Prospective identification of myogenic endothelial cells in human skeletal muscle, Nature biotechnology, 25 (2007) 1025-1034.

[83] A. Dellavalle, M. Sampaolesi, R. Tonlorenzi, E. Tagliafico, B. Sacchetti, L. Perani, A. Innocenzi, B.G. Galvez, G. Messina, R. Morosetti, S. Li, M. Belicchi, G. Peretti, J.S. Chamberlain, W.E. Wright, Y. Torrente, S. Ferrari, P. Bianco, G. Cossu, Pericytes of human skeletal muscle are myogenic precursors distinct from satellite cells, Nature cell biology, 9 (2007) 255-267.

[84] R. Benchaouir, M. Meregalli, A. Farini, G. D'Antona, M. Belicchi, A. Goyenvalle, M. Battistelli, N. Bresolin, R. Bottinelli, L. Garcia, Y. Torrente, Restoration of human dystrophin following transplantation of exon-skipping-engineered DMD patient stem cells into dystrophic mice, Cell stem cell, 1 (2007) 646-657.

[85] A. Farini, P. Razini, S. Erratico, Y. Torrente, M. Meregalli, Cell based therapy for Duchenne muscular dystrophy, Journal of cellular physiology, 221 (2009) 526-534.

[86] M. Dezawa, H. Ishikawa, Y. Itokazu, T. Yoshihara, M. Hoshino, S. Takeda, C. Ide, Y. Nabeshima, Bone marrow stromal cells generate muscle cells and repair muscle degeneration, Science, 309 (2005) 314-317.

[87] R. Darabi, R.W. Arpke, S. Irion, J.T. Dimos, M. Grskovic, M. Kyba, R.C. Perlingeiro, Human ES- and iPS-derived myogenic progenitors restore DYSTROPHIN and improve contractility upon transplantation in dystrophic mice, Cell stem cell, 10 (2012) 610-619.

[88] D. Hockemeyer, H. Wang, S. Kiani, C.S. Lai, Q. Gao, J.P. Cassady, G.J. Cost, L. Zhang, Y. Santiago, J.C. Miller, B. Zeitler, J.M. Cherone, X. Meng, S.J. Hinkley, E.J. Rebar, P.D. Gregory, F.D. Urnov, R. Jaenisch, Genetic engineering of human pluripotent cells using TALE nucleases, Nature biotechnology, 29 (2011) 731-734.

[89] K. Mamchaoui, C. Trollet, A. Bigot, E. Negroni, S. Chaouch, A. Wolff, P.K. Kandalla, S. Marie, J. Di Santo, J.L. St Guily, F. Muntoni, J. Kim, S. Philippi, S. Spuler, N. Levy, S.C. Blumen, T. Voit, W.E. Wright, A. Aamiri, G. Butler-Browne, V. Mouly, Immortalized pathological human myoblasts: towards a universal tool for the study of neuromuscular disorders, Skeletal muscle, 1 (2011) 34.

[90] T. Tamaki, Y. Okada, Y. Uchiyama, K. Tono, M. Masuda, M. Wada, A. Hoshi, T. Ishikawa, A. Akatsuka, Clonal multipotency of skeletal muscle-derived stem cells between mesodermal and ectodermal lineage, Stem cells, 25 (2007) 2283-2290.

[91] Z. Qu-Petersen, B. Deasy, R. Jankowski, M. Ikezawa, J. Cummins, R. Pruchnic, J. Mytinger, B. Cao, C. Gates, A. Wernig, J. Huard, Identification of a novel population of muscle stem cells in mice: potential for muscle regeneration, The Journal of cell biology, 157 (2002) 851-864.

[92] B.M. Deasy, B.M. Gharaibeh, J.B. Pollett, M.M. Jones, M.A. Lucas, Y. Kanda, J. Huard, Long-term self-renewal of postnatal muscle-derived stem cells, Molecular biology of the cell, 16 (2005) 3323-3333.

[93] G.M. Mueller, T. O'Day, J.F. Watchko, M. Ontell, Effect of injecting primary myoblasts versus putative muscle-derived stem cells on mass and force generation in mdx mice, Human gene therapy, 13 (2002) 1081-1090.

[94] M.G. Minasi, M. Riminucci, L. De Angelis, U. Borello, B. Berarducci, A. Innocenzi, A. Caprioli, D. Sirabella, M. Baiocchi, R. De Maria, R. Boratto, T. Jaffredo, V. Broccoli, P. Bianco, G. Cossu, The meso-angioblast: a multipotent, self-renewing cell that originates from the dorsal aorta and differentiates into most mesodermal tissues, Development, 129 (2002) 2773-2783.

[95] G. Cossu, P. Bianco, Mesoangioblasts--vascular progenitors for extravascular mesodermal tissues, Current opinion in genetics & development, 13 (2003) 537-542.

[96] M. Sampaolesi, S. Blot, G. D'Antona, N. Granger, R. Tonlorenzi, A. Innocenzi, P. Mognol, J.L. Thibaud, B.G. Galvez, I. Barthelemy, L. Perani, S. Mantero, M. Guttinger, O. Pansarasa, C. Rinaldi, M.G. Cusella De Angelis, Y. Torrente, C. Bordignon, R.

Bottinelli, G. Cossu, Mesoangioblast stem cells ameliorate muscle function in dystrophic dogs, Nature, 444 (2006) 574-579.

[97] R. Darabi, F.N. Santos, R.C. Perlingeiro, The therapeutic potential of embryonic and adult stem cells for skeletal muscle regeneration, Stem cell reviews, 4 (2008) 217-225.

[98] Y. Torrente, M. Belicchi, M. Sampaolesi, F. Pisati, M. Meregalli, G. D'Antona, R. Tonlorenzi, L. Porretti, M. Gavina, K. Mamchaoui, M.A. Pellegrino, D. Furling, V. Mouly, G.S. Butler-Browne, R. Bottinelli, G. Cossu, N. Bresolin, Human circulating AC133(+) stem cells restore dystrophin expression and ameliorate function in dystrophic skeletal muscle, The Journal of clinical investigation, 114 (2004) 182-195.

[99] M.F. Pittenger, A.M. Mackay, S.C. Beck, R.K. Jaiswal, R. Douglas, J.D. Mosca, M.A. Moorman, D.W. Simonetti, S. Craig, D.R. Marshak, Multilineage potential of adult human mesenchymal stem cells, Science, 284 (1999) 143-147.

[100] Y. Liu, X. Yan, Z. Sun, B. Chen, Q. Han, J. Li, R.C. Zhao, Flk-1+ adipose-derived mesenchymal stem cells differentiate into skeletal muscle satellite cells and ameliorate muscular dystrophy in mdx mice, Stem cells and development, 16 (2007) 695-706.

[101] G. Di Rocco, M.G. Iachininoto, A. Tritarelli, S. Straino, A. Zacheo, A. Germani, F. Crea, M.C. Capogrossi, Myogenic potential of adipose-tissue-derived cells, Journal of cell science, 119 (2006) 2945-2952.

[102] M. Breitbach, T. Bostani, W. Roell, Y. Xia, O. Dewald, J.M. Nygren, J.W. Fries, K. Tiemann, H. Bohlen, J. Hescheler, A. Welz, W. Bloch, S.E. Jacobsen, B.K. Fleischmann, Potential risks of bone marrow cell transplantation into infarcted hearts, Blood, 110 (2007) 1362-1369.

[103] J. Chan, S.N. Waddington, K. O'Donoghue, H. Kurata, P.V. Guillot, C. Gotherstrom, M. Themis, J.E. Morgan, N.M. Fisk, Widespread distribution and muscle differentiation of human fetal mesenchymal stem cells after intrauterine transplantation in dystrophic mdx mouse, Stem cells, 25 (2007) 875-884.

[104] R. Pecanha, L.L. Bagno, M.B. Ribeiro, A.B. Robottom Ferreira, M.O. Moraes, G. Zapata-Sudo, T.H. Kasai-Brunswick, A.C. Campos-de-Carvalho, R.C. Goldenberg, J.P. Saar Werneck-de-Castro, Adipose-derived stem-cell treatment of skeletal muscle injury, The Journal of bone and joint surgery. American volume, 94 (2012) 609-617.

[105] S. Bhagavati, W. Xu, Generation of skeletal muscle from transplanted embryonic stem cells in dystrophic mice, Biochemical and biophysical research communications, 333 (2005) 644-649.

[106] H. Kamochi, M.S. Kurokawa, H. Yoshikawa, Y. Ueda, C. Masuda, E. Takada, K. Watanabe, M. Sakakibara, Y. Natuki, K. Kimura, M. Beppu, H. Aoki, N. Suzuki, Transplantation of myocyte precursors derived from embryonic stem cells transfected with IGFII gene in a mouse model of muscle injury, Transplantation, 82 (2006) 516-526.

[107] R. Darabi, K. Gehlbach, R.M. Bachoo, S. Kamath, M. Osawa, K.E. Kamm, M. Kyba, R.C. Perlingeiro, Functional skeletal muscle regeneration from differentiating embryonic stem cells, Nature medicine, 14 (2008) 134-143.

[108] M.P. Lutolf, H.M. Blau, Artificial stem cell niches, Adv Mater, 21 (2009) 3255-3268.

[109] A. Urciuolo, M. Quarta, V. Morbidoni, F. Gattazzo, S. Molon, P. Grumati, F. Montemurro, F.S. Tedesco, B. Blaauw, G. Cossu, G. Vozzi, T.A. Rando, P. Bonaldo, Collagen VI regulates satellite cell self-renewal and muscle regeneration, Nature communications, 4 (2013) 1964.

[110] Y.S. Choi, L.G. Vincent, A.R. Lee, M.K. Dobke, A.J. Engler, Mechanical derivation of functional myotubes from adipose-derived stem cells, Biomaterials, 33 (2012) 2482-2491.

[111] C. Borselli, C.A. Cezar, D. Shvartsman, H.H. Vandenburgh, D.J. Mooney, The role of multifunctional delivery scaffold in the ability of cultured myoblasts to promote muscle regeneration, Biomaterials, 32 (2011) 8905-8914.

[112] C.A. Rossi, M. Pozzobon, P. De Coppi, Advances in musculoskeletal tissue engineering: moving towards therapy, Organogenesis, 6 (2010) 167-172.

[113] Z. Qu, L. Balkir, J.C. van Deutekom, P.D. Robbins, R. Pruchnic, J. Huard, Development of approaches to improve cell survival in myoblast transfer therapy, The Journal of cell biology, 142 (1998) 1257-1267.

[114] L. Boldrin, N. Elvassore, A. Malerba, M. Flaibani, E. Cimetta, M. Piccoli, M.D. Baroni, M.V. Gazzola, C. Messina, P. Gamba, L. Vitiello, P. De Coppi, Satellite cells delivered by micro-patterned scaffolds: a new strategy for cell transplantation in muscle diseases, Tissue engineering, 13 (2007) 253-262.

[115] E. Serena, M. Flaibani, S. Carnio, L. Boldrin, L. Vitiello, P. De Coppi, N. Elvassore, Electrophysiologic stimulation improves myogenic potential of muscle precursor cells grown in a 3D collagen scaffold, Neurological research, 30 (2008) 207-214.

[116] C. Borselli, H. Storrie, F. Benesch-Lee, D. Shvartsman, C. Cezar, J.W. Lichtman, H.H. Vandenburgh, D.J. Mooney, Functional muscle regeneration with combined delivery of angiogenesis and myogenesis factors, Proceedings of the National Academy of Sciences of the United States of America, 107 (2010) 3287-3292.

[117] A. Musaro, C. Giacinti, G. Borsellino, G. Dobrowolny, L. Pelosi, L. Cairns, S. Ottolenghi, G. Cossu, G. Bernardi, L. Battistini, M. Molinaro, N. Rosenthal, Stem cell-mediated muscle regeneration is enhanced by local isoform of insulin-like growth factor 1, Proceedings of the National Academy of Sciences of the United States of America, 101 (2004) 1206-1210.

[118] G. Dobrowolny, C. Giacinti, L. Pelosi, C. Nicoletti, N. Winn, L. Barberi, M. Molinaro, N. Rosenthal, A. Musaro, Muscle expression of a local Igf-1 isoform protects motor neurons in an ALS mouse model, The Journal of cell biology, 168 (2005) 193-199.

[119] S. Badylak, J. Obermiller, L. Geddes, R. Matheny, Extracellular matrix for myocardial repair, The heart surgery forum, 6 (2003) E20-26.

[120] T.W. Gilbert, A.M. Stewart-Akers, A. Simmons-Byrd, S.F. Badylak, Degradation and remodeling of small intestinal submucosa in canine Achilles tendon repair, The Journal of bone and joint surgery. American volume, 89 (2007) 621-630.

[121] J.E. Valentin, N.J. Turner, T.W. Gilbert, S.F. Badylak, Functional skeletal muscle formation with a biologic scaffold, Biomaterials, 31 (2010) 7475-7484.

[122] R.D. Record, D. Hillegonds, C. Simmons, R. Tullius, F.A. Rickey, D. Elmore, S.F. Badylak, In vivo degradation of 14C-labeled small intestinal submucosa (SIS) when used for urinary bladder repair, Biomaterials, 22 (2001) 2653-2659.

[123] A.J. Beattie, T.W. Gilbert, J.P. Guyot, A.J. Yates, S.F. Badylak, Chemoattraction of progenitor cells by remodeling extracellular matrix scaffolds, Tissue engineering. Part A, 15 (2009) 1119-1125.

[124] B.M. Sicari, J.P. Rubin, C.L. Dearth, M.T. Wolf, F. Ambrosio, M. Boninger, N.J. Turner, D.J. Weber, T.W. Simpson, A. Wyse, E.H. Brown, J.L. Dziki, L.E. Fisher, S. Brown, S.F. Badylak, An acellular biologic scaffold promotes skeletal muscle formation in mice and humans with volumetric muscle loss, Science translational medicine, 6 (2014) 234ra258.

[125] M.T. Wolf, K.A. Daly, J.E. Reing, S.F. Badylak, Biologic scaffold composed of skeletal muscle extracellular matrix, Biomaterials, 33 (2012) 2916-2925.

[126] N.J. Turner, J.S. Badylak, D.J. Weber, S.F. Badylak, Biologic Scaffold Remodeling in a Dog Model of Complex Musculoskeletal Injury, The Journal of surgical research, (2011).

[127] M.H. Snow, Myogenic cell formation in regenerating rat skeletal muscle injured by mincing. II. An autoradiographic study, The Anatomical record, 188 (1977) 201-217.

[128] J.D. Rosenblatt, A.I. Lunt, D.J. Parry, T.A. Partridge, Culturing satellite cells from living single muscle fiber explants, In vitro cellular & developmental biology. Animal, 31 (1995) 773-779.

[129] G. Shefer, D.P. Van de Mark, J.B. Richardson, Z. Yablonka-Reuveni, Satellite-cell pool size does matter: defining the myogenic potency of aging skeletal muscle, Developmental biology, 294 (2006) 50-66.

[130] M. Gaster, S.R. Kristensen, H. Beck-Nielsen, H.D. Schroder, A cellular model system of differentiated human myotubes, APMIS : acta pathologica, microbiologica, et immunologica Scandinavica, 109 (2001) 735-744.

[131] M. Juhas, N. Bursac, Roles of adherent myogenic cells and dynamic culture in engineered muscle function and maintenance of satellite cells, Biomaterials, (2014).

[132] M. Juhas, G.C. Engelmayr, Jr., A.N. Fontanella, G.M. Palmer, N. Bursac, Biomimetic engineered muscle with capacity for vascular integration and functional maturation in vivo, Proceedings of the National Academy of Sciences of the United States of America, (2014).

[133] S. Fukada, Y. Ma, T. Ohtani, Y. Watanabe, S. Murakami, M. Yamaguchi, Isolation, characterization, and molecular regulation of muscle stem cells, Frontiers in physiology, 4 (2013) 317.

[134] T.A. Rando, H.M. Blau, Primary mouse myoblast purification, characterization, and transplantation for cell-mediated gene therapy, The Journal of cell biology, 125 (1994) 1275-1287.

[135] H.H. Vandenburgh, P. Karlisch, L. Farr, Maintenance of highly contractile tissue-cultured avian skeletal myotubes in collagen gel, In vitro cellular & developmental biology : journal of the Tissue Culture Association, 24 (1988) 166-174.

[136] S. Grefte, S. Vullinghs, A.M. Kuijpers-Jagtman, R. Torensma, J.W. Von den Hoff, Matrigel, but not collagen I, maintains the differentiation capacity of muscle derived cells in vitro, Biomed Mater, 7 (2012) 055004.

[137] J.R. Sanes, J.W. Lichtman, Induction, assembly, maturation and maintenance of a postsynaptic apparatus, Nat Rev Neurosci, 2 (2001) 791-805.

[138] S.L. Goodman, R. Deutzmann, V. Nurcombe, Locomotory competence and laminin-specific cell surface binding sites are lost during myoblast differentiation, Development, 105 (1989) 795-802.

[139] R.G. Ham, J.A. St Clair, C. Webster, H.M. Blau, Improved media for normal human muscle satellite cells: serum-free clonal growth and enhanced growth with low serum, In vitro cellular & developmental biology : journal of the Tissue Culture Association, 24 (1988) 833-844.

[140] Z. Yablonka-Reuveni, T.M. Balestreri, D.F. Bowen-Pope, Regulation of proliferation and differentiation of myoblasts derived from adult mouse skeletal muscle by specific isoforms of PDGF, The Journal of cell biology, 111 (1990) 1623-1629.

[141] R.S. Krauss, F. Cole, U. Gaio, G. Takaesu, W. Zhang, J.S. Kang, Close encounters: regulation of vertebrate skeletal myogenesis by cell-cell contact, Journal of cell science, 118 (2005) 2355-2362.

[142] S.R. Chowdhury, Y. Muneyuki, Y. Takezawa, M. Kino-oka, A. Saito, Y. Sawa, M. Taya, Growth and differentiation potentials in confluent state of culture of human skeletal muscle myoblasts, Journal of bioscience and bioengineering, 109 (2010) 310-313.

[143] H.M. Blau, C. Webster, Isolation and characterization of human muscle cells, Proceedings of the National Academy of Sciences of the United States of America, 78 (1981) 5623-5627.

[144] D. Gawlitta, K.J. Boonen, C.W. Oomens, F.P. Baaijens, C.V. Bouten, The influence of serum-free culture conditions on skeletal muscle differentiation in a tissue-engineered model, Tissue engineering. Part A, 14 (2008) 161-171.

[145] C.W. McAleer, J.W. Rumsey, M. Stancescu, J.J. Hickman, Functional myotube formation from adult rat satellite cells in a defined serum-free system, Biotechnology progress, (2015).

[146] H. Fujita, A. Endo, K. Shimizu, E. Nagamori, Evaluation of serum-free differentiation conditions for C2C12 myoblast cells assessed as to active tension generation capability, Biotechnology and bioengineering, 107 (2010) 894-901.

[147] C. Murre, P.S. McCaw, D. Baltimore, A new DNA binding and dimerization motif in immunoglobulin enhancer binding, daughterless, MyoD, and myc proteins, Cell, 56 (1989) 777-783.

[148] R. Benezra, R.L. Davis, A. Lassar, S. Tapscott, M. Thayer, D. Lockshon, H. Weintraub, Id: a negative regulator of helix-loop-helix DNA binding proteins. Control of terminal myogenic differentiation, Annals of the New York Academy of Sciences, 599 (1990) 1-11.

[149] M.R. Weist, M.S. Wellington, J.E. Bermudez, T.Y. Kostrominova, C.L. Mendias, E.M. Arruda, L.M. Larkin, TGF-beta1 enhances contractility in engineered skeletal muscle, Journal of tissue engineering and regenerative medicine, 7 (2013) 562-571.

[150] B.D. Cosgrove, P.M. Gilbert, E. Porpiglia, F. Mourkioti, S.P. Lee, S.Y. Corbel, M.E. Llewellyn, S.L. Delp, H.M. Blau, Rejuvenation of the muscle stem cell population restores strength to injured aged muscles, Nature medicine, 20 (2014) 255-264.

[151] C. Xu, M. Tabebordbar, S. Iovino, C. Ciarlo, J. Liu, A. Castiglioni, E. Price, M. Liu, E.R. Barton, C.R. Kahn, A.J. Wagers, L.I. Zon, A Zebrafish Embryo Culture System Defines Factors that Promote Vertebrate Myogenesis across Species, Cell, 155 (2013) 909-921.

[152] X. Fu, J. Xiao, Y. Wei, S. Li, Y. Liu, J. Yin, K. Sun, H. Sun, H. Wang, Z. Zhang, B.T. Zhang, C. Sheng, H. Wang, P. Hu, Combination of inflammation-related cytokines promotes long-term muscle stem cell expansion, Cell Res, 25 (2015) 655-673.

[153] R.C. Strohman, E. Bayne, D. Spector, T. Obinata, J. Micou-Eastwood, A. Maniotis, Myogenesis and histogenesis of skeletal muscle on flexible membranes in vitro, In vitro

cellular & developmental biology : journal of the Tissue Culture Association, 26 (1990) 201-208.

[154] H. Takahashi, T. Shimizu, M. Nakayama, M. Yamato, T. Okano, The use of anisotropic cell sheets to control orientation during the self-organization of 3D muscle tissue, Biomaterials, 34 (2013) 7372-7380.

[155] L. Madden, M. Juhas, W.E. Kraus, G.A. Truskey, N. Bursac, Bioengineered human myobundles mimic clinical responses of skeletal muscle to drugs, eLife, 4 (2015).

[156] J. Koffler, K. Kaufman-Francis, Y. Shandalov, D. Egozi, D.A. Pavlov, A. Landesberg, S. Levenberg, Improved vascular organization enhances functional integration of engineered skeletal muscle grafts, Proceedings of the National Academy of Sciences of the United States of America, 108 (2011) 14789-14794.

[157] S. Levenberg, J. Rouwkema, M. Macdonald, E.S. Garfein, D.S. Kohane, D.C. Darland, R. Marini, C.A. van Blitterswijk, R.C. Mulligan, P.A. D'Amore, R. Langer, Engineering vascularized skeletal muscle tissue, Nature biotechnology, 23 (2005) 879-884.

[158] W. Bian, B. Liau, N. Badie, N. Bursac, Mesoscopic hydrogel molding to control the 3D geometry of bioartificial muscle tissues, Nature protocols, 4 (2009) 1522-1534.

[159] U. Mayer, Integrins: redundant or important players in skeletal muscle?, The Journal of biological chemistry, 278 (2003) 14587-14590.

[160] Y. Katagiri, T. Hiroyama, N. Akamatsu, H. Suzuki, H. Yamazaki, K. Tanoue, Involvement of alpha v beta 3 integrin in mediating fibrin gel retraction, The Journal of biological chemistry, 270 (1995) 1785-1790.

[161] A.C. Paul, P.W. Sheard, S.J. Kaufman, M.J. Duxson, Localization of alpha 7 integrins and dystrophin suggests potential for both lateral and longitudinal transmission of tension in large mammalian muscles, Cell and tissue research, 308 (2002) 255-265.

[162] C.S. Cheng, B.N. Davis, L. Madden, N. Bursac, G.A. Truskey, Physiology and metabolism of tissue-engineered skeletal muscle, Experimental biology and medicine (Maywood, N.J.), (2014).

[163] S. Rangarajan, L. Madden, N. Bursac, Use of Flow, Electrical, and Mechanical Stimulation to Promote Engineering of Striated Muscles, Ann Biomed Eng, 42 (2014) 1391-1405.

[164] H.H. Vandenburgh, P. Karlisch, Longitudinal growth of skeletal myotubes in vitro in a new horizontal mechanical cell stimulator, In vitro cellular & developmental biology : journal of the Tissue Culture Association, 25 (1989) 607-616.

[165] G. Moon du, G. Christ, J.D. Stitzel, A. Atala, J.J. Yoo, Cyclic mechanical preconditioning improves engineered muscle contraction, Tissue engineering. Part A, 14 (2008) 473-482.

[166] B.T. Corona, M.A. Machingal, T. Criswell, M. Vadhavkar, A.C. Dannahower, C. Bergman, W. Zhao, G.J. Christ, Further development of a tissue engineered muscle repair construct in vitro for enhanced functional recovery following implantation in vivo in a murine model of volumetric muscle loss injury, Tissue engineering. Part A, 18 (2012) 1213-1228.

[167] M.L. Langelaan, K.J. Boonen, K.Y. Rosaria-Chak, D.W. van der Schaft, M.J. Post, F.P. Baaijens, Advanced maturation by electrical stimulation: Differences in response between C2C12 and primary muscle progenitor cells, Journal of tissue engineering and regenerative medicine, 5 (2011) 529-539.

[168] A. Khodabukus, L.M. Baehr, S.C. Bodine, K. Baar, Role of Contraction Duration in Inducing Fast-To-Slow Contractile and Metabolic Protein and Functional Changes in Engineered Muscle, Journal of cellular physiology, (2015).

[169] D.W. van der Schaft, A.C. van Spreeuwel, H.C. van Assen, F.P. Baaijens, Mechanoregulation of vascularization in aligned tissue-engineered muscle: a role for vascular endothelial growth factor, Tissue engineering. Part A, 17 (2011) 2857-2865.

[170] H. Vandenburgh, J. Shansky, F. Benesch-Lee, V. Barbata, J. Reid, L. Thorrez, R. Valentini, G. Crawford, Drug-screening platform based on the contractility of tissue-engineered muscle, Muscle & nerve, 37 (2008) 438-447.

[171] P.H. Lee, H.H. Vandenburgh, Skeletal muscle atrophy in bioengineered skeletal muscle: a new model system, Tissue engineering. Part A, 19 (2013) 2147-2155.

[172] L. Wang, J. Shansky, H. Vandenburgh, Induced formation and maturation of acetylcholine receptor clusters in a defined 3D bio-artificial muscle, Molecular neurobiology, 48 (2013) 397-403.

[173] T.A. Davis, M.L. Fiorotto, Regulation of muscle growth in neonates, Curr Opin Clin Nutr, 12 (2009) 78-85.

[174] J.A. Faulkner, S.V. Brooks, R.G. Dennis, Measurement of recovery of function following whole muscle transfer, myoblast transfer, and gene therapy, Methods in molecular medicine, 18 (1999) 155-172.

[175] H. Vandenburgh, J. Shansky, F. Benesch-Lee, K. Skelly, J.M. Spinazzola, Y. Saponjian, B.S. Tseng, Automated drug screening with contractile muscle tissue engineered from dystrophic myoblasts, FASEB journal : official publication of the Federation of American Societies for Experimental Biology, 23 (2009) 3325-3334.

[176] J. Nakai, M. Ohkura, K. Imoto, A high signal-to-noise Ca(2+) probe composed of a single green fluorescent protein, Nature biotechnology, 19 (2001) 137-141.

[177] L. Tian, S.A. Hires, T. Mao, D. Huber, M.E. Chiappe, S.H. Chalasani, L. Petreanu, J. Akerboom, S.A. McKinney, E.R. Schreiter, C.I. Bargmann, V. Jayaraman, K. Svoboda, L.L. Looger, Imaging neural activity in worms, flies and mice with improved GCaMP calcium indicators, Nature methods, 6 (2009) 875-881.

[178] T.W. Chen, T.J. Wardill, Y. Sun, S.R. Pulver, S.L. Renninger, A. Baohan, E.R. Schreiter, R.A. Kerr, M.B. Orger, V. Jayaraman, L.L. Looger, K. Svoboda, D.S. Kim, Ultrasensitive fluorescent proteins for imaging neuronal activity, Nature, 499 (2013) 295-300.

[179] T.L. Criswell, B.T. Corona, Z. Wang, Y. Zhou, G. Niu, Y. Xu, G.J. Christ, S. Soker, The role of endothelial cells in myofiber differentiation and the vascularization and innervation of bioengineered muscle tissue in vivo, Biomaterials, 34 (2013) 140-149.

[180] M.L. Williams, T.Y. Kostrominova, E.M. Arruda, L.M. Larkin, Effect of implantation on engineered skeletal muscle constructs, Journal of tissue engineering and regenerative medicine, 7 (2013) 434-442.

[181] H. Wu, L. Mei, Morphological analysis of neuromuscular junctions by immunofluorescent staining of whole-mount mouse diaphragms, Methods in molecular biology, 1018 (2013) 277-285.

[182] G.M. Palmer, A.N. Fontanella, S. Shan, G. Hanna, G. Zhang, C.L. Fraser, M.W. Dewhirst, In vivo optical molecular imaging and analysis in mice using dorsal window chamber models applied to hypoxia, vasculature and fluorescent reporters, Nature protocols, 6 (2011) 1355-1366.

[183] L.E. Freed, F. Guilak, X.E. Guo, M.L. Gray, R. Tranquillo, J.W. Holmes, M. Radisic, M.V. Sefton, D. Kaplan, G. Vunjak-Novakovic, Advanced tools for tissue engineering: scaffolds, bioreactors, and signaling, Tissue engineering, 12 (2006) 3285-3305.

[184] A.M. De Jesus, E.A. Sander, Observing and quantifying fibroblast-mediated fibrin gel compaction, Journal of visualized experiments : JoVE, (2014) e50918.

[185] R. Close, Dynamic Properties of Fast + Slow Skeletal Muscles of Rat during Development, J Physiol-London, 173 (1964) 74-&.

[186] W. Yan, S. George, U. Fotadar, N. Tyhovych, A. Kamer, M.J. Yost, R.L. Price, C.R. Haggart, J.W. Holmes, L. Terracio, Tissue engineering of skeletal muscle, Tissue engineering, 13 (2007) 2781-2790.

[187] G. Mutungi, J. Trinick, K.W. Ranatunga, Resting tension characteristics in differentiating intact rat fast- and slow-twitch muscle fibers, J Appl Physiol (1985), 95 (2003) 2241-2247.

[188] V.I. Sikavitsas, G.N. Bancroft, A.G. Mikos, Formation of three-dimensional cell/polymer constructs for bone tissue engineering in a spinner flask and a rotating wall vessel bioreactor, Journal of biomedical materials research, 62 (2002) 136-148.

[189] J.E. Frith, B. Thomson, P.G. Genever, Dynamic three-dimensional culture methods enhance mesenchymal stem cell properties and increase therapeutic potential, Tissue engineering. Part C, Methods, 16 (2010) 735-749.

[190] G.Z. Jin, J.H. Park, S.J. Seo, H.W. Kim, Dynamic cell culture on porous biopolymer microcarriers in a spinner flask for bone tissue engineering: a feasibility study, Biotechnology letters, (2014).

[191] C.M. Lo, H.B. Wang, M. Dembo, Y.L. Wang, Cell movement is guided by the rigidity of the substrate, Biophys J, 79 (2000) 144-152.

[192] M. Ghibaudo, J.M. Di Meglio, P. Hersen, B. Ladoux, Mechanics of cell spreading within 3D-micropatterned environments, Lab on a chip, 11 (2011) 805-812.

[193] S. Song, H. Han, U.H. Ko, J. Kim, J.H. Shin, Collaborative effects of electric field and fluid shear stress on fibroblast migration, Lab on a chip, 13 (2013) 1602-1611.

[194] J.Y. Park, S.J. Yoo, L. Patel, S.H. Lee, S.H. Lee, Cell morphological response to low shear stress in a two-dimensional culture microsystem with magnitudes comparable to interstitial shear stress, Biorheology, 47 (2010) 165-178.

[195] D.J. Glass, Signalling pathways that mediate skeletal muscle hypertrophy and atrophy, Nature cell biology, 5 (2003) 87-90.

[196] N.E. Brooks, K.H. Myburgh, Skeletal muscle wasting with disuse atrophy is multi-dimensional: the response and interaction of myonuclei, satellite cells and signaling pathways, Frontiers in physiology, 5 (2014) 99.

[197] M.J. Rennie, R.H. Edwards, D. Halliday, D.E. Matthews, S.L. Wolman, D.J. Millward, Muscle protein synthesis measured by stable isotope techniques in man: the effects of feeding and fasting, Clinical science, 63 (1982) 519-523.

[198] J.W. Triplett, R. O'Riley, K. Tekulve, S.M. Norvell, F.M. Pavalko, Mechanical loading by fluid shear stress enhances IGF-1 receptor signaling in osteoblasts in a PKCzeta-dependent manner, Molecular & cellular biomechanics : MCB, 4 (2007) 13-25.

[199] A.G. Passerini, A. Milsted, S.E. Rittgers, Shear stress magnitude and directionality modulate growth factor gene expression in preconditioned vascular endothelial cells, Journal of vascular surgery, 37 (2003) 182-190.

[200] S. Kuang, S.B. Charge, P. Seale, M. Huh, M.A. Rudnicki, Distinct roles for Pax7 and Pax3 in adult regenerative myogenesis, J Cell Biol, 172 (2006) 103-113.

[201] C. Lepper, T.A. Partridge, C.M. Fan, An absolute requirement for Pax7-positive satellite cells in acute injury-induced skeletal muscle regeneration, Development, 138 (2011) 3639-3646.

[202] S. Kuang, M.A. Gillespie, M.A. Rudnicki, Niche regulation of muscle satellite cell self-renewal and differentiation, Cell stem cell, 2 (2008) 22-31.

[203] D.D. Cornelison, B.J. Wold, Single-cell analysis of regulatory gene expression in quiescent and activated mouse skeletal muscle satellite cells, Developmental biology, 191 (1997) 270-283.

[204] K.J. Wilschut, H.P. Haagsman, B.A. Roelen, Extracellular matrix components direct porcine muscle stem cell behavior, Experimental cell research, 316 (2010) 341-352.

[205] R. Moore, F.S. Walsh, The cell adhesion molecule M-cadherin is specifically expressed in developing and regenerating, but not denervated skeletal muscle, Development, 117 (1993) 1409-1420.

[206] Y. Pouliot, M. Gravel, P.C. Holland, Developmental regulation of M-cadherin in the terminal differentiation of skeletal myoblasts, Developmental dynamics : an official publication of the American Association of Anatomists, 200 (1994) 305-312.

[207] D. Brohl, E. Vasyutina, M.T. Czajkowski, J. Griger, C. Rassek, H.P. Rahn, B. Purfurst, H. Wende, C. Birchmeier, Colonization of the satellite cell niche by skeletal muscle progenitor cells depends on Notch signals, Developmental cell, 23 (2012) 469-481.

[208] A.S. Brack, T.A. Rando, Tissue-specific stem cells: lessons from the skeletal muscle satellite cell, Cell stem cell, 10 (2012) 504-514.

[209] R. Sambasivan, R. Yao, A. Kissenpfennig, L. Van Wittenberghe, A. Paldi, B. Gayraud-Morel, H. Guenou, B. Malissen, S. Tajbakhsh, A. Galy, Pax7-expressing satellite cells are indispensable for adult skeletal muscle regeneration, Development, 138 (2011) 3647-3656.

[210] G.M. Palmer, A.N. Fontanella, S. Shan, M.W. Dewhirst, High-resolution in vivo imaging of fluorescent proteins using window chamber models, Methods in molecular biology, 872 (2012) 31-50.

[211] N. Badie, L. Satterwhite, N. Bursac, A method to replicate the microstructure of heart tissue in vitro using DTMRI-based cell micropatterning, Ann Biomed Eng, 37 (2009) 2510-2521.

[212] R. Couteaux, J.C. Mira, A. d'Albis, Regeneration of muscles after cardiotoxin injury. I. Cytological aspects, Biology of the cell / under the auspices of the European Cell Biology Organization, 62 (1988) 171-182.

[213] J. Dhawan, T.A. Rando, Stem cells in postnatal myogenesis: molecular mechanisms of satellite cell quiescence, activation and replenishment, Trends in cell biology, 15 (2005) 666-673.

[214] J.R. Florini, K.A. Magri, Effects of growth factors on myogenic differentiation, Am J Physiol, 256 (1989) C701-711.

[215] M. Marti, N. Montserrat, C. Pardo, L. Mulero, L. Miquel-Serra, A.M. Rodrigues, J. Andres Vaquero, B. Kuebler, C. Morera, M.J. Barrero, J.C. Izpisua Belmonte, M-cadherin-mediated intercellular interactions activate satellite cell division, Journal of cell science, 126 (2013) 5116-5131.

[216] R. Srikuea, C. Pholpramool, Y. Kitiyanant, T. Yimlamai, Satellite cell activity in muscle regeneration after contusion in rats, Clinical and experimental pharmacology & physiology, 37 (2010) 1078-1086.

[217] Y. Jin, N. Murakami, Y. Saito, Y. Goto, K. Koishi, I. Nonaka, Expression of MyoD and myogenin in dystrophic mice, mdx and dy, during regeneration, Acta neuropathologica, 99 (2000) 619-627.

[218] J.W. Sanger, J. Wang, B. Holloway, A. Du, J.M. Sanger, Myofibrillogenesis in skeletal muscle cells in zebrafish, Cell motility and the cytoskeleton, 66 (2009) 556-566.

[219] J.W. Sanger, S. Kang, C.C. Siebrands, N. Freeman, A. Du, J. Wang, A.L. Stout, J.M. Sanger, How to build a myofibril, Journal of muscle research and cell motility, 26 (2005) 343-354.

[220] A. Kontrogianni-Konstantopoulos, M.A. Ackermann, A.L. Bowman, S.V. Yap, R.J. Bloch, Muscle giants: molecular scaffolds in sarcomerogenesis, Physiological reviews, 89 (2009) 1217-1267.

[221] L. Urbani, M. Piccoli, C. Franzin, M. Pozzobon, P. De Coppi, Hypoxia increases mouse satellite cell clone proliferation maintaining both in vitro and in vivo heterogeneity and myogenic potential, PloS one, 7 (2012) e49860.

[222] P. Fraisl, M. Mazzone, T. Schmidt, P. Carmeliet, Regulation of angiogenesis by oxygen and metabolism, Developmental cell, 16 (2009) 167-179.

[223] S.L. Lee, W.C. Pevec, R.C. Carlsen, Functional outcome of new blood vessel growth into ischemic skeletal muscle, Journal of vascular surgery, 34 (2001) 1096-1102.

[224] H. Vandenburgh, High-content drug screening with engineered musculoskeletal tissues, Tissue engineering. Part B, Reviews, 16 (2010) 55-64.

[225] G.A. Truskey, H.E. Achneck, N. Bursac, H. Chan, C.S. Cheng, C. Fernandez, S. Hong, Y. Jung, T. Koves, W.E. Kraus, K. Leong, L. Madden, W.M. Reichert, X. Zhao, Design considerations for an integrated microphysiological muscle tissue for drug and tissue toxicity testing, Stem cell research & therapy, 4 Suppl 1 (2013) S10.

[226] N. Hayashiji, S. Yuasa, Y. Miyagoe-Suzuki, M. Hara, N. Ito, H. Hashimoto, D. Kusumoto, T. Seki, S. Tohyama, M. Kodaira, A. Kunitomi, S. Kashimura, M. Takei, Y. Saito, S. Okata, T. Egashira, J. Endo, T. Sasaoka, S. Takeda, K. Fukuda, G-CSF supports long-term muscle regeneration in mouse models of muscular dystrophy, Nature communications, 6 (2015) 6745.

[227] B. Deng, M. Wehling-Henricks, S.A. Villalta, Y. Wang, J.G. Tidball, IL-10 triggers changes in macrophage phenotype that promote muscle growth and regeneration, Journal of immunology, 189 (2012) 3669-3680.

[228] L. Pelosi, C. Giacinti, C. Nardis, G. Borsellino, E. Rizzuto, C. Nicoletti, F. Wannenes, L. Battistini, N. Rosenthal, M. Molinaro, A. Musaro, Local expression of IGF-1 accelerates muscle regeneration by rapidly modulating inflammatory cytokines and chemokines, FASEB journal : official publication of the Federation of American Societies for Experimental Biology, 21 (2007) 1393-1402.

[229] E.R. Stanley, Murine bone marrow-derived macrophages, Methods in molecular biology, 75 (1997) 301-304.

[230] E. Kanters, M.J. Gijbels, I. van der Made, M.N. Vergouwe, P. Heeringa, G. Kraal, M.H. Hofker, M.P. de Winther, Hematopoietic NF-kappaB1 deficiency results in small atherosclerotic lesions with an inflammatory phenotype, Blood, 103 (2004) 934-940.

[231] M. Soleimani, S. Nadri, A protocol for isolation and culture of mesenchymal stem cells from mouse bone marrow, Nature protocols, 4 (2009) 102-106.

[232] M. Maleki, F. Ghanbarvand, M. Reza Behvarz, M. Ejtemaei, E. Ghadirkhomi, Comparison of mesenchymal stem cell markers in multiple human adult stem cells, International journal of stem cells, 7 (2014) 118-126.

[233] N. Jetten, S. Verbruggen, M.J. Gijbels, M.J. Post, M.P. De Winther, M.M. Donners, Anti-inflammatory M2, but not pro-inflammatory M1 macrophages promote angiogenesis in vivo, Angiogenesis, 17 (2014) 109-118.

[234] J.Y. Qin, L. Zhang, K.L. Clift, I. Hulur, A.P. Xiang, B.Z. Ren, B.T. Lahn, Systematic comparison of constitutive promoters and the doxycycline-inducible promoter, PloS one, 5 (2010) e10611.

[235] B. Sun, S.P. Young, P. Li, C. Di, T. Brown, M.Z. Salva, S. Li, A. Bird, Z. Yan, R. Auten, S.D. Hauschka, D.D. Koeberl, Correction of multiple striated muscles in murine Pompe disease through adeno-associated virus-mediated gene therapy, Molecular therapy : the journal of the American Society of Gene Therapy, 16 (2008) 1366-1371.

[236] H. Wang, S. Loof, P. Borg, G.A. Nader, H.M. Blau, A. Simon, Turning terminally differentiated skeletal muscle cells into regenerative progenitors, Nature communications, 6 (2015) 7916.

[237] F.O. Martinez, S. Gordon, The M1 and M2 paradigm of macrophage activation: time for reassessment, F1000prime reports, 6 (2014) 13.

[238] J.G. Tidball, K. Dorshkind, M. Wehling-Henricks, Shared signaling systems in myeloid cell-mediated muscle regeneration, Development, 141 (2014) 1184-1196.

[239] A.A. Tarique, J. Logan, E. Thomas, P.G. Holt, P.D. Sly, E. Fantino, Phenotypic, functional, and plasticity features of classical and alternatively activated human macrophages, American journal of respiratory cell and molecular biology, 53 (2015) 676-688.

[240] F. Porcheray, S. Viaud, A.C. Rimaniol, C. Leone, B. Samah, N. Dereuddre-Bosquet, D. Dormont, G. Gras, Macrophage activation switching: an asset for the resolution of inflammation, Clinical and experimental immunology, 142 (2005) 481-489.

[241] F. Marchildon, D. Fu, N. Lala-Tabbert, N. Wiper-Bergeron, CCAAT/enhancer binding protein beta protects muscle satellite cells from apoptosis after injury and in cancer cachexia, Cell death & disease, 7 (2016) e2109.

[242] C. Leeuwenburgh, C.M. Gurley, B.A. Strotman, E.E. Dupont-Versteegden, Age-related differences in apoptosis with disuse atrophy in soleus muscle, American journal of physiology. Regulatory, integrative and comparative physiology, 288 (2005) R1288-1296.

[243] S. Yasuhara, M.E. Perez, E. Kanakubo, Y. Yasuhara, Y.S. Shin, M. Kaneki, T. Fujita, J.A. Martyn, Skeletal muscle apoptosis after burns is associated with activation of proapoptotic signals, American journal of physiology. Endocrinology and metabolism, 279 (2000) E1114-1121.

[244] J. Du, X. Wang, C. Miereles, J.L. Bailey, R. Debigare, B. Zheng, S.R. Price, W.E. Mitch, Activation of caspase-3 is an initial step triggering accelerated muscle proteolysis in catabolic conditions, The Journal of clinical investigation, 113 (2004) 115-123.

[245] A. McArdle, A. Maglara, P. Appleton, A.J. Watson, I. Grierson, M.J. Jackson, Apoptosis in multinucleated skeletal muscle myotubes, Laboratory investigation; a journal of technical methods and pathology, 79 (1999) 1069-1076.

[246] B.A. Citron, P.M. Arnold, C. Sebastian, F. Qin, S. Malladi, S. Ameenuddin, M.E. Landis, B.W. Festoff, Rapid upregulation of caspase-3 in rat spinal cord after injury: mRNA, protein, and cellular localization correlates with apoptotic cell death, Experimental neurology, 166 (2000) 213-226.

[247] K. Boland, L. Flanagan, J.H. Prehn, Paracrine control of tissue regeneration and cell proliferation by Caspase-3, Cell death & disease, 4 (2013) e725.

[248] T.M. Caserta, A.N. Smith, A.D. Gultice, M.A. Reedy, T.L. Brown, Q-VD-OPh, a broad spectrum caspase inhibitor with potent antiapoptotic properties, Apoptosis : an international journal on programmed cell death, 8 (2003) 345-352.

[249] D. Vucic, V.M. Dixit, I.E. Wertz, Ubiquitylation in apoptosis: a post-translational modification at the edge of life and death, Nature reviews. Molecular cell biology, 12 (2011) 439-452.

[250] H. Bruunsgaard, M. Pedersen, B.K. Pedersen, Aging and proinflammatory cytokines, Current opinion in hematology, 8 (2001) 131-136.

[251] R.A. Collins, M.D. Grounds, The role of tumor necrosis factor-alpha (TNF-alpha) in skeletal muscle regeneration. Studies in TNF-alpha(-/-) and TNF-alpha(-/-)/LT-alpha(-/-) mice, The journal of histochemistry and cytochemistry : official journal of the Histochemistry Society, 49 (2001) 989-1001.

[252] E.E. Pistilli, J.R. Jackson, S.E. Alway, Death receptor-associated pro-apoptotic signaling in aged skeletal muscle, Apoptosis : an international journal on programmed cell death, 11 (2006) 2115-2126.

[253] S.J. Lees, K.A. Zwetsloot, F.W. Booth, Muscle precursor cells isolated from aged rats exhibit an increased tumor necrosis factor- alpha response, Aging cell, 8 (2009) 26-35.

[254] S. Kuru, A. Inukai, T. Kato, Y. Liang, S. Kimura, G. Sobue, Expression of tumor necrosis factor-alpha in regenerating muscle fibers in inflammatory and non-inflammatory myopathies, Acta neuropathologica, 105 (2003) 217-224.

[255] P. Hu, Z. Han, A.D. Couvillon, R.J. Kaufman, J.H. Exton, Autocrine tumor necrosis factor alpha links endoplasmic reticulum stress to the membrane death receptor pathway through IRE1alpha-mediated NF-kappaB activation and down-regulation of TRAF2 expression, Mol Cell Biol, 26 (2006) 3071-3084.

[256] R. Uemura, M. Xu, N. Ahmad, M. Ashraf, Bone marrow stem cells prevent left ventricular remodeling of ischemic heart through paracrine signaling, Circulation research, 98 (2006) 1414-1421.

[257] R. Schindler, J. Mancilla, S. Endres, R. Ghorbani, S.C. Clark, C.A. Dinarello, Correlations and interactions in the production of interleukin-6 (IL-6), IL-1, and tumor necrosis factor (TNF) in human blood mononuclear cells: IL-6 suppresses IL-1 and TNF, Blood, 75 (1990) 40-47.

[258] I. Tassiulas, K.H. Park-Min, Y. Hu, L. Kellerman, D. Mevorach, L.B. Ivashkiv, Apoptotic cells inhibit LPS-induced cytokine and chemokine production and IFN responses in macrophages, Human immunology, 68 (2007) 156-164.

[259] K.R. Knight, A. Messina, J.V. Hurley, B. Zhang, W.A. Morrison, A.G. Stewart, Muscle cells become necrotic rather than apoptotic during reperfusion of ischaemic skeletal muscle, Int J Exp Pathol, 80 (1999) 169-175.

[260] K.L. Spiller, R.R. Anfang, K.J. Spiller, J. Ng, K.R. Nakazawa, J.W. Daulton, G. Vunjak-Novakovic, The role of macrophage phenotype in vascularization of tissue engineering scaffolds, Biomaterials, 35 (2014) 4477-4488.

[261] R. Mittermayr, P. Slezak, N. Haffner, D. Smolen, J. Hartinger, A. Hofmann, J. Schense, D. Spazierer, J. Gampfer, A. Goppelt, H. Redl, Controlled release of fibrin

matrix-conjugated platelet derived growth factor improves ischemic tissue regeneration by functional angiogenesis, Acta biomaterialia, 29 (2016) 11-20.

[262] L.S. Nierobisz, B. Cheatham, B.M. Buehrer, J.Z. Sexton, High-content screening of human primary muscle satellite cells for new therapies for muscular atrophy/dystrophy, Current chemical genomics and translational medicine, 7 (2013) 21-29.

[263] C.F. Bentzinger, Y.X. Wang, J. von Maltzahn, V.D. Soleimani, H. Yin, M.A. Rudnicki, Fibronectin regulates Wnt7a signaling and satellite cell expansion, Cell stem cell, 12 (2013) 75-87.

[264] W. Liu, Y. Wen, P. Bi, X. Lai, X.S. Liu, X. Liu, S. Kuang, Hypoxia promotes satellite cell self-renewal and enhances the efficiency of myoblast transplantation, Development, 139 (2012) 2857-2865.

[265] J.Q. Davies, S. Gordon, Isolation and culture of human macrophages, Methods in molecular biology, 290 (2005) 105-116.

[266] B. van Wilgenburg, C. Browne, J. Vowles, S.A. Cowley, Efficient, long term production of monocyte-derived macrophages from human pluripotent stem cells under partly-defined and fully-defined conditions, PloS one, 8 (2013) e71098.

[267] J. Wu, S.D. Hunt, H. Xue, Y. Liu, R. Darabi, Generation and validation of PAX7 reporter lines from human iPS cells using CRISPR/Cas9 technology, Stem Cell Res, 16 (2016) 220-228.

[268] M. Akiyama, Y. Kaneko, H. Kondo, T. Takeuchi, Comparison of the clinical effectiveness of tumour necrosis factor inhibitors and abatacept after insufficient response to tocilizumab in patients with rheumatoid arthritis, Clin Rheumatol, (2016).

[269] M. Quattrocelli, M. Sampaolesi, The mesmiRizing complexity of microRNAs for striated muscle tissue engineering, Advanced drug delivery reviews, 88 (2015) 37-52.

[270] M. Guescini, D. Guidolin, L. Vallorani, L. Casadei, A.M. Gioacchini, P. Tibollo, M. Battistelli, E. Falcieri, L. Battistin, L.F. Agnati, V. Stocchi, C2C12 myoblasts release micro-vesicles containing mtDNA and proteins involved in signal transduction, Experimental cell research, 316 (2010) 1977-1984.

[271] A. Forterre, A. Jalabert, K. Chikh, S. Pesenti, V. Euthine, A. Granjon, E. Errazuriz, E. Lefai, H. Vidal, S. Rome, Myotube-derived exosomal miRNAs downregulate Sirtuin1 in myoblasts during muscle cell differentiation, Cell cycle, 13 (2014) 78-89.

[272] Y. Nakamura, S. Miyaki, H. Ishitobi, S. Matsuyama, T. Nakasa, N. Kamei, T. Akimoto, Y. Higashi, M. Ochi, Mesenchymal-stem-cell-derived exosomes accelerate skeletal muscle regeneration, FEBS letters, 589 (2015) 1257-1265.

[273] N. Ismail, Y. Wang, D. Dakhlallah, L. Moldovan, K. Agarwal, K. Batte, P. Shah, J. Wisler, T.D. Eubank, S. Tridandapani, M.E. Paulaitis, M.G. Piper, C.B. Marsh,

Macrophage microvesicles induce macrophage differentiation and miR-223 transfer, Blood, 121 (2013) 984-995.

[274] D. Joshi, H. Patel, D.M. Baker, X. Shiwen, D.J. Abraham, J.C. Tsui, Development of an in vitro model of myotube ischemia, Laboratory investigation; a journal of technical methods and pathology, 91 (2011) 1241-1252.

[275] R. Shechter, A. London, C. Varol, C. Raposo, M. Cusimano, G. Yovel, A. Rolls, M. Mack, S. Pluchino, G. Martino, S. Jung, M. Schwartz, Infiltrating blood-derived macrophages are vital cells playing an anti-inflammatory role in recovery from spinal cord injury in mice, PLoS medicine, 6 (2009) e1000113.

[276] V.E. Miron, A. Boyd, J.W. Zhao, T.J. Yuen, J.M. Ruckh, J.L. Shadrach, P. van Wijngaarden, A.J. Wagers, A. Williams, R.J. Franklin, C. ffrench-Constant, M2 microglia and macrophages drive oligodendrocyte differentiation during CNS remyelination, Nature neuroscience, 16 (2013) 1211-1218.

[277] J.R. Plemel, V. Wee Yong, D.P. Stirling, Immune modulatory therapies for spinal cord injury--past, present and future, Experimental neurology, 258 (2014) 91-104.

Biography

Born on February 7th, 1988. Grew up in Webster, New York and graduated from Webster Thomas High School in 2006.

EDUCATION

2010 – 2016	PhD, Biomedical Engineering, April 2016 Duke University, Durham, NC
2006 – 2010	BS, Bioengineering, May 2010 University of Pittsburgh, Pittsburgh, PA

FELLOWSHIPS

Graduate Research Fellowship from the National Science Foundation (2010 – 2013)

PUBLICATIONS

N. Bursac, **M. Juhas**, T. Rando, 'Synergizing Engineering and Biology to Treat and Model Skeletal Muscle Injury and Disease', Annual Review of Biomedical Engineering, 17 (2015)**, 217-42**.

M. Juhas, J. Ye, N. Bursac, 'Design, Evaluation, and Application of Engineered Skeletal Muscle', Methods Journal, 15 (2015).

L. Madden, **M Juhas**, W. E. Kraus, G. A. Truskey, N. Bursac, 'Bioengineered human myobundles mimic clinical responses of skeletal muscle to druges', eLife, 4 (2015).

M. Juhas and N. Bursac, 'Roles of adherent myogenic cells and dynamic culture in engineered muscle function and maintenance of satellite cells', Biomaterials, 35 (2014), 9438-46.

M. Juhas, G. C. Engelmayr, Jr., A. N. Fontanella, G. M. Palmer, and N. Bursac, 'Biomimetic Engineered Muscle with Capacity for Vascular Integration and Functional Maturation in Vivo', Proc Natl Acad Sci USA, 15 (2014), 5508-13.

M. Juhas, and N. Bursac, 'Engineering Skeletal Muscle Repair', Curr Opin Biotechnol, 24 (2013), 880-6.

W. Bian, **M. Juhas**, and N. Bursac, 'Engineering of Skeletal Muscle Regeneration: Principles, Current State, and Challenges'. Tissue and Organ Regeneration: Advances in Micro and Nanotechnology (2013).

W. Bian, **M. Juhas**, T. W. Pfeiler, and N. Bursac, 'Local Tissue Geometry Determines Contractile Force Generation of Engineered Muscle Networks', Tissue Eng Part A, 18 (2012), 957-67.

N. T. Remlinger, C. A. Czajka, **M. E. Juhas**, D. A. Vorp, D. B. Stolz, S. F. Badylak, S. Gilbert, and T. W. Gilbert, 'Hydrated Xenogeneic Decellularized Tracheal Matrix as a Scaffold for Tracheal Reconstruction', Biomaterials, 31 (2010), 3520-6.

J. T. Samosky, P. Allen, S. Boronyak, B. Branstetter, S. Hein, **M. Juhas**, D. A. Nelson, S. Orebaugh, R. Pinto, A. Smelko, M. Thompson, and R. A. Weaver, 'Toward a Comprehensive Hybrid Physical-Virtual Reality Simulator of Peripheral Anesthesia with Ultrasound and Neurostimulator Guidance', Stud Health Technol Inform, 163 (2011), 552-4.

PRESENTATIONS

M. Juhas and N. Bursac. “Engineering Self-regenerative Muscle Tissue.” regenerationNEXT Community Meeting, Durham, NC, Janurary 2016. Oral presentation.

M. Juhas, J. Ye, and N. Bursac. “Engineering Regenerative Skeletal Muscle Tissues.” TERMIS World Conference, Boston, MA, September 2015. Poster.

M. Juhas, J. Ye, G. Engelmayr, and N. Bursac. “Engineering Skeletal Muscle Tissues Capable of Regeneration.” NCTERMS, Durham, NC, October 2014. Poster.

L. Madden, **M. Juhas**, and N. Bursac. “Functional Maturation of Engineered 3D Human Skeletal Muscle.” NCTERMS, Durham, NC, October 2014. Poster.

M. Juhas, G. Engelmayr, and N. Bursac. “Bioengineered Skeletal Muscle With Functional Stem Cell Pool and Capacity for Vascular Integration and Maturation In Vivo.” American Soicety of Gene & Cell Therapy 17th Annual Meeting, Washington, DC, 2014. Poster.

M. Juhas, G. Engelmayr, and N. Bursac. “Bioengineered skeletal muscle with capacity for vascular integration and functional maturation in vivo.” NCTERMS, Winston Salem, NC, October 2013. Poster.

M. Juhas, G. Engelmayr, and N. Bursac. “3D tissue-engineered muscle with satellite cell niche exhibits unparallel contractile function and robust vascularization.” EMBO Workshop: Molecular mechanisms of muscle growth and wasting in health and disease, Ascona, Switzerland, September 2013. Oral presentation.

M. Juhas and N. Bursac. “Tissue-engineered Skeletal Muscle: potential for on-site muscle repair and model in vitro system.” Duke Biomedical Engineering Retreat, Beaufort, NC, May 2013. Oral presentation.

M. Juhas and N. Bursac. “Engineering Skeletal Muscle Tissue Replicating Structure and Function of Native Muscle.” Biomedical Engineering Society Conference, Atlanta, GA, October 2012. Oral presentation.

M. Juhas and N. Bursac. “Engineering Muscle with Improved Force Production.” TERMIS North America Conference, Houston, TX, December 2011, Oral presentation.